ON THE SYNTHESIS AND CHARACTERIZATION OF

THE OPTICAL PROPERTIES OF EUROPIUM- AND

RUTHENIUM-DOPED SOL–GEL-DERIVED

MATERIALS AND SODIUM SULFATES

By

LOWELL RALPH MATTHEWS

Bachelor of Science

University of Tulsa

Tulsa, Oklahoma

1990

Submitted to the Faculty of the
Graduate College of the
Oklahoma State University
in partial fulfillment of
the requirements for
the Degree of
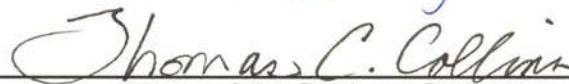DOCTOR OF PHILOSOPHY
May, 1995

ON THE SYNTHESIS AND CHARACTERIZATION OF

THE OPTICAL PROPERTIES OF EUROPIUM- AND

RUTHENIUM-DOPED SOL–GEL-DERIVED

MATERIALS AND SODIUM SULFATES

Thesis Approved:

_____
Thesis Adviser

_____
Lionel M. Raff

_____

_____

_____
Thomas C. Collins
Dean of the Graduate College
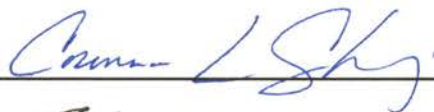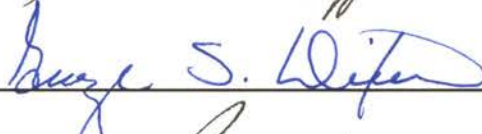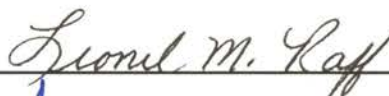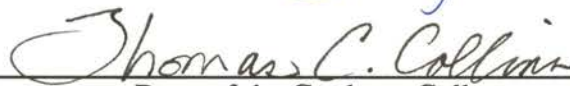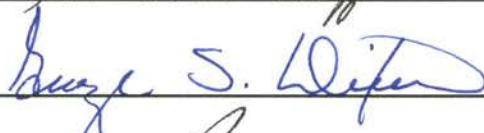
ON THE SYNTHESIS AND CHARACTERIZATION OF

THE OPTICAL PROPERTIES OF EUROPIUM- AND

RUTHENIUM-DOPED SOL–GEL-DERIVED

MATERIALS AND SODIUM SULFATES

Thesis Approved:

_____

Thesis Adviser

_____

Leonel M. Raff

_____

_____

_____

_____

Thomas C. Collins

Dean of the Graduate College

PREFACE

This research project was conducted in order to gain new understandings of the behavior of fluorescent metalorganic complexes of europium(III) and ruthenium(II) when incorporated into sol–gel-derived solid-state hosts, with a desired objective of producing new optical sources. The project included the characterization of a number of europium(III) β-diketonates incorporated into sol–gel silica, followed by the incorporation of the most luminescent subjects, complexes of europium(III) with 4,4,4-trifluoro-1-(2′-thienyl)-1,3-butanedione, into organically modified silicate materials. Subsequently, tris(2,2′-bipyridyl)ruthenium(II) chloride was incorporated into the same set of host materials. Finally, the knowledge of europium(III) fluorescence spectroscopy gained during the previous studies was used to characterize high-temperature phases of sodium sulfate stabilized to room temperature by the incorporation of europium(III).

I would like to offer my sincere appreciation to the members of my doctoral committee—Drs. Neil Purdie (Chair), Lionel M. Raff, George S. Dixon, Corinna Czekaj, and Edward T. Knobbe, my research advisor, saving the most influential for last. Thank you for putting up with me for four years! I must also thank the past and present Knobbe researchers for their support—L. M. (Trace) Yates III, Xiaodong Sun, Diane M. Arbuthnot, James Greuel, Robert Parkhill, and Drs. Xiaojun Wang and Monica Sorescu—and Drs. K. D. Berlin, E. M. Holt, Warren T. Ford, Shanmin Zhang, Roger R. Petrin, Roger J. Reeves, R. J. Hauenstein, and many others for assistance and expertise over the years. But none of my professional accomplishments would be possible without the support of my wonderful wife, Jeannine, our son Stephen, our extended families, and most of all, my Lord and Savior, Jesus Christ.

TABLE OF CONTENTS

LIST OF TABLES

LIST OF FIGURES

NOMENCLATURE*

bpy	2,2'-bipyridine or bipyridyl
BLL	Beer–Lambert Law
CP	Cross-polarization (NMR)
cw	Continuous wave
DMF	N,N-dimethylformamide
DTA	Differential thermal analysis
ED	Electric dipole
EG	Ethylene glycol or 1,2-ethanediol
EIMS	Electron impact mass spectrometry
en	Ethylenediamine or 1,2-diaminoethane
ET	Energy transfer
FAB	Fast atom bombardment (mass spectrometry)
GPTMS	3-Glycidoxypropyltrimethoxysilane
Hacac	Acetylacetone or 2,4-pentanedione; also, acac⁻ for its enolate ion
Hba	Benzoylacetone or 1-phenyl-1,3-butanedione; also, ba⁻ for its enolate ion
Hbtfa	Benzoyltrifluoroacetone or 4,4,4-trifluoro-1-phenyl-1,3-butanedione; also, btfa⁻ for its enolate ion
Hdbm	Dibenzoylmethane or 1,3-diphenyl-1,3-propanedione; also, dbm⁻ for its enolate ion
Hdik	A generic β-diketone, $R^1C(O)CH_2C(O)R^2$; also, dik⁻ for its enolate ion

---

*   Where two names are given for a chemical compound, the first is the common name and the second is the official name assigned by the International Union for Pure and Applied Chemistry (IUPAC). Where a single name is given, it is the IUPAC name.

HTf	Triflic acid or trifluoromethylsulfonic acid, HSO_3CF_3; also, Tf^- for the triflate ion
Htfaa	Trifluoroacetylacetone or 1,1,1-trifluoro-2,4-pentanedione; also, $tfaa^-$ for its enolate ion
Httfa	Thenoyltrifluoroacetone or 4,4,4-trifluoro-1-(2′-thienyl)-1,3-butanedione; also, $ttfa^-$ for its enolate ion
IR	Infrared
LMET	Ligand-to-metal energy transfer
Ln	A generic lanthanide element (La–Lu)
LSIMS	Liquid secondary ion mass spectrometry
M	Molar
MAS	Magic-angle-spinning (NMR)
MD	Magnetic dipole
MLCT	Metal-to-ligand charge transfer
MMA	Methyl methacrylate
NMR	Nuclear magnetic resonance
OPD	One-pulse-with-proton-decoupling (NMR)
Pip	Piperidine; also, $PipH^+$ for the protonated piperidinium ion
PMMA	Poly(methyl methacrylate)
PMT	Photomultiplier tube
Q	A generic nitrogenous organic base; also, Q^+ for the protonated ion
RT	Room temperature ($\approx$290 K)
RuB	Tris(2,2′-bipyridyl)ruthenium(II) chloride
S/A	Silica–acrylate ormosil
TEOS	Tetraethyl orthosilicate or tetraethoxysilane

TG	Thermogravimetry
TMOS	Tetramethyl orthosilicate or tetramethoxysilane
TMSPM	3-(Trimethoxysilyl)propyl methacrylate

LIST OF SYMBOLS

α or α_{Abs}	Absorption coefficient (cm^{-1})
Δ	Change or difference in
ϵ	Molar extinction coefficient ((M cm)$^{-1}$)
η_{21}	Integrated intensity ratio
λ	Wavelength (usually nm)
λ_{em}	Emission wavelength (nm)
λ_{em-max}	Wavelength of maximum emission (nm)
λ_{ex}	Excitation wavelength (nm)
λ_{ex-max}	Wavelength of maximum excitation (nm)
ν	Vibrational mode (cm^{-1})
σ	Conductivity (S/cm or (Ω cm)$^{-1}$)
σ_0	Conductivity pre-exponential constant (S cm^{-1} K or (Ω cm)$^{-1}$ K)
σ_{Abs}	Absorption cross-section (cm^2)
σ_{SpE}	Spontaneous emission cross section (cm^2)
τ or τ_d	Fluorescence lifetime or decay time (usually μs)
τ_r	Fluorescence rise time (usually ns)
$^{(2S+1)}L_J$	Angular momentum term symbol, where $S \equiv$ total spin angular momentum (0, 1/2, 1, 3/2, ...); $L \equiv$ total orbital angular momentum (0, 1, 2, 3, ..., written S, P, D, F, ...); and $J \equiv$ total angular momentum ($L + S, L + S - 1$, ..., $|L - S|$). Thus, the ground state of europium(III), with $L = 3$, $S = 3$, and $J = 0$ has the term symbol $^7F_0$.
C_x, D_x	Schönflies symmetry classification symbols
E_J	Abbreviation for the $^5D_0 \rightarrow {}^7F_J$ emissions of europium(III), $J = 0$–4.
I	Intensity (usually emission intensity)

k	Boltzmann's constant (J/K or eV/K)
K	Equilibrium constant (subscripts a, b, and f indicate acid, base, and formation equilibrium constants, respectively)
K'	Partition coefficient (mL/g)
N	Number density (cm^{-3})
pK	Equilibrium constant in logarithmic form ($pK = -\log K$)
Q	Quantum efficiency (photons emitted per photon absorbed)
Q^n	Silicon atom coordinated to $n = 0\text{--}4$ other silicon atoms by oxygen bridges (a term used in ^{29}Si NMR)
Q_c	Activation energy of ionic motion (J, J/mol, or eV)
R	Gas constant (J mol^{-1} K^{-1}) or water-to-alkoxide ratio
S	Integrated emission intensity
T	Absolute temperature (K)

CHAPTER 1

EFFECTS OF LIGAND VARIATION ON THE LUMINESCENCE BEHAVIOR OF

EUROPIUM(III) β-DIKETONATES INCORPORATED INTO SOL–GEL SILICA

I. Introduction

The sol–gel method has been shown to be a suitable approach for the preparation of

novel inorganic and composite materials, into which fluorophores can be incorporated.

Much recent work has focused on the development of solid-state tunable dye laser media

using organic dye dopants in sol–gel hosts,[1–12] and several researchers have demonstrated

laser action in such media.[1–7] Typically, dopants are incorporated into gel hosts via disso-

lution of soluble species into the initial precursor sol. Solutions may be coated onto

various substrates, pulled into free-standing fibers, or cast into bulk monoliths. Thus, gel-

based media appear to be promising candidates for the development of new bulk lasers and

integrated optical device sources. Unfortunately, from the engineering point of view, most

of the organic dyes photodecompose fairly quickly, thereby limiting useful application life-

times.[2–3, 8] Efforts have been directed toward improving the photostability of dye-doped

gel materials through changing matrix composition and processing parameters, and more

recently reported materials possess substantially enhanced stability behavior, by orders of

magnitude in some cases.[6, 9–11] A second problem associated with organic dye-doped

materials involves luminescence quenching at high laser repetition rates, as intersystem

crossing to relatively long-lived triplet states tends to reduce the stimulated emission cross-

section of these systems at pump-pulse rates greater than 5 Hz, whereas many dye-laser

applications require pump rates of 10–50 Hz. For these reasons, it is of interest to explore

alternative luminescent species for use in optical source applications. The research

1

presented herein seeks to extend earlier work regarding luminescent doped sol–gel matrices to include complexed rare earth ion dopants.

Compounds containing rare earth ions have long been used as phosphors and laser materials because of their sharp, intensely luminescent f–f electronic transitions. In particular, europium(III) has five narrow emission bands corresponding to the $^5D_0 \rightarrow {}^7F_J$ transitions, where J = 0, 1, 2, 3, or 4. The strongest emission, $^5D_0 \rightarrow {}^7F_2$ or E_2,[†] occurs at approximately 610 nanometers, the characteristic "europium red" luminescence.[13] Among their widespread applications, europium(III) phosphors have been used as red emission sources in cathode-ray tubes.[13] The E_2 transition has also been shown to exhibit laser emission under appropriate conditions in Eu^{3+}-doped crystals and glasses[14] and from Eu^{3+} organometallic complexes in solution.[15]

Mack $et\ al.$, Sanchez, and Campostrini $et\ al.$ have previously examined the luminescence behavior of $EuCl_3$[16–17] and $Eu(NO_3)_3$[18] salts adsorbed into porous glasses and doped into sol–gel hosts. $EuCl_3$-doped silica gels produced in our laboratory were found to exhibit both highly quenched luminescence and relatively inefficient absorption of excitation energy due to the Laporte-forbidden nature of Eu^{3+} f–f transitions. Thus, it is of great interest to modify the local environment of Eu^{3+} ions to improve their absorptive characteristics and to reduce nonradiative decay mechanisms from the excited state. One approach is the use of complex-forming ligands such as the β-diketones. This method affords a rare earth ion that is substantially shielded from the immediate local surroundings by the organic ligand shell. Some β-diketonate ligands are also highly asymmetric, thereby reducing the local field symmetry of the metal ion and making the f–f radiative transitions somewhat more allowed. Brecher $et\ al.$ demonstrated that organometallic complexes of europium showed intense fluorescence in a variety of solutions, including protic systems such as ethanol and methyl methacrylate.[19] The emission intensities of these complexes were found to be greater than those of inorganic salts, such as $EuCl_3$, after dissolution into

---

[†] In Chapters 1 and 8, the symbol E_J is an abbreviation for the $^5D_0 \rightarrow {}^7F_J$ emission.

comparable solvents. In the reported work twelve different europium(III) β-diketonate metalorganic complexes, the *tris* and *tetrakis* complexes of six different ligands, have been prepared, and the eight most luminescent have been doped into silica hosts prepared by the sol–gel method. The luminescence behaviors of the resulting composite materials are described. (For more detailed background information, see Appendices A–C.)

II. Experimental Methods

A. Syntheses

Europium(III) chelates were prepared using six different β-diketones, illustrated and listed in Figure 1-1, which differ mainly in the structure of their R^1 and R^2 groups. These compounds as a class are known to undergo keto–enol tautomerization. Although the keto form (Fig. 1-1a) is, in general, favored under neutral or acidic conditions, the enolic hydrogen (the OH group, Fig. 1-1b) is sufficiently acidic to dissociate in the presence of a base (Eq. 1a–1b), forming the conjugated enolate (β-diketonate) anion (Fig. 1-1c). This anion may react with metal ions to form organometallic complexes.[20] In the presence of stoichiometric quantities of Eu^{3+}, they can produce tris (Eq. 2a) or tetrakis (Eq. 2b) chelate complexes, depending upon the synthetic conditions used:

(1a) $\quad$ Hdik + NaOH → Na(dik) + H_2O

(1b) $\quad$ Hdik + Pip → (PipH)(dik)

(2a) $\quad$ 3 Na(dik) + $EuCl_3$ → Eu(dik)$_3$ + 3 NaCl

(2b) $\quad$ 4 (PipH)(dik) + $EuCl_3$ → (PipH)[Eu(dik)$_4$] + 3 (PipH)Cl
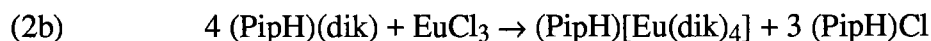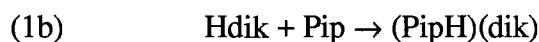
where Hdik and dik⁻ are a β-diketone and its β-diketonate anion, respectively, and Pip and $PipH^+$ are piperidine and the piperidinium cation, respectively (see Fig. 1-1d). The indicated syntheses were initially described by Whan and Crosby[21] for Hba and Hdbm (see Fig. 1-1) and later expanded by Brecher *et al.*,[19] who fully detailed the preparation of a number of tris and tetrakis europium(III) β-diketonates; Lyle and Witts[22] have written a

critical review of various synthetic methods for producing rare-earth β-diketonates. These complexes are highly soluble in N,N-dimethylformamide (DMF), which is known to be compatible with sol–gel preparative techniques for silica gel.[23] The tris and tetrakis europium(III) complexes of all six β-diketonates listed in Figure 1-1 were initially chosen for incorporation into silica gel; however, the acetylacetonate and trifluoroacetylacetonate complexes were found to be effectively nonluminescent in both DMF solution and silica gel systems and were therefore eliminated from further consideration. In accordance with the theory discussed in Section III below, two likely reasons for their lack of luminescence are lack of extended conjugation to either R group and insufficient overlap between the ligands' T_1 and the Eu^{3+} $^5D_0$ energy levels.

Figure 1-1: Structures and Nomenclature

(a) R^1 ... R^2

(b) R^1 ... R^2

(c) R^1 ... R^2

(d)
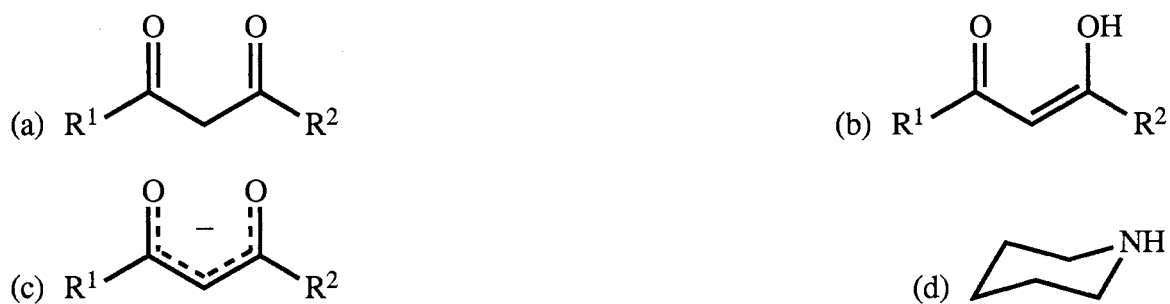
Symbol	β-Diketone (Common and IUPAC Names)	R^1	R^2
Hacac	Acetylacetone 2,4-Pentanedione	CH_3	CH_3
Hba	Benzoylacetone 1-Phenyl-1,3-butanedione	C_6H_5	CH_3
Hbtfa	Benzoyltrifluoroacetone 4,4,4-Trifluoro-1-phenyl-1,3-butanedione	C_6H_5	CF_3
Hdbm	Dibenzoylmethane 1,3-Diphenyl-1,3-propanedione	C_6H_5	C_6H_5
Htfaa	Trifluoroacetylacetone 1,1,1-Trifluoro-2,4-pentanedione	CF_3	CH_3
Httfa	Thenoyltrifluoroacetone 4,4,4-Trifluoro-1-(2'-thienyl)-1,3-butanedione	C_4H_3S	CF_3

FIGURE 1-1: Structures and symbols of the ligands, base, and solvent. (a) A generic β-diketone, keto form. (b) The enol form. (c) The generic enolate (β-diketonate) anion. (d) Organic base piperidine (Pip, $C_5H_{11}N$). (e) Solvent N,N-dimethylformamide.

4

The host silica gel matrix was prepared by the hydrolysis and condensation of tetraethoxysilane (TEOS) according to the "sonogel" procedure as described by de la Rosa-Fox, Esquivias, and Zarzycki.[24] A 4:1 water to alkoxide mole ratio was used, with acid catalysis. Typical early syntheses included 10 mL of H_2O, 31 mL of TEOS, and a drop of concentrated HCl; in later syntheses, 10 mL of 0.040 M HCl was used in place of water and concentrated HCl for more accurate pH selection. In either case, the batches were processed in disposable polypropylene beakers, which were immersed in an ice bath contained within a Bransonic® model 3 ultrasonic cleaner. The two-phase reaction mixture was stirred at intervals with a disposable transfer pipette; the single-phase sol usually formed within 20–30 minutes with noticeable exothermicity. It has been observed that fresh sols provide a small improvement in reproducibility over older sols, which when stored in a freezer stay liquid for months.

Chelate-doped gel samples were prepared by the addition of aliquots of the organo-europium complex, dissolved in DMF at 5 mM, to the silica precursor solution. The resulting sol was subsequently cast into transparent polystyrene cuvettes. The samples were kept in covered containers at room temperature until the onset of gellation, which occurred within 5–9 days. Aging and drying were allowed to proceed under ambient conditions over a period of several weeks, during which the luminescence activity was monitored. Dried xerogel samples retained approximately 20% of their original volume, as determined from the recorded sol volumes and measurements of the physical dimensions of the solid samples, averaged over about 20 samples. Using this value for the final volume, the final concentration (number density) of the organometallic guest species in the host gel increases approximately fivefold, to 5.0 mM (3.0×10^{18} cm^{-3}).

B.   *Characterization*

The samples' luminescence characteristics were measured using a Spex Industries Model F112 spectrofluorimeter interfaced to an IBM-compatible personal computer. Emission and excitation spectra were made in the "front face" orientation, and all spectra

were corrected for instrumental response by using the "correction factor" files in the Spex software. The integrated emission intensity values (necessary to obtain quantum efficiencies) were computed via the integration function of the Spex software.

C.   Discussion of Characterization Methods

Characterization of doped gels by NMR, infrared, and mass spectroscopic techniques has proved to be difficult because of the relatively small amount of dopant present with respect to the matrix. A series of solid-state NMR experiments (including nuclides ^{1}H, ^{13}C, and ^{29}Si, see Appendix C) on the silica gel introduced in this Chapter and the organically modified silicate *(ormosil)* host materials introduced in Chapters 3 and 4 identified a number of features belonging to the host matrices, but subsequent experiments on doped versions failed to identify significant differences from the undoped materials. Furthermore, attempts to detect nuclides unique to the dopants (including ^{151}Eu and ^{153}Eu) failed to produce a detectable signal. Likewise, while the utility of IR and mass spectroscopic techniques has been demonstrated in the characterization of the dopants when pure, IR techniques proved insensitive to the doped materials and the physical properties of the doped materials proved incompatible with the requirements of mass spectroscopy.

In contrast, many europium(III) compounds are detectable in extremely low concentrations by such optical techniques as ultraviolet/visible/near infrared absorption spectroscopy, particularly by fluorescence emission and excitation spectroscopies. In solution, europium(III) fluorescence detection limits as low as 2.0×10^{-12} M have been reported.[25] Europium(III) fluorescence is also highly sensitive to alterations in the immediate surroundings of the Eu^{3+} ion. It can therefore be used as a luminescent probe to characterize its environment in detail, and numerous examples of this use appear in the literature.[18, 26] For these reasons, as well as meeting the experimental objective of preparing luminescent materials through chemical optimization for use as potential optical sources, fluorescence and absorption spectroscopies were chosen as the principal characterization techniques for the work described throughout this thesis.

6

In the following sections, changes in the luminescence behavior of eight europium(III) β-diketonates are presented as luminescence emission and excitation spectra in Figures 1-3 to 1-18. In general, the first spectrum in each set is that of the compound dissolved in DMF at 1.0 mM (6.0×10^{17} cm^{-3}), the next is the comparable silica sol (also 1.0 mM), and the subsequent spectra were recorded as the silica host ages from sol to gel to xerogel, reaching a final concentration near 5.0 mM (3.0×10^{18} cm^{-3}). In all eight cases, the compound's fluorescence intensity is higher in DMF, an aprotic solvent, than in the sol–gel silica, and the spectra in DMF are scaled accordingly. Spectra in ethanol have been observed to be very similar to those in silica sol.

All of the visible features in the emission spectra can be attributed to the characteristic europium(III) emissions described in the introduction; they arise from the $^5D_0$ level, which lies about 17,300 cm^{-1} above the $^7F_0$ ground state. These emissions are located at 578, 585–595, 605–625, 645–655, and 685–705 nm and correspond to the transitions $^5D_0 \rightarrow {}^7F_J$, $J = 0$–4, (abbreviated E_{0-4}) respectively.[13] The E_2 and E_4 features are most prominent, while the E_0 and E_3 features are frequently almost nonexistent. Furthermore, the wavelengths of the emission features—related to the energy separation between emitting and receiving levels—are fairly constant; the significant changes are in the branching ratios between the various emission features and in absolute intensity.

The interpretation of the excitation spectra is not so straightforward, however. In inorganic salts like europium(III) chloride or nitrate, the Eu^{3+} center is excited directly from its $^7F_0$ ground state to one of a large number of higher-lying energy levels; the most prominent transition is the "E" band[27] or $^7F_0 \rightarrow {}^5L_6$ transition near 393 nm.[28]‡ However, the

‡   Through the rest of Chapter 1, the energy level term symbols and the wavelengths and oscillator strengths of transitions from the $^7F_0$ ground state to various excited states of europium(III) have been adapted from the experimental data (in wavenumbers) presented by Carnall, Fields, and Rajnak in Table VII of Ref. 28.

dominant excitation mechanism in europium(III) chelates is ligand-to-metal energy transfer (LMET). In this process, the ligands absorb radiant energy to reach an excited singlet state ($S_0 \rightarrow S_1$), undergo intersystem crossing to the lowest triplet state ($S_1 \rightarrow T_1$), transfer energy via intramolecular pathways to relax to the ligand ground state while exciting the Eu^{3+} center (ligand $T_1 \rightarrow S_0$; Eu^{3+} $^7F_0 \rightarrow {}^5D_0$ or higher levels, frequently $^5D_1$). The Eu^{3+} center then undergoes nonradiative decay to the $^5D_0$ emitting level, from which it fluoresces ($^5D_0 \rightarrow {}^7F_{0-4}$).[15, 29] In most of the excitation spectra, particularly those in DMF solution, the europium(III) features become part of the LMET peak.

Throughout this study, it was observed that the species of the ligand was far more important in determining spectral features and overall luminescence intensity than was the tris or tetrakis nature of the chelate. Of the six ligands originally included in the study, btfa⁻ and ttfa⁻ were clearly observed to be the most luminescent in solution, indistinguishable to the eye; ba⁻ and dbm⁻ had lesser but still discernible luminescence; acac⁻ and tfaa⁻ were only faintly luminescent and were therefore not incorporated into sol–gel silica hosts. There are three notable differences between btfa⁻ and ttfa⁻ and the other four ligands: in both btfa⁻ and ttfa⁻, their structures allow conjugation between their R^1 groups and the central three-carbon chain (see Fig. 1-1c); they are highly asymmetric, $R^1 \neq R^2$; and their R^2 groups (CF_3) are highly polar. The R^1 group is nonpolar in btfa⁻ and somewhat polar in ttfa⁻. In contrast, acac⁻ and tfaa⁻ lack conjugation outside the central portion; dbm⁻ is conjugated but symmetric; and ba⁻ is conjugated and asymmetric but lacks a strongly withdrawing R^2 group.

The differences in fluorescence behavior between different complexes and for the same complex in different matrices arise from the complex interaction of a number of factors. Fluorescence requires efficient population of the europium(III) $^5D_0$ emitting level, hence any alteration of the efficiency of population of the $^5D_0$ level via ligand-to-metal energy transfer or of $^5D_0 \rightarrow {}^7F_J$ transition probabilities can have a profound effect upon the observed fluorescence, including changes in absolute intensity and branching ratios. The

energy level structure, particularly conjugation and the location of the T_1 level, and the symmetry properties of the complexed ligand appear to be the most important parameters. Conjugation increases the ligand's overall ability to absorb energy and tends to lower its excited energy levels. The ligand's energy level structure affects the energy transfer rates: if $T_1 < {}^5D_0$ or $T_1 \gg {}^5D_0$, the Eu^{3+} ${}^5D_0$ level will not be efficiently populated and any excitation energy present will tend to dissipate via nonradiative means rather than fluorescence, especially when $T_1 < {}^5D_0$. Sample ligand and metal energy levels are illustrated in Figure 1-2. Ligand energy levels are also much more sensitive to external perturbations than are rare-earth-ion energy levels. Incorporation into a solid-state matrix is accompanied by such factors as physical compression which tend to elevate ligand energy levels; in one case, the value of T_1 in $Eu(ttfa)_3$ powder was increased by 1,800 cm^{-1} upon its incorporation into poly(methyl methacrylate).[30] This effect can be at least partly attributed to pressure-induced physical distortions (*e.g.* twisting) causing a loss of conjugation in the ligand and a concomitant decrease in its ability to absorb energy.

Ligand symmetry directly affects the Eu^{3+} ion's crystal field—highly asymmetric ligands ($R^1 \neq R^2$) promote fluorescence by making Eu^{3+} transitions more allowed (a relaxation of the Laporte rule), increasing transition probabilities. Changes in the Eu^{3+} ion's local environment are most readily observed through changes in the absolute and relative intensities of the E_1 and E_2 emissions. The E_1 emission is a magnetic-dipole (MD) transition, a transition which follows the selection rules (chiefly $\Delta J = \pm 1$) for the absorption or emission of radiation by an oscillating magnetic dipole, and is therefore relatively insensitive to changes in symmetry of the crystal field, which is primarily electrostatic, not magnetic. Changes in E_1 are driven by other factors (*e.g.* changes in the ${}^5D_0$ level's population and quenching). In contrast, the E_2 emission is a forced electric-dipole (ED) transition (which involves the absorption or emission of radiation by an oscillating electric dipole) subject to electrostatic perturbations and therefore very sensitive to changes in the crystal field. Therefore, an absolute increase of the integrated intensity (S) of E_2 and a

relative increase of $S(E_2)$ to $S(E_1)$ (the η_{21} ratio) is correlated to the lowering of symmetry, particularly the removal of inversion symmetry at the Eu^{3+} site, and increased bond strength between Eu^{3+} and its neighbors.[31-32] Values of $S(E_1)$, $S(E_2)$, and η_{21} obtained from the emission spectra described in the following sections are presented in Table 1-1.

Figure 1-2: Energy Level Diagram
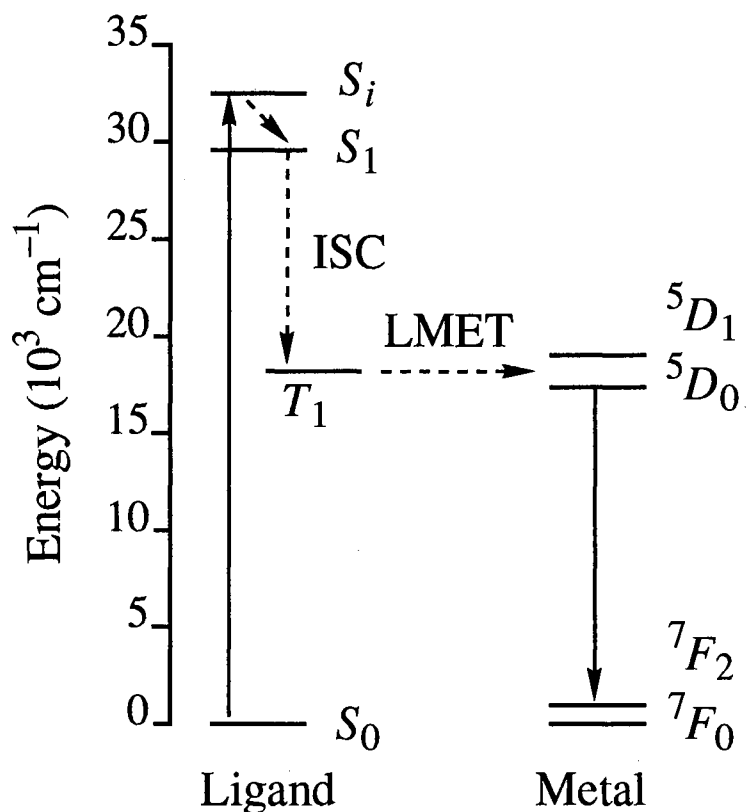
FIGURE 1-2: Energy levels of $Eu(ttfa)_3$ powder (values from Ref. 30). Solid and dashed arrows represent radiative and nonradiative transitions, respectively. For clarity, only two each of the five ^5D and seven ^7F levels of Eu^{3+} are included. Both radiative and nonradiative $ttfa^- \, T_1 \to S_0$ and nonradiative $Eu^{3+} \, ^5D_0 \to {}^7F_J$ transitions may also occur.

TABLE 1-1

A. Eu(ba)$_3$

Medium	$S(E_1)$	$S(E_2)$	η_{21}
DMF	5.70×10^{-3}	1.03×10^{-1}	18.13
Sol	3.46×10^{-4}	1.18×10^{-3}	3.40
Gel 9	3.54×10^{-4}	1.16×10^{-3}	3.26
Gel 25	4.58×10^{-4}	1.52×10^{-3}	3.31
Gel 50	4.92×10^{-4}	1.63×10^{-3}	3.32
Gel 125	7.50×10^{-4}	2.35×10^{-3}	3.13

B. (PipH)[Eu(ba)$_4$]

Medium	$S(E_1)$	$S(E_2)$	η_{21}
DMF	5.01×10^{-3}	9.14×10^{-2}	18.24
Sol	2.42×10^{-4}	9.15×10^{-4}	3.78
Gel 7	3.39×10^{-4}	1.03×10^{-3}	3.04
Gel 25	4.10×10^{-4}	1.34×10^{-3}	3.28
Gel 50	4.72×10^{-4}	1.58×10^{-3}	3.35
Gel 125	5.49×10^{-4}	2.16×10^{-3}	3.93

C. Eu(btfa)$_3$

Medium	$S(E_1)$	$S(E_2)$	η_{21}
Sol	8.73×10^{-4}	1.19×10^{-2}	13.60
Gel 24	5.61×10^{-3}	1.06×10^{-1}	18.88
Gel 43	3.91×10^{-3}	7.66×10^{-2}	19.60

D. (PipH)[Eu(btfa)$_4$]

Medium	$S(E_1)$	$S(E_2)$	η_{21}
DMF	4.48×10^{-2}	8.09×10^{-1}	18.08
Sol	9.77×10^{-4}	1.18×10^{-2}	12.08
Gel 5	1.61×10^{-3}	2.19×10^{-2}	13.59
Gel 25	1.84×10^{-3}	2.49×10^{-2}	13.49
Gel 43	3.70×10^{-3}	5.75×10^{-2}	15.54
Gel 100	5.34×10^{-3}	9.16×10^{-2}	17.17

E. Eu(dbm)$_3$

Medium	$S(E_1)$	$S(E_2)$	η_{21}
DMF	7.46×10^{-4}	1.54×10^{-2}	20.62
Sol	1.60×10^{-4}	5.33×10^{-4}	3.33
Gel 7	1.66×10^{-4}	4.68×10^{-4}	2.83
Gel 20	4.06×10^{-5}	1.22×10^{-4}	3.01
Gel 37	3.29×10^{-5}	1.67×10^{-4}	5.09
Gel 59[a]	3.98×10^{-5}	2.79×10^{-4}	7.00
Gel 121[a]	3.25×10^{-5}	3.54×10^{-4}	10.89

TABLE 1-1 (Continued)

F. (PipH)[Eu(dbm)₄]

Medium	$S(E_1)$	$S(E_2)$	η_{21}
DMF	8.21×10^{-4}	1.73×10^{-2}	21.06
Sol	1.56×10^{-4}	4.90×10^{-4}	3.13
Gel 6	1.38×10^{-4}	4.17×10^{-4}	3.03
Gel 20	1.70×10^{-5}	7.57×10^{-5}	4.46
Gel 35[a]	2.29×10^{-5}	2.39×10^{-4}	10.43
Gel 59[a]	3.65×10^{-5}	3.91×10^{-4}	10.72
Gel 111[a]	5.46×10^{-5}	9.14×10^{-4}	16.75

G. Eu(ttfa)₃

Medium	$S(E_1)$	$S(E_2)$	η_{21}
DMF	4.04×10^{-3}	6.05×10^{-2}	15.01
Sol	8.20×10^{-4}	9.80×10^{-3}	11.95
Gel 8	9.80×10^{-4}	1.13×10^{-2}	11.52
Gel 25	1.27×10^{-3}	1.71×10^{-2}	13.46
Gel 43	2.79×10^{-3}	4.32×10^{-2}	15.51
Gel 100	6.65×10^{-3}	1.14×10^{-1}	17.18

H. (PipH)[Eu(ttfa)₄]

Medium	$S(E_1)$	$S(E_2)$	η_{21}
DMF	2.77×10^{-2}	4.73×10^{-1}	17.10
Sol	9.23×10^{-4}	1.24×10^{-2}	13.46
Gel 24	1.15×10^{-2}	2.15×10^{-1}	18.72
Gel 43	9.71×10^{-3}	1.91×10^{-1}	19.71
Gel 114	5.21×10^{-2}	1.00×10^{-0}	19.19

TABLE 1-1: Integrated emission intensities (S) for the $^5D_0 \rightarrow {}^7F_{1-2}$ (E_{1-2}) fluorescence emissions of europium(III) chelates in DMF solution and sol–gel silica hosts, normalized to $S(E_2)$ of (PipH)[Eu(ttfa)₄] in silica xerogel, the highest value observed; and their $E_2{:}E_1$ intensity ratios, $\eta_{21} \equiv S(E_2)/S(E_1)$. Those values for Eu(dbm)$_x$ marked "a" apply to the red-shifted (top) spectrum in Figures 1-11 and 1-13. The reader should refer back to this Table for subsequent references to values of S or η_{21} in this Chapter.

One external interaction is the quenching of europium(III) fluorescence by multi-phonon absorptions in hydroxyl-containing species, which are theoretically completely absent in DMF solution but which are present as water, alcohols, and silanols in silica gels; even in xerogels they are still present albeit in reduced numbers. However, ligands which promote the Eu^{3+} transition probabilities can reduce quenching by decreasing the time available for multiphonon events.

A.   *Tris(1-phenyl-1,3-butanedionato-O,O′)europium(III), Eu(ba)₃, Figures 1-3 and 1-4*

From Figure 1-3, it may be observed that the emission behavior of Eu(ba)$_3$ is significantly quenched in sol–gel silica relative to DMF solution, requiring the use of a large scaling factor for the DMF-solution spectrum. The main differences between the DMF spectrum and all six silica spectra appear to arise from the diminution of the highest-energy portion of the E_2 peak (610 nm) relative to the other features, which leads to a huge drop in η_{21} upon going from DMF to silica; such a drop is consistent with a significant increase in Eu^{3+} site symmetry. Because both R groups of ba$^-$ are hydrophobic, this effect may be due to a decrease in repulsive interactions upon going from DMF, an extremely polar solvent, to the less polar silica environment, which could allow the complex to relax into a more symmetric configuration. It can be noted that more hydrophilic ligands (*e.g.* btfa$^-$) behave much differently.

All five silica spectra in Figure 1-3 show a remarkable consistency in the shape and position of the spectral features, with no significant changes in the branching ratios. The only change is a gradual increase in total intensity, in which the emission maxima increase from 0.6 to 1.0 units as the silica gel ages. This increase is significantly less than the projected fivefold increase in concentration; the complex therefore does not appear to obey the Beer–Lambert Law (BLL), which states that intensity should be directly proportional to concentration, at least not in this region of concentration. Such behavior is consistent with the onset of quenching behavior, in this case probably via dopant intermolecular energy transfer, as concentration increases.

13

In Figure 1-4, the excitation spectra show substantive luminescence change upon going from DMF solution to sol–gel silica. The smooth curve in the DMF spectrum is fairly typical of europium(III) β-diketonate behavior in that all the Eu^{3+} features become part of the LMET peak, in this case centered near 383 nm. It should be noted that there are no transitions from the Eu^{3+} $^{7}F_{0}$ ground state to energy levels corresponding to this wavelength; the nearest are to the $^{5}L_{6}$ near 393 nm and the much weaker $^{5}G_{4-6}$ set near 375 nm. The band must therefore be almost completely LMET in character.

The silica spectra are all very similar to one another, varying only in intensity; a new feature near 393 nm dominates the 383-nm peak and a shoulder peak centered near 375 nm. While the 393- and 375-nm features do correspond to europium(III) ground-state transitions (to the $^{5}L_{6}$ and $^{5}G_{4-6}$ levels, respectively), they are significantly broader than the Eu^{3+} absorption peaks and should therefore contain a substantial amount of LMET character. These peak energies and their differences from the DMF spectrum may be interpreted as a quenching of fluorescence emission from those excitation energies which do not completely overlap a receptor level in the Eu^{3+} center. As in the emission spectra (Fig. 1-3), the observed increase in excitation intensity less than that expected for BLL behavior, probably due to the onset of intermolecular quenching effects.

Figure 1-3: Eu(ba)$_3$, 10^{-3} M, Emission Spectra
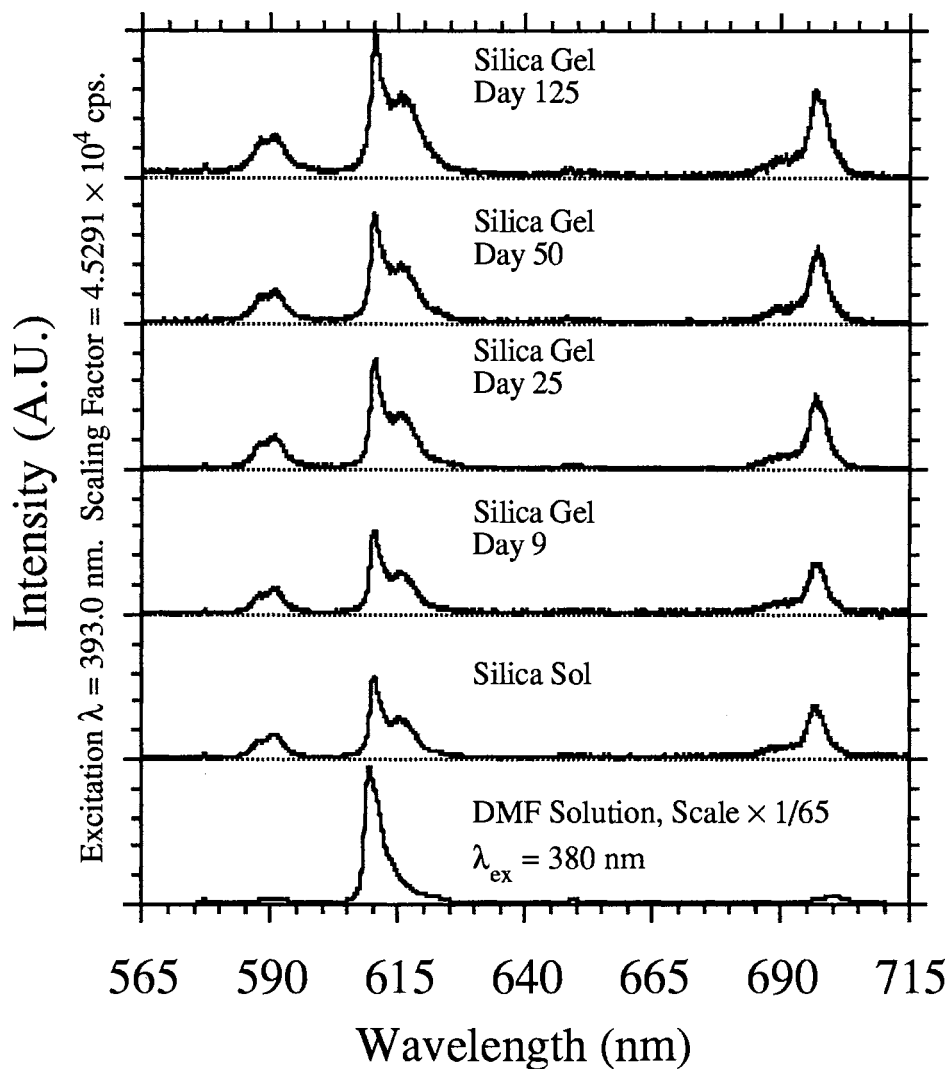
FIGURE 1-3: Emission spectra for Eu(ba)$_3$ in DMF solution and sol–gel silica. The given scaling factor is that of the silica gel day 125 spectrum in photon counts per second (cps), an instrument-dependent parameter removed by normalization. The DMF solution spectrum has been divided by 65 and has a different excitation wavelength (λ_{ex}).

Figure 1-4: Eu(ba)$_3$, 10^{-3} M, Excitation Spectra

FIGURE 1-4: Excitation spectra for Eu(ba)$_3$ in DMF solution and sol–gel silica. The given scaling factor is that of the silica gel day 125 spectrum. The DMF solution spectrum has been divided by 60 and has a slightly different emission wavelength (λ_{em}).

B. *Piperidinium Tetrakis(1-phenyl-1,3-butanedionato-O,O')europate(III), (PipH)-[Eu(ba)₄], Figures 1-5 and 1-6*

As is the case for Eu(ba)$_3$ (Fig. 1-3), the emission behavior of (PipH)[Eu(ba)$_4$] (Fig. 1-5) is significantly quenched in sol–gel silica relative to DMF solution, although somewhat less so than Eu(ba)$_3$. The same large decrease in η_{21} observed for Eu(ba)$_3$ is also observed for (PipH)[Eu(ba)$_4$], presumably for the same reason, a large increase in Eu^{3+} local site symmetry. Once more, the main differences between the DMF spectrum and all five silica spectra appear to arise from the diminution of the highest-energy portion of the E_2 peak (610 nm) relative to the other features. The most notable difference from the DMF spectrum of Eu(ba)$_3$ is that at least two lower-energy features in the E_2 transition are much more prominent in the (PipH)[Eu(ba)$_4$] DMF spectrum. Such an increase in the splitting of the $2J + 1 = 5$ Stark components of the E_2 peak is consistent with a decrease in local site symmetry in (PipH)[Eu(ba)$_4$] relative to Eu(ba)$_3$.

As before, the six silica spectra have consistent spectral features with no significant changes in their branching ratios while showing a gradual increase in total intensity, in which the emission maxima increase from 0.5 to 1.0 units, again at a significantly lower rate than BLL behavior consistent with the onset of intermolecular quenching forces.

The (PipH)[Eu(ba)$_4$] excitation spectra (Fig. 1-6) show nearly identical behavior to those of Eu(ba)$_3$ (Fig. 1-4), indicating that the same factors discussed previously are still in operation.

Figure 1-5: (PipH)[Eu(ba)$_4$], 10^{-3} M, Emission Spectra

FIGURE 1-5: Emission spectra for (PipH)[Eu(ba)4] in DMF solution and sol–gel silica. The given scaling factor is that of the silica gel day 125 spectrum. The DMF solution spectrum has been divided by 45 and has a different λ_{ex}.

Figure 1-6: (PipH)[Eu(ba)$_4$], 10^{-3} M, Excitation Spectra

FIGURE 1-6: Excitation spectra for (PipH)[Eu(ba)$_4$] in DMF solution and sol–gel silica. The given scaling factor is that of the silica gel day 125 spectrum. The DMF solution spectrum has been divided by 45 and has a slightly different λ_{em}.

19

C.   Tris(4,4,4-trifluoro-1-phenyl-1,3-butanedionato-O,O')europium(III), Eu(btfa)₃, Figures 1-7 and 1-8

The emission spectra of Eu(btfa)$_3$ (Fig. 1-7) show a much larger increase in intensity with aging of the silica host than do the Eu(ba)$_x$ (x = 3, 4) spectra. In fact, the emission maximum increases by a factor of about 17, much greater than the factor of 5 expected for BLL behavior; it is therefore likely to arise from reduced quenching interactions as the solvents evaporate. This trend is the opposite of that observed in Eu(ba)$_x$ and points to a significant difference in the way in which the dopant–matrix interactions affect intermolecular quenching processes. As noted earlier, the main difference between Eu(ba)$_x$ and Eu(btfa)$_x$ is the much greater polarity of the latter; because silica is a polar matrix, it may be hypothesized that in such an environment the relatively nonpolar Eu(ba)$_x$ molecules will tend to aggregate, leading to intermolecular quenching, whereas Eu(btfa)$_x$ will not. This process would make intermolecular quenching relatively insignificant in Eu(btfa)$_x$ while solvent quenching diminishes with solvent evaporation, leading to an increase in fluorescence intensity higher than that expected for an increase in concentration.

The most notable spectral change other than intensity occurs in the high- (609 and 611 nm) and low-energy (616 nm) portions of the E_2 band, in which the branching ratio changes from favoring the 616-nm peak in the sol to the 609- and 611-nm peaks in the gel, indicative of changes in local-site symmetry as the silica cage forms and contracts.

The excitation spectra (Fig. 1-8) show that the wavelength of maximum excitation ($\lambda_{ex\text{-}max}$) has shifted by more than 10 nm to lower energies, a bathochromic shift. This is most likely due to a lowering of the complex's S_1 energy level induced by environmental changes (*e.g.* polarity, compression) accompanying solvent evaporation. In the two gel spectra, all the Eu^{3+} features have been completely incorporated into the LMET peak, but in the sol spectrum, a shoulder is visible at 393 nm which indicates some direct excitation of the Eu^{3+} $^5L_6$ level.

20

Figure 1-7: Eu(btfa)$_3$, 10^{-3} M, Emission Spectra
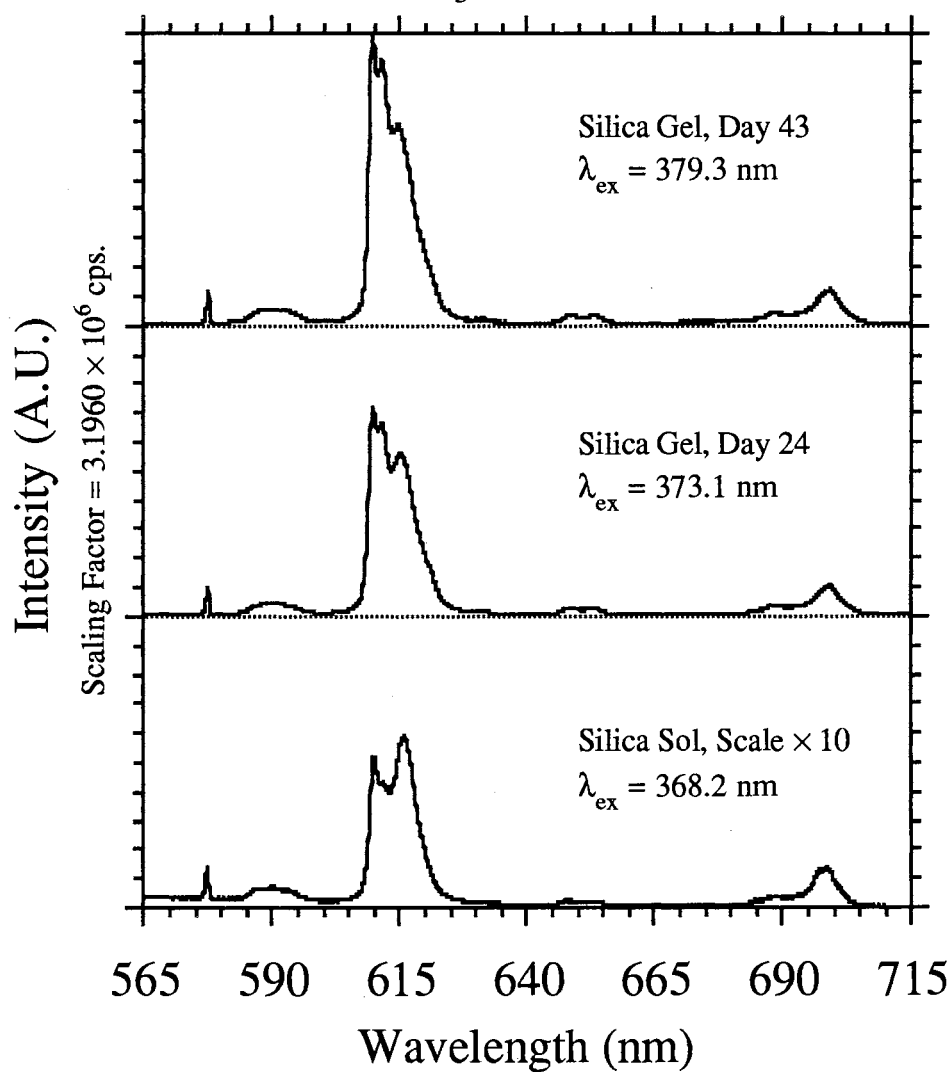
FIGURE 1-7: Emission spectra for Eu(btfa)$_3$ in sol–gel silica. The given scaling factor is that of the silica gel day 43 spectrum. The silica sol spectrum has been multiplied by 10 for clarity. Each spectrum has a different λ_{ex} due to the change in $\lambda_{ex\text{-}max}$ (see Fig. 1-8). A DMF solution spectrum was not available.

Figure 1-8: Eu(btfa)$_3$, 10^{-3} M, Excitation Spectra

y-axis: Intensity (A.U.)

y-axis (inner label): Emission λ = 609.9 nm. Scaling Factor = 1.3812×10^6 cps.

Silica Gel
Day 43

Silica Gel
Day 24

Silica Sol, Scale $\times$ 10
λ_{em} = 616.1 nm

x-axis: Wavelength (nm)

330   350   370   390   410   430
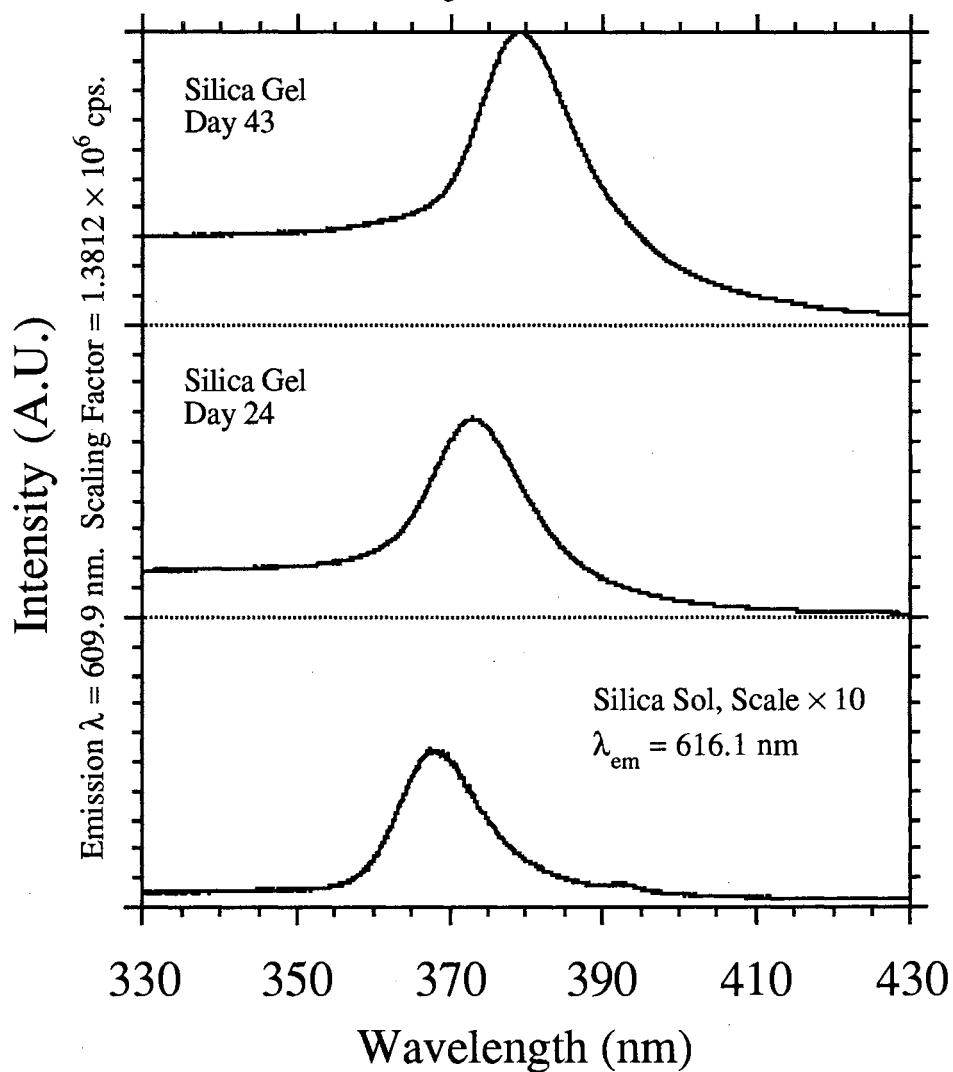
FIGURE 1-8: Excitation spectra for Eu(btfa)$_3$ in sol–gel silica. The given scaling factor is that of the silica gel day 43 spectrum. The silica sol spectrum has been multiplied by 10 for clarity and has a different λ_{em}.

D.   *Piperidinium Tetrakis(4,4,4-trifluoro-1-phenyl-1,3-butanedionato-O,O')europate-*
       (III), (PipH)[Eu(btfa)₄], Figures 1-9 and 1-10

While the emission of (PipH)[Eu(btfa)$_4$] in sol–gel silica is quenched relative to

DMF solution, the quenching is significantly less severe than for the Eu(ba)$_x$ and the

overall intensities are quite high, almost two orders of magnitude higher than in Eu(ba)$_x$.

Because of the similarity of ba$^-$ and btfa$^-$ ligands, changes in behavior must arise from the

substitution of CF$_3$ for CH$_3$ at the R^2 position; the CF$_3$ group is both electron-withdrawing

(affecting resonance, hence the ligand energy levels) and polar (affecting solvent inter-

actions).   In DMF, $S(E_1)$ for (PipH)[Eu(btfa)$_4$] is a decade higher than that of

(PipH)[Eu(ba)$_4$], indicating much more efficient LMET. As in Eu(ba)$_x$, however, the dif-

ferences between the DMF and silica spectra are due to a reduced contribution from the

610-nm feature of the E_2 peak relative to the other features; in all the spectra, the E_2 peak

completely dominates the other four. As the silica ages from sol to xerogel, the E_2 Stark

splitting gradually changes to favor the 610-nm feature associated with decreasing

symmetry.

For this compound, the intensity change of the emission maxima with aging is

much closer to the fivefold increase predicted by the BLL than the preceding compounds.

If this increase were purely due to BLL behavior, however, there should be no change in

the branching ratios or Stark splitting. While the change in the E_2 peak shape is small, it is

nevertheless present; therefore, small changes in the molecular environment are present

which cannot be accounted for solely by the BLL. Such changes in the molecular envi-

ronment should be expected to occur with the removal of solvent species.

In Figure 1-10, the silica excitation spectra show a gradual shift to longer wave-

lengths during the aging process until the $\lambda_{ex\text{-}max}$ of the "Day 100" spectrum is within 5 nm

of the peak associated with the DMF spectrum, indicating a return to a more similar envi-

ronment (*e.g.* containing fewer hydroxyl species) as solvents evaporate. However, this

bathochromic shift in $\lambda_{ex\text{-}max}$ for (PipH)[Eu(btfa)$_4$] in silica is not as large as that for

Eu(btfa)$_3$. All the Eu^{3+} transitions are completely incorporated into the LMET band. The major difference between the DMF and silica spectra is the appearance in the silica spectra, particularly in "Day 100," of an excitation "plateau" at energies higher than that of $\lambda_{ex\text{-}max}$, indicating that excitation of the Eu^{3+} $^5D_0$ level retains efficiency throughout this regime, whereas the excitation coupling in DMF solution is centered within the 360–400-nm region. Certain nonradiative decay pathways present in DMF solution must be diminished in silica xerogel; encapsulation of the dopant molecules within the silica network may reduce the amount of nonradiative intermolecular ligand–ligand interactions possible in the liquid phase.

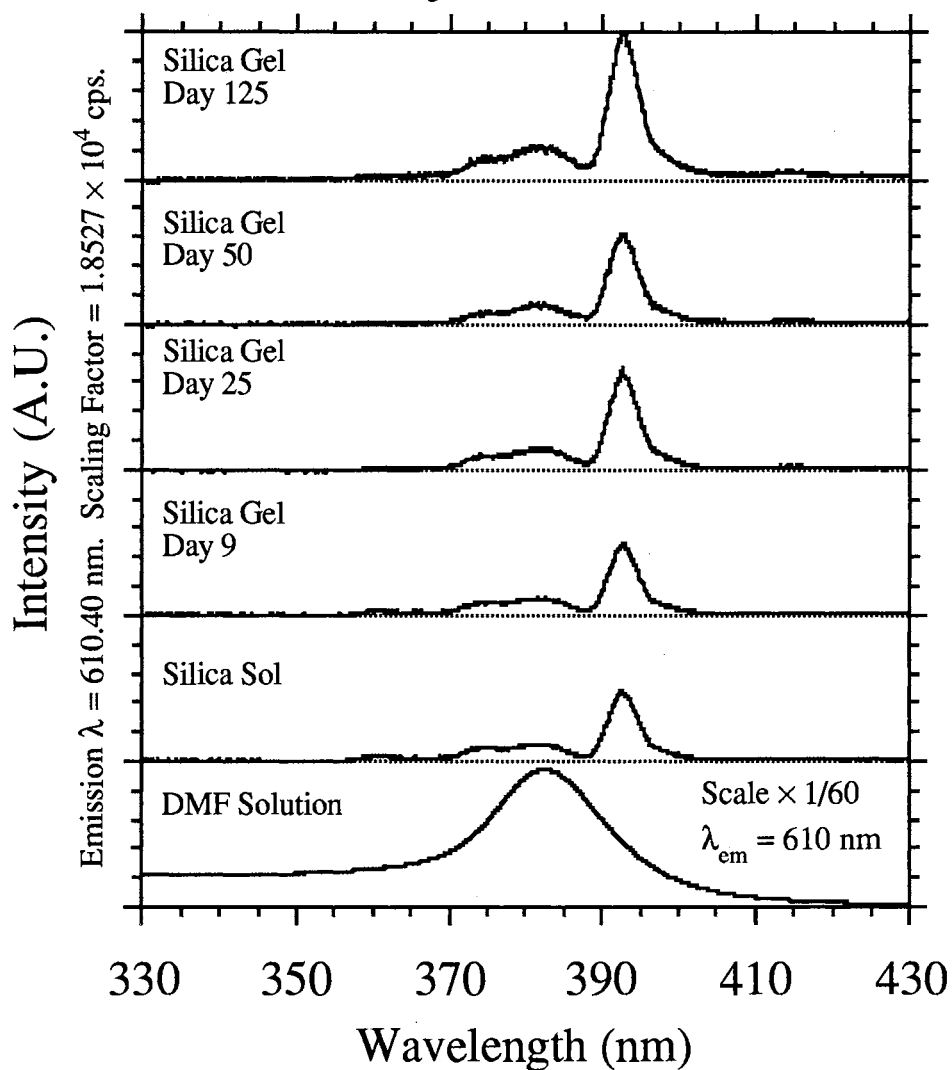# Figure 1-9: (PipH)[Eu(btfa)$_4$], 10^{-3} M, Emission Spectra

FIGURE 1-9: Emission spectra for (PipH)[Eu(btfa)$_4$] in DMF solution and sol–gel silica. The given scaling factor is that of the silica gel day 100 spectrum. The DMF solution spectrum has been divided by 12. Each spectrum has a different λ_{ex} due to the change in λ_{ex-max} (see Fig. 1-10).

Figure 1-10: (PipH)[Eu(btfa)$_4$], 10^{-3} M, Excitation Spectra

FIGURE 1-10: Excitation spectra for (PipH)[Eu(btfa)$_4$] in DMF solution and sol–gel silica. The given scaling factor is that of the silica gel day 100 spectrum. The DMF solution spectrum has been multiplied by 2/3 and has a slightly different λ_{em}.

E.   Tris(1,3-diphenyl-1,3-propanedionato-O,O')europium(III),   Eu(dbm)₃,   Figures 1-11 and 1-12

From Figures 1-11 for Eu(dbm)₃ and 1-13 for (PipH)[Eu(dbm)₄], it may be observed that these Eu(dbm)$_x$ complexes undergo severe quenching in drier silica gels relative to DMF solution or even silica sol, whereas the previously discussed Eu(ba)$_x$ and Eu(btfa)$_x$ complexes are most quenched in the sol and recover luminescence intensity during the drying process. In fact, the Eu(dbm)$_x$ complexes, particularly Eu(dbm)₃, suffer the most severe quenching of all the complexes in this study. As before, the E_2 band in the DMF spectrum is dominant relative to the other transitions; in this case, it has four clearly resolved components (at 609, 611, 615, and 623 nm) in contrast to two components in all the silica spectra (at 610 and 616 nm).

The excitation spectra (Fig. 1-12) show a possible cause for the intriguing fall and rise of the emission spectrum as the silica host ages. There is a clear difference in the nature of the excitation coupling in DMF solution and in silica sol, because $\lambda_{ex\text{-}max}$ undergoes a 20-nm hypsochromic shift from DMF (415 nm) to silica sol (395 nm) and is two decades less intense. As there are no Eu^{3+} transitions between 393 and 464 nm, the excitation band in DMF must be due to LMET; as for Eu(ba)$_x$ in silica, the 393-nm excitation peak in the sol and "Day 7" spectra does correspond to a Eu^{3+} transition. It may be observed that as the silica gel dries, the 393-nm component decreases relative to a broad new band centered near 405 nm, which approaches the value in DMF and probably arises from a matrix-induced lowering of the ligand's S_1 energy level.
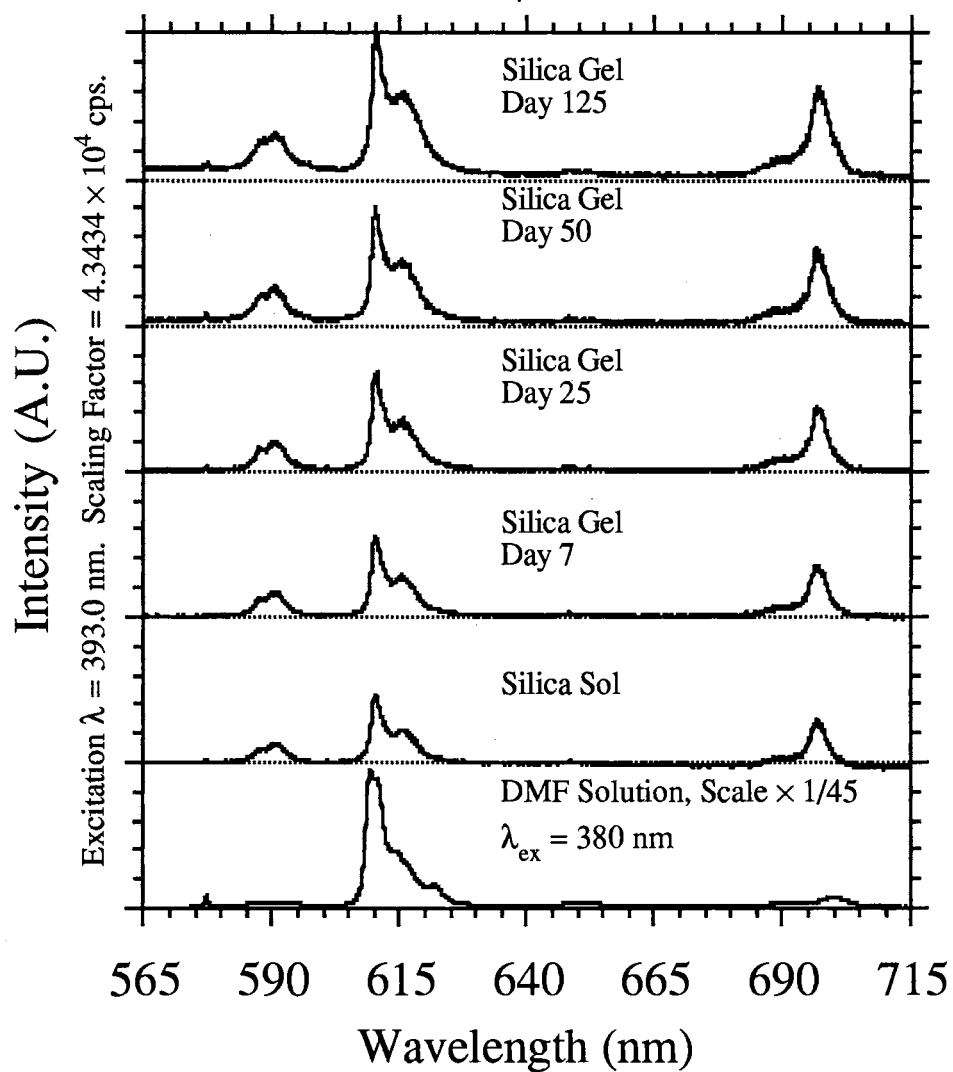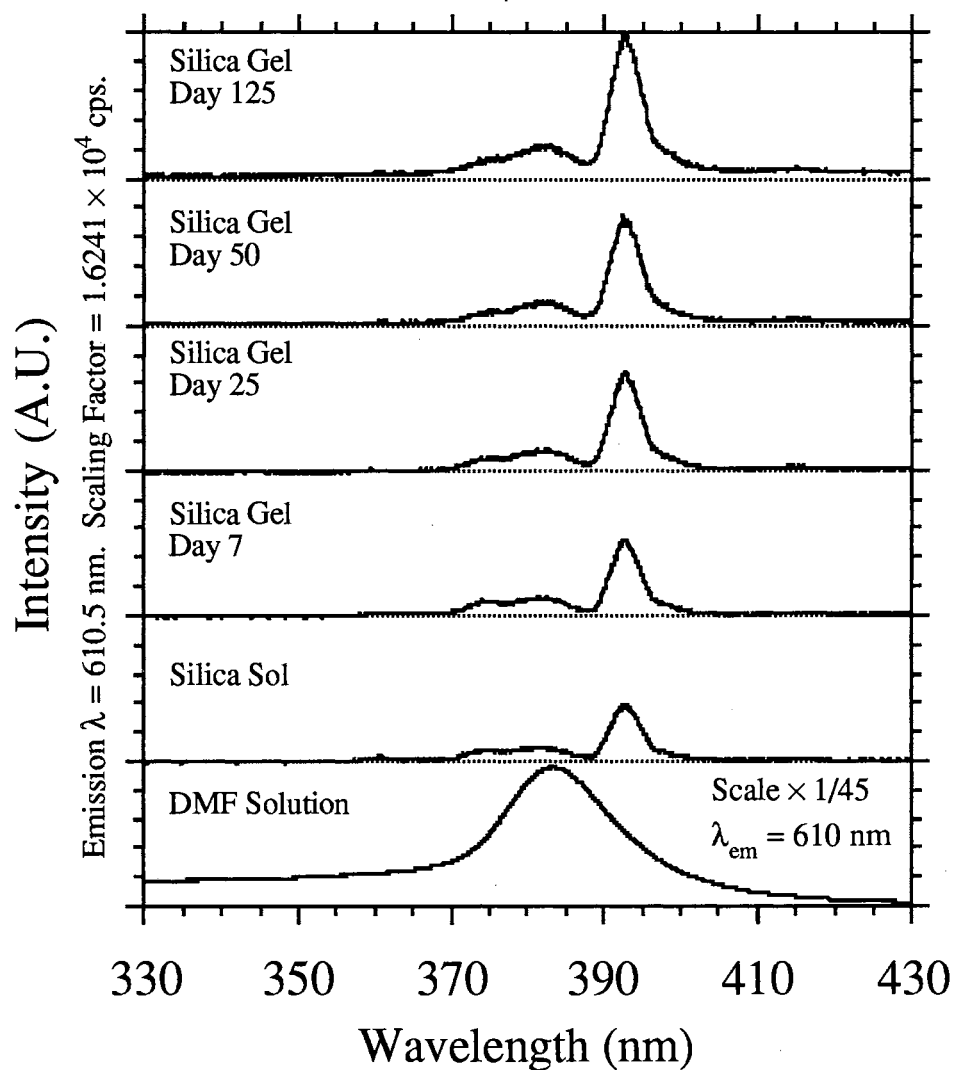
Figure 1-11: Eu(dbm)$_3$, 10^{-3} M, Emission Spectra
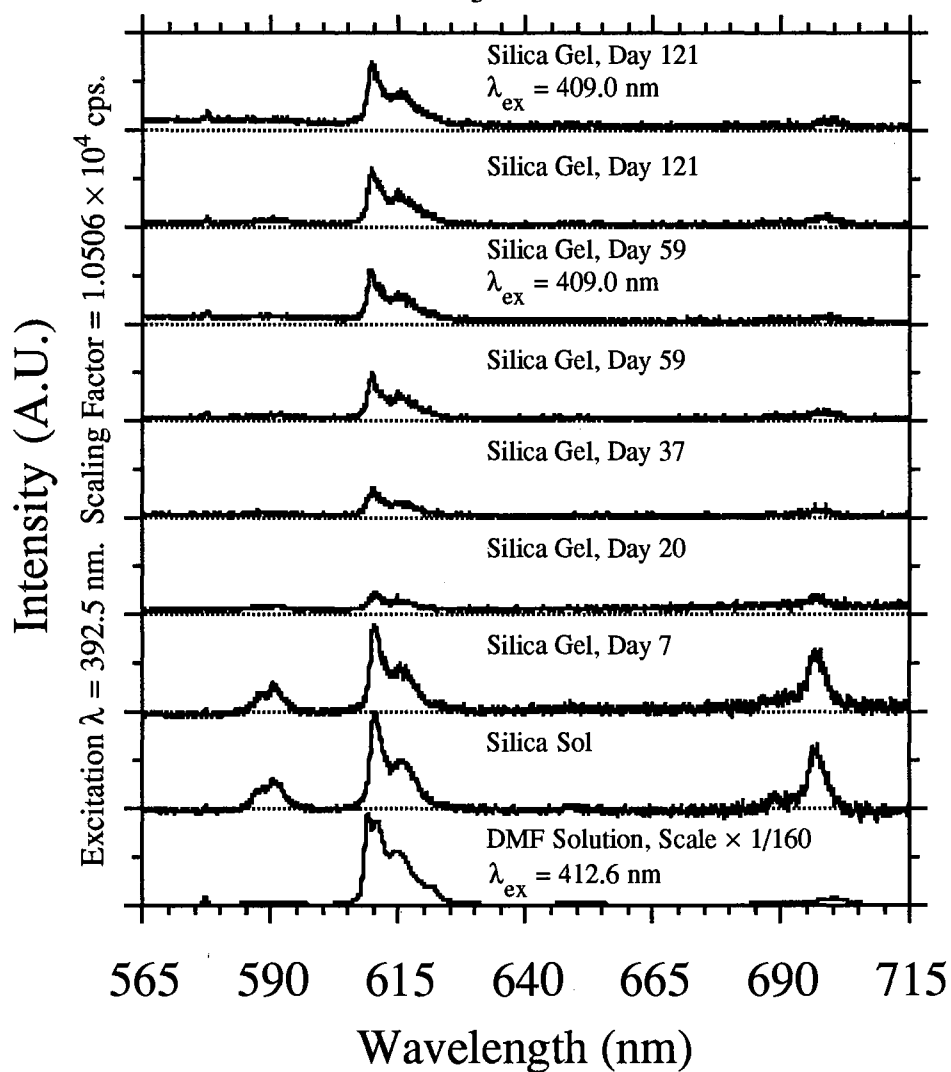
FIGURE 1-11: Emission spectra for Eu(dbm)$_3$ in DMF solution and sol–gel silica. The given scaling factor is that of the silica sol spectrum. The DMF solution spectrum has been divided by 160 and has a significantly different λ_{ex}. Two spectra each are presented for days 59 and 121 to illustrate the red-shift in $\lambda_{ex\text{-}max}$.

Figure 1-12: Eu(dbm)$_3$, 10^{-3} M, Excitation Spectra

FIGURE 1-12: Excitation spectra for Eu(dbm)$_3$ in DMF solution and sol–gel silica. The given scaling factor is that of the silica sol spectrum. The DMF solution spectrum has been divided by 180 and has a slightly different λ_{em}.

F.   *Piperidinium Tetrakis(1,3-diphenyl-1,3-propanedionato-O,O')europate(III), (PipH)[Eu(dbm)4], Figures 1-13–1-14*

Both emission (Fig. 1-13) and excitation spectra (Fig. 1-14) of (PipH)[Eu(dbm)$_4$] are very similar to those of Eu(dbm)$_3$ (Figs. 1-11 and 1-12), indicating that the same type of physical and chemical interactions are present in both systems. The emission spectra show the same change in Stark splittings, going from a four-component E_2 band in DMF solution to a two-component band in silica, indicative of an increase in site symmetry. In this case, however, a xerogel spectrum ("Day 111, λ_{ex} = 406.0 nm") has a greater maximum emission intensity than the sol spectrum, probably indicating a slightly decreased tendency of the charged tetrakis species to aggregate. The excitation spectra show the same 20-nm shift from DMF to silica sol and a similar drop in intensity. The quenching of the 393-nm component relative to a broad band at 405 nm as the silica host dries is also consistent with the behavior observed for Eu(dbm)$_3$.

Figure 1-13: (PipH)[Eu(dbm)$_4$], 10^{-3} M, Emission Spectra

FIGURE 1-13: Emission spectra for (PipH)[Eu(dbm)4] in DMF solution and sol–gel silica. The given scaling factor is that of the second silica gel day 111 spectrum, λ_{ex} = 406.0 nm. The DMF solution spectrum has been divided by 125 and has a significantly different λ_{ex}. Two spectra each are presented for days 35, 59, and 111 to illustrate the red-shift in $\lambda_{ex\text{-}max}$.

Figure 1-14: $(PipH)[Eu(dbm)_4]$, 10^{-3} M, Excitation Spectra
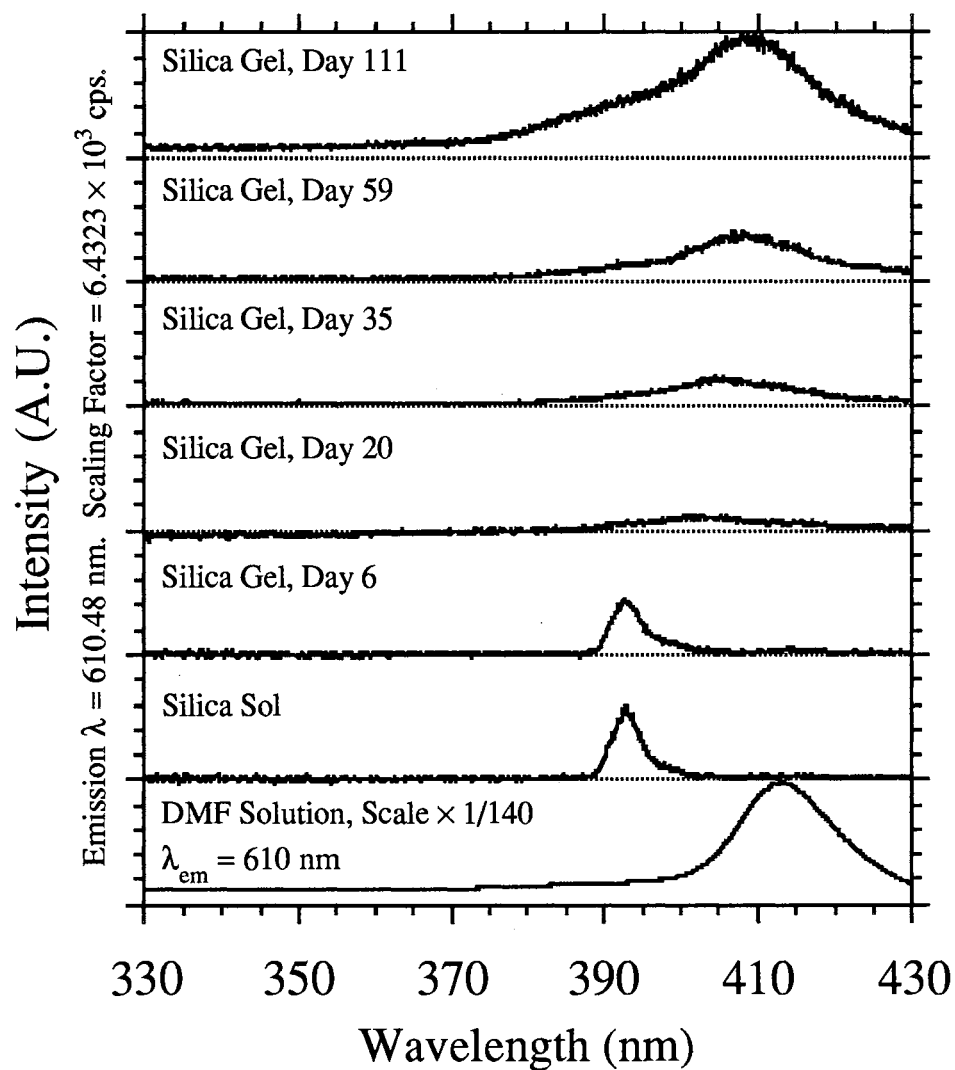
FIGURE 1-14: Excitation spectra for $(PipH)[Eu(dbm)_4]$ in DMF solution and sol–gel silica. The given scaling factor is that of the silica gel day 111 spectrum. The DMF solution spectrum has been divided by 140 and has a slightly different λ_{em}.

G.   Tris(4,4,4-trifluoro-1-(2'-thienyl)-1,3-butanedionato-O,O')europium(III), Eu(ttfa)₃, Figures 1-15 and 1-16

As for the $Eu(btfa)_x$ compounds, the $Eu(ttfa)_x$ compounds are highly luminescent in solution and retain much of their luminescence intensity in sol–gel silica. Once more, the differences between the DMF and silica spectra of $Eu(ttfa)_3$ are due to a reduced contribution from the higher-energy features of the E_2 peak, which dominates the other spectral features. Its solution spectrum is somewhat different in that the 612-nm peak is more intense than the 610-nm peak, but in silica this line shape reverts to that observed in the previous compounds.

The intensity of the $Eu(ttfa)_3$ emission maxima in silica xerogel is nearly 20 times greater than that in the sol, a significantly larger increase than that predicted by BLL behavior. In that regard, the behavior of $Eu(ttfa)_3$ is very similar to that of $Eu(btfa)_3$ and is probably also due to a reduction in quenching forces accompanying solvent evaporation. As discussed earlier, when the opposite trend occurs, $i.e.$ in $Eu(ba)_x$, this reduction in solvent quenching is probably outweighed by intermolecular quenching forces introduced by dopant aggregation.

As observed for $Eu(btfa)_3$, the silica excitation spectra of $Eu(ttfa)_3$ exhibit a bathochromic shift during aging process until the $\lambda_{ex\text{-}max}$ of the day 100 spectrum is nearly equal that of the DMF spectrum. While it is likely, judging from the smooth, broad character of the excitation peak in DMF and the older gels, that the excitation arises from LMET, the peaks' location in the 390–395-nm region shows a probable coupling with the europium(III) $^5L_6$ level. The excitation "plateau" at $\lambda < \lambda_{ex\text{-}max}$ observed for $(PipH)[Eu(btfa)_4]$ in silica is also present in $Eu(ttfa)_3$, but for the former it was not present in the DMF spectrum, whereas it does appear in the DMF spectrum and all the silica spectra of the latter compound. For $Eu(ttfa)_3$, therefore, at least a few energy migration pathways to the Eu^{3+} $^5D_0$ level are available at energies greater than the resonance level. In fact, by day 100 the plateau is nearly as efficient in exciting the E_2 emission as is $\lambda_{ex\text{-}max}$.

Figure 1-15: $Eu(ttfa)_3$, 10^{-3} M, Emission Spectra

Silica Gel, Day 100
$\lambda_{ex} = 389.9$ nm

Silica Gel, Day 43
$\lambda_{ex} = 390.0$ nm

Silica Gel, Day 25
$\lambda_{ex} = 386.5$ nm

Silica Gel, Day 8, Scale × 10
$\lambda_{ex} = 380.2$ nm

Silica Sol, Scale × 10
$\lambda_{ex} = 375.4$ nm

DMF Solution, Scale × 5/8
$\lambda_{ex} = 390.6$ nm

Intensity (A.U.)

Scaling Factor = 3.4524×10^6 cps.

565   590   615   640   665   690   715

Wavelength (nm)
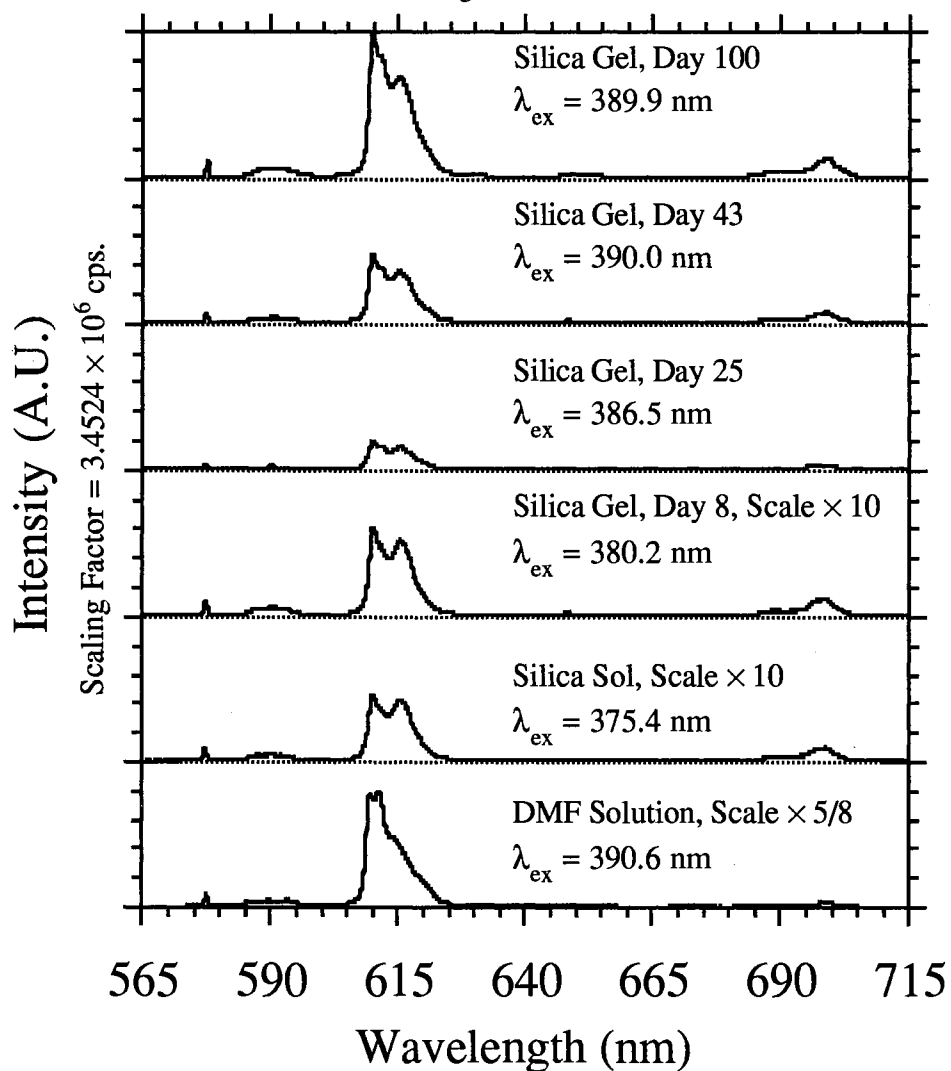
FIGURE 1-15: Emission spectra for $Eu(ttfa)_3$ in DMF solution and sol–gel silica. The given scaling factor is that of the silica gel day 100 spectrum. The DMF solution spectrum has been multiplied by 5/8. The silica sol and gel day 8 spectra have been multiplied by 10 for clarity. Each spectrum has a different λ_{ex} due to the change in $\lambda_{ex\text{-}max}$ (see Fig. 1-16).

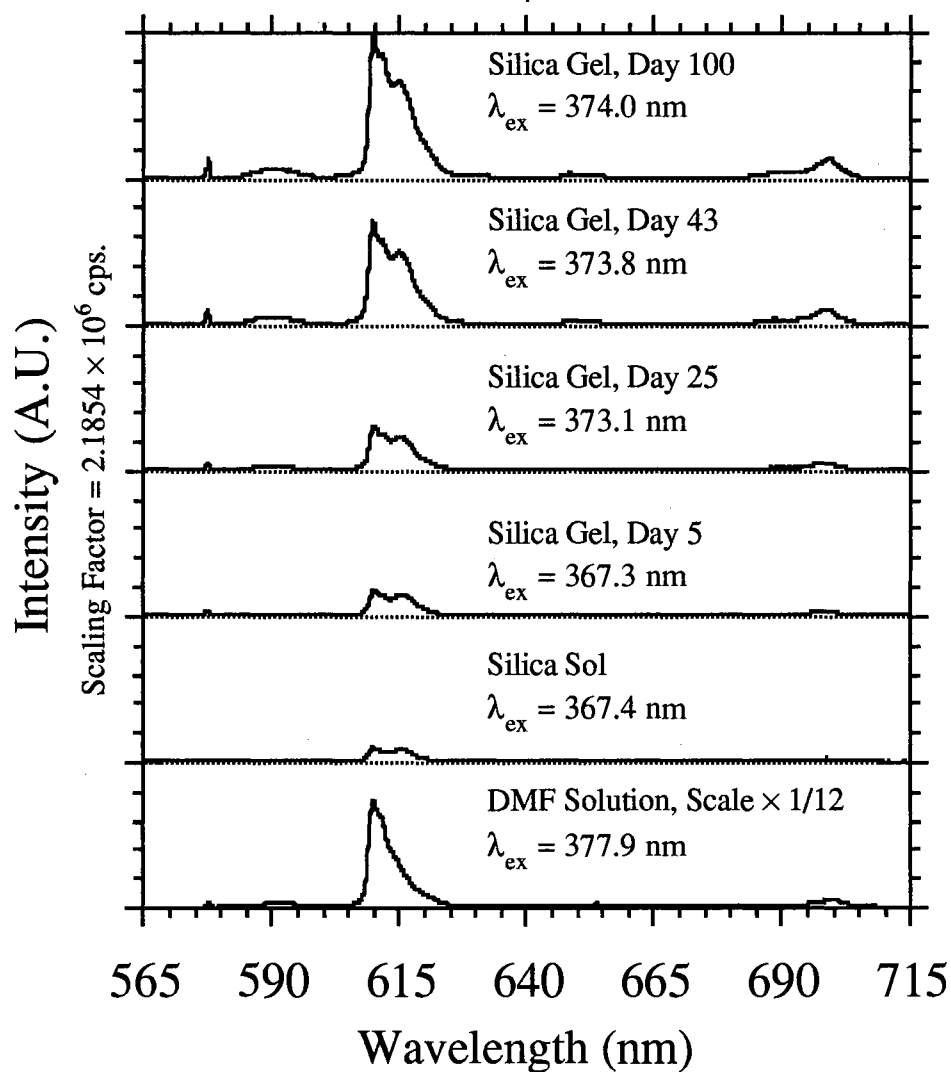# Figure 1-16: $Eu(ttfa)_3$, 10^{-3} M, Excitation Spectra
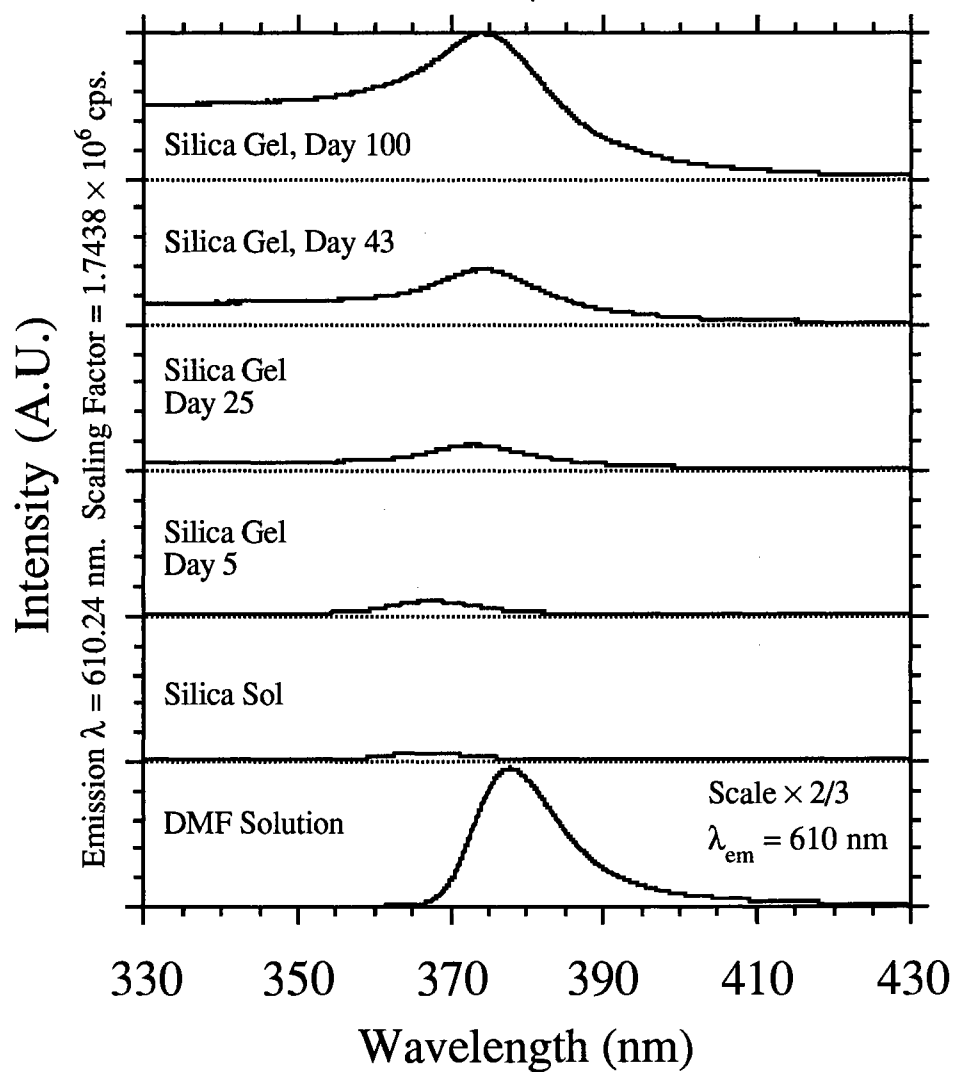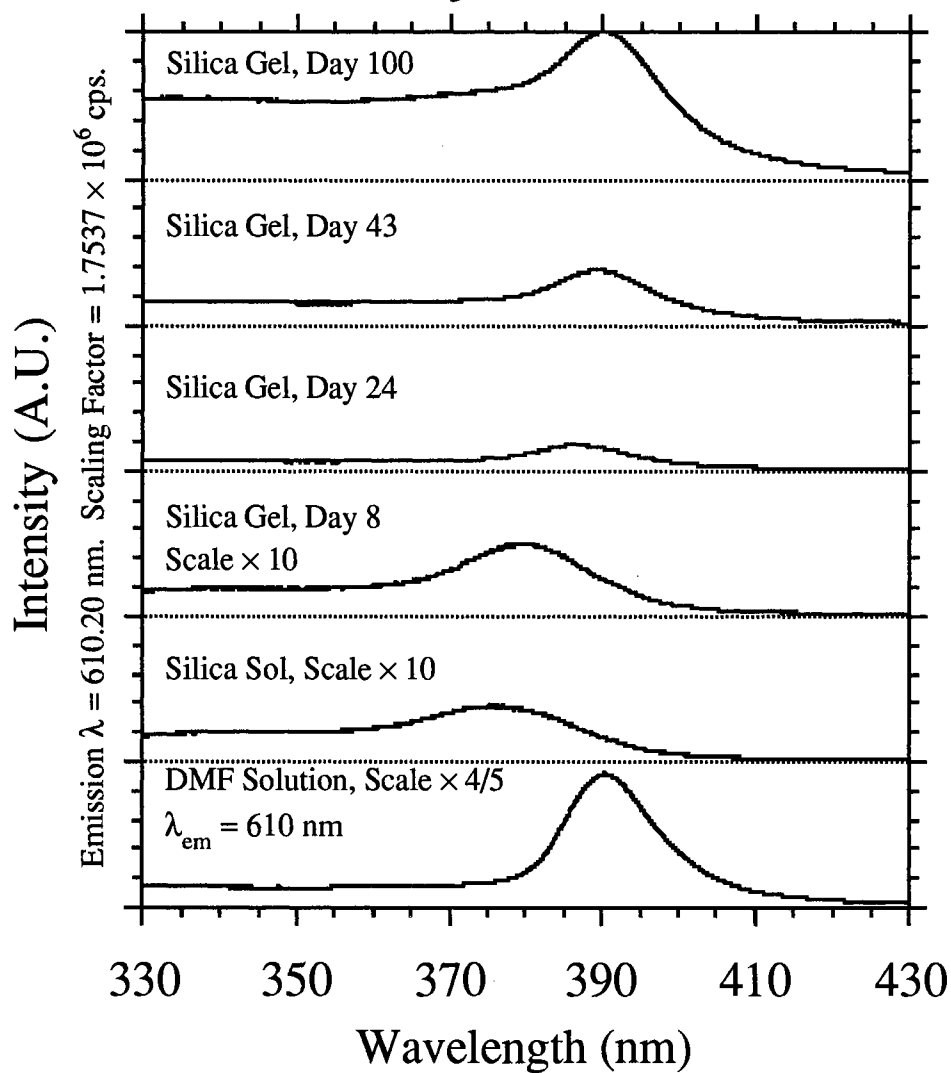

FIGURE 1-16: Excitation spectra for $Eu(ttfa)_3$ in DMF solution and sol–gel silica. The given scaling factor is that of the silica gel day 100 spectrum. The DMF solution spectrum has been multiplied by 4/5 and has a slightly different λ_{em}.

H.   Piperidinium Tetrakis(4,4,4-trifluoro-1-(2'-thienyl)-1,3-butanedionato-O,O')europate(III), (PipH)[Eu(ttfa)₄], Figures 1-17–1-18

The emission (Fig. 1-17) spectra of (PipH)[Eu(ttfa)$_4$] are very similar to those of Eu(ttfa)$_3$ (Fig. 1-15). A very similar branching-ratio change occurs on going from DMF solution to silica, including the prominence of the 612-nm E_2 component in DMF, but for (PipH)[Eu(ttfa)$_4$] the 616-nm component becomes more intense than the higher-energy components in silica sol. Its increase in maximum emission intensity from sol to xerogel is even greater than that of Eu(ttfa)$_3$ at 25, indicating that either (PipH)[Eu(ttfa)$_4$] is more subject to solvent quenching than Eu(ttfa)$_3$ or that its dopant–matrix interactions are more conducive to fluorescence enhancement (*i.e.* induce greater asymmetry) than those of Eu(ttfa)$_3$. The observation of more prominent E_2 Stark splitting in (PipH)[Eu(ttfa)$_4$] indicates that the latter effect is probably the more important.

The excitation spectra of the Eu(ttfa)$_x$ compounds (Figs. 1-16 and 1-18) show similar behavior for the two compounds in silica but very different behavior in DMF solution. The position of $\lambda_{ex\text{-}max}$ for both compounds in the xerogel is near 390 nm, having settled at that position from slightly higher energies during the drying process, but their $\lambda_{ex\text{-}max}$ positions in DMF are fully 10 nm apart, at 380 and 390 nm for (PipH)[Eu(ttfa)$_4$] and Eu(ttfa)$_3$, respectively. For these two chelates, then, there is a difference in coupling to Eu^{3+} in DMF; one possible cause is the charged character of the tetrakis chelate, which could lead to a stronger interaction with the highly polar solvent which elevates its S_1 level above that of the tris chelate.

Figure 1-17: (PipH)[Eu(ttfa)$_4$], 10^{-3} M, Emission Spectra
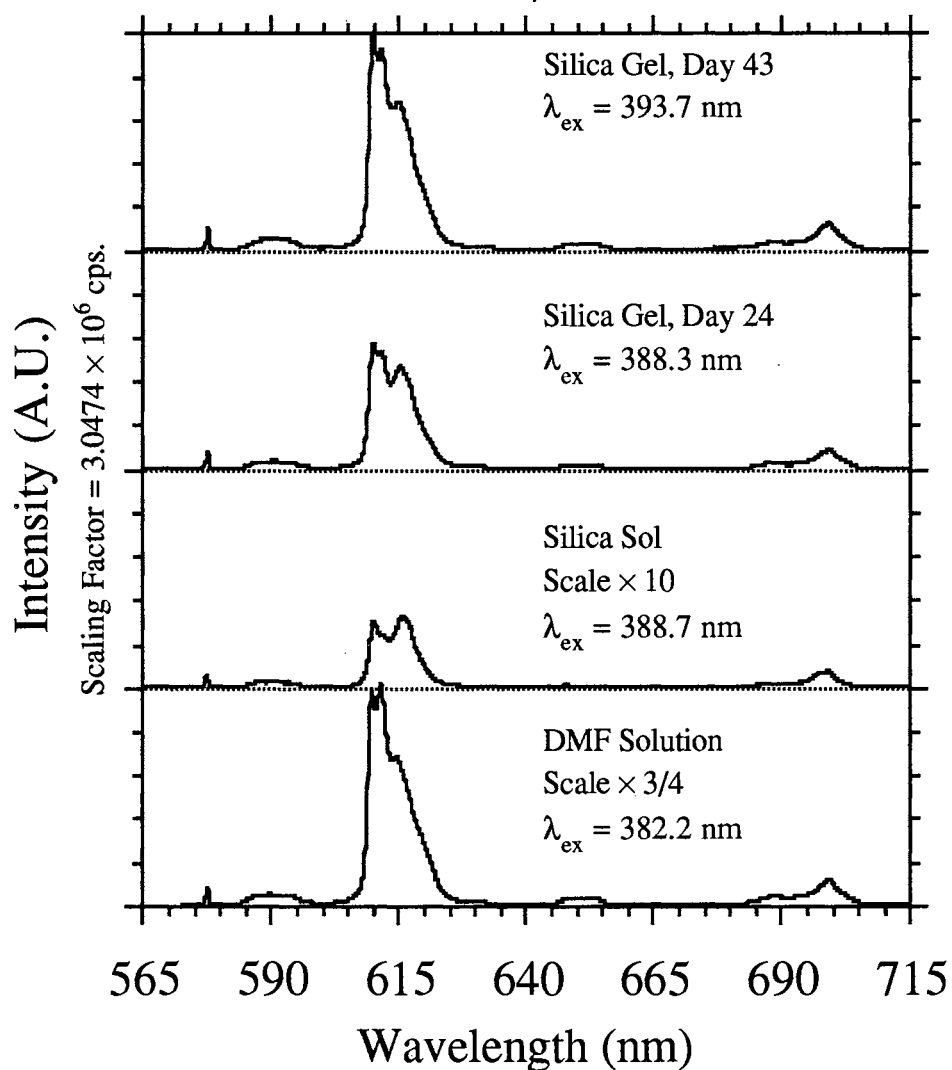
FIGURE 1-17: Emission spectra for (PipH)[Eu(ttfa)4] in DMF solution and sol–gel silica. The given scaling factor is that of the silica gel day 43 spectrum. The silica sol spectrum has been multiplied by 10 for clarity. The DMF solution spectrum has been multiplied by 3/4. Each spectrum has a different λ_{ex} due to the change in $\lambda_{ex\text{-}max}$ (see Fig. 1-18).

Figure 1-18: $(PipH)[Eu(ttfa)_4]$, 10^{-3} M, Excitation Spectra
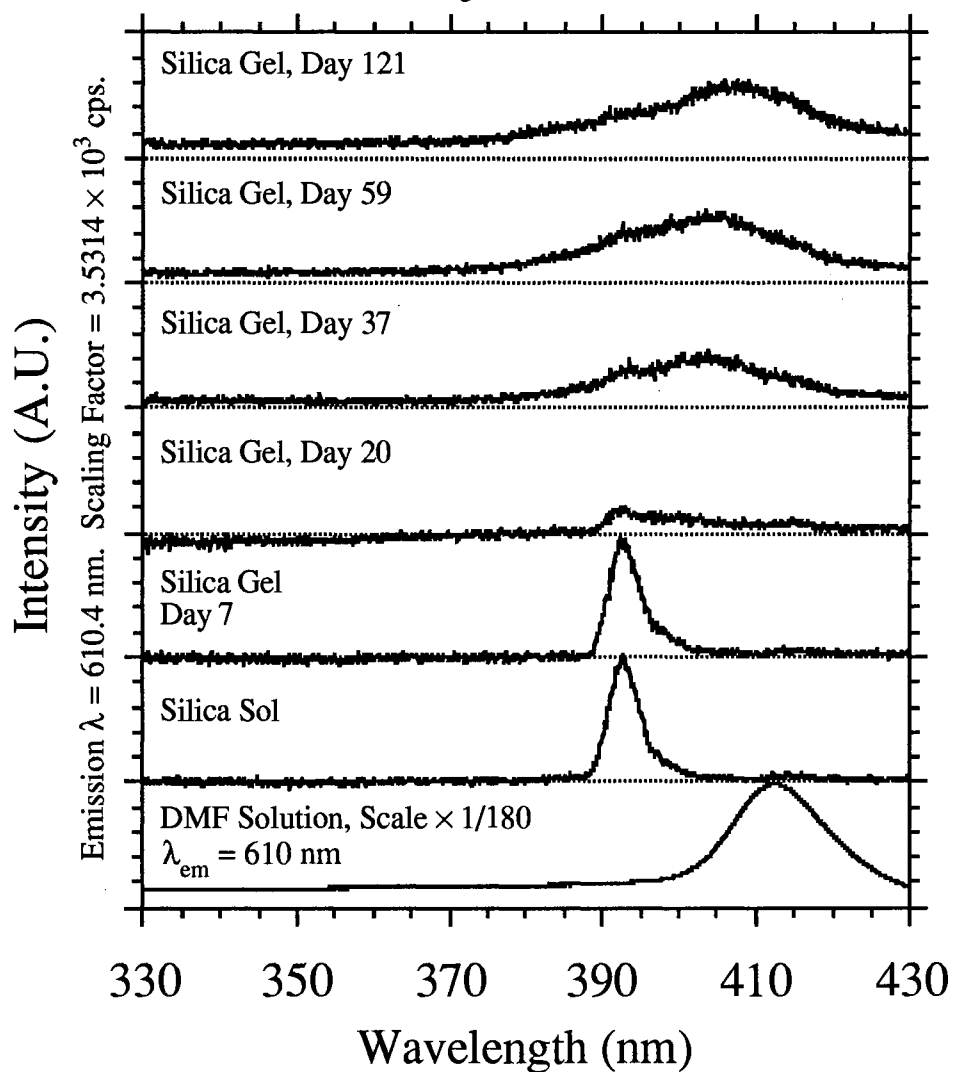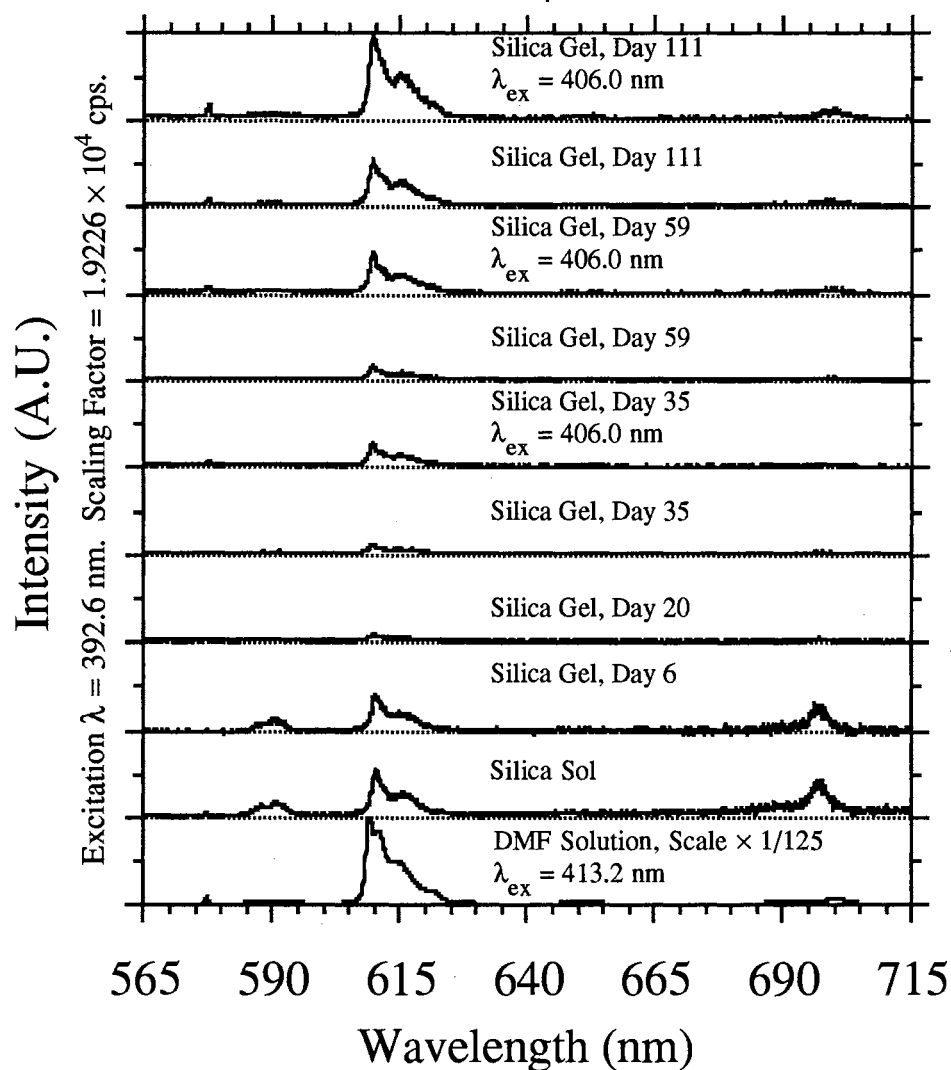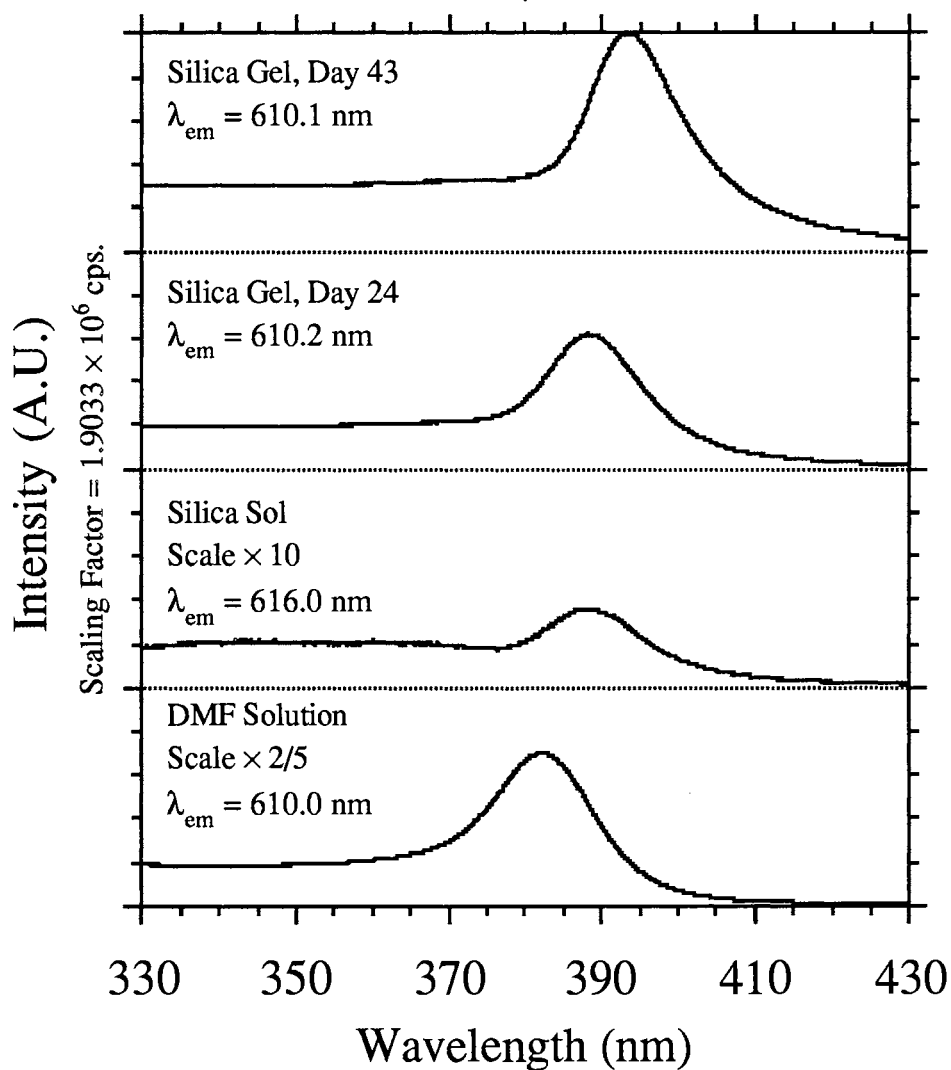

FIGURE 1-18: Excitation spectra for $(PipH)[Eu(ttfa)_4]$ in DMF solution and sol–gel silica. The given scaling factor is that of the silica gel day 43 spectrum. The silica sol spectrum has been multiplied by 10. The DMF solution spectrum has been multiplied by 2/5. Each spectrum has a different λ_{em} due to the change in $\lambda_{em\text{-}max}$ (see Fig. 1-17).

I.   *Comparative Fluorescence Output*

The final Figure for this Chapter, 1-19, displays the fluorescence output of the eight europium(III) β-diketonates incorporated into sol–gel silica. In this case, the measure of fluorescence output used is the integrated emission intensity, which may be expressed as:

(3) $S = \int I(\lambda)\, d\lambda$

where $I(\lambda)$ is the emission intensity in arbitrary units at a particular wavelength λ and S is the value of the integral (S has units of length from the $d\lambda$ term, but S and I are generally used in a context which renders them effectively dimensionless). Theoretically, this integration includes all wavelengths, but in practice limits are chosen at the points where each spectral peak becomes indistinguishable from the baseline; the bases of Eu^{3+} peaks are generally 10–40 nm wide. At least for comparative purposes, the integrated intensity is a reliable measure of the number of photons emitted at all relevant energies. This is essentially the same quantity reported for individual emission peaks in Table 1-1; but in this Figure the intensity is integrated over all five emission peaks.

It may be observed from Figure 1-19 that for all eight compounds in DMF solution, the S values all lie within the order of magnitude between $10^{7.2}$ and $10^{8.2}$.[††] This variance is much less extreme than that of the comparable values in silica, which range from less than $10^{4.6}$ to over $10^{7.8}$, more than three orders of magnitude. Clearly, the various ligands react differently to incorporation into the silica network. The ligand species appears to be far more important in determining luminescence intensity than the type of chelate, because the values of the tris and tetrakis chelates of a particular ligand are very close to one another. In silica, there is no consistent preference for one chelate form over the other, but the tendency, noted by early researchers like Brecher *et al.*,[19] for tetrakis chelates to be more luminescent than the tris chelates in solution appears to hold true.

[††] The missing value for $Eu(btfa)_3$ in DMF should be approximately 8.0.

Figure 1-19: Europium β-Diketonates, 10^{-3} M
Comparative Fluorescence Output
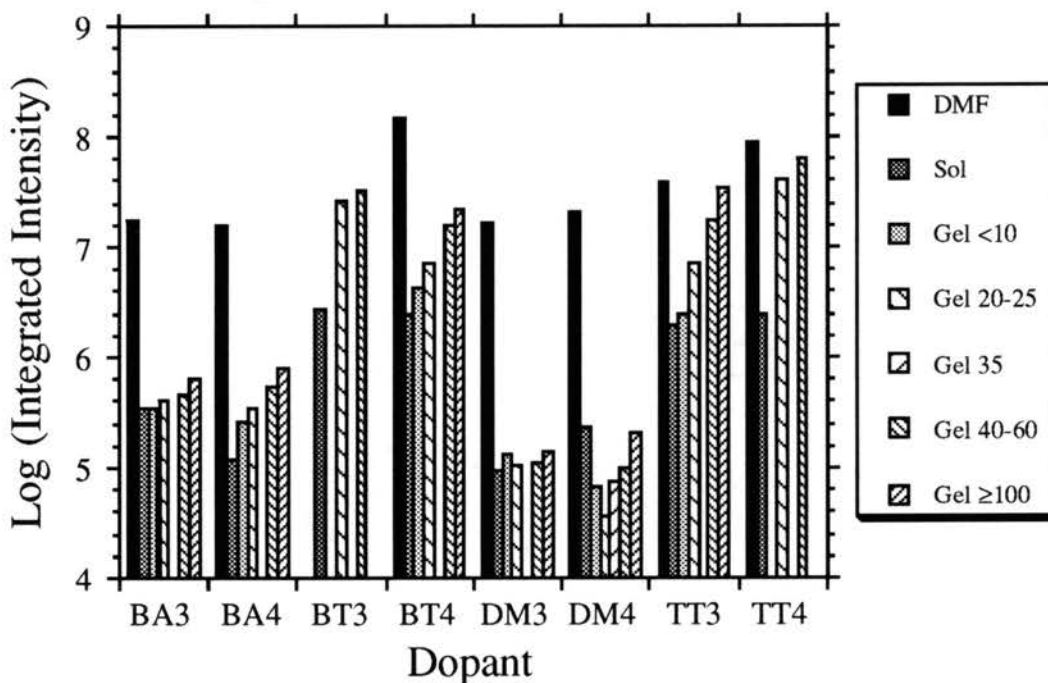
FIGURE 1-19: Comparative fluorescence output, measured as integrated emission intensity on a logarithmic scale, for the eight europium(III) β-diketonates in DMF solution and in sol–gel silica as shown in Figures 1-3–1-18. The letter codes on the horizontal axis refer to the ligand (BA = ba⁻, BT = btfa⁻, DM = dbm⁻, TT = ttfa⁻); the numbers (3, 4) represent tris (EuL_3) or tetrakis (EuL_4^-) chelates. The numbers on the legend are days of drying time (only DM4 has a value for "Day 35").

Since the key step in transferring energy from the ligand to the europium(III) center involves an overlap between the ligand T_1 excited state and various Eu^{3+} excited states, one possible explanation for the difference in ligand behavior in silica is that the energies of the relevant T_1 levels are altered in such a way as to reduce the overlap with the Eu^{3+} levels. In particular, if the T_1 level were to be lowered below the Eu^{3+} $^5D_0$ level, the complex would preferentially undergo nonradiative de-excitation.

Ligand energy-level alterations can arise from a number of factors. Important differences between environments of the DMF solution and sol–gel silica include the lower polarity of silica relative to DMF; the presence of protic quenching species (*i.e.* ROH) in silica sol, reduced in silica gel and not present in DMF; and forces arising from the entrapment of solute molecules in silica gel but not in DMF or silica sol. The latter two influences are more difficult to separate because they are concurrent.

For $Eu(ba)_x$, the dominant force appears to be the polarity difference between DMF and silica sol, because the spectral changes (especially the large decrease in η_{21}) become immediately apparent upon going from DMF to silica sol and change relatively little as the silica ages. As discussed above, the lower polarity of the silica apparently allows the relatively nonpolar ba^- complexes to relax into a more symmetric configuration, which leads to a decrease in absolute intensity and a lower η_{21}. While intensity does increase from the sol value as the gel ages, the increase is less than that predicted by the BLL, an indicator of dopant aggregation (*e.g.* dimerization) and resultant nonradiative intermolecular energy transfer.

For $Eu(btfa)_x$ and $Eu(dbm)_x$, the difference between DMF and silica sol is readily apparent, but as the silica ages the S and η_{21} values in silica begin to approach those of DMF as the linked influences of solvent evaporation and entrapment become dominant. Solvent evaporation decreases the concentration of hydroxyl-containing species and leads to increases in absolute intensity. In $Eu(btfa)_x$, this appears to be the dominant process because the intensity increase is greater than BLL behavior; if present, dopant aggregation

apparently does not cause significant quenching, and this difference from the behavior of Eu(ba)$_x$ has been attributed to the greater polarity of Eu(btfa)$_x$.

While solvent evaporation must influence the behavior of Eu(dbm)$_x$, the forces arising from entrapment appear to be more important, providing an environment closer to that of DMF. Because Eu(dbm)$_x$ is relatively nonpolar like Eu(ba)$_x$, similar behavior should be expected; it is in fact observed only in the sol and younger gels. Although both Eu(ba)$_x$ and Eu(dbm)$_x$ exhibit a marked drop in η_{21} (hence an increase in symmetry) upon going from DMF to silica sol, η_{21} does not increase appreciably with aging in Eu(ba)$_x$ but does increase in Eu(dbm)$_x$, to at least half its DMF value. The main difference between ba$^-$ and dbm$^-$ is the substitution of a phenyl group in dbm$^-$ for the methyl group of ba$^-$ at R^2, which changes the ligand's size and also allows extends its conjugation along its entire length, which should increase its rigidity. It may be hypothesized that the observed increase in η_{21} with gel aging (hence a decrease in symmetry) for Eu(dbm)$_x$ may arise from the response of a rigid ligand to entrapment forces as a preference for shifting the arrangement of its bonding to the Eu^{3+} center (causing a decrease in local site symmetry) over a weakening of its extended conjugation.

In Eu(ttfa)$_x$, which contains the most polar ligand, the intensity in aged silica gel actually exceeds that of DMF; the polarity difference causes relatively minor effects compared to those of silica aging.

IV. Conclusions

In comparing the fluorescence behavior of different europium(III) β-diketonate complexes in solution and in a silica host created by the sol–gel method, a number of significant ligand-dependent differences in fluorescence behavior have been observed. The identity of the ligand was found to be of much greater importance in determining luminescence behavior than was the number of ligands (three or four) present in the complex.

42

While all the complexes in the experiment lost fluorescence intensity upon incorporation into the sol–gel system relative to their solution values, the benzoylacetonate and dibenzoylmethide complexes lost a significantly larger fraction of their fluorescence intensity than did the benzoyltrifluoroacetonate and thenoyltrifluoroacetonate complexes. As a result, the latter four complexes would be much better suited to optical source applications, where intense fluorescence is desired, than would the former four, while the dibenzoylmethide complexes would be best suited to those applications where quenched fluorescence was desired. The new solid-state materials constructed in the experiment, particularly those containing the thenoyltrifluoroacetonates, were deemed worthy of the further investigations reported in Chapter 2.

V. References

1. U. Itoh, M. Takakusa, T. Moriya, and S. Saito, *Japan. J. Appl. Phys.* **16** (1977) 1059.

2. R. M. O'Connell and T. T. Saito, *Opt. Eng.* **22** (1983) 393.

3. D. A. Gromov, K. M. Dyumaev, A. A. Manenkov, A. P. Maslyukov, G. A. Matyushin, V. S. Nechitailo, and A. M. Prokhorov, *J. Opt. Soc. Am. B* **2** (1985) 1028.

4. R. Reisfeld, D. Brusilovsky, and M. Eyal, in *French-Israeli Workshop on Solid State Lasers,* Proceedings of SPIE 1182 (Bellingham, WA: The Society of Photo-Optical Instrumentation Engineers, 1988), p. 230.

5. B. Dunn, E. Knobbe, J. M. McKiernan, J. C. Pouxviel, and J. I. Zink, in C. Jeffrey Brinker, David E. Clark, and Donald R. Ulrich, *Better Ceramics Through Chemistry III,* MRS Symposium Proceedings 121 (Pittsburgh, PA: Materials Research Society, 1989), p. 331.

6.   E. T. Knobbe, B. Dunn, P. D. Fuqua, F. and Nishida, *Appl. Opt.* **29** (1990) 2729.

7.   B. Dunn, "Dye-Doped Sol-Gel Tunable Lasers," Fifth International Conference on Ultrastructure Processing of Ceramics, Glasses, Composites, Ordered Polymers, and Advanced Optical Materials (Orlando, FL, February 1991).

8.   I. P. Kaminow, L. W. Stulz, E. A. Chandross, and C. A. Pryde, *Appl. Opt.* **11** (1972) 1563.

9.   D. Avnir, D. Levy, and R. Reisfeld, *J. Phys. Chem.* **88** (1984) 5956.

10.   D. Avnir, V. R. Kaufman, and R. Reisfeld, *J. Non-Cryst. Solids* **74** (1985) 395.

11.   Carol A. Capozzi and L. David Pye, in Proceedings of SPIE 970 (Bellingham, WA: The Society of Photo-Optical Instrumentation Engineers, 1988), p. 135.

12.   A. J. Berry and T. A. King, *J. Phys. D, Appl. Phys.* **22** (1989) 1419.

13.   S. P. Sinha, *Europium* (New York: Springer-Verlag New York, Inc., 1967).

14.   N. C. Chang, *J. Appl. Phys.* **34** (1963) 3500.

15.   A. Lempicki, and H. Samelson, *Phys. Lett.* **4** (1963) 133.

16.   H. Mack, R. Reisfeld, and D. Avnir, *Chem. Phys. Lett.* **99** (1983) 238.

17.   Clément Sanchez, in J. D. Mackenzie and D. R. Ulrich, *Sol–Gel Optics, Proceedings of SPIE 1328* (Bellingham, WA: The Society of Photo-Optical Instrumentation Engineers, 1990), p. 40.

18.   R. Campostrini, G. Carturan, M. Ferrari, M. Montagna, and O. Pilla, *J. Mater. Res.* **7** (1992) 745.

19.   C. Brecher, H. Samelson, and A. Lempicki, *J. Chem. Phys.* **42** (1965) 1081.

20.   A. Streitwieser, Jr., and C. H. Heathcock, *Introduction to Organic Chemistry* (New York: Macmillan Publishing Co., Inc., 1976).

21.   R. E. Whan and G. A. Crosby, *J. Mol. Spectrosc.* **8** (1962) 315.

22.   S. J. Lyle and Alan D. Witts, *Inorg. Chim. Acta* **5** (1971) 481.

23. (a) T. Adachi and S. Sakka, *J. Mater. Sci.* **22** (1987) 4407. (b) T. Adachi and S. Sakka, *J. Non-Cryst. Solids* **99** (1988) 118.

24. (a) N. de la Rosa-Fox, L. Esquivias, and J. Zarzycki, *Diffusion and Defect Data* **53–54** (1987) 363. (b) L. Esquivias and J. Zarzycki, in J. D. Mackenzie and D. R. Ulrich, *Ultrastructure Processing of Advanced Ceramics* (New York: John Wiley & Sons, Inc., 1988), p. 255.

25. (a) Guiyun Zhu, Zhikun Si, Ping Liu, and Wei Jiang, *Anal. Chim. Acta* **247** (1991) 37. (b) Zhi-Kun Si, Gui-Yun Zhu, and Jie Li, *Analyst* **116** (1991) 309.

26. (a) Michael Albin and William DeW. Horrocks, Jr., *Inorg. Chem.* **24** (1985) 895. (b) Jean-Claude G. Bünzli and Georges-Olivier Pradervand, *J. Chem. Phys.* **85** (1986) 2489. (c) Béatrice Alpha, Vincenzo Balzani, Jean-Marie Lehn, Siglinda Perathoner, and Nanda Sabbatini, *Angew. Chem. Intl. Ed. Engl.* **26** (1987) 1266. (d) M. F. Hazenkamp and G. Blasse, *Chem. Mater.* **2** (1990) 105. (e) K. Devlin, B. O'Kelly, Z. R. Tang, C. McDonagh, and J. F. McGilp, *J. Non-Cryst. Solids* **135** (1991) 8. There are many other publications on this subject.

27. G. H. Dieke and H. M. Crosswhite, *Appl. Opt.* **2** (1963) 675.

28. W. T. Carnall, P. R. Fields, and K. Rajnak, *J. Chem. Phys.* **49** (1968) 4412.

29. N. E. Wolff and R. J. Pressley, *Appl. Phys. Lett.* **2** (1963) 152.

30. A. V. Hayes and H. G. Drickamer, *J. Chem. Phys.* **76** (1982) 114.

31. M. J. Lochhead, P. R. Wamsley, and K. L. Bray, *Inorg. Chem.*, in press.

32. R. Reisfeld, V. Chernyak, M. Eyal, and C. K. Jørgensen, in W. Strek, W. Ryba-Romanowski, J. Legendziewicz, and B. Jezowska-Trzebiatowska, *The Second International School on Excited States of Transition Elements* (Singapore; New Jersey; London; Hong Kong: World Scientific Publishing Co. Pte. Ltd., 1992), p. 247.

CHAPTER 2

THE LUMINESCENCE BEHAVIOR OF EUROPIUM(III)

4,4,4-TRIFLUORO-1-(2'-THIENYL)-1,3-BUTANEDIONATES

INCORPORATED INTO SOL–GEL SILICA*

I. Introduction

In Chapter 1, it was stated and demonstrated that the sol–gel method is a suitable approach for the preparation of novel inorganic and composite fluorophore-doped materials, including a wide variety of organic dyes reported by previous researchers[†] and fluorescent β-diketonate complexes of europium(III). The research presented in the present Chapter focuses more closely on the luminescence behavior of the tris and tetrakis complexes of europium(III) with one particular β-diketonate ligand, 4,4,4-trifluoro-1-(2'-thienyl)-1,3-butanedionate or thenoyltrifluoroacetonate (ttfa⁻). The solid-state materials made from doping these complexes into silica xerogel were found to be highly luminescent during the work described in the preceding Chapter. In fact, of all the β-diketonate complexes tested (Fig. 1-1, p. 3), the ttfa⁻ complexes retained the most luminescence intensity in silica xerogel. Therefore, in the present work, tris(4,4,4-trifluoro-1-(2'-thienyl)-1,3-butanedionate-O,O')europium(III) dihydrate, Eu(ttfa)$_3 \cdot 2H_2O$, and piperidinium tetrakis-(4,4,4-trifluoro-1-(2'-thienyl)-1,3-butanedionate-O,O')europate(III), (PipH)[Eu(ttfa)$_4$], metalorganic complexes have been doped into silica prepared by the sol–gel technique. The luminescence behaviors of the resulting composite materials are described.

---

*   Substantial portions of the work presented in this Chapter appeared in L. R. Matthews and E. T. Knobbe, *Chem. Mater.* **5** (1993) 1697.

†   See References 1–12 in Chapter 1, pp. 32–33.

A.   *Syntheses*

Europium(III) chelates were prepared using 4,4,4-trifluoro-1-(2'-thienyl)-1,3-butanedione or thenoyltrifluoroacetone (Httfa, Fig. 2-1). As described in the preceding Chapter, compounds of this type can form a stable, conjugated anion (ttfa⁻) in the presence of a base, which may then act as bidentate ligands in the formation of metalorganic complexes with a wide variety of metal ions. This includes the trivalent ions of the rare-earth metals, specifically europium(III); furthermore, this ion is sufficiently large as to allow coordination with either three or four bidentate ligands in its preferred eight- to ninefold coordination.[1-3] The synthetic reactions take place as follows:

(1a) $Httfa + NaOH \rightarrow Na(ttfa) + H_2O$

(1b) $Httfa + Pip \rightarrow (PipH)(ttfa)$

(2a) $3\ Na(ttfa) + EuCl_3 + 2\ H_2O \rightarrow Eu(ttfa)_3 \cdot 2H_2O + 3\ NaCl$

(2b) $4\ (PipH)(ttfa) + EuCl_3 \rightarrow (PipH)[Eu(ttfa)_4] + 3\ (PipH)Cl$
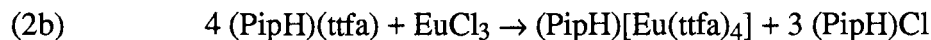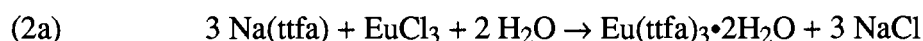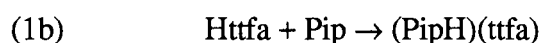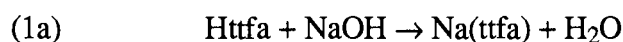
where Pip and PipH⁺ are piperidine and the piperidinium cation, respectively. The synthetic procedures followed were those of Whan and Crosby[4] and Brecher, Samelson, and Lempicki[5] (detailed in Chapter 1). Both complexes were found to be soluble in *N,N*-dimethylformamide (DMF), a solvent which has been used a drying control chemical additive to reduce cracking in sol–gel silica.[6] Ligand, base, and predicted complex structures[7-8] are shown in Figure 2-1.

The complexes' chemical compositions were partially verified by FAB mass spectrometry at the OSU Mass Spectrometry Facility: for $Eu(ttfa)_3 \cdot 2H_2O$, the parent-ion peak was identifiable, there were no peaks at higher masses, and fragmentation peaks corresponding to water, ttfa⁻, and $Eu(ttfa)_{3-x}$ groups were found; for $(PipH)[Eu(ttfa)_4]$, a small but identifiable parent-ion peak was present, in addition to similar fragmentation peaks to $Eu(ttfa)_3 \cdot 2H_2O$.

Attempts to grow crystals suitable for X-ray diffraction studies proved only marginally successful. No Eu(ttfa)$_3 \cdot$2H$_2$O crystals larger than fine powders were ever obtained. A number of apparently good, optical-quality, needle-shaped crystals of (PipH)[Eu(ttfa)$_4$] were grown from toluene in a vapor-diffusion chamber containing pentane. However, the X-ray studies conducted by Dr. Elizabeth M. Holt of OSU showed that the crystals were polymorphic, probably due to the presence of several different stereoisomers.

A typical synthesis of Eu(ttfa)$_3 \cdot$2H$_2$O involved two solutions. In the first container, 5 mmol of EuCl$_3 \cdot$6H$_2$O (Pfaltz & Bauer) were dissolved into about 20 mL of water or 50% water–ethanol. In the second container, a stoichiometric amount, 15 mmol, of Httfa (Aldrich) was dissolved in the appropriate stoichiometric amount of aqueous sodium hydroxide (Fisher), typically 1.0×10^{-2} M. (The anionic form, ttfa$^-$, is significantly more water-soluble than Httfa, so it proved desirable to include the base from the beginning.) The first solution was slowly added to the second to produce a precipitate which was then collected by vacuum filtration and dried in a dessicator over anhydrous calcium sulfate. Drying under these mild conditions produced the dihydrate; the water of hydration could have been removed by heating under stronger vacuum.[5]

A typical synthesis of (PipH)[Eu(ttfa)$_4$] also involved two solutions. In the first container, 5 mmol of EuCl$_3 \cdot$6H$_2$O were dissolved into about 20 mL of ethanol. In the second container, a slight excess of Httfa, $\geq$ 20 mmol, was also dissolved in about 20 mL of ethanol to form a faintly amber solution. To the second container was added a slightly greater excess of piperidine (Aldrich[‡]), $\geq$ mmol Httfa; the reaction was immediate and produced a noticeable darkening of the amber color. The EuCl$_3$ solution was added slowly to the (PipH)(ttfa) solution to form a milky, fluorescent precipitate which was then collected and dried.

---

‡ Because piperidine is a controlled-substance precursor, Aldrich requires special purchaser certification before delivery.

Figure 2-1: Chemical Structures

(a) 4,4,4-Trifluoro-1-(2'-thienyl)-
1,3-butanedione
(Thenoyltrifluoroacetone, Httfa)
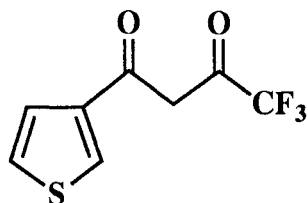
(b) Thenoyltrifluoroacetonate
Ion (ttfa⁻)
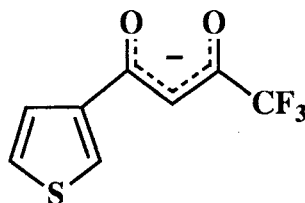
(c) Piperidine (Pip)
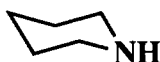
(d) Tris(4,4,4-trifluoro-1-(2'-thienyl)-
1,3-butanedionato-O,O')europium(III)
Dihydrate, Eu(ttfa)₃•2H₂O
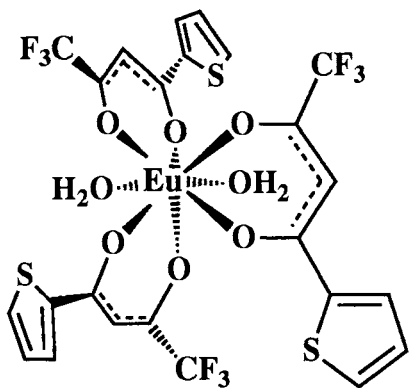
(e) Piperidinium Tetrakis(4,4,4-trifluoro-
1-(2'-thienyl)-1,3-butanedionato-O,O')-
europate(III), (PipH)[Eu(ttfa)₄]
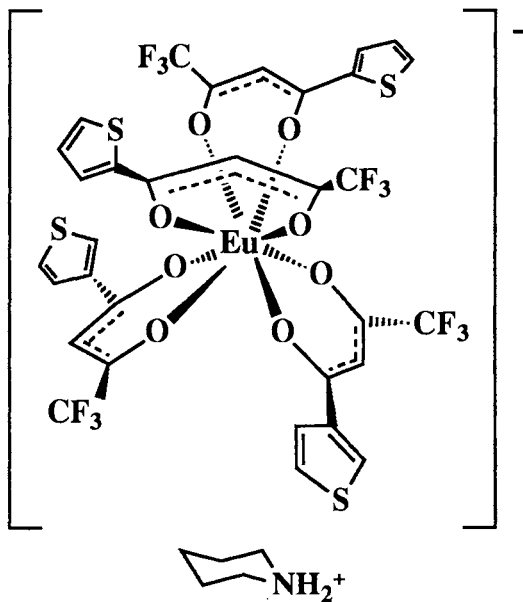
FIGURE 2-1: (a) 4,4,4-Trifluoro-1-(2'-thienyl)-1,3-butanedione or thenoyltrifluoroacetone (Httfa), in its keto form. (b) Enolate form, thenoyltrifluoroacetonate (ttfa⁻). (c) Base piperidine (Pip). (d) Tris(4,4,4-trifluoro-1-(2'-thienyl)-1,3-butanedionato-O,O')europium(III) dihydrate, Eu(ttfa)₃•2H₂O (Ref. 7). (e) Piperidinium tetrakis(4,4,4-trifluoro-1-(2'-thienyl)-1,3-butanedionato-O,O')europate(III), (PipH)[Eu(ttfa)₄] (Ref. 8).

As described in Chapter 1, the silica host matrix was prepared from tetraethoxy-silane (TEOS, Aldrich) and 0.040 M aqueous HCl (Aldrich) following the "sonogel" procedure of de la Rosa-Fox, Esquivias, and Zarzycki.[9]

B. Spectroscopic Analysis

Luminescence characteristics were measured using a Spex Industries Model F112 spectrofluorimeter; absorption spectra were obtained using a Cary model 5 spectrophotometer. Emission and excitation spectra were made in the "front face" orientation, and all spectra were corrected by using the "correction factor" files in the Spex software. Quantum efficiencies (Q) were calculated by the reference technique of Demas and Crosby[10] using rhodamine 6G chloride in ethanol, reported to have a Q of 95%.[11] Absorption cross-sections (σ_{Abs}) were calculated according to:

$$(3) \qquad \sigma_{Abs} = \frac{\alpha_{Abs}}{\Delta N}$$

where α_{Abs} is the absorption coefficient (cm^{-1}) at the excitation wavelength and ΔN is the difference between ground (N_0) and excited (N_1) state number densities (cm^{-3}).[12] Excited state population densities were assumed to be negligible compared to the ground state population densities ($\Delta N \approx N_0$) under the spectrofluorometric excitation conditions used. The spontaneous-emission cross-section (σ_{SpE}), a measure of the relative "brightness" of a luminous source, was obtained using the following:

$$(4) \qquad \sigma_{SpE} = Q\,\sigma_{Abs}.$$

III. Discussion of Results

Figure 2-2 shows the emission spectra of (PipH)[Eu(ttfa)$_4$], Eu(ttfa)$_3$, and EuCl$_3$ in aged silica gel upon excitation of the $^7F_0 \rightarrow {}^5D_2$ europium transition. The maximum intensity of the $^5D_0 \rightarrow {}^7F_2$ peak (610–620 nm) in (PipH)[Eu(ttfa)$_4$] was observed to be slightly higher than that of Eu(ttfa)$_3$ and approximately 50 times that of EuCl$_3$. Only minor

differences were seen between the relative emission peak heights of the various compounds when characterizing the organoeuropium spectra in DMF solution with respect to comparable concentrations in the silica precursor sol and the final dried silica gel. No indication of the presence of luminescent europium(II) species, known to have spectrally broad emission peaks near 428 and 507 nm in silicate materials,[13] was found.

Figure 2-3 shows the associated excitation spectra, detailing pump transitions resulting in radiative relaxation from the $^5D_0 \rightarrow {}^7F_2$ levels. Both chelates were observed to exhibit greatly increased $^5D_0 \rightarrow {}^7F_2$ luminescence emission cross-section, by approximately an order of magnitude with respect to comparable $EuCl_3$-doped samples, following excitation of the $^7F_0 \rightarrow {}^5D_2$ transition. While this increase is notable, a substantially larger emission cross-section results upon excitation of the chelate absorption band. Excitation of
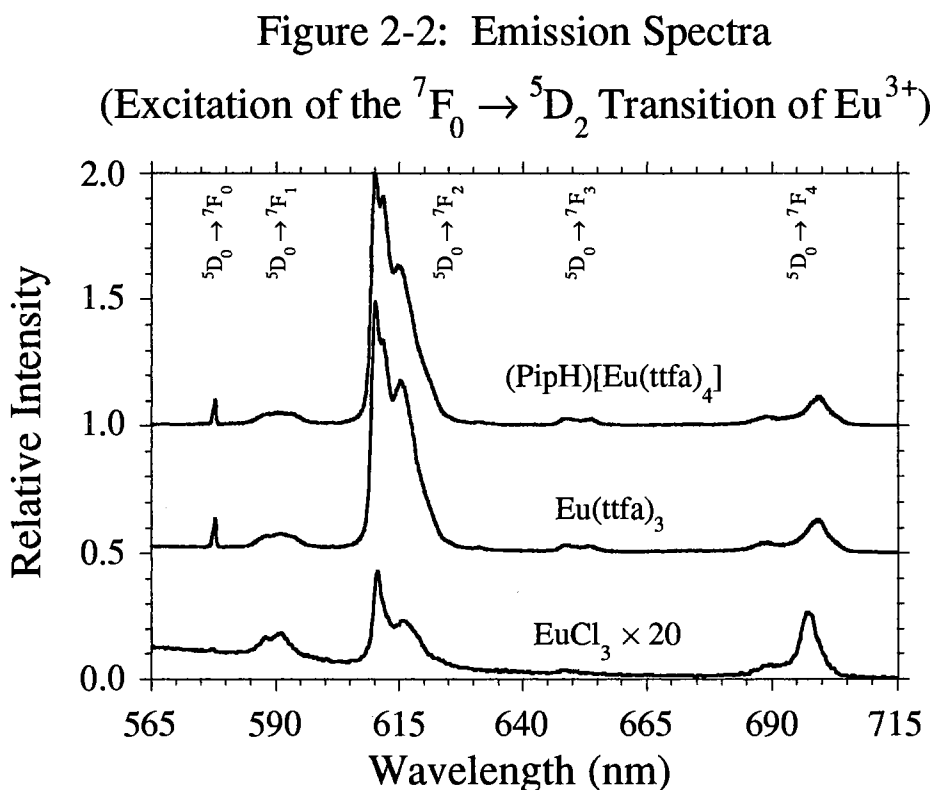
Figure 2-2: Emission Spectra

(Excitation of the $^7F_0 \rightarrow {}^5D_2$ Transition of Eu^{3+})

FIGURE 2-2: Emission spectra for (PipH)[Eu(ttfa)$_4$] (top, offset 1.0 relative intensity units), Eu(ttfa)$_3$ (center, offset 0.5 units), and EuCl$_3$ in aged silica gel. Spectra were normalized to the maximum emission intensity of (PipH)[Eu(ttfa)$_4$]. The spectrum of EuCl$_3$ has been increased by a factor of 20 times to make the salient structural features observable.

51

the ligand band, which couples (via ligand-to-metal charge transfer) into the $^5D_3$ (near 400 nm) and higher levels of europium(III), was observed to result in emission cross-sections which were larger than comparable $EuCl_3$-doped gel samples by three orders of magnitude.

The effect of complex formation on the luminescence behavior of europium(III) in the gel hosts was examined by exciting the $^7F_0 \rightarrow {}^5D_2$ transition of Eu^{3+} at 464 nm, a lower excitation energy than the chelates' charge-transfer band. The complexes' quantum efficiencies and emission cross-sections were found to be significantly higher than those of $EuCl_3$ in solid- and liquid-phase hosts (Table 2-1, Sections 1 and 2), indicating that radiative relaxation processes associated with the Eu^{3+} ion are indeed enhanced by the chelate cage.
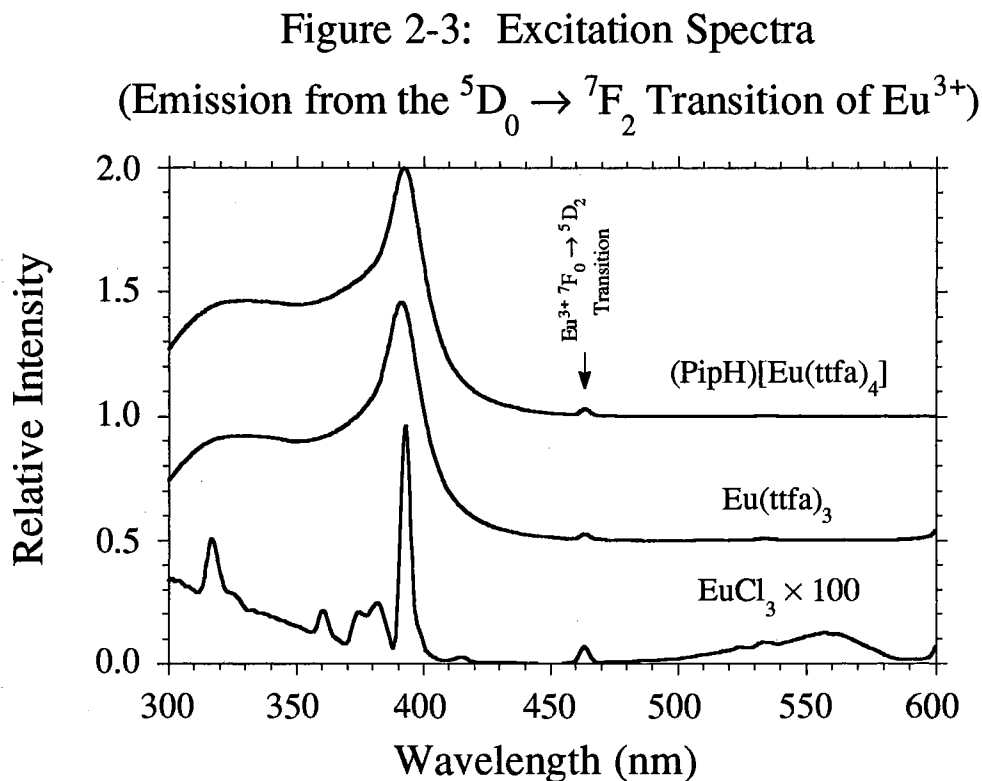
Figure 2-3: Excitation Spectra
(Emission from the $^5D_0 \rightarrow {}^7F_2$ Transition of Eu^{3+})

FIGURE 2-3: Excitation spectra for (PipH)[Eu(ttfa)$_4$] (top, offset 1.0 relative intensity units), Eu(ttfa)$_3$ (center, offset 0.5 units), and $EuCl_3$ in aged silica gel. Spectra were normalized to the maximum emission intensity of (PipH)[Eu(ttfa)$_4$]. The spectrum of $EuCl_3$ has been increased by a factor of 100 times to make the salient structural features observable.

The spontaneous-emission cross-sections of the rare earth complexes, which are a measure of the radiated emission intensity from a given sample volume, were found to be 14 and 16 times larger for the tris and tetrakis chelates, respectively, than the comparable EuCl$_3$-doped silica gel material when excited at the $^7F_0 \rightarrow {}^5D_2$ transition (Table 2-1, Section 2). Luminescence behavior of the chelates greatly increased when pumped at wavelengths near 390 nm, corresponding to excitation at the red edge of the complexes' intense ultraviolet absorption bands (Table 2-1, Sections 3 and 4). The corresponding emission cross-sections of gels doped with Eu(ttfa)$_3$ and (PipH)[Eu(ttfa)$_4$] were observed to be 4,800 and 7,600 times larger, respectively, than comparable gel samples doped with EuCl$_3$. Quantum efficiencies of the chelate-doped gels were calculated to be between 15% and 23%. While the Q of the chloride-doped gels is also about 10%, the overall fluorescence output is substantially reduced by the significantly lower α_{Abs} and σ_{Abs} values of EuCl$_3$. The difference in σ_{SpE} between the chelate- and chloride-doped gels are much more indicative of the true difference in luminescence performance.

53

TABLE 2-1

Fluorescence Yield Comparison

Dopants in DMF Solution and Aged Silica Gel

	λ_{ex} (nm)	α_{Abs} (cm^{-1})	σ_{Abs} (cm^2)	Q	σ_{SpE} (cm^2) (λ_{em} 612 nm)
1. Excitation of the Europium $^7F_0 \rightarrow {}^5D_2$ Transition, DMF Solution (6.02 $\times 10^{17}$ cm^{-3})					
EuCl$_3$	464.0	0.0007	1.1×10^{-21}	8.5%	9.1×10^{-23}
Eu(ttfa)$_3$	463.8	0.0051	8.5×10^{-21}	10.2%	8.7×10^{-22}
(PipH)[Eu(ttfa)$_4$]	463.9	0.0053	8.8×10^{-21}	10.6%	9.3×10^{-22}
2. Excitation of the Europium $^7F_0 \rightarrow {}^5D_2$ Transition, Silica Gel (3.10 $\times 10^{18}$ cm^{-3})					
EuCl$_3$	463.3	0.0087	2.9×10^{-21}	1.0%	2.9×10^{-23}
Eu(ttfa)$_3$	463.7	0.0193	6.4×10^{-21}	6.3%	4.1×10^{-22}
(PipH)[Eu(ttfa)$_4$]	463.6	0.0235	7.8×10^{-21}	5.9%	4.6×10^{-22}
3. Excitation of the Chelate, DMF Solution (6.02 $\times 10^{17}$ cm^{-3})					
Eu(ttfa)$_3$	389.5	1.34	2.2×10^{-18}	37.3%	8.3×10^{-19}
(PipH)[Eu(ttfa)$_4$]	389.0	1.50	2.5×10^{-18}	31.9%	8.0×10^{-19}
4. Excitation of the Chelate, Silica Gel (3.10 $\times 10^{18}$ cm^{-3})					
Eu(ttfa)$_3$	391.0	2.63	8.7×10^{-19}	15.8%	1.4×10^{-19}
(PipH)[Eu(ttfa)$_4$]	392.0	1.01	1.0×10^{-18}	22.2%	2.2×10^{-19}

All the compounds in groups 1 and 3 were studied as 1.0 millimolar solutions (number density 6.0×10^{17} cm^{-3}) in N,N-dimethylformamide. The solid-state samples in groups 2 and 4 were calculated from length measurements to have dopant concentrations of 5.0 mM (number density 3.0×10^{18} cm^{-3}).

IV. Conclusions

Rare-earth complex doped silica gels have been observed to exhibit substantially improved luminescence characteristics with respect to comparable materials containing simple metal salts. A number of factors contribute to the enhanced fluorescence performance of the tris and tetrakis europium(III) thenoyltrifluoroacetonates relative to europium(III) chloride. First, the chelating ligands act as "antennae" which capture a much larger fraction of the available excitation energy than the Eu^{3+} ion captures itself, as evidenced by the much larger absorption cross-sections exhibited by the chelates relative to the chloride. Second, because the Eu^{3+} ion in the chelate complexes is excited primarily by energy transfer instead of direct excitation, it may be excited by a much broader range of energies than in the chloride. Third, the chelating ligands at least partially protect the Eu^{3+} ion from intermolecular quenching effects which lower the efficiency of the ion's radiative relaxation processes. A further observation is that both the tris and tetrakis chelates enhance Eu^{3+} fluorescence in very similar ways relative to the inorganic salt. In conclusion, the relatively high efficiency and large spontaneous-emission cross-sections exhibited by these systems makes them promising candidates for potential use as optical sources.

V. References

1. Herbert Bauer, Joseph Blanc, and Daniel L. Ross, *J. Am. Chem. Soc.* **86** (1964) 5125.

2. Jean-Claude G. Bünzli and Bernard Klein, in G. J. McCarthy, H. B. Silber, and J. J. Rhyne, *The Rare Earths in Modern Science and Technology,* Volume 3 (New York; London: Plenum Press, 1982), p. 97.

3. S. P. Sinha, *Europium* (New York: Springer-Verlag New York, Inc., 1967).

4. R. E. Whan and G. A. Crosby, *J. Mol. Spectrosc.* **8** (1962) 315.

5. C. Brecher, H. Samelson, and A. Lempicki, *J. Chem. Phys.* **42** (1965) 1081.

6. (a) T. Adachi and S. Sakka, *J. Mater. Sci.* **22** (1987) 4407. (b) T. Adachi and S. Sakka, *J. Non-Cryst. Solids* **99** (1988) 118.

7. J. G. White, *Inorg. Chim. Acta* **16** (1976) 159.

8. H. Bauer, J. Blanc, and D. L. Ross, *J. Am. Chem. Soc.* **86** (1964) 5125.

9. (a) N. de la Rosa-Fox, L. Esquivias, and J. Zarzycki, *Diffusion and Defect Data* **53–54** (1987) 363. (b) L. Esquivias and J. Zarzycki, in J. D. Mackenzie and D. R. Ulrich, *Ultrastructure Processing of Advanced Ceramics* (New York: John Wiley & Sons, Inc., 1988), p. 255.

10. J. N. Demas and G. A. Crosby, *J. Phys. Chem.* **75** (1971) 991.

11. (a) K. H. Drexhage, in F. D. Schäfer, *Dye Lasers*, second edition (New York, Berlin, Heidelberg: Springer-Verlag, 1977). (b) K. H. Drexhage, "Design of Laser Dyes," VII International Quantum Electronics Conference (Montreal, 1972). (c) K. H. Drexhage, *Laser Focus* **9** (1973) 35.

12. O. Svelto, *Principles of Lasers,* second edition (New York: Plenum Press, 1982).

13. Xiao Zhang and Xingren Liu, *J. Electrochem. Soc.* **139** (1992) 622.

CHAPTER 3

LUMINESCENCE OF TRIS(4,4,4-TRIFLUORO-1-(2′-THIENYL)-1,3-BUTANEDIONATO-O,O')EUROPIUM(III) IN SOL–GEL-DERIVED SILICA AND ACRYLATE ORMOSIL HOST MATERIALS*

I. Introduction

The preceding Chapter reported the incorporation of europium(III) thenoyltrifluoroacetonate complexes, which have been shown to exhibit intense fluorescence and laser emission in solution,[1] into silica gel hosts via the sol–gel process. The organo-rare earth complex-doped gels proved to have intense fluorescence characteristics, especially with respect to comparable $EuCl_3$-doped samples. However, silica xerogels have a notable, unfortunate mechanical fragility which tends to preclude, to a large extent, optical shaping and polishing operations. (Of course, crystalline or dense-glass silica has no such problems.) Organically modified silicate *(ormosil)* materials, by contrast, tend to have a superior mechanical toughness and crack-resistance which permits, in many instances, optical grinding and polishing operations to be performed.[2] For that reason, the most efficient emitter molecule from Chapters 1–2, tris(4,4,4-trifluoro-1-(2′-thienyl)-1,3-butanedionato-O,O')europium(III) n-hydrate, Eu(ttfa)$_3$, was incorporated into such a matrix. The research presented herein extends the earlier work on silica gel matrices (Ch. 1–2) to include a silica–acrylate (S/A) ormosil matrix. The present Chapter is focused on the assessment of dopant concentration and dopant–matrix interaction effects in rare earth complex-doped silicate and organically modified materials.

The tris(4,4,4-trifluoro-1-(2'-thienyl)-1,3-butanedionato-*O,O'*)europium(III) trihydrate, Eu(ttfa)$_3$•3H$_2$O, was obtained from Kodak Chemicals and used without further purification or characterization. The structure of the complex is shown in Figure 3-1.[3]

FIGURE 3-1: Chemical structure of Eu(ttfa)$_3$•3H$_2$O (modified from Ref. 3).

Silica gel was prepared from tetraethoxysilane (TEOS, Aldrich Chemical Company) according to the "sonogel" procedure described previously (Ch. 1–2 and Ref. 4). S/A ormosil was prepared from tetramethoxysilane (TMOS, Fluka Chemie AG), 3-(trimethoxysilyl)propyl methacrylate (TMSPM, Aldrich), and methyl methacrylate monomer (MMA, Aldrich) via the "sonogel" procedure using mild acid catalysis and a mole ratio of 7 H$_2$O : 1 TMOS : 1 TMSPM : 1 MMA. A typical synthesis included reacting 14.7 mL of TMOS, 23.7 mL of TMSPM, and 6.3 mL of 0.040 *N* HCl in a sonicator for about 15 minutes, then adding 10.7 mL of MMA to the mixture. The precursor sols (after the addition of MMA) were hydrolyzed overnight before doping.

Chelate-doped silica samples were prepared by adding aliquots of Eu(ttfa)$_3$ dissolved in *N,N*-dimethylformamide (DMF, EM Science) at five times the target concentration to the silica precursor sol, as described in Chapters 1–2. The target sample concentrations selected were 1.0×10^{-1}, 10^{-2}, and 10^{-3} *M* (number densities $N = 6.0 \times 10^{19}$, 10^{18}, and 10^{17} cm^{-3}), requiring the DMF solutions to be 5.0×10^{-1}, 10^{-2}, and 10^{-3} *M* (3.0×10^{20}, 10^{19}, and 10^{18} cm^{-3}), respectively. These same target concentrations were also used for the ormosil samples to allow for a more meaningful comparison of the two host

58

matrices. Unfortunately, DMF proved to be incompatible with S/A ormosil, so doped ormosil samples were prepared by dissolving the desired amount of Eu(ttfa)$_3$ directly into the S/A precursor solution. The surfactant Triton® X-100 (an alkylaryl polyether alcohol obtained from Rohm and Haas Company via J. T. Baker) was added, in the amount of 5 volume percent, to the ormosil samples to inhibit phase separation in the gel samples. The resulting solutions were cast into transparent polystyrene cuvettes and kept in covered containers at room temperature until the onset of gellation. Aging and drying were allowed to proceed under ambient conditions over a period of several weeks. In this series of experiments, silica xerogel samples retained approximately 30% of their original volume and S/A xerogel samples retained approximately 40% of their initial volume. This shrinkage has the effect of increasing the dopant concentration in the xerogels relative to those in the sols by factors of 3.33 for silica and 2.50 for S/A ormosil.

Luminescence characteristics were measured using a Spex Industries Model F112 spectrofluorimeter, and absorption spectra were recorded using a Cary 5 spectrophotometer. Relative quantum efficiencies (Q), absorption cross-sections (σ_{Abs}), and spontaneous emission cross-sections (σ_{SpE}) were calculated by the methods described in Chapter 2.

III. Discussion of Results

Figure 3-2 shows a representative emission spectrum for Eu(ttfa)$_3$ in the S/A ormosil host. The sample was excited at 464 nm, corresponding to the $^7F_0 \rightarrow {}^5D_2$ band of Eu^{3+}. The final dopant number density in the dried host of this particular sample was calculated to be 1.6×10^{20} cm^{-3} (270 mM). The observable emission peaks result from relaxation out of the $^5D_0$ excited state to the first five levels of the ^7F ground manifold; the $^5D_0 \rightarrow {}^7F_2$ emission is the one usually associated with laser behavior.[5] The positions and branching ratios of the salient spectral features of the Eu(ttfa)$_3$-doped silica and ormosil samples were found to be effectively concentration independent over the three-

59

Figure 3-2: Sample Emission Spectrum

$Eu(ttfa)_3$ in S/A, 1.6×10^{20} cm^{-3}, Excited at the $^7F_0 \rightarrow {}^5D_2$ Transition
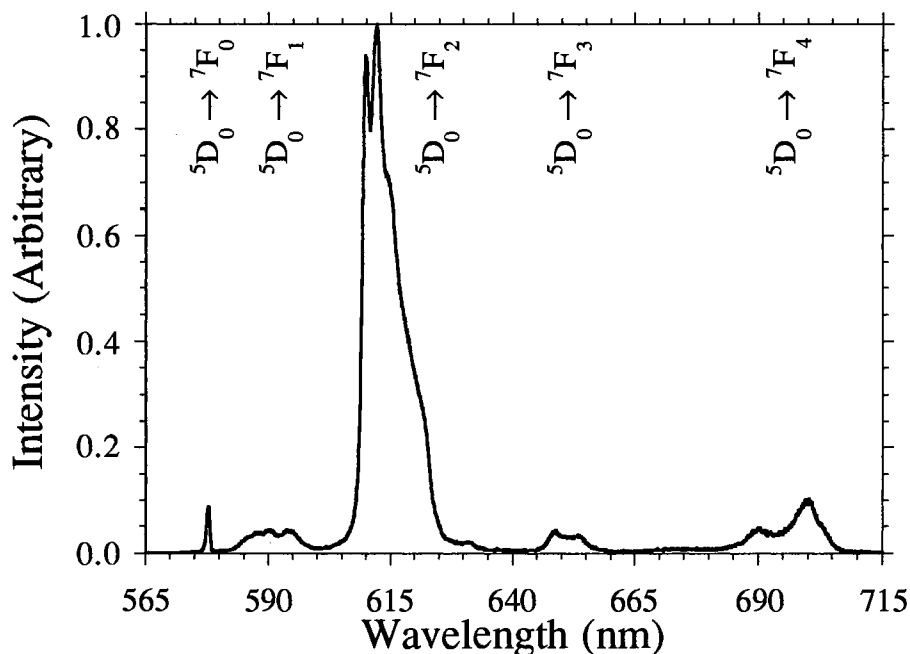
decade range of the experiment; predictably, intensity decreased with decreasing concentration.

Figure 3-3 shows the comparable excitation spectrum associated with emission from the $^5D_0 \rightarrow {}^7F_2$ transition of Eu^{3+}; the emission wavelength was 612 nm. The broad band centered at 430 nm was found to correspond to the red edge of the ligand's intense absorption band; Eu^{3+} fluorescence from excitation in this region comes from ligand-to-metal energy transfer (LMET).[1,6] The other three features, at 464, 535, and 580 nm, arise from europium(III) transitions from the $^7F_0$ ground state to the ^5D manifold.[5] The positions of the three europium(III) excitation peaks were found to be independent of changes in the matrix composition and/or dopant concentration. The relative intensities of these three peaks were found to vary in a nearly linear fashion as a function of dopant number density, which was varied from 6.0×10^{17} up to 1.6×10^{20} cm^{-3} (1.0 to 270 mM). This europium-peak concentration behavior was observed in both matrices in the sol and in the

Figure 3-3: Sample Excitation Spectrum

$Eu(ttfa)_3$ in S/A, $1.6 \times 10^{20}\,cm^{-3}$, Emission Via the $^5D_0 \to {}^7F_2$ Relaxation

Intensity (Arbitrary) vs. Wavelength (nm). Labels: Ligand-Metal Energy Transfer Band; $^7F_0 \to {}^5D_2$; $^7F_0 \to {}^5D_1$; $^7F_0 \to {}^5D_0$.
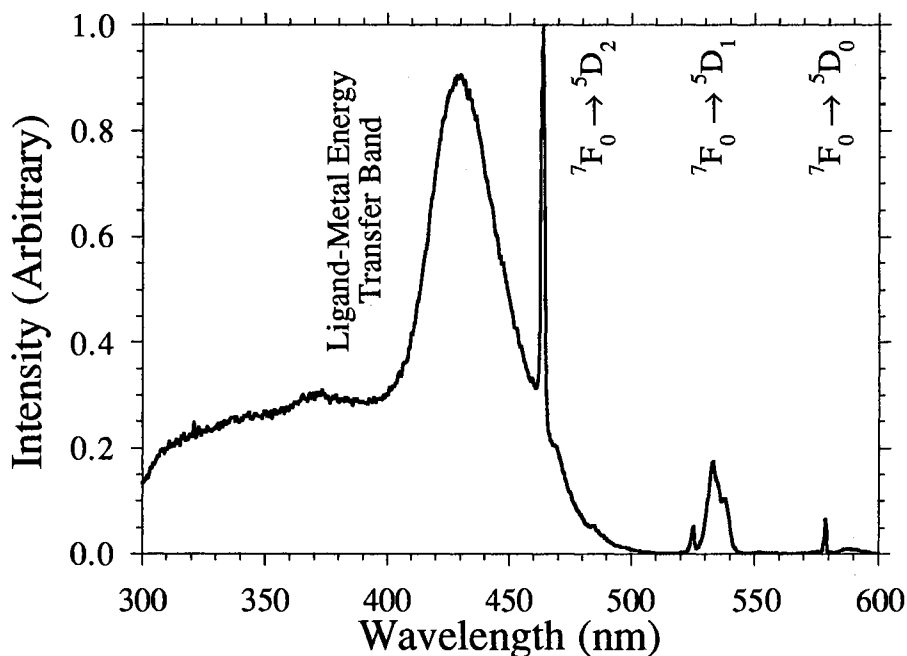
xerogels. In contrast, the position of the LMET peak was observed to have a strong concentration dependence in both hosts. There was a clearly resolved hypsochromic (blue) shift of the peak with decreasing $Eu(ttfa)_3$ concentration, e.g. from 430 nm at 1.6×10^{20} cm^{-3} (270 mM) to 395 nm at 1.5×10^{18} cm^{-3} (2.5 mM).

Intense luminescence via excitation of the LMET peak was found to predominate at the lower dopant concentrations. At the highest concentrations ($N \geq 10^{20}$ cm^{-3} or 170 mM), however, the amplitude of the Eu^{3+} $^7F_0 \to {}^5D_2$ excitation peak surpassed that of the LMET peak. The spectrum shown in Figure 3-3 highlights one of the notable features of the rare earth complex luminophores. The ligand imparts a very broad, intense excitation band, leading to emission from the complexed europium(III) ion. Thus, these species may be efficiently pumped by broad-band sources such as flashlamps. The excitation efficiency of comparable inorganic europium(III) salts, such as $EuCl_3$, is substantially lower (by at least two decades) when using broad-band pump schemes.

Figures 3-4 and 3-5 show the quantum efficiencies of $Eu(ttfa)_3$ in S/A gel and silica gel hosts over three decades of concentration. The samples were excited at the Eu^{3+} $^7F_0 \rightarrow {}^5D_2$ peak (464 nm) and at the LMET peak (390–430 nm), respectively. The starting dopant concentrations in the initial sol were 1.0×10^{-3}, 10^{-2}, and 10^{-1} M, corresponding to number densities 6.0×10^{17}, 10^{18}, and 10^{19} cm^{-3}, respectively. The final dopant number densities in dried gel were 1.5×10^{18}, 1.7×10^{19}, and 1.6×10^{20} cm^{-3} (2.5, 28, and 270 mM) for S/A ormosil and 2.2×10^{18}, 1.9×10^{19}, and 1.9×10^{20} cm^{-3} (3.7, 32, and 320 mM) for silica.

In the S/A matrix (samples S/A 17, 18, and 19), the quantum efficiency under direct pumping of the Eu^{3+} excitation peak decreases as concentration increases (Fig. 3-4), but the efficiency of the LMET peak remains nearly constant (Fig. 3-5). Similar trends were observed in both sol and gel states. The decrease in quantum efficiency with elevated dopant levels, as seen for S/A samples in the ormosil host, is consistent with a tendency for luminescence quenching by a cross-relaxation mechanism between adjacent europium(III) species. In the silica matrix, however, the efficiency of both excitation peaks was seen to increase with increasing dopant concentration. This phenomenon is counter to the previously described trend and therefore suggests a fundamentally different type of ligand–matrix interaction. At the lower concentrations, the quantum efficiency of $Eu(ttfa)_3$ in the S/A host is clearly greater than that of $Eu(ttfa)_3$ in the silica host for both excitations; the two hosts approach parity at the highest concentration. One potential mechanism by which such a phenomenon might occur involves matrix modification by the dopant species. Gellation times for the silica samples were noted to be shortened as more dopant was added, and it is postulated that elevated dopant densities resulted in changes to the basic gel microstructure. Such changes to the gel structure or overall density would be expected to result in modification of vibronic coupling events through the gel network, thermal conductivity, local dielectric constant, etc. Unfortunately,

Figure 3-4: Quantum Efficiencies I

Excitation at the Europium $^7F_0 \rightarrow ^5D_2$ Transition
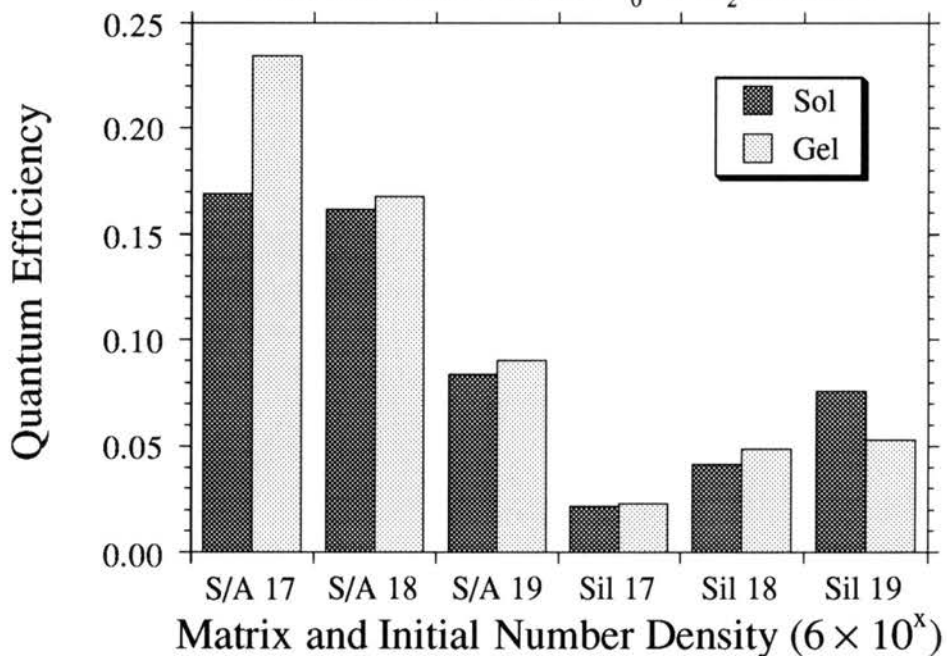
Figure 3-5: Quantum Efficiencies II

Excitation at the Ligand-to-Metal Energy Transfer Band
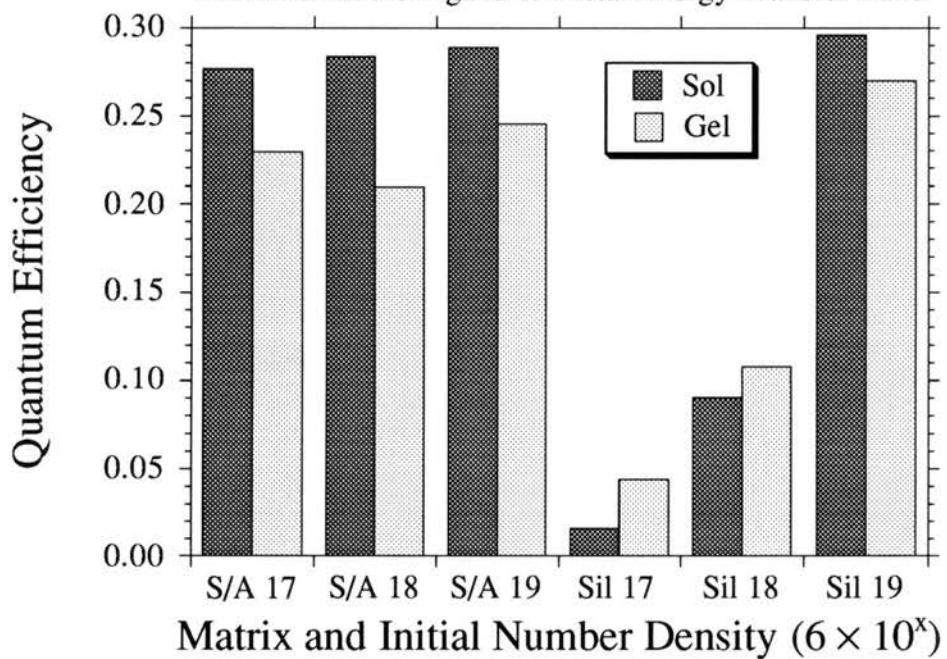
attempts to verify this hypothesis by IR and NMR spectroscopy proved unsuccessful (see also Appendix C).

The corresponding spontaneous-emission cross-sections (σ_{SpE}) are presented in Figures 3-6 and 3-7, respectively. This quantity measures the emitting cross-sectional area per atom and is directly related to the absorption cross-section (σ_{Abs}) (the absorbing area per atom) through the quantum efficiency (Q):

$$(1) \qquad \sigma_{SpE} = Q\sigma_{Abs}$$

As dopant concentrations increase, there is a concomitant tendency for molecules such as Eu(ttfa)$_3$ to oligomerize, thereby resulting in lower absorption cross-sections. As the stimulated-emission cross-section is a function of both quantum efficiency and absorption cross-section, it is a sensitive measure of the combined effects of concentration-dependent cross-relaxation events as well as oligomerization and/or phase separation.

In the S/A matrix, the spontaneous-emission cross-section decreases as concentration increases under both sets of excitation conditions, in the sol and gel states. This behavior is consistent with lower quantum efficiencies and absorption cross-sections. In the silica matrix, the emission cross-section due to excitation of the LMET band (Fig. 3-7) also generally conforms to this trend. The emission cross-section from excitation of the Eu^{3+} transition (Fig. 3-6) increases with increasing dopant concentration. This is due, primarily, to the increase in quantum efficiency as previously described.

64

Figure 3-6: Spontaneous Emission Cross-Sections I

Excitation at the Europium $^7F_0 \rightarrow {}^5D_2$ Transition
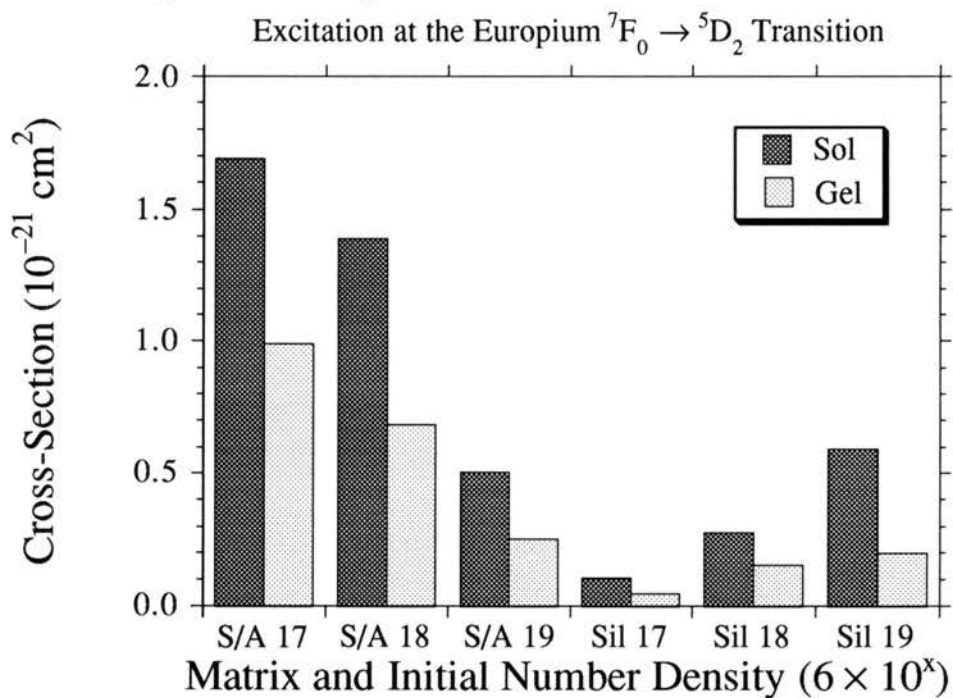
Figure 3-7: Spontaneous Emission Cross-Sections II

Excitation at the Ligand-to-Metal Energy Transfer Band
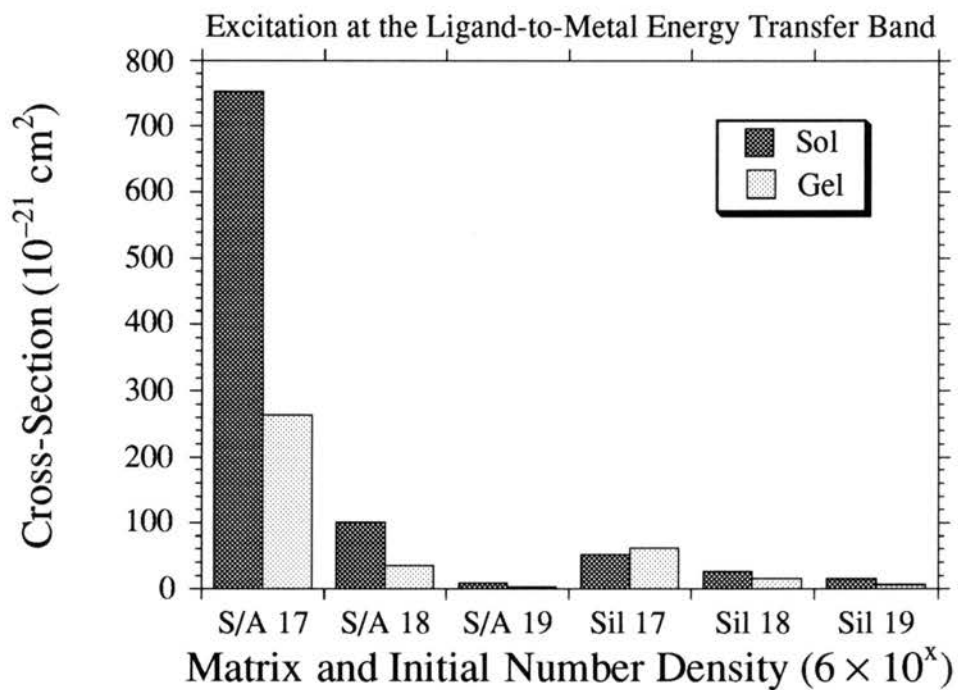
IV. Conclusions

The presence of dopant–dopant interactions may be inferred because both quantum efficiency and spontaneous-emission cross-section are functions of concentration for all the samples in the study. The quenching observed in the S/A ormosil materials with elevated dopant levels is presumably a form of concentration quenching, due to cross-relaxation between dopant molecules. The increase in quantum efficiency for doped silica gels may be due to some ligand–matrix interactions which result in a modified gel structure as previously described. Another possibility is that changes in the silica gel microstructure at high dopant concentrations make the radiative transitions in the europium(III) complex more allowed, due to changes in symmetry, and therefore more efficient. Since the optical spectroscopy techniques used in this experiment do not answer this question unequivocally and IR and NMR techniques provided no useful information, different techniques like high-resolution microscopy might provide some of the answers.

The relatively high quantum efficiencies and spontaneous emission cross-sections exhibited by Eu(ttfa)$_3$ in both matrices make them promising candidates for use as optical sources. However, because the S/A ormosil gel has improved mechanical properties and reduced quenching at lower dopant concentrations when compared to silica gel, it appears to be the preferable host matrix for Eu(ttfa)$_3$.

V. References

1. A. Lempicki and H. Samelson, *Phys. Lett.* **4** (1963) 133.

2. (a) C. A. Capozzi and L. D. Pye, in Proceedings of SPIE 970 (Bellingham, WA: Society of Photo-Optical Instrumentation Engineers, 1988), p. 135; (b) H. Schmidt and B. Seiferling, in C. J. Brinker, D. E. Clark, and D. R. Ulrich, *Better Ceramics Through Chemistry II,* Materials Research Society Symposium Proceedings 73 (Pittsburgh, PA: Materials Research Society, 1986), p. 739.

3. J. G. White, *Inorg. Chim. Acta* **16** (1976) 159.

4. (a) N. de la Rosa-Fox, L. Esquivias, and J. Zarzycki, *Diffusion and Defect Data* **53–54** (1987) 363. (b) L. Esquivias and J. Zarzycki, in J. D. Mackenzie and D. R. Ulrich, *Ultrastructure Processing of Advanced Ceramics* (New York: John Wiley & Sons, Inc., 1988), p. 255.

5. G. H. Dieke and H. M. Crosswhite, *Appl. Opt.* **2** (1963) 675.

6. N. E. Wolff and R. J. Pressley, *Appl. Phys. Lett.* **2** (1963) 152.

CHAPTER 4

LUMINESCENCE BEHAVIOR OF INORGANIC AND METALORGANIC

EUROPIUM(III) DOPANTS INCORPORATED INTO SILICA AND

EPOXIDE ORMOSIL SOL–GEL-DERIVED HOSTS*

I. Introduction

In Chapters 2 and 3, the incorporation of europium(III) thenoyltrifluoroacetonate

complexes into silica and acrylate–silica organically modified silicate *(ormosil)* gel hosts

via the sol–gel method was described. These dopants are of interest for use in solution-

derived matrices as they have been shown to exhibit intense fluorescence and laser emis-

sion in solution.[1] Similarly, gels doped with the rare earth metalorganic complex were

previously shown to possess intense fluorescence characteristics, especially with respect

to comparable gels doped with inorganic europium(III) salts such as the chloride (Ch. 2–

3, Refs. 2–4) or nitrate (Ref. 5).

Silica xerogels (but not dense glasses or crystals) tend to be mechanically fragile,

which largely precludes optical shaping and polishing operations. Ormosil materials, in

contrast, have improved mechanical stability and are thus compatible with various optical

grinding and polishing operations.[6–7] Thus, there is interest in the investigation of addi-

tional organoeuropium complex-doped gel systems, as novel optical media may be

prepared in useful embodiments via this route. The study of alternate host matrix com-

positions is especially salient if guest–host interactions are found to make an important

contribution to the overall luminescence behavior of these systems, as the local chemical

environment of the matrix is readily modified within ormosil media. The research

---

presented herein extends the earlier work on the silica and acrylate ormosil gels to include an epoxide–ethylene glycol or "epoxy–diol" ormosil composition. The work presented in this Chapter is focused on the assessment of dopant chemistry, dopant concentration, and dopant–matrix interaction effects in rare earth-doped silicate and modified silicate materials.

II. Experimental Methods

The tris(4,4,4-trifluoro-1-(2'-thienyl)-1,3-butanedionato-O,O')europium(III) tri-hydrate, Eu(ttfa)$_3 \cdot 3H_2O$, called Eu(ttfa)$_3$, was obtained from Kodak Chemicals and used without further purification or characterization. The structure of the complex was presented in Figure 3-1.[8]

The epoxy–diol (ED) ormosil host *(matrix E)* was prepared under mildly acidic conditions using tetramethoxysilane (TMOS, Fluka Chemie AG), 3-glycidoxypropyltri-methoxysilane (GPTMS, Aldrich Chemical Company), ethylene glycol (Fisher Scientific Company), and 0.040 M HCl in water as previously described.[9–10] Molar ratios of 4.5 H_2O : 1 TMOS : 1 GPTMS : 1 ethylene glycol were employed. A typical synthesis involved reacting 15.7 mL of TMOS and 6.7 mL of 0.040 M HCl in the sonicator until it forms a sol (usually within 5 minutes), then adding 23.6 mL of GPTMS, 1.9 mL of additional 0.040 M HCl, and 5.9 mL of ethylene glycol to the mixture. The resulting sol was allowed to react in the sonicator for 10–20 minutes and then aged overnight before use. Silica *(matrix S)* specimens were prepared as described in the preceding Chapters. Doping was achieved by the addition of aliquots of EuCl$_3$ or Eu(ttfa)$_3$ dissolved in methanol at five times the target concentration, generally 1–10 mM. The resulting solutions were cast into transparent polystyrene cuvettes and kept in covered containers at room temperature until the onset of gellation. Aging and drying were allowed to proceed under ambient conditions over a period of several weeks. ED ormosil and silica

specimens in this series of experiments were found to retain approximately 60% and 30%, respectively, of their initial volumes, producing an increase in dopant concentration in the xerogel by factors of 1.7 and 3.3 over the sol concentrations, respectively. For purposes of direct comparison of matrix performance, solid-state samples having xerogel number densities (N) of approximately 2×10^{19} cm^{-3} were selected from a pair of concentration series for this study.

Luminescence (emission and excitation) spectra were measured using a Spex Industries Model F112 spectrofluorimeter. Absorption spectra were determined using a Cary 5 spectrophotometer. All spectra were corrected for instrumental response by the Spex software. Fluorescence lifetimes were measured by exciting the samples, while positioned in the spectrofluorimeter sample chamber, with radiation from a Lambda Physik LPD 500 fs dye laser (pumped by a Lambda Physik LEXtra 200 excimer laser oscillating at 308 nm). Two laser excitation wavelengths were utilized: 441 nm and 543 nm. Temporally-resolved luminescence transients were characterized through the use of a Tektronix model 2440 digital storage oscilloscope (500 MHz bandwidth) in conjunction with the spectrofluorimeter's R928 PMT output. Relative quantum efficiencies were calculated by the reference technique described in Chapter 2.

III. Discussion of Results

Figures 4-1 through 4-4 show representative emission spectra for EuCl$_3$ and Eu(ttfa)$_3$ in the different host matrices. Relative emission intensities have been normalized with respect to that of Eu(ttfa)$_3$ in the epoxy–diol ormosil host, Eu(ttfa)$_3$:E, excited at 408 nm (Fig. 4-4). The spectra shown in Figures 4-1 and 4-2 represent emission upon excitation at 464 nm, corresponding to the $^7F_0 \rightarrow {}^5D_2$ absorptive transition of Eu^{3+}; this wavelength was chosen because it lies outside the main absorption band of the (ttfa)$^-$ ligand, thereby facilitating the direct comparison of europium-only transitions as a function

of the local chemical environment. In Figures 4-3 and 4-4, the samples were excited at higher photon energies; $EuCl_3$ (Fig. 4-4) was excited at 393 nm, corresponding to the "E" band of Dieke and Crosswhite[11] (later designated $^7F_0 \rightarrow {}^5L_6$)[12] which was found to be the most intense excitation band of the inorganic salt. The emission spectrum of $Eu(ttfa)_3$ (Fig. 4-4) was recorded using an excitation wavelength (λ_{ex}) of 408 nm, which corresponds to the maximum of the organo-rare earth complex excitation peak. This decay mechanism is associated with excitation of the organic ligand and subsequent radiative relaxation from the incorporated Eu^{3+} ion following ligand-to-metal energy transfer (LMET).[1, 13] This emission is the most intense observed in the present study and has therefore been assigned the value of 1.00 normalized relative emission intensity units. The 393-nm and 408-nm excitation wavelengths were selected so that maximum luminescence intensities could be quantified as a function of ligand and matrix interactions. In all cases the observable emission peaks result from relaxation out of the $^5D_0$ excited state of Eu^{3+} to the first five levels of the ^7F ground manifold; the $^5D_0 \rightarrow {}^7F_2$ emission is the one usually associated with laser behavior in Eu^{3+}-based systems.[11]

Changes in the local chemical environment, either by variation of the ligand or gel matrix composition, were found to leave the essential spectral features of europium(III) essentially unchanged as a function of the local conditions, although distinct perturbations to the radiative branching ratios were observed. There were, however, pronounced chemistry-related effects on the relative emission intensity characteristics. Under a given set of conditions (matrix composition and excitation band), the $Eu(ttfa)_3$ complex's emission was found to be at least 30 and as much as 2000 times more intense than that of $EuCl_3$ in equivalent matrices (compare Figure 4-1 with Figure 4-2 and Figure 4-3 with Figure 4-4).

Figure 4-1: EuCl₃ Emission Spectra I

EuCl$_3$, λ_{ex} = 464 nm

E: N = 2.2 × 10^{19} cm^{-3}

S: N = 2.1 × 10^{19} cm^{-3}

All transitions marked are emissions from the $^5D_0$ excited state.

Matrix E

Matrix S × 10
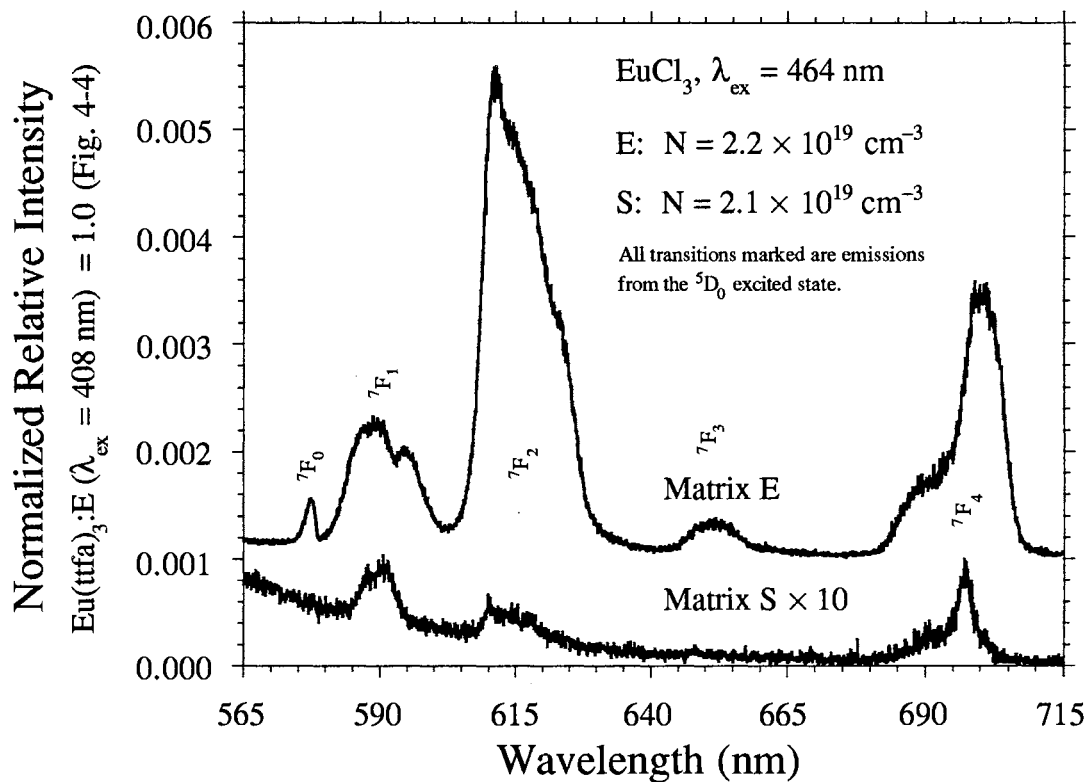
FIGURE 4-1: Fluorescence emission spectrum of EuCl$_3$, 2.2 × 10^{19} cm^{-3} in epoxy–diol ormosil (E) and 2.1 × 10^{19} cm^{-3} in silica (S) gels, excited at the $^7F_0 \rightarrow {}^5D_2$ transition of Eu^{3+} near 464 nm. Spectrum E is offset 0.001 normalized relative intensity units. All emission spectra in Figures 4-1–4-4 are normalized to Eu(ttfa)$_3$ in matrix E, excited at 408 nm (Fig. 4-4).

Figure 4-2: Eu(ttfa)₃ Emission Spectra I

FIGURE 4-2: Fluorescence emission spectrum of Eu(ttfa)₃, 2.2×10^{19} cm^{-3} in matrix E and 2.1×10^{19} cm^{-3} in matrix S, excited at the $^7F_0 \rightarrow {}^5D_2$ transition of Eu^{3+} near 464 nm. Spectrum E is offset 0.2 normalized relative intensity units.

Figure 4-3: EuCl₃ Emission Spectra II

FIGURE 4-3: Fluorescence emission spectrum of EuCl₃, 2.2×10^{19} cm⁻³ in matrix E and 2.1×10^{19} cm⁻³ in matrix S, excited at the "E" band or $^7F_0 \rightarrow ^5L_6$ transition of Eu³⁺ near 393 nm. Spectrum E is offset 0.005 normalized relative intensity units.

Figure 4-4: Eu(ttfa)₃ Emission Spectra II

Eu(ttfa)$_3$, λ_{ex} = 408 nm

E: N = 2.2 × 10^{19} cm^{-3}

S: N = 2.1 × 10^{19} cm^{-3}

All transitions marked are emissions from the $^5D_0$ excited state.

$^7F_0$ $^7F_1$ $^7F_2$ $^7F_3$ $^7F_4$

Matrix E

Matrix S

FIGURE 4-4: Fluorescence emission spectrum of Eu(ttfa)₃, 2.2×10^{19} cm^{-3} in matrix E and 2.1×10^{19} cm^{-3} in matrix S, excited at the maximum value of the ligand-to-metal energy transfer (LMET) band, which is located near 408 nm at these particular number densities. Spectrum E is offset 0.2 normalized relative intensity units.

Regarding matrix effects, Eu(ttfa)$_3$ luminescence was observed to be at least twice as intense in the ormosil matrix as in the silica matrix (see Figures 4-2 and 4-4). This indicates that the denser and less porous, organically modified silicate host tends to promote radiative decay from the metalorganic complex to a greater extent than when it is entrapped in a lower density, purely inorganic host; this was observed, however, to be a relatively small effect. One possible explanation for this effect is that in a medium with a smaller pore size, intracavity pressures are higher and ligand–matrix interactions are more prevalent; either could modify the conditions for ligand-to-metal energy transfer and thereby promote fluorescence in the ormosil relative to silica. The radiative intensity of EuCl$_3$ was found to be much more heavily influenced by matrix effects, as shown in Figures 4-1 and 4-3. The relative luminescence intensities of the salt increased by factors ranging from 25 to nearly 100 upon incorporation into the ormosil host, a much greater difference than that observed in the case of the metalorganic complex. This discrepancy has been attributed to a fundamental difference between the guest–host interactions associated with the two dopant species. Eu(ttfa)$_3$, by nature of its bulky, shielding ligands, is substantially less sensitive to the local environment than EuCl$_3$, whose free Eu^{3+} ion may interact to a much greater extent with the surrounding matrix. In the case of EuCl$_3$:S, there is extensive quenching which is presumably due to the presence of abundant hydroxyl species (*i.e.* $\equiv$SiOH, ROH, H$_2$O). EuCl$_3$:E, however, is substantially less quenched, despite the large hydroxyl activity in such materials. It appears that chelation between the Eu^{3+} and select groups of the epoxy–diol ormosil may make an important contribution in this system. It is likely that interactions with α,β-diol or other α,β-dioxy groups, present in the matrix E medium, may be responsible for such behavior. Similar effects were not observed in the case of EuCl$_3$-doped acrylate ormosil hosts (Ch. 3), indicating that an inherently different dopant–matrix interaction exists in the EuCl$_3$:E material.

Figures 4-5 and 4-6 show the excitation spectra of $EuCl_3$ and $Eu(ttfa)_3$ associated with emission from the $^5D_0 \rightarrow {}^7F_2$ transition of Eu^{3+} (λ_{em} = 612 nm). In contrast to Figures 4-1–4-4, which indicate that the Eu^{3+} emission processes in the two dopant species are fundamentally similar (although again subject to perturbations in the branching ratios), Figures 4-5 and 4-6 indicate that the excitation processes which populate the Eu^{3+} $^5D_0$ level in the two dopants are distinctly different at wavelengths shorter than 450 nm. The broad, strong excitation band of $Eu(ttfa)_3$ has been found to correspond to the red-most edge of the complex's intense ligand absorption band, which is shown in the case of a thin film in Figure 4-7. The absorption band of the thin film contains at least two components, centered at 341 nm and approximately 350 nm, but in bulk samples the red edge extends out to well beyond 400 nm. Europium(III) fluorescence from excitation of $Eu(ttfa)_3$ in this region reportedly originates from the ligand-to-metal energy transfer (LMET) mechanism.[1, 8] The LMET band nearly obscures Eu^{3+} features in this region, including the strong $^7F_0 \rightarrow {}^5L_6$ transition (393 nm) clearly visible in the case of $EuCl_3$-doped gels (Fig. 4-5). Outside this region, however, the $^7F_0 \rightarrow {}^5D_{0-2}$ Eu^{3+} features are visible and subject to similar matrix effects—both dopants are clearly more luminescent in the epoxy–diol ormosil than in the silica gel. Significantly, the $Eu(ttfa)_3$ spectra (Fig. 4-6) show that, as noted above, matrix composition affects overall excitation intensity but causes little or no perturbation to spectral features as the $(ttfa)^-$ ligands largely shield the Eu^{3+} ion from the surrounding matrix.

Conversely, the $EuCl_3$ spectra (Fig. 4-5) show that relatively free Eu^{3+} ions can interact extensively with the host matrix. In the $EuCl_3$:S sample spectrum, all the observable features correspond to transitions from the $^7F_0$ ground state to well-documented Eu^{3+} energy levels,[11–12] most notably the $^5L_6$ "E"-band. The $EuCl_3$:E sample spectrum also shows the predominant $^7F_0 \rightarrow {}^5D_{0-3}$ and $^7F_0 \rightarrow {}^5L_6$ transitions, with an increased intensity indicative of reduced quenching effects. More interesting, however, is the appearance of a new, broad, intense excitation band centered at approximately 350 nm. This

band resembles the LMET band of $Eu(ttfa)_3$, yet does not completely overwhelm the sharp Eu^{3+} $f \rightarrow f$ transition features; in particular, the $^5D_4$ and $^5H_6$ peaks are still discernible. It appears that the epoxy–diol ormosil matrix either (a) transfers energy to the Eu^{3+} $^5D_0$ level by LMET (or some related mechanism) or (b) it activates Eu^{3+} levels in this region (330–390 nm) which are not normally associated with transitions from the ground state (i.e., $^5G_{2-3}$, $^5L_{7-10}$, and $^5H_{3-5, 7}$). In either case, as indicated by emission spectroscopy, chelation between Eu^{3+} and oxygen-containing groups on the side chains of matrix E is a probable cause of this new excitation band.

Table 4-1 displays the optical parameters of quantum efficiency, relative emission intensity, and fluorescence lifetime for the four dopant–matrix compositions. Each composition was excited at the Eu^{3+} $^7F_0 \rightarrow {}^5D_2$ peak (464 nm) and at two higher energies (408 and 393 nm), as before. Quantum efficiency values indicate that both dopants are significantly less quenched in matrix E than in matrix S, as expected from the luminescence spectroscopy data. The quantum efficiencies of $Eu(ttfa)_3$:E were found to be quite high for materials of this sort, and appear to have some promise in terms of potential optical source applications.

A description of the integrated emission intensity values has been included as they more effectively quantify the radiance or "brightness" of the specimens. Such comparisons are particularly useful in the case, for example, of materials to be used as phosphors. When excited at 464 nm, where the only differences in energy absorption between $Eu(ttfa)_3$ and $EuCl_3$ arise from ligand modification of the immediate environment of Eu^{3+}, $Eu(ttfa)_3$:E specimens had 7 times greater integrated intensity values than $Eu(ttfa)_3$:S samples, and $EuCl_3$:E materials were found to have integrated emission intensity values which were 16 times more intense than $EuCl_3$:S materials. Relative to ligation effects, the $Eu(ttfa)_3$:E specimen had an integrated emission intensity which was 41 times more intense than the comparable $EuCl_3$:E system. Thus, quenching behavior is much less predominant in the epoxy–diol ormosil host.

Figure 4-5: EuCl₃ Excitation Spectra
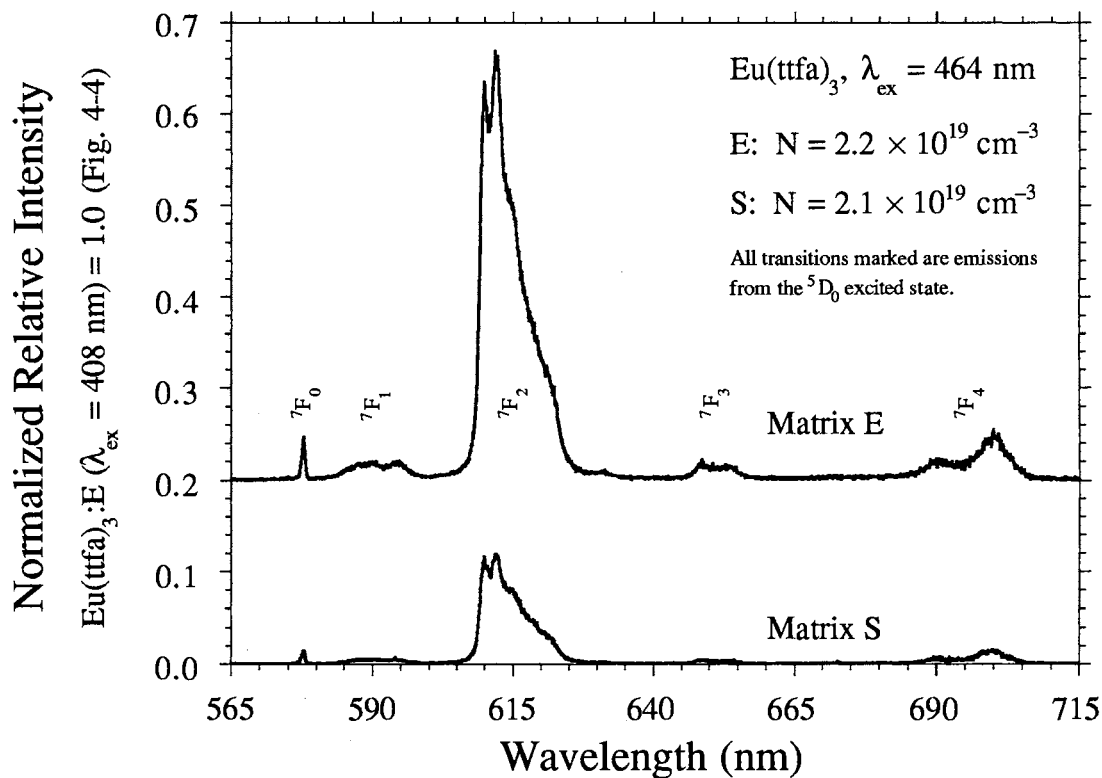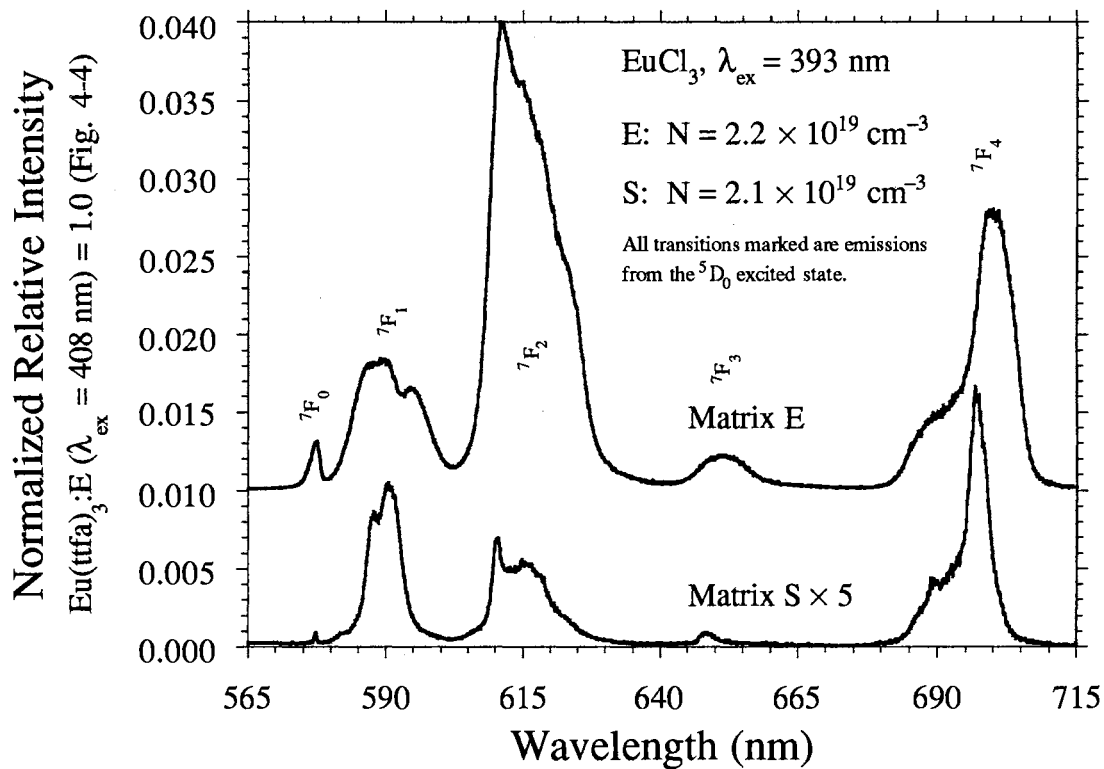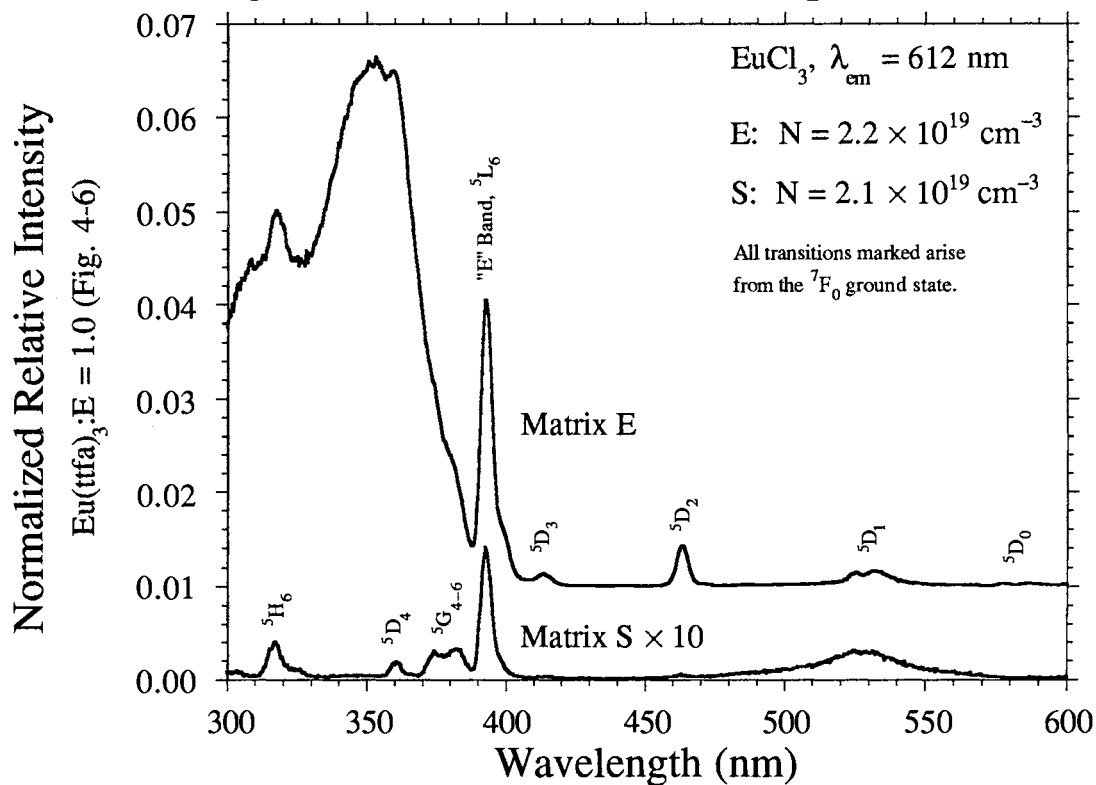

FIGURE 4-5: Fluorescence excitation spectrum of EuCl$_3$, 2.2×10^{19} cm^{-3} in matrix E and 2.1×10^{19} cm^{-3} in matrix S, viewed at the $^5D_0 \rightarrow {}^7F_2$ transition of Eu^{3+} near 612 nm. Spectrum E is offset 0.01 normalized relative intensity units. All excitation spectra in Figures 4-5–4-6 are normalized to Eu(ttfa)$_3$ in matrix E (Fig. 4-6).
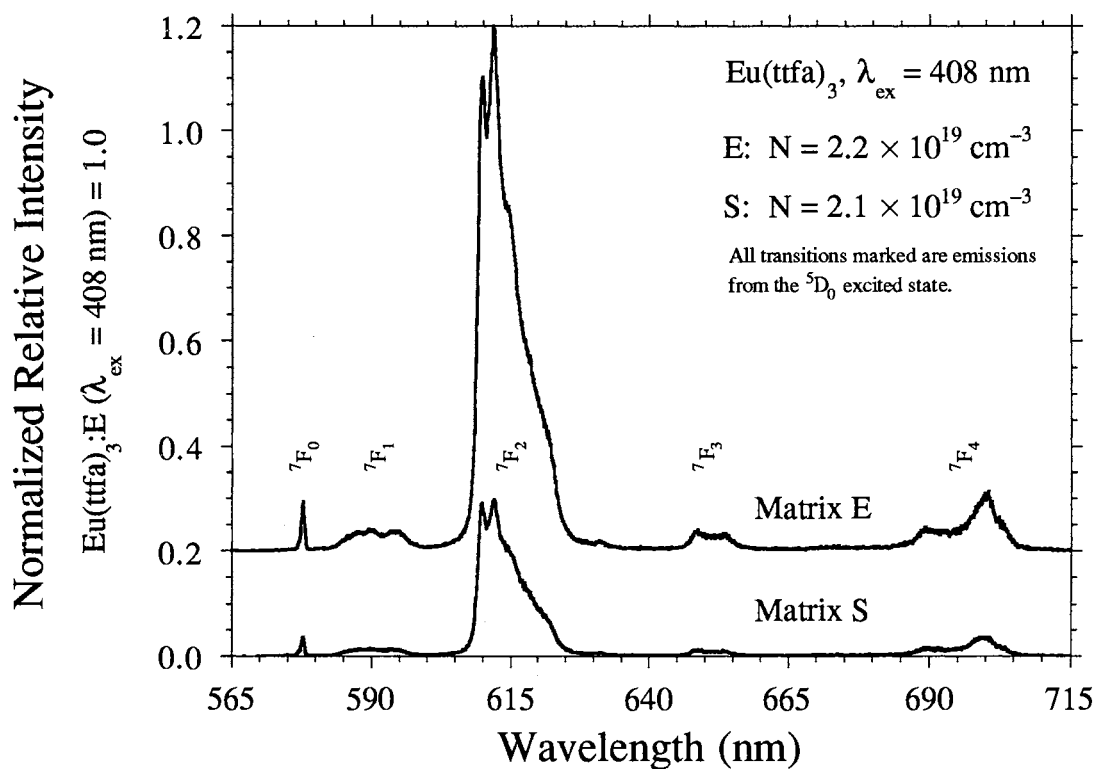
Figure 4-6: Eu(ttfa)₃ Excitation Spectra
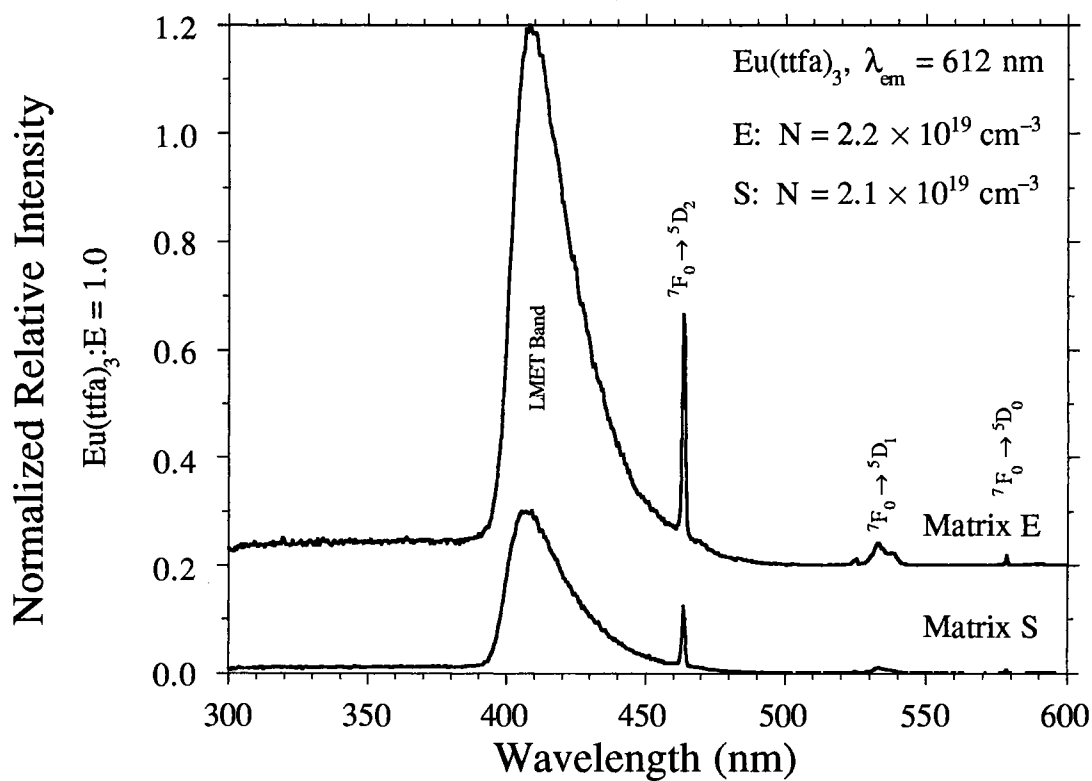
FIGURE 4-6: Fluorescence excitation spectrum of Eu(ttfa)3, 2.2×10^{19} cm^{-3} in matrix E and 2.1×10^{19} cm^{-3} in matrix S, viewed at the $^5D_0 \rightarrow {}^7F_2$ transition of Eu^{3+} near 612 nm. Spectrum E is offset 0.2 normalized relative intensity units.

Figure 4-7: Eu(ttfa)₃ Absorption Spectrum
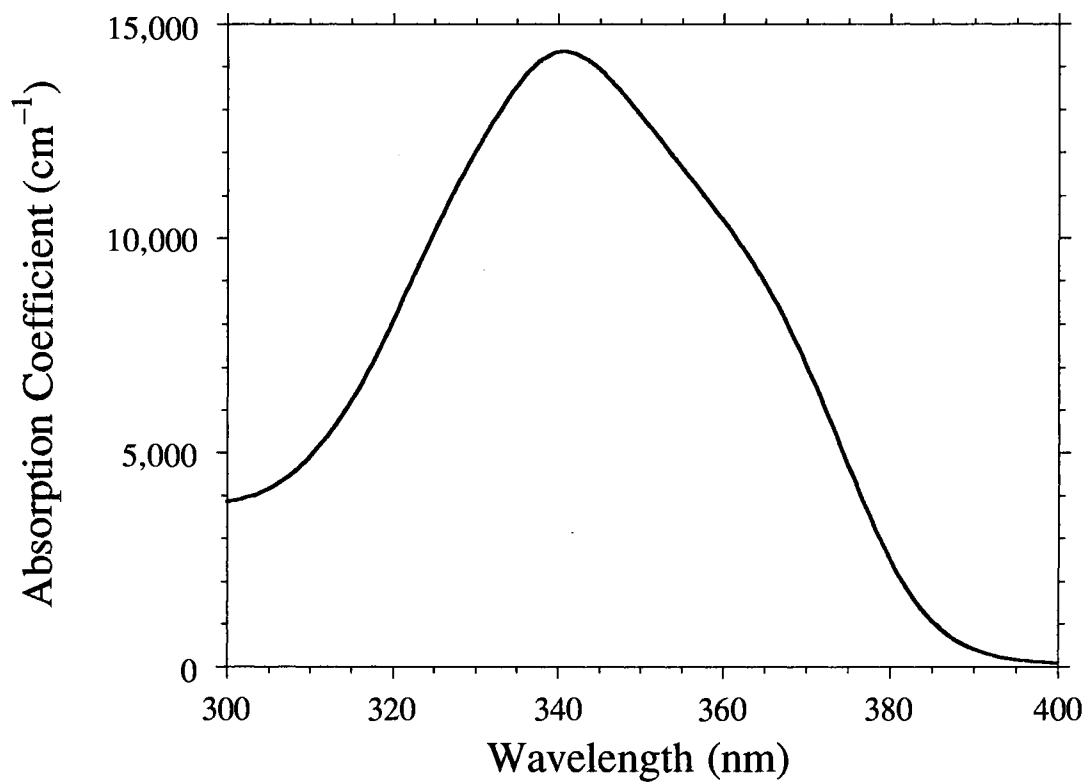
FIGURE 4-7: Absorption spectrum of Eu(ttfa)$_3$, 2.2×10^{19} cm^{-3} in matrix E. The specimen was cast on a glass slide as a two-layer thin film of approximately 1 μm total thickness.

TABLE 4-1

	EuCl$_3$:E	EuCl$_3$:S	Eu(ttfa)$_3$:E	Eu(ttfa)$_3$:S
Number Density (cm^{-3})	2.2×10^{19}	2.1×10^{19}	2.2×10^{19}	2.1×10^{19}
Quantum Efficiency, λ_{ex} 464 nm	10.6%	7.6%	46.3%	16.4%
Quantum Efficiency, λ_{ex} 393 or 408 nm	11.0%	1.2%	41.1%	12.3%
Relative Integrated Emission Intensity, λ_{ex} 464 nm	1.15×10^{-2}	7.09×10^{-4}	4.75×10^{-1}	6.72×10^{-2}
Relative Integrated Emission Intensity, λ_{ex} 393 or 408 nm	7.48×10^{-2}	6.04×10^{-3}	1.00×10^{0}	3.01×10^{-1}
Fluorescence Lifetime (μs)	710	116	290	180
Fluorescence Rise Time (ns)			420	310

TABLE 4-1: Optical parameters for all four dopant–matrix compositions. Quantum efficiency and normalized relative integrated emission intensity each have two excitation values, the first at the $^7F_0 \rightarrow {}^5D_2$ transition of Eu^{3+} near 464 nm, and the second at the "E" band or $^7F_0 \rightarrow {}^5L_6$ transition of Eu^{3+} near 393 nm for EuCl$_3$ or at the maximum value of the LMET band ($\approx$408 nm) for Eu(ttfa)$_3$. The fluorescence lifetimes and rise times of the $^5D_0 \rightarrow {}^7F_2$ emission were measured by laser excitation. EuCl$_3$ was excited at 543 nm, roughly corresponding to the relatively weak $^7F_0 \rightarrow {}^5D_1$ transition of Eu^{3+}. Eu(ttfa)$_3$ was excited at 441 nm, which lies just within the red wing of the LMET band.

The fluorescence lifetime of the $^5D_0 \rightarrow {}^7F_2$ relaxation event was also studied in the four dopant–matrix systems. The lifetime of EuCl$_3$ in matrix S, 116 µs, is very close to that reported for crystalline EuCl$_3$·6H$_2$O, 122 µs.[14] In matrix E, however, the lifetime was observed to increase by a factor of 6, up to a value of 710 µs, indicating a significantly different chemical environment for the Eu^{3+} ion. This increase must be associated with the elimination of one or more pathways for nonradiative decay events out of the $^5D_0$ state. A lifetime of 710 µs is, in fact, comparable to those reported for similar concentrations of Eu(ClO$_4$)$_3$ (775 µs) and Eu(NO$_3$)$_3$ (680 µs) in acetonitrile (CH$_3$CN),[15] a solvent which lacks the hydroxyl groups which are the most probable quenching agents in aqueous and silicate environments. The lifetime of Eu(ttfa)$_3$ does increase in matrix E relative to matrix S, but the effect is not as dramatic as for EuCl$_3$. This indicates that the increase is presumably due to the overall reduced level of quenching in matrix E rather than a drastic change in Eu^{3+} environment. This is consistent with other observations indicating that the (ttfa)$^-$ ligand effectively shields Eu^{3+} from the surrounding matrix.

IV. Conclusions

The luminescence behavior of EuCl$_3$ and a metalorganic complex, Eu(ttfa)$_3$, doped into sol–gel derived hosts have been studied. Comparisons between matrix- and ligand-associated interactions have been presented and compared with previously observed results using an acrylate ormosil. In both host matrices, Eu(ttfa)$_3$ exhibits higher quantum efficiencies and greater emission intensities than comparable EuCl$_3$-doped specimens. These increases are attained without significant changes to the fundamental features of the Eu^{3+} emission spectrum. Introduction of the LMET band, however, makes excitation via broad-band pump source a much more efficient method by which to excite Eu(ttfa)$_3$ than the comparable EuCl$_3$. These factors make Eu(ttfa)$_3$ an interesting candidate for use as an optical source.

Eu(ttfa)$_3$- and EuCl$_3$-doped epoxy–diol ormosil hosts featured clear spectroscopic differences with respect to silica systems. In the case of Eu(ttfa)$_3$, the most significant difference is the reduction in quenching interactions as demonstrated by increases in quantum efficiency, integrated intensity, and fluorescence lifetime. For EuCl$_3$, the preceding effects are augmented by the possible Eu^{3+} ligand-like modification which introduces a new excitation band, offering some of the characteristics noted for the fully complexed Eu(ttfa)$_3$. The anomalously long lifetime observed for the EuCl$_3$:E system is not well understood, and bears further study.

V. References

1. A. Lempicki and H. Samelson, *Phys. Lett.* **4** (1963) 133.

2. H. Mack, R. Reisfeld, and D. Avnir, *Chem. Phys. Lett.* **99** (1983) 238.

3. D. Levy, R. Reisfeld, and D. Avnir, *Chem. Phys. Lett.* **109** (1984) 593.

4. C. Sanchez, in *Sol-Gel Optics,* Proceedings of SPIE, v. 1328 (Bellingham, WA: Society of Photo-Optical Instrumentation Engineers, 1990), p. 40.

5. R. Campostrini, G. Carturan, M. Ferrari, M. Montagna, and O. Pilla, *J. Mater. Res.* **7** (1992) 745.

6. C. A. Capozzi and L. D. Pye, in Proceedings of SPIE v. 970 (Bellingham, WA: Society of Photo-Optical Instrumentation Engineers, 1988), p. 135.

7. H. Schmidt and B. Seiferling, in C. J. Brinker, D. E. Clark, and D. R. Ulrich, *Better Ceramics Through Chemistry II,* Materials Research Society Symposium Proceedings, v. 73 (Pittsburgh, PA: Materials Research Society, 1986), p. 739.

8. J. G. White, *Inorg. Chim. Acta* **16** (1976) 159.

9. (a) N. de la Rosa-Fox, L. Esquivias, and J. Zarzycki, *Diffusion and Defect Data* **53–54** (1987) 363. (b) L. Esquivias and J. Zarzycki, in J. D. Mackenzie and D. R. Ulrich, *Ultrastructure Processing of Advanced Ceramics* (New York: John Wiley & Sons, Inc., 1988), p. 255.

10. E. T. Knobbe, B. Dunn, P. D. Fuqua, and F. Nishida, *Appl. Opt.* **29** (1990) 2729.

11. G. H. Dieke and H. M. Crosswhite, *Appl. Opt.* **2** (1963) 675.

12. W. T. Carnall, P. R. Fields, and K. Rajnak, *J. Chem. Phys.* **49** (1968) 4412.

13. N. E. Wolff and R. J. Pressley, *Appl. Phys. Lett.* **2** (1963) 152.

14. J. Heber and K. H. Hellwege, in H. M. Crosswhite and H. W. Moos, *Optical Properties of Ions in Crystals* (New York, London, Sydney: Interscience Publishers Division of John Wiley & Sons, Inc., 1967), p. 457.

15. Y. Haas and G. Stein, *J. Phys. Chem.* **75** (1971) 3668.

CHAPTER 5

CONCENTRATION EFFECTS ON THE LUMINESCENCE

BEHAVIOR OF EUROPIUM(III) CHLORIDE- AND

ORGANOEUROPIUM-DOPED SILICATE GELS*

I. Introduction

The incorporation of tris(4,4,4-trifluoro-1-(2'-thienyl)-1,3-butanedionato-

O,O')europium(III), commonly referred to as europium(III) thenoyltrifluoroacetonate

(Eu(ttfa)$_3$), into silica and two different organically modified silicate *(ormosil)* gel hosts

via the sol–gel process has been described in the preceding Chapters. Europium(III) β-

diketonate complexes like Eu(ttfa)$_3$ are of interest for use in solution-derived gel hosts as

they have been shown to exhibit intense fluorescence and laser emission in protic solu-

tions.[1] Silica xerogels doped with this complex have demonstrated significantly

increased fluorescence intensities with respect to comparable gels doped with the inor-

ganic europium(III) chloride salt (Ch. 2). Unfortunately, the mechanical fragility of silica

xerogels frequently precludes the shaping and polishing operations necessary for optical

applications; in contrast, ormosil materials are more suitable for such operations.[2]

Observations of significant differences in the guest–host interactions present in the three

gel systems, presumably caused by the differences in chemical structure between pure

silica and the two ormosil xerogels, have been discussed in Chapters 3 and 4. With the

research presented herein, the earlier work on the silica, acrylate ormosil, and epoxide

ormosil gels doped with Eu(ttfa)$_3$ and EuCl$_3$ is extended to include concentration effects

---

86

in each matrix. This work has been done in order to characterize the luminescence behavior of Eu(ttfa)$_3$ in the solid-state host as a function of dopant concentration. Thus, dopant–matrix and dopant–dopant interactions have been characterized. Such studies are important for the potential development of these systems as photonic media, as in the case of phosphors or optical gain media.

II. Experimental Methods

Europium(III) chloride hexahydrate, EuCl$_3$•6H$_2$O, and tris(4,4,4-trifluoro-1-(2′-thienyl)-1,3-butanedionato-O,O′)europium(III) trihydrate, Eu(ttfa)$_3$•3H$_2$O, were obtained from Pfaltz & Bauer and Kodak Chemicals, respectively, and used without further purification or characterization. The structure of the metalorganic complex was previously presented as Figure 3-1.[3]

The silica *(matrix S),* acrylate ormosil *(matrix A),* and epoxide ormosil *(matrix E)* were prepared according to procedures described in the preceding Chapters.[4–5] Precursors used for the gels were tetramethoxysilane (TMOS, Fluka Chemie AG) and water containing 0.040 molar hydrochloric acid as a catalyst for silica (mole ratio 1 TMOS : 4 H$_2$O); TMOS, 3-(trimethoxysilyl)propyl methacrylate (TMSPM, Aldrich Chemical Company), methyl methacrylate (MMA, Aldrich), and 0.040 *M* HCl for acrylate ormosil (1 TMOS : 1 TMSPM : 1 MMA : 7 H$_2$O); and TMOS, 3-glycidoxypropyl-trimethoxysilane (GPTMS, Aldrich), ethylene glycol (Fisher Scientific Company), and water for epoxide ormosil (1 TMOS : 1 GPTMS : 1 (CH$_2$OH)$_2$: 4.5 H$_2$O). Acrylate ormosil, epoxide ormosil, and silica xerogel specimens were found to retain approximately 50%, 60%, and 30%, respectively, of their initial sol–gel solution volumes.

Luminescence (emission and excitation) spectra were measured using a Spex Industries Model F112 spectrofluorimeter. Absorption characteristics were determined using a Cary 5 spectrophotometer. Spectra were corrected for instrumental response by

the correction features in the Spex software. Fluorescence lifetimes were measured by exciting the samples, while positioned in the spectrofluorimeter sample chamber, with the radiation from a Lambda Physik LPD 500 fs dye laser (pumped by a Lambda Physik LEXtra 308-nm xenon chloride excimer laser) at 441 or 543 nm. Signal from the R928 PMT was temporally characterized using a Tektronix 2440 digital storage oscilloscope (500 MHz bandwidth). Relative quantum efficiencies were calculated by the methods described in Chapter 2.

III. Discussion of Results

The initial and final dopant concentrations of both $EuCl_3$ and $Eu(ttfa)_3$ in each matrix are shown in Table 5-1. Figure 5-1 shows representative emission spectra for $EuCl_3$ and $Eu(ttfa)_3$ in each of the three host matrices, with intensities normalized to that of $Eu(ttfa)_3$:A. The spectral intensities of $EuCl_3$-doped hosts have been increased by a factor of 40, as noted in the figure. Each specimen was optically pumped at the wavelength corresponding to the most intense excitation transition for the particular dopant compound. For $EuCl_3$, this is the "E" band[6] or $^7F_0 \rightarrow {}^5L_6$ transition[7] near 393 nm. As discussed in Chapters 3 and 4, for $Eu(ttfa)_3$, the absorption band which produces the maximum emission is due to ligand-to-metal energy transfer (LMET)[1, 8] and its position has been found to be a function of concentration (385 nm $\leq \lambda_{ex-max} \leq$ 430 nm). In all six cases the observable emission peaks result from relaxation out of the $^5D_0$ excited state of Eu^{3+} to the first five levels of its ^7F ground state manifold; the $^5D_0 \rightarrow {}^7F_2$ emission is the one usually associated with phosphorescence and/or laser behavior.[6]

Figure 5-2 shows the comparable excitation spectra associated with emission from the $^5D_0 \rightarrow {}^7F_2$ transition of Eu^{3+} near 612 nm. In the $EuCl_3$ samples, all spectral features except the broad band centered at 350 nm in $EuCl_3$:E correspond to classical Eu^{3+} energy levels.[6]

TABLE 5-1

Initial Sol Concentration (Molar)	Initial Sol Number Density (cm^{-3})	Final Number Density (cm^{-3}), Xerogel A	Final Number Density (cm^{-3}), Xerogel E	Final Number Density (cm^{-3}), Xerogel S
0.001	6.0×10^{17}	1.2×10^{18}	1.1×10^{18}	2.1×10^{18}
0.002	1.2×10^{18}	2.4×10^{18}	2.2×10^{18}	4.2×10^{18}
0.004	2.4×10^{18}	4.8×10^{18}	4.3×10^{18}	8.4×10^{18}
0.010	6.0×10^{18}	1.2×10^{19}	1.1×10^{19}	2.1×10^{19}
0.020	1.2×10^{19}	2.4×10^{19}	2.2×10^{19}	4.2×10^{19}
0.040	2.4×10^{19}	4.8×10^{19}	4.3×10^{19}	8.4×10^{19}
0.100	6.0×10^{19}	1.2×10^{20}	1.1×10^{20}	2.1×10^{20}

TABLE 5-1: Initial and final concentrations or dopant levels for both EuCl$_3$ and Eu(ttfa)$_3$.

Figures 5-3 and 5-4 show the quantum efficiencies (Q) of EuCl$_3$ and Eu(ttfa)$_3$ in the three host matrices, over three orders of dopant concentration magnitude. The specimens were excited at the same two wavelengths used in Figure 5-1, namely the $^7F_0 \to {}^5L_6$ band (393 nm) for EuCl$_3$ (Fig. 5-3) and the LMET peak maximum (385–430 nm) for Eu(ttfa)$_3$ (Fig. 5-4). Under ideal conditions, the quantum efficiency for this radiative transition would be independent of concentration at room temperature. It is observed, however, to decrease with increasing concentration in most real systems. This concentration quenching is usually caused by cross-relaxation between neighboring Eu^{3+} ions; it is somewhat reduced in complexes relative to uncomplexed ions because interionic separations are increased.[10] Figure 5-3 shows that the quantum efficiency behavior of EuCl$_3$ is nearly ideal within ~5% experimental error above 3×10^{18} cm^{-3}; that is, it is nearly independent of concentration. In contrast, the quantum efficiency behavior for Eu(ttfa)$_3$ (Fig. 5-4) is found to be highly concentration-dependent in all three matrices.

Emission Spectra

Excited at Eu^{3+} $^7F_0 \to {}^5L_6$ Band ($\approx$393 nm) for

$EuCl_3$ or LMET ($\approx$408 nm) for $Eu(ttfa)_3$
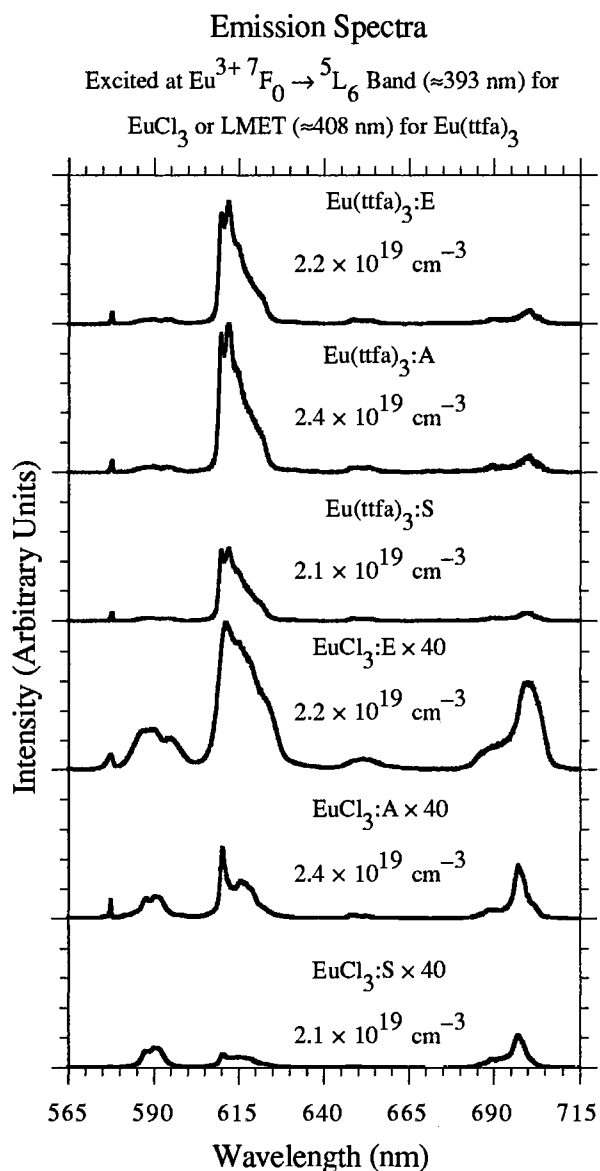
FIGURE 5-1: Sample fluorescence emission spectra of $Eu(ttfa)_3$ and $EuCl_3$ in epoxide ormosil (E), 2.2×10^{19} cm^{-3}; acrylate ormosil (A), 2.4×10^{19} cm^{-3}; and silica (S) gels, 2.1×10^{19} cm^{-3}; excited at the "E" band or $^7F_0 \to {}^5L_6$ transition near 393 nm for $EuCl_3$ or the maximum value of the LMET band for $Eu(ttfa)_3$ (see Table 5-2). The emission spectra are normalized to the intensity of $Eu(ttfa)_3$:A. The spectra of $EuCl_3$ are multiplied by 40 for clarity.

Excitation Spectra

Viewed at Eu^{3+} $^5D_0 \to {}^7F_2$ ($\approx$612 nm)

Eu(ttfa)$_3$:E

2.2×10^{19} cm^{-3}

Eu(ttfa)$_3$:A

2.4×10^{19} cm^{-3}

Eu(ttfa)$_3$:S

2.1×10^{19} cm^{-3}

EuCl$_3$:E × 20

2.2×10^{19} cm^{-3}

EuCl$_3$:A × 50

2.4×10^{19} cm^{-3}

EuCl$_3$:S × 200

2.1×10^{19} cm^{-3}

Intensity (Arbitrary Units)

Wavelength (nm)
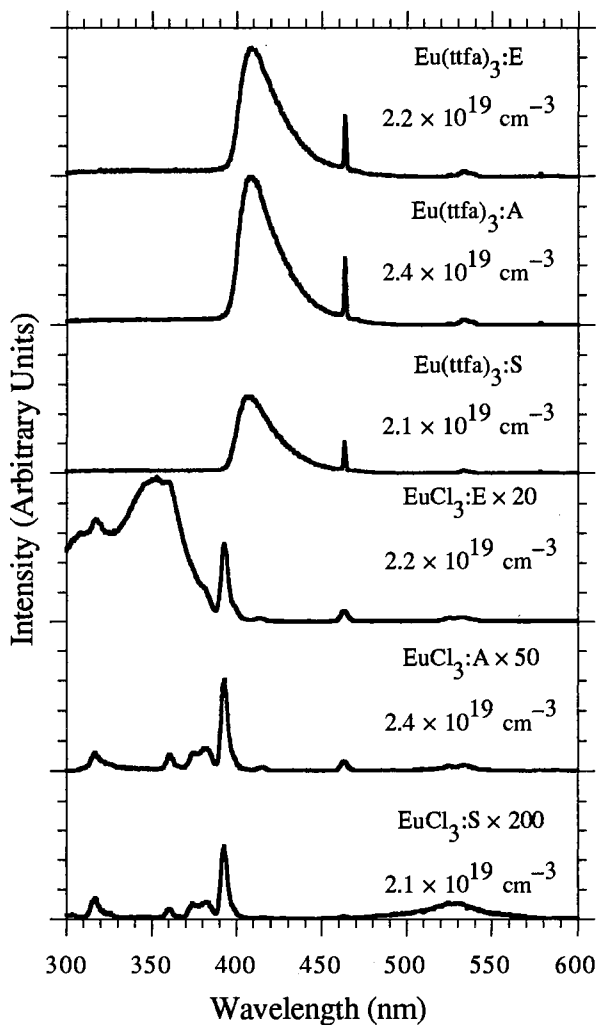
FIGURE 5-2: Fluorescence excitation spectrum of Eu(ttfa)$_3$ and EuCl$_3$ in matrices E, A, and S at the same concentrations as in Figure 5-1; viewed at the $^5D_0 \to {}^7F_2$ transition of Eu^{3+} near 612 nm. The excitation spectra are normalized to the intensity of Eu(ttfa)$_3$:A. The spectra of EuCl$_3$ are multiplied by factors of 20 (E), 50 (A), and 200 (S) for clarity.

91

EuCl$_3$ Quantum Efficiencies
Excited at Eu^{3+} ^{7}F$_0 \rightarrow$ ^{5}L$_6$ (393 nm)
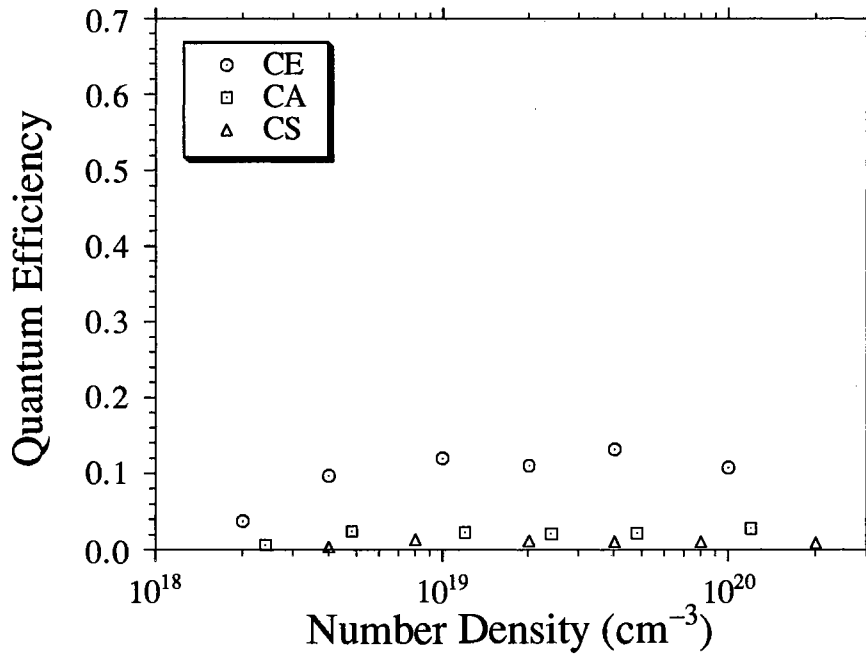
FIGURE 5-3: Quantum efficiency as a function of concentration for EuCl$_3$ (legend C) in

matrices E, A, and S; excited at the $^7F_0 \rightarrow {}^5L_6$ transition of Eu^{3+} near 393 nm.

Eu(ttfa)$_3$ Quantum Efficiencies
Excited at LMET
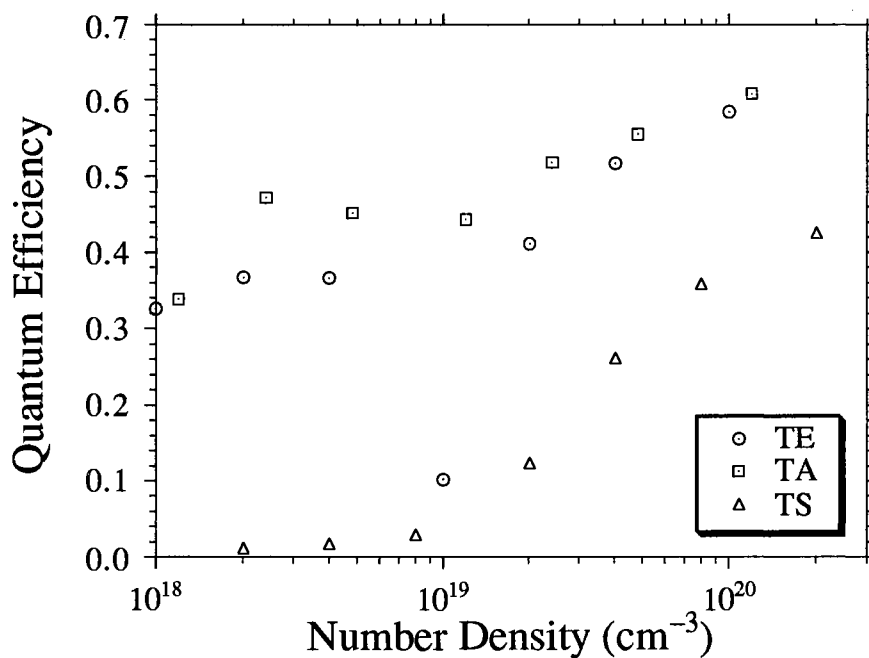
FIGURE 5-4: Quantum efficiency as a function of concentration for Eu(ttfa)$_3$ (legend T) in matrices E, A, and S; excited at the maximum value of the LMET band (see Table 5-2). The value for Eu(ttfa)$_3$:E at 10^{19} cm^{-3} is out of bounds.

Figures 5-5 and 5-6 indicate that the total integrated emission intensity quantitatively increases with concentration in all six cases, confirming the qualitative observation that sample brightness increases as a function of concentration for both compounds. This effect is most dramatic for the $EuCl_3$ dopant. It is also noted that $Eu(ttfa)_3$ is significantly brighter than $EuCl_3$ at all concentrations.

Figure 5-7 shows the fluorescence lifetimes of the $^5D_0 \rightarrow {}^7F_2$ emission of $EuCl_3$ in all three host matrices. The lifetimes in silica are close to that reported for crystalline $EuCl_3 \cdot 6H_2O$, 122 μs,[11] and change little with concentration. Those in acrylate ormosil are nearly double the silica lifetimes at the lower concentrations (200 μs), approaching comparable value with the silica lifetimes at elevated concentrations. In $EuCl_3$:E, however, the lifetimes are four to five times as long as those in acrylate ormosil and silica. In Figure 5-8, it can be seen that the lifetimes of $Eu(ttfa)_3$:S specimens exhibit an overall increase with concentration, but those of $Eu(ttfa)_3$:A and $Eu(ttfa)_3$:E are relatively independent of dopant density at the lower concentrations. Double-exponential decay behavior is observed in the three highest concentrations of $Eu(ttfa)_3$:A, but not in $Eu(ttfa)_3$:E. In the latter case, only a slight lifetime decrease (consistent with concentration quenching) is observed at higher concentrations.

EuCl$_3$ Integrated Emission Intensities

Excited at Eu^{3+} ^{7}F$_0 \rightarrow$ ^{5}L$_6$ (393 nm)
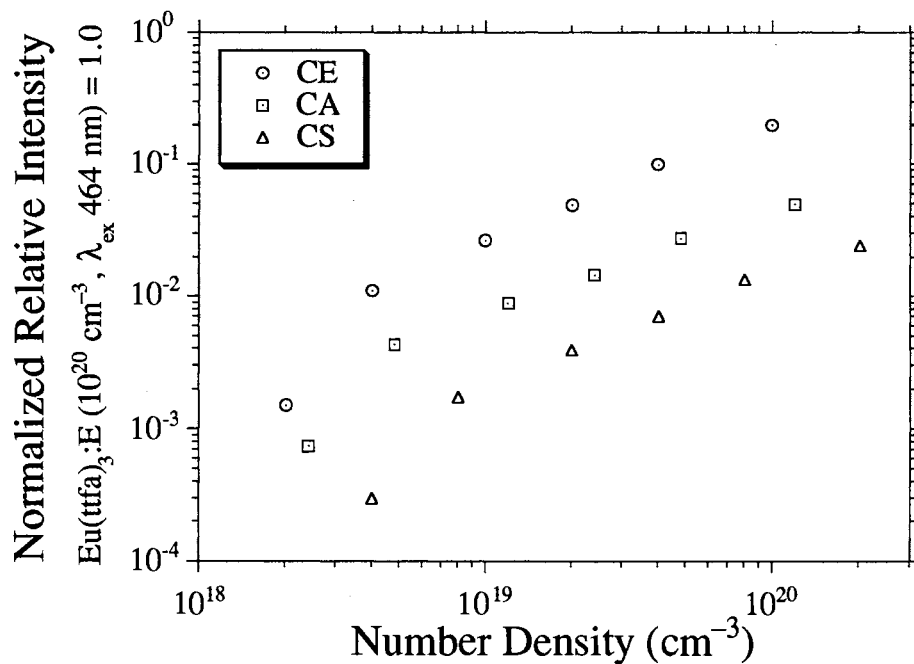
FIGURE 5-5: Integrated emission intensity as a function of concentration for EuCl$_3$ (legend C) in matrices E, A, and S; excited at the $^7F_0 \rightarrow$ $^5L_6$ transition of Eu^{3+} near 393 nm, normalized to the value of Eu(ttfa)$_3$:A at 10^{20} cm^{-3} (Fig. 5-6).

Eu(ttfa)$_3$ Integrated Emission Intensities
Excited at LMET
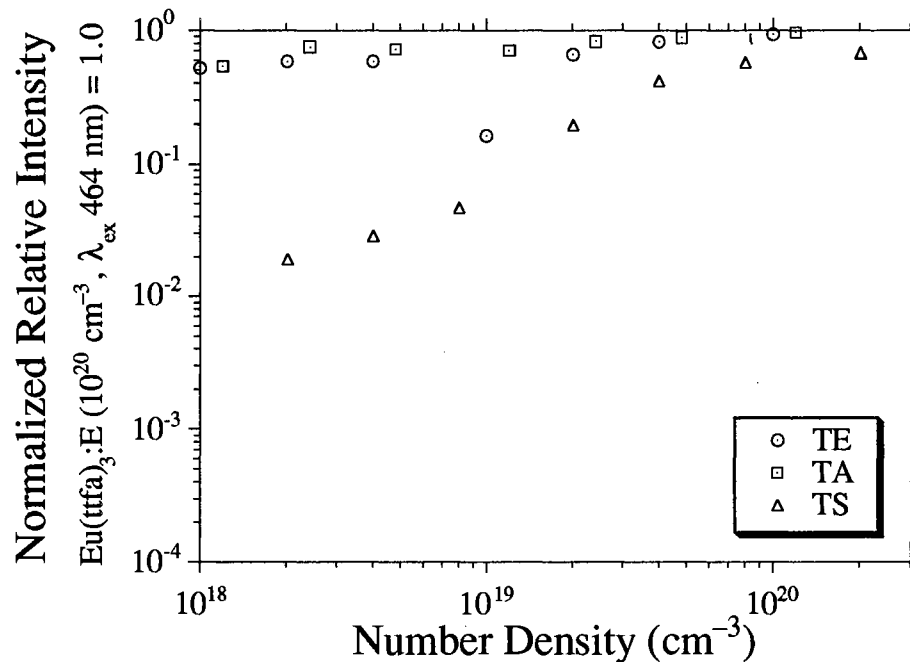
FIGURE 5-6: Integrated emission intensity as a function of concentration for Eu(ttfa)$_3$ (legend T) in matrices E, A, and S; excited at the maximum value of the LMET band (see Table 5-2), normalized to the value of Eu(ttfa)$_3$:E at 10^{20} cm^{-3} (this Figure). The value for Eu(ttfa)$_3$:E at 10^{19} cm^{-3} is out of bounds.

EuCl$_3$ Fluorescence Lifetimes
Excited at 543 nm
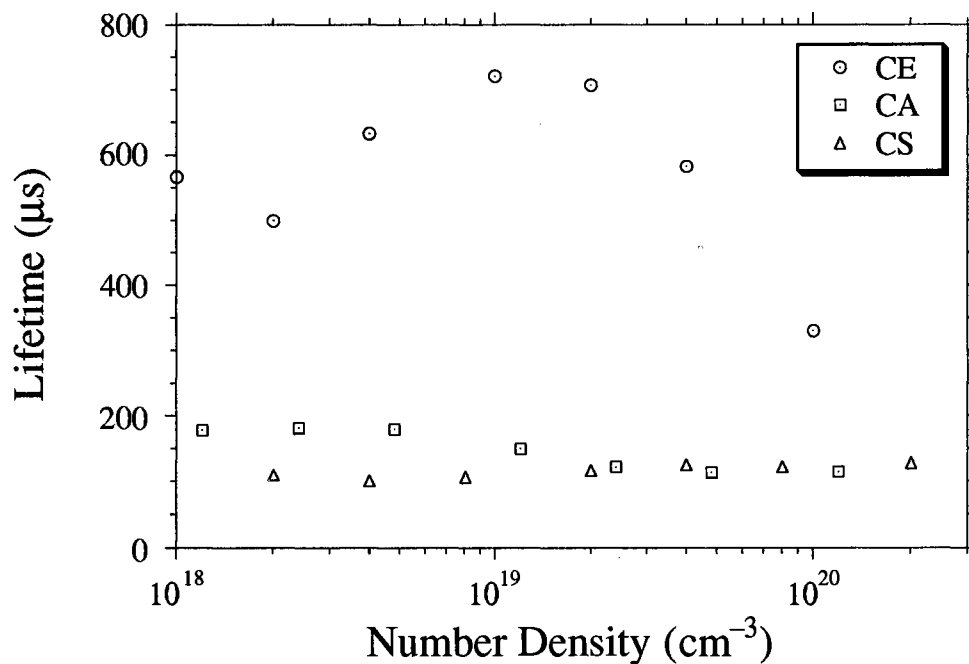
FIGURE 5-7: Fluorescence lifetimes (μs) of the $^5D_0 \to {}^7F_2$ emission for EuCl$_3$. The samples were excited by a 500-fs-pulse dye laser operating at 543 nm, which roughly corresponds to the relatively weak Eu^{3+} $^7F_0 \to {}^5D_1$ absorption. The value for EuCl$_3$:E at 2×10^{18} cm^{-3} is out of bounds.
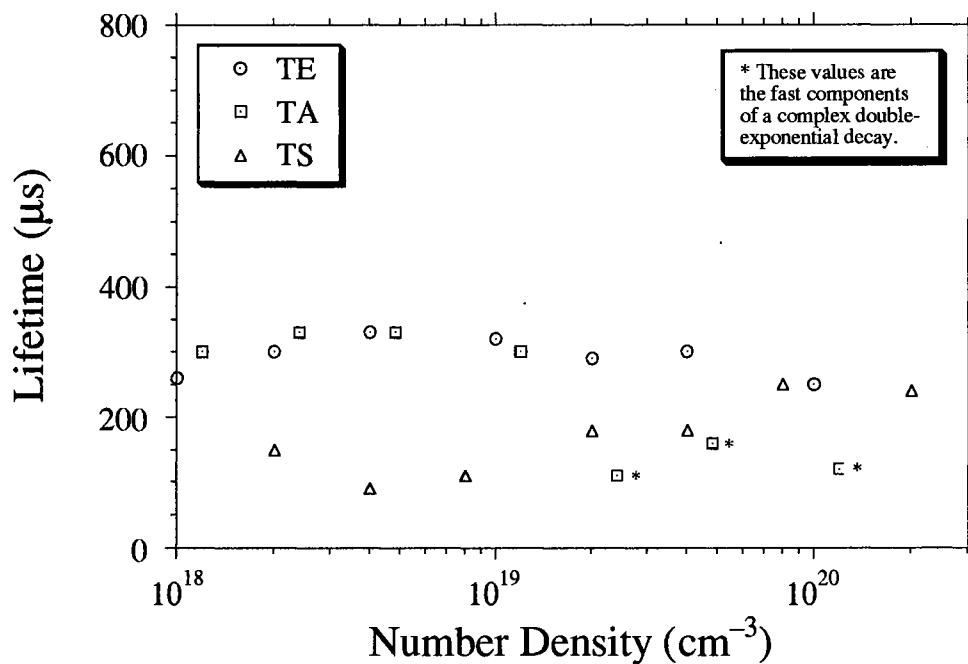
FIGURE 5-8: Fluorescence lifetimes (μs) of the $^5D_0 \rightarrow {}^7F_2$ emission for Eu(ttfa)₃. The samples were excited by a 500-fs-pulse dye laser operating at 441 nm, which lies within the red wing of the LMET band.

Changes in the local chemical environment experienced by the europium dopant (i.e. two different ligands and three different matrices) were observed to result in substantial variations in emission peak branching ratios and bandwidth broadening effects (Fig. 5-1). The peak locations, however, are essentially unperturbed, thus demonstrating the relative insensitivity of the Eu^{3+} $4f^6$ electron energy levels to local matrix effects. The relative emission intensity, however, has a significant dependence upon ligand and matrix character. Ligand effects cause the luminescence of $Eu(ttfa)_3$ to be at least 40 times more intense than that of $EuCl_3$ in all three matrices. These effects presumably arise from increased shielding of Eu^{3+} from quenching collisions in $Eu(ttfa)_3$ relative to $EuCl_3$, increased asymmetry in the Eu^{3+} site (which enhances transition probabilities) in $Eu(ttfa)_3$ relative to $EuCl_3$, and ligand energy capture (which can only occur in complexes like $Eu(ttfa)_3$). Dopant–matrix interactions cause $Eu(ttfa)_3$ luminescence to be at least twice as intense in both ormosils as in silica. This is likely due to reduced quenching phenomena as a result of differences in the host network structure. Finally, the relative intensity of $EuCl_3$ luminescence yields have been previously observed to increase by orders of magnitude upon changing from silica and acrylate ormosil to epoxide ormosil, primarily due to the hypothesized complexation between Eu^{3+} and the side chains of the epoxide ormosil (Ch. 4).[†]

The excitation spectra (Fig. 5-2) show significant differences between $EuCl_3$ and $Eu(ttfa)_3$, particularly in their interactions with the three matrices. As reported in Chapter 4, the broad 350-nm band in $EuCl_3$:E resembles the ligand excitation band observed in $Eu(ttfa)_3$ and may indicate a significant degree of chelation between the Eu^{3+} from $EuCl_3$ and α,β-diol or other α,β-dioxy groups present in the glycidoxypropyl side chain of the epoxide ormosil.[9] If these oxygen-containing side chains were indeed chelating Eu^{3+} ions, these linkages could be expected to accelerate the rate of cross-linking in the matrix,

---

[†] To date, attempts to test this complexation hypothesis by IR and NMR spectroscopy have proved inconclusive.

leading to shorter gellation times; in fact, an approximately 40% decrease in gellation time for $EuCl_3$:E relative to $Eu(ttfa)_3$:E at equivalent concentrations has been observed. The features of Figure 5-2 near 464, 535, and 580 nm arise from Eu^{3+} transitions from the $^7F_0$ ground state to the $^5D_{0-2}$ terms.[6] The position of these three Eu^{3+} excitation peaks has been found to be independent of changes in chemical species, matrix composition, and dopant concentration, and their relative intensities were found to vary in a nearly linear fashion as a function of dopant concentration N, which was varied from 6.0×10^{17} up to 6.0×10^{19} cm^{-3} in the initial sols (Table 5-1). This behavior was observed in the case of each europium(III) compound and in all three host matrices (both sol and dried gels). Certain higher-energy features of the $EuCl_3$ spectra, notably the $^7F_0 \rightarrow {}^5L_6$ transition near 393 nm, exhibit similar concentration dependence.

In contrast to the f-f excitation peaks of $EuCl_3$ and of $Eu(ttfa)_3$ (above 460 nm), the position of the $Eu(ttfa)_3$ LMET excitation peak below 450 nm has been observed to have a strong concentration dependence in all three hosts. The most notable effect is a clearly resolved red-shift of the peak maximum with increasing $Eu(ttfa)_3$ concentration from about 385 to 430 nm (Table 5-2). The red edge of this broad excitation band has been found to correspond to the red edge of the complex's intense ligand absorption band. As reported in Chapter 4, this absorption band has been observed to have at least two components, centered at 341 and 350 nm. Maximum excitation has been found to occur at the wavelength (λ_{ex-max}) where the value of the absorption coefficient (α) of the absorption band's red edge is approximately 2.0 cm^{-1}. At excitation energy (and α values) higher than that of λ_{ex-max}, excitation via the LMET mechanism appears to be quenched due to the activation of nonradiative relaxation mechanisms. Ligand–ligand exchange phenomena are presumed to play a role in this behavior, probably through the interaction of ligand excited states.

TABLE 5-2

Initial Number Density (cm^{-3})	$\lambda_{ex\text{-}max}$ Acrylate Ormosil	$\lambda_{ex\text{-}max}$ Epoxide Ormosil	$\lambda_{ex\text{-}max}$ Silica
6.0×10^{17}	390.5	390.0	387.5
1.2×10^{18}	394.5	394.5	392.0
2.4×10^{18}	397.5	397.0	394.5
6.0×10^{18}	403.0	403.5	401.5
1.2×10^{19}	408.5	408.0	409.0
2.4×10^{19}	413.0	415.5	412.5
6.0×10^{19}	423.5	424.5	426.5

TABLE 5-2: Wavelength positions of the maximum ligand-to-metal energy transfer (LMET) excitation ($\lambda_{ex\text{-}max}$, nm) for Eu(ttfa)$_3$ as a function of concentration.

In Eu(ttfa)$_3$, intense luminescence via excitation of the LMET band is dominant at the lower dopant concentrations; however, at the highest concentrations ($N \geq 10^{20}$ cm^{-3}) the amplitude of the Eu^{3+} $^7F_0 \rightarrow {}^5D_2$ excitation peak surpasses that of the LMET band. This occurs because the two excitation phenomena obey different intensity–concentration relationships. The intensity of the LMET band increases at a much slower rate than that expected for a Beer–Lambert relationship, while the Eu^{3+} transition generally obeys Beer–Lambert behavior.

The quantum efficiency behaviors of EuCl$_3$ and Eu(ttfa)$_3$ differ significantly. The quantum efficiency behavior of EuCl$_3$ (Fig. 5-3) is nearly independent of concentration, but the quantum efficiency of Eu(ttfa)$_3$ (Fig. 5-4) tends to increase with increasing concentration and exhibits much more statistical variation than EuCl$_3$. The rate of increase, however, is much steeper in silica than in the acrylate or epoxide hosts, which exhibit comparable behavior. The quantum efficiency of Eu(ttfa)$_3$:A and Eu(ttfa)$_3$:E are

relatively high (approaching 60% at moderate dopant densities), an important feature in potential optical source applications.

The phenomenon in which the quantum efficiency of Eu(ttfa)$_3$:S *increases* with concentration, first described in Chapter 3, has been observed consistently over four separate sample series, when excited at both the LMET band and the $^7F_0 \rightarrow {}^5D_2$ transition of Eu^{3+} (464 nm), outside the ligand absorption band. A suggested mechanism involves modification of the matrix microstructure or nanostructure by the dopant species. It has been observed that the gellation time for Eu(ttfa)$_3$:S is much shorter than that of EuCl$_3$:S at equivalent concentrations (generally 5–7 days). The most concentrated Eu(ttfa)$_3$:S samples gelled within 5–10 minutes of casting, with the others following from highest to lowest concentrations within 0.5–2 days. It has been reported that the presence of F$^-$ in acid-catalyzed sol–gel reactions greatly decreases gellation times relative to those sols containing Cl$^-$ or NO$_3^-$;[12] it is therefore likely that the presence of the nine fluorine atoms from the highly polarized trifluoromethyl groups on the exterior of each organoeuropium complex species accelerates the sol–gel condensation reaction in silica. Possible means by which this process could increase the quantum efficiency of embedded Eu(ttfa)$_3$ are through geometric modification of the ligands, changes to the shape of the molecular complex, or nanostructural dopant-induced modifications to the gel host, leading to greater asymmetry at the Eu^{3+} site and decreased quenching, perhaps through reduced phonon coupling to the matrix.

With regard to total integrated emission intensity (Figs. 5-5 and 5-6), EuCl$_3$ adheres much more closely than Eu(ttfa)$_3$ to a simple Beer–Lambert relationship, with an intensity increase slightly less than ten for a tenfold concentration increase. (The deviation below 4×10^{18} cm^{-3} is probably due to serial dilution error accumulation.) The intensities of Eu(ttfa)$_3$ in matrices A and E exhibit a steady increase as a function of concentration, but only by a factor of about two for a one-hundred-fold increase in

concentration. The intensity of Eu(ttfa)$_3$:S actually increases by a factor greater than ten at moderate concentrations.

Fluorescence lifetime behaviors (Figs. 5-7 and 5-8) were observed to vary significantly, not only between the two dopant species but also between the various dopant–matrix combinations. While the lifetimes of EuCl$_3$:S specimens were not significantly dependent upon concentration, those of EuCl$_3$ in both matrices A and E exhibit substantive concentration dependence. At low concentrations, EuCl$_3$:A lifetimes are nearly double those of the corresponding EuCl$_3$:S specimens, but the lifetimes associated with EuCl$_3$:A decrease rapidly with increasing concentration to values which approximate the comparable EuCl$_3$:S materials. Thus, EuCl$_3$:A is less subject to matrix quenching than EuCl$_3$:S at the lower dopant concentrations, but concentration quenching effects become dominant at the higher concentrations. The exceptionally long lifetimes of EuCl$_3$:E clearly indicate that the Eu^{3+} ion exists in a significantly different environment in the epoxide ormosil than in the other two hosts. This long lifetime, plus the previously noted appearance of the new broad, intense excitation band, strongly suggests the formation of a complex between Eu^{3+} and the side chains of the epoxide ormosil as described in the preceding Chapter.

In the case of Eu(ttfa)$_3$:S, the increasing lifetimes with concentration correspond with the observed increase in quantum efficiency. The lifetime values for Eu(ttfa)$_3$:A are relatively unchanged as a function of dopant density until the onset of double-exponential decay behavior (three highest concentrations), which is probably associated with cross-relaxation and/or dimerization effects. The values for Eu(ttfa)$_3$:E are also fairly constant, decreasing slightly at high concentrations (presumably due to concentration quenching), but are consistently higher than those for Eu(ttfa)$_3$:S. Longer radiative lifetimes are generally associated with reduced quenching, indicating that matrix E is a promising ormosil host for optical source applications.

IV. Conclusions

In summary, strong dopant concentration dependence yields widely varying luminescence results in europium-doped silicate gels. This is found to be largely influenced by the nature of the particular dopant and matrix species utilized. $EuCl_3$ was found to demonstrate Beer–Lambert-like luminescence characteristics, even in the complex-forming matrix. $Eu(ttfa)_3$-doped specimens, on the other hand, show only a modest increase in luminescence intensity as a function of dopant concentration. The relatively high quantum efficiencies and emission intensities exhibited by $Eu(ttfa)_3$ in all three matrices and by $EuCl_3$:E make them promising candidates for use as optical sources. Because ormosil matrices have improved mechanical and optical properties, and generally reduced quenching characteristics relative to silica gel, they appear to be promising host matrices for $Eu(ttfa)_3$-based systems. $EuCl_3$ clearly exhibits more promising optical characteristics in the epoxide ormosil host. Quantum efficiency, integrated intensity, and fluorescence lifetime measurements indicate that concentration quenching effects for $Eu(ttfa)_3$ become significant only at concentrations above 10^{20} cm^{-3} in both ormosil hosts. Thus, this dopant is particularly resistant to deleterious concentration effects in sol–gel hosts and is a promising candidate for the development of a wide variety of optical sources.

V. References

1. (a) A. Lempicki and H. Samelson, *Phys. Lett.* **4** (1963) 133; (b) A. Lempicki, H. Samelson, and C. Brecher, *Appl. Opt. Suppl.* **2** (1965) 205.

2. (a) C. A. Capozzi and L. D. Pye, in Proceedings of SPIE 970 (Bellingham, WA: The Society of Photo-Optical Instrumentation Engineers, 1988), p. 135; (b) H. Schmidt and B. Seiferling, in C. J. Brinker, D. E. Clark, and D. R. Ulrich, eds., *Better Ceramics Through Chemistry II,* MRS Symposium Proceedings 73 (Pittsburgh, PA: Materials Research Society, 1986), p. 739.

3. J. G. White, *Inorg. Chim. Acta* **16** (1976) 159.

4. (a) N. de la Rosa-Fox, L. Esquivias, and J. Zarzycki, *Diffusion and Defect Data* **53–54** (1987) 363. (b) L. Esquivias and J. Zarzycki, in J. D. Mackenzie and D. R. Ulrich, *Ultrastructure Processing of Advanced Ceramics* (New York: John Wiley & Sons, Inc., 1988), p. 255.

5. E. T. Knobbe, B. Dunn, P. D. Fuqua, and F. Nishida, *Appl. Opt.* **29** (1990) 2729.

6. G. H. Dieke and H. M. Crosswhite, *Appl. Opt.* **2** (1963) 675.

7. W. T. Carnall, P. R. Fields, and K. Rajnak, *J. Chem. Phys.* **49** (1968) 4412.

8. N. E. Wolff and R. J. Pressley, *Appl. Phys. Lett.* **2** 152 (1963).

9. G. Philipp and H. Schmidt, *J. Non-Cryst. Solids* **82** (1986) 31.

10. S. R. Chinn, in M. J. Weber, ed., *CRC Handbook of Laser Science and Technology, Volume I, Lasers and Masers* (Boca Raton, FL: CRC Press, Inc., 1982), p. 147.

11. J. Heber and K. H. Hellwege, H. M. Crosswhite and H. W. Moos, eds., *Optical Properties of Ions in Crystals* (New York; London; Sydney: Interscience Publishers Division of John Wiley & Sons, Inc., 1967), p. 457.

12. C. J. Brinker and G. W. Scherer, *Sol–Gel Science: The Physics and Chemistry of Sol–Gel Processing* (Boston: Academic Press, 1990).

CHAPTER 6

ENERGY TRANSFER AND EMISSION PROCESSES IN SOL–GEL-DERIVED

MATERIALS DOPED WITH EUROPIUM(III) COMPLEXES*

I. Introduction

In the previous Chapters regarding the incorporation of tris(4,4,4-trifluoro-1-(2'-thienyl)-1,3-butanedionato-O,O')europium(III), Eu(ttfa)$_3$, into sol–gel-derived silica and organically modified silicate *(ormosil)* hosts, the objective has been the development of enhanced luminescence characteristics through variations in ligand and matrix chemistry and concentration-related effects. Sol–gel derived (and similar) media have good potential with regard to the development of device-integrated optical sources, in that these materials are prepared at temperatures below 100°C. Thus, such materials are compatible with a number of existing device architectures, including coatings, films, and fibers. The research presented herein extends the studies of Eu(ttfa)$_3$-doped gels to include the observation of time-resolved energy transfer (ET) processes in these systems, and observations associated with changes in ET behavior as a function of host matrix and dopant concentration levels.

II. Experimental Methods

Tris(4,4,4-trifluoro-1-(2'-thienyl)-1,3-butanedionato-O,O')europium(III) trihydrate, Eu(ttfa)$_3$•3H$_2$O, was obtained from Kodak Chemicals and used without further

106

purification or characterization. The previously determined structure of this metalorganic complex was presented in Figure 3-1.[1]

Silica *(matrix S)*, acrylate ormosil *(matrix A)*, and epoxide ormosil *(matrix E)* host materials were prepared according to the procedures described in the preceding Chapters.[2] Silica samples were prepared using tetramethoxysilane (TMOS, Fluka Chemie AG) and 0.040 molar aqueous hydrochloric acid precursors (mole ratios of 1.0 TMOS : 4.0 H_2O : 2.9 $\times$ 10^{-3} HCl). Acrylate ormosil samples were prepared using TMOS, 3-(trimethoxysilyl)propyl methacrylate (TMSPM, Aldrich Chemical Company), methyl methacrylate (MMA, Aldrich), and 0.040 M aqueous HCl precursors (mole ratios of 1.0 TMOS : 1.0 TMSPM : 1.0 MMA : 7.0 H_2O : 5.0 $\times$ 10^{-3} HCl). Epoxide ormosil samples were prepared using TMOS, 3-glycidoxypropyltrimethoxysilane (GPTMS, Aldrich), ethylene glycol (EG, Fisher Scientific Company), and 0.040 M aqueous HCl precursors (mole ratios of 1.0 TMOS : 1.0 GPTMS : 1.0 EG : 4.5 H_2O : 3.2 $\times$ 10^{-3} HCl). Acrylate ormosil, epoxide ormosil, and silica xerogel specimens in this study were found to retain approximately 50%, 60%, and 30%, respectively, of their initial precursor solution volumes.

Fluorescence rise times (τ_r) and radiative decay times (τ_d) were measured by exciting the samples with 308-nm laser radiation, produced by a Lambda Physik LEXtra xenon chloride excimer laser (10-ns pulse width). This photon energy (32,500 cm^{-1}) can result in the direct excitation of the ttfa$^-$ ligand. Luminescent signal was collected using a double-grating, 0.22-m monochromator (SPEX model 1680) and focused onto a thermo-electrically cooled R928 PMT. Time-resolved events were characterized using a Tektronix 2440 digital storage oscilloscope (500 MHz bandwidth) interfaced to an IBM-compatible computer.

Figure 6-1 shows representative continuous-wave (cw) emission spectra for Eu(ttfa)$_3$ in each of the three host matrices, with intensities normalized to that of Eu(ttfa)$_3$:A as in Chapter 5. The samples were pumped at the wavelength corresponding to the maximum emission resulting from excitation of the β-diketonate ligand followed by ligand-to-metal energy transfer (LMET) as described in Chapters 3–5.[3] The observable emission peaks result from relaxation out of the $^5D_0$ excited state of Eu^{3+} to the first five levels ($k = 0$–4) of the ^7F_k ground-state manifold;[4] the $^5D_0 \rightarrow \, ^7F_2$ emission near 612 nm is the one usually associated with optical source applications.[4] As in Chapter 5, it is the emission wavelength for the excitation spectra presented in Figure 6-2.

According to the mechanism first proposed by Crosby, Whan, and Alire,[5] ET (sensitized) emission from rare-earth (RE) chelates proceeds through the following steps: (1) ligand absorption of pump radiation via singlet–singlet ($S_0 \rightarrow S_i$) transition, (2) intersystem crossing (ISC) to the ligand triplet state ($S_i \rightarrow T_i$), (3) intramolecular energy transfer (more specifically, ligand-to-metal energy transfer, LMET) to excited metal ion states ($T_i \rightarrow Eu^{3+} \, ^5D_j, j \geq 0$), (4) internal conversion via nonradiative relaxation to the metal ion's emitting level ($Eu^{3+} \, ^5D_j \rightarrow \, ^5D_0$), and finally (5) emission ($Eu^{3+} \, ^5D_0 \rightarrow \, ^7F_k, k = 0, 1, 2, 3, 4; k = 2$ dominant). These processes are indicated in Figure 6-3.

The temporal rise times of radiative events can be related to absorption and energy transfer processes and energy state levels in metalorganic complexes. The initial optical absorption step in such systems is fully allowed (singlet–singlet) and, accordingly, is a very fast (*i.e.*, $\leq$ 10-ps) transition. ISC in metal-free systems is spin-forbidden and relatively slow, but has been found to be very fast (~10 ps) in rare-earth metalorganic chelates due to heavy ion effects and the existence of both $n\pi^*$ and $\pi\pi^*$ states in the ligands.[6] LMET in RE chelate systems has also been reported to be fast (~100 ps).[6-7]

Emission Spectra
Excited at LMET ($\approx$408 nm)

0 **1** **2** **3** **4**

Intensity (Arbitrary Units)

Eu(ttfa)$_3$:E

Eu(ttfa)$_3$:A

Eu(ttfa)$_3$:S

565   590   615   640   665   690   715
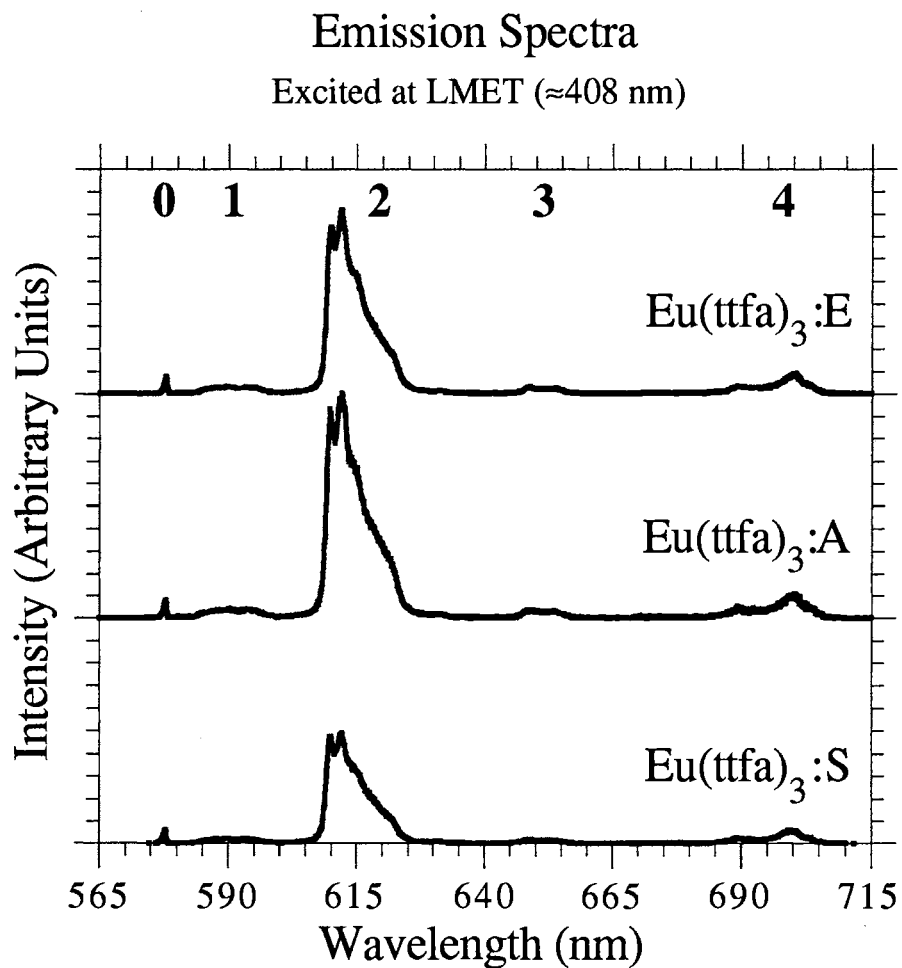
Wavelength (nm)

FIGURE 6-1: Sample fluorescence emission spectra of Eu(ttfa)$_3$ in sol–gel hosts; excitation at the peak wavelength resulting in LMET emission (393 nm $\leq \lambda_{ex\text{-}max} \leq$ 420 nm). Emission spectra are normalized to the intensity of Eu(ttfa)$_3$:A. Peak labels (boldface numbers) are the k values of the transitions $^5D_0 \to {}^7F_k$.

Excitation Spectra

Viewed at Eu^{3+} $^5D_0 \rightarrow {}^7F_2$ ($\approx$612 nm)

LMET

2   **1**   **0**

Intensity (Arbitrary Units)

$Eu(ttfa)_3$:E

$Eu(ttfa)_3$:A

$Eu(ttfa)_3$:S

300   350   400   450   500   550   600

Wavelength (nm)
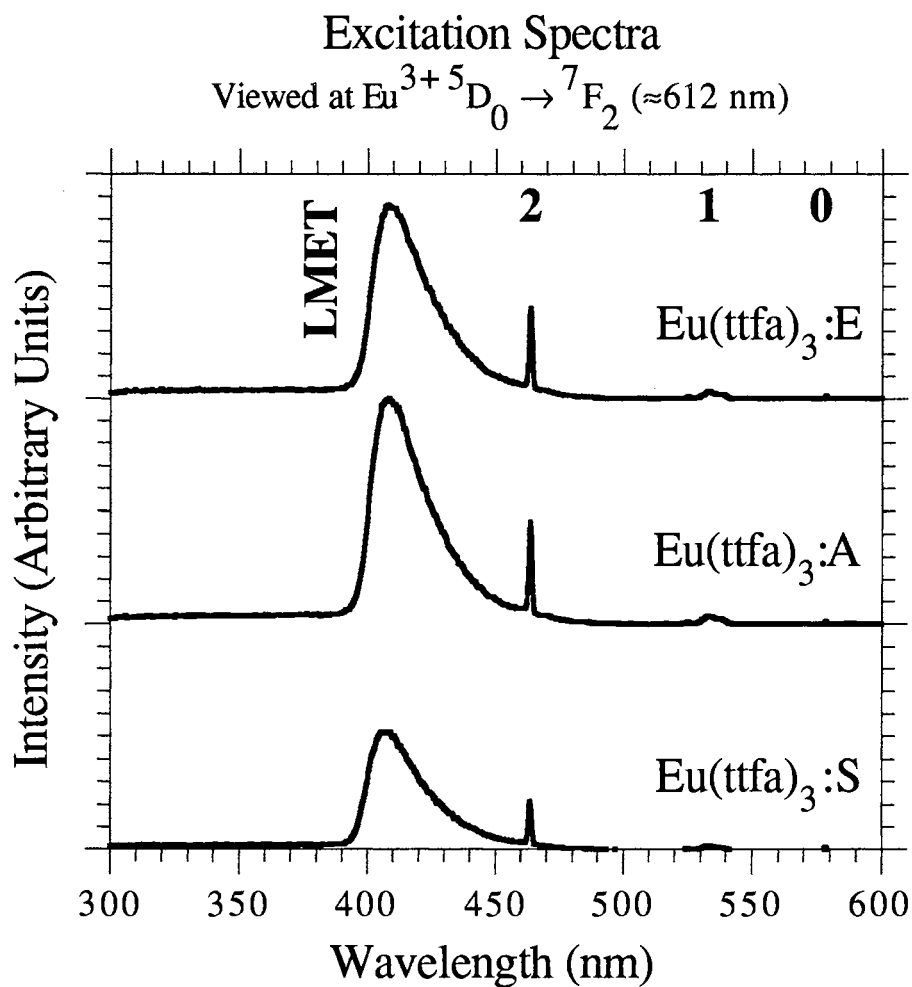
FIGURE 6-2: Fluorescence excitation spectrum of Eu(ttfa)₃ in matrices E, A, and S at the same concentrations as in Figure 6-1; $\lambda_{em} \approx$ 612 nm, associated with the $^5D_0 \rightarrow {}^7F_2$ radiative transition of Eu^{3+}. Excitation spectra are normalized to the intensity of Eu(ttfa)₃:A. Peak labels (boldface numbers) are the j values of the transitions $^7F_0 \rightarrow {}^5D_j$; the LMET band is labeled also.
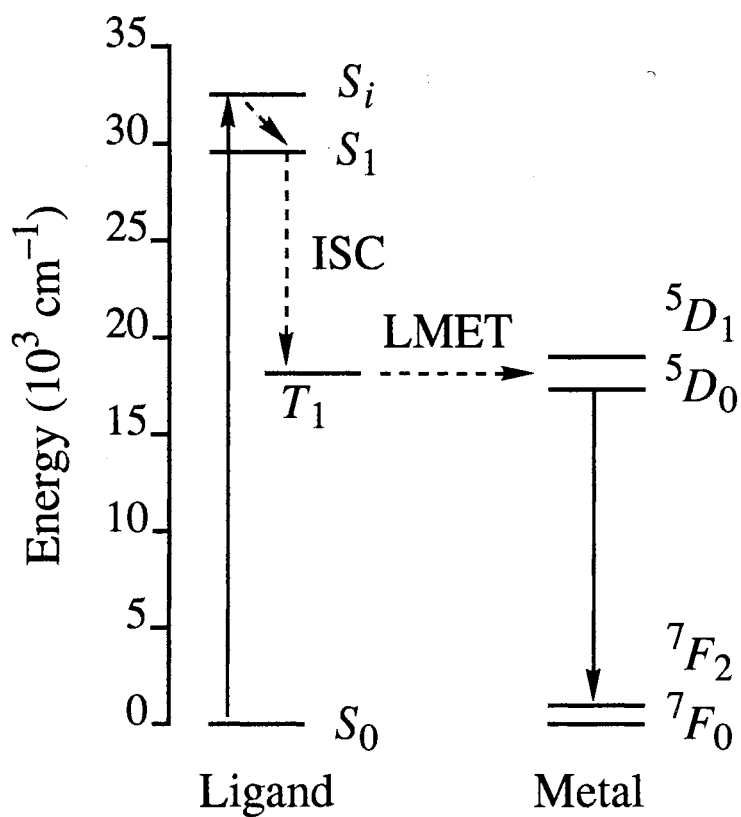
FIGURE 6-3: Energy level diagram for Eu(ttfa)$_3$ powder, using values from Ref. 11. Solid and dashed arrows represent radiative and nonradiative transitions, respectively. For clarity, only two each of the five ^5D_j and seven ^7F_k Eu^{3+} levels are included. Both radiative and nonradiative ttfa$^-$ $T_1 \rightarrow S_0$ and nonradiative Eu^{3+} $^5D_0 \rightarrow$ ^7F_k transitions may also occur.

Kleinerman[8] reported that LMET occurs by a *spin-allowed* short-range exchange interaction in such systems. Thus, the three steps which lead to an excited ^5D_j state in the europium(III) ion via LMET are expected to occur over a temporal period of between 100 ps and 1 ns (10^{-10}–10^{-9} s).

Figure 6-4 shows a plot of the experimentally observed Eu^{3+} $^5D_0 \rightarrow {}^7F_2$ radiative rise time (τ_r) in Eu(ttfa)$_3$:E specimens at two dopant concentrations (1.0×10^{19} and 1.0×10^{20} cm^{-3}) upon excitation at 308 nm (10-ns pulse width).

The calculated rise times, 350–420 ns, leading to relaxation from the $^5D_0$ level of Eu^{3+} (Fig. 6-4) indicate that population of the $^5D_0$ level does not occur by a direct LMET mechanism. Thus, one or more intermediate steps must take place in order to account for the difference between initial excitation of the europium(III) ion (100 ps to 1 ns) and population of its $^5D_0$ state (350–420 ns). Europium(III) internal conversion, $^5D_1 \rightarrow {}^5D_0$, has been shown to be a relatively slow process which can be the rate-limiting step leading to $^5D_0 \rightarrow {}^7F_2$ emission. It has been noted that the rise time of the $^5D_0$ level is approximately equal to the decay time of the $^5D_1$ level observed in the relatively weak $^5D_1 \rightarrow {}^7F_0$ emission; $\tau_r({}^5D_0)$ values for similar europium(III) chelates, such as Eu(dbm)$_3$ (where dbm is the dibenzoylmethide or 1,3-diphenyl-1,3-propanedionato ion), have been reported to range from 1.1–2.0 μs at 77 K.[9–10] Such events would be expected to be somewhat faster at room temperature. Bhaumik[9] noted that, when predicted by transition probabilities, $\tau_d({}^5D_1)$ should be ~10 ms, shortened to ~1 ms in chelates. The experimentally observed $\tau_d({}^5D_1)$ = 1 μs, however, is too short to be a radiative transition; instead, it must represent nonradiative decay to the $^5D_0$ level. Watson *et al.*[10] demonstrated that Eu(8-hq)$_3$ (where 8-hq is the 8-hydroxyquinolate ion), a chelate system in which the ligand T_1 state is lower in energy than the $^5D_1$ state of Eu^{3+}, exhibits a $^5D_0$ rise time of less than 100 ns. Luminescence from the $^5D_1$ level is not observed in these compounds, thus verifying that the 1-μs $\tau_r({}^5D_0)$ component originates due to internal conversion from the $^5D_1$ level.

Fluorescence Rise Time

Graph showing Intensity (Arbitrary Units) on the y-axis (0.0 to 1.0) versus Time (μs) on the x-axis (0.0 to 3.0).

Eu(ttfa)$_3$:E, 256 Pulses

λ_{ex} = 308 nm, λ_{em} = 612 nm

A: 1.0×10^{19} cm^{-3}, 420 ns
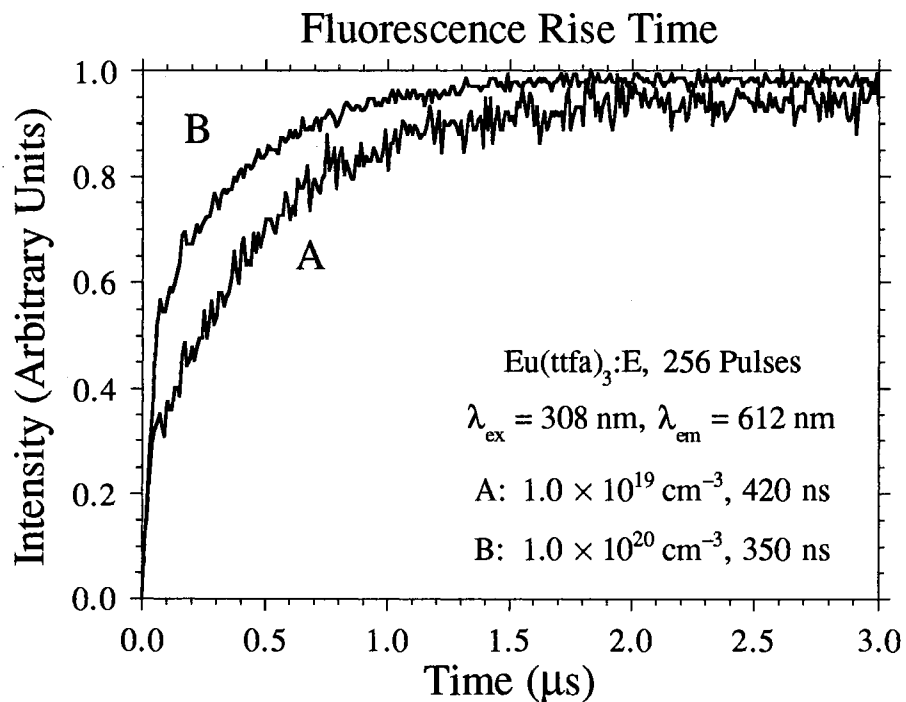
B: 1.0×10^{20} cm^{-3}, 350 ns

FIGURE 6-4: Fluorescence rise time (τ_r) of the $^5D_0 \rightarrow {}^7F_2$ emission of Eu(ttfa)$_3$:E, 1.0×10^{19} and 1.0×10^{20} cm^{-3}, excited at 308 nm, averaged over 256 pulses. Fitted solutions indicate τ_r values of 420 and 350 ns, respectively.

Hayes and Drickamer[11] experimentally demonstrated that the ligand energy levels of rare-earth chelates are much more sensitive to external conditions than the RE ion levels, and that ligand levels in the powder are generally much lower in energy than the corresponding levels when the complex is doped into solid-state host media such as poly(methyl methacrylate) (PMMA). In compositionally pure $Eu(ttfa)_3$ crystalline powder, the relative energy levels associated with $^5D_0$ emission via the LMET mechanism are: $^5D_1$ (19,000 cm^{-1}) > T_1 (18,200 cm^{-1}) > $^5D_0$ (17,300 cm^{-1}). Hayes and Drickamer predicted that $\tau_r(^5D_0)$ for such a system should be less than 100 ns, as the T_1 ligand level is associated with direct excitation of the $^5D_0$ state upon LMET. This researcher has confirmed their prediction by an observation of $Eu(ttfa)_3$ powder in which the rise time of the $^5D_0 \rightarrow {}^7F_2$ emission was found to be at least as fast as the 10-ns pulse width of the laser system used in the experiment. When dissolved in PMMA, however, the T_1 level was observed by Hayes and Drickamer to be dramatically increased, up to approximately 20,000 cm^{-1}. In a PMMA host, therefore, the ttfa$^-$ ligand's T_1 level is higher in energy than the Eu^{3+} $^5D_1$ level.[11] This researcher's observation of $\tau_r(^5D_0)$ values in the 300–500 ns range (room temperature) is consistent with previously described population rates associated with $^5D_1 \rightarrow {}^5D_0$ transition events. The implication of these findings is that the triplet T_1 state of the ttfa$^-$ ligand is elevated, as a result of ligand–matrix interaction effects (e.g. physical compression) in all three host systems studied, to an energy level substantially greater than that reported for $Eu(ttfa)_3$ in powder form (T_1 = 18,200 cm^{-1}). The efficiency of ET processes in these compounds indicates that T_1 is probably perturbed such that it becomes very comparable in energy to the $^5D_1$ level of Eu^{3+} (19,000 cm^{-1}). These results are in good agreement with the previous findings for $Eu(ttfa)_3$ dopant behavior in solid-state PMMA hosts.[11]

It may also be noted, by examination of Figure 6-4, that the sample with the higher concentration (1.0 × 10^{20} cm^{-3}) exhibits a somewhat shorter $^5D_0$ rise time (350 ns), but remains in the same order of magnitude. It was reported in Chapter 5 that the

radiative decay time of the $^5D_0 \rightarrow \, ^7F_2$ transition also decreases over this concentration interval. This is consistent with increased quenching of both $^5D_1$ and $^5D_0$ levels as a function of higher dopant concentrations, presumably due to intermolecular energy transfer events (perhaps through the ligand T_1 or Eu^{3+} $^5D_0$ states) associated with reduced intermolecular spacing. Figure 6-5 shows the concentration dependence of the $^5D_0$ rise times in all three host matrices upon excitation at 308 nm. The rise times were observed to decrease in a nearly semi-logarithmic fashion with concentration in all three matrices over the number density range 10^{18}–10^{20} cm^{-3}. Thus, concentration quenching mechanisms associated with Eu(ttfa)$_3$ dopants in the three gel hosts are likely to be substantially the same.

Figure 6-6 shows representative logarithmic decay curves of Eu(ttfa)$_3$ in the acrylate ormosil host (matrix A) at number densities of 1.2×10^{19} and 1.2×10^{20} cm^{-3}. The development of intermolecular ET processes with increasing concentration is indicated by the appearance of double-exponential $\tau_d(^5D_0)$ behavior. This effect was observed to be most significant in matrix A, in which double-exponential behavior first appears at the dopant level of 2.4×10^{19} cm^{-3}. The temporally short and long radiative decay components are shown as a function of concentration and matrix in Table 6-1. In matrix E, the onset of double-exponential behavior was not observed until a number density of 1.0×10^{20} cm^{-3} was achieved. This difference in behavior is possibly related to the differing polarities and network structures of the two matrices.

Rise Time Concentration Dependence
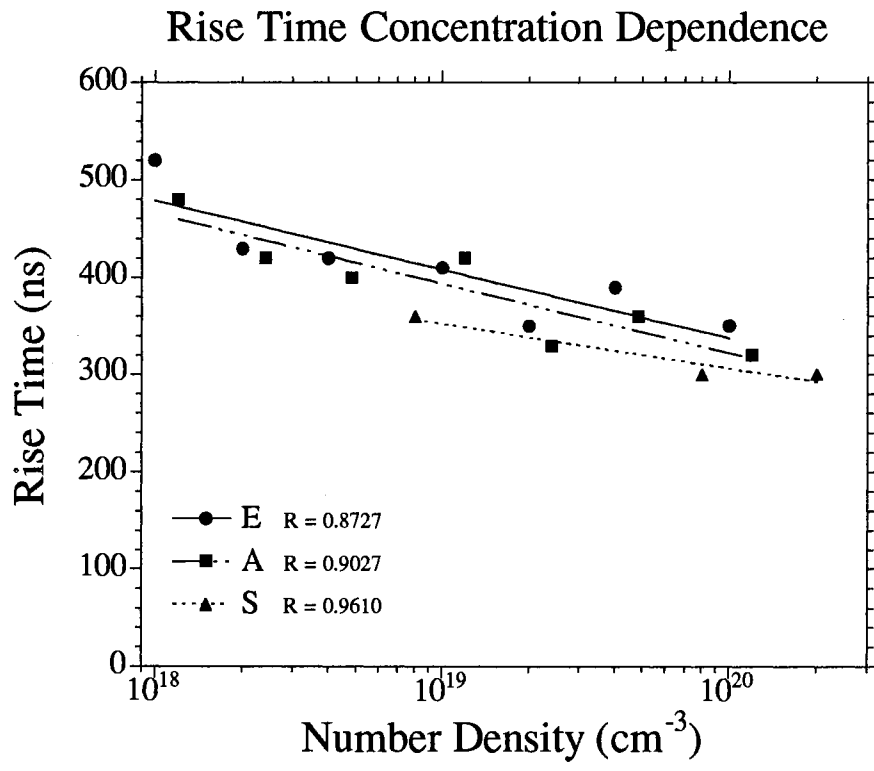
FIGURE 6-5: Fluorescence rise time (τ_r) of the $^5D_0$ level of Eu(ttfa)$_3$, measured as τ_r of the $^5D_0 \rightarrow {}^7F_2$ emission, as a function of concentration in matrices E, A, and S; excited at 308 nm, averaged over 256 pulses, and exponentially fitted. The R values are linear regression correlation factors for the lines shown.

116

Fluorescence Decay Curve
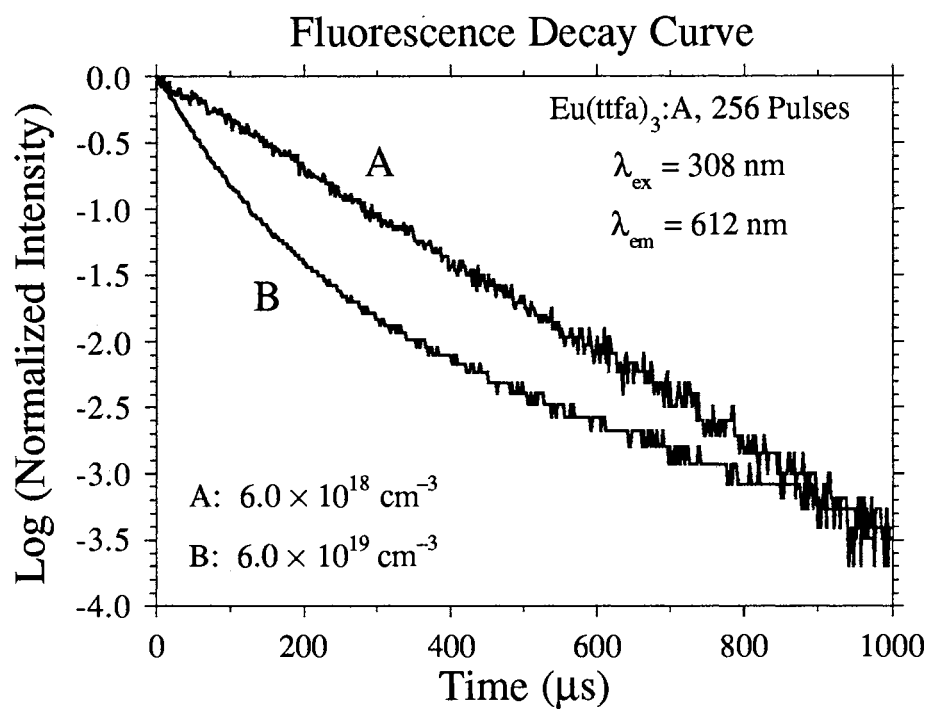
FIGURE 6-6: Logarithmic fluorescence decay (τ_d) of the $^5D_0 \rightarrow {}^7F_2$ emission of Eu(ttfa)$_3$:A at 6.0×10^{18} and 6.0×10^{19} cm^{-3}, excited at 308 nm, averaged over 256 pulses.

TABLE 6-1

Lifetime (τ_d) Behavior of Eu(ttfa)$_3$ $^5D_0 \rightarrow {}^7F_2$ Emission by Matrix and Concentration

Acrylate Ormosil (Matrix A)		Epoxide Ormosil (Matrix E)		
Number Density (cm^{-3})	Lifetime Components (μs)		Number Density (cm^{-3})	Lifetime Components (μs)
1.2×10^{19}	300		1.0×10^{19}	320
2.4×10^{19}	110	400	2.0×10^{19}	310
4.8×10^{19}	160	370	4.0×10^{19}	300
1.2×10^{20}	120	350	1.0×10^{20}	250 350

IV. Conclusions

In summary, changes in matrix and concentration cause distinctive perturbations to the energy transfer process associated with Eu(ttfa)$_3$-doped silicate gels. Comparison with earlier work on a similar host matrix (PMMA) shows that the ligand energy levels of Eu(ttfa)$_3$ are elevated in these gel matrices with respect to the pure Eu(ttfa)$_3$ powder. The triplet state energy is sufficiently increased to result in the population of the $^5D_1$ level of Eu^{3+} (rather than the $^5D_0$ level). The increase in the $^5D_1$ decay rate (equivalent to a decrease in $^5D_0$ rise time) and onset of double-exponential $^5D_0$ decay behavior as concentration increases point to intermolecular energy transfer interactions of the sort commonly encountered as concentration quenching. Thus, fundamental guest–host interactions have been found to dictate the essential nature of ET and luminescence phenomena in these systems.

118

V. References

1. J. G. White, *Inorg. Chim. Acta* **16** (1976) 159.

2. (a) N. de la Rosa-Fox, L. Esquivias, and J. Zarzycki, *Diffusion and Defect Data* **53–54** (1987) 363. (b) L. Esquivias and J. Zarzycki, in J. D. Mackenzie and D. R. Ulrich, *Ultrastructure Processing of Advanced Ceramics* (New York: John Wiley & Sons, Inc., 1988), p. 255. (c) E. T. Knobbe, B. Dunn, P. D. Fuqua, and F. Nishida, *Appl. Opt.* **29** (1990) 2729.

3. (a) A. Lempicki and H. Samelson, *Phys. Lett.* **4** (1963) 133. (b) A. Lempicki, H. Samelson, and C. Brecher, *Appl. Opt. Suppl.* **2** (1965) 205. (c) N. E. Wolff and R. J. Pressley, *Appl. Phys. Lett.* **2** (1963) 152.

4. G. H. Dieke and H. M. Crosswhite, *Appl. Opt.* **2** (1963) 675.

5. G. A. Crosby, S. E. Whan, and R. M. Alire, *J. Chem. Phys.* **34** (1961) 743.

6. M. L. Bhaumik and M. A. El-Sayed, *J. Chem. Phys.* **42** (1965) 787.

7. J. Yu, R. B. Lessard, L. E. Bowman, and D. G. Nocera, *Chem. Phys. Lett.* **187** (1991) 263.

8. M. Kleinerman, *J. Chem. Phys.* **51** (1969) 2370.

9. M. L. Bhaumik, *J. Chem. Phys.* **41** (1964) 574.

10. W. M. Watson, R. P. Zerger, J. T. Yardley, and G. D. Stucky, *Inorg. Chem.* **14** (1975) 2765.

11. A. V. Hayes and H. G. Drickamer, *J. Chem. Phys.* **76** (1982) 114.

CHAPTER 7

LUMINESCENCE BEHAVIOR OF ORGANO-RUTHENIUM COMPLEXES ENTRAPPED WITHIN SOL–GEL HOSTS*

I. Introduction

The preceding Chapters have described the incorporation of tris(4,4,4-trifluoro-1-(2'-thienyl)-1,3-butanedionato-O,O')europium(III), Eu(ttfa)$_3$, into silica and two different organically modified silicate *(ormosil)* gel hosts via the sol–gel process. Complexes like Eu(ttfa)$_3$ and tris(2,2'-bipyridyl)ruthenium(II) chloride ([Ru(bpy)$_3$]Cl$_2$, referred to as *RuB* hereafter) are of interest because they exhibit pronounced luminescence in solid-state sol–gel hosts, which may be prepared at very low processing temperatures (at or near room temperature).

RuB is particularly interesting because of its useful photo- and electrochemical properties. Thus, a large body of previous work exists in the area of organo-ruthenium-doped gel systems. Prior research on RuB in conjunction with sol–gel chemistry has focused on determinations of optical, photochemical, and electrochemical properties of this compound entrapped within silica hosts. Reisfeld *et al.*[1–2] studied the optical characteristics of RuB entrapped within sol–gel silica hosts; they described absorption and emission spectra, and reported values for fluorescence lifetime (τ = 1.34 μs) and quantum efficiency (Q = 10%). An important feature of the work is that the quantum efficiency was found to be higher in solid-state glass hosts than in comparable solution, due to the absence of collisional de-excitation. Matsui *et al.*[3] observed that the blue shift in the

---

120

wavelength of maximum RuB emission (λ_{em-max}), a phenomenon which occurs during the sol–gel aging process as the motion of solvent molecules becomes restricted, is a function of both solution viscosity and pH in sol–gel silica. Slama-Schwok et al.[4] observed photo-induced electron transfer between RuB and the iridium bipyridyl complex Ir[(bpy)$_2$-(C^{3}N'bpy)]$^{3+}$, both entrapped in sol–gel silica, with the aid of a diffusible electron carrier (1,4-dimethoxybenzene). Dvorak and De Armond[5] coated platinum and indium tin oxide (ITO) electrodes with films of sol–gel silica containing RuB and observed that entrapped RuB retains its photochemical and electrochemical activity upon entrapment. MacCraith et al.[6] prepared an optically coupled oxygen (O$_2$) sensor by coating optical fibers with sol–gel silica films containing RuB and [Ru(dpp)$_3$]$^{2+}$ (where dpp = 4,7-diphenyl-1,10-phenanthroline). Clearly, RuB-doped gels have stimulated research in widely varied fields, as a desirable combination of physicochemical properties may be achieved in such media.

In the preceding Chapters, it has been observed that (a) Eu(ttfa)$_3$-doped gels have significantly greater fluorescence intensities than comparable EuCl$_3$-doped gels, (b) that significant differences in the guest–host interactions are present in the three gel systems investigated, and (c) that the effects of concentration differ as a function of both dopant species and matrix. The present work involves the extension of the earlier work to include RuB, in order to characterize its luminescence behavior in the solid-state hosts and in order to gain a further understanding of dopant–matrix interactions and other parameters important for the potential development of such systems as photonic materials (e.g. phosphors and/or optical source media).

II. Experimental Methods

Tris(2,2′-bipyridyl)ruthenium(II) chloride hexahydrate, [Ru(bpy)$_3$]Cl$_2$•6H$_2$O (RuB), was obtained from Aldrich Chemical Company and used without further

wavelength of maximum RuB emission ($\lambda_{em\text{-}max}$), a phenomenon which occurs during the sol–gel aging process as the motion of solvent molecules becomes restricted, is a function of both solution viscosity and pH in sol–gel silica. Slama-Schwok et al.[4] observed photo-induced electron transfer between RuB and the iridium bipyridyl complex Ir[(bpy)$_2$-(C^{3}N'bpy)]$^{3+}$, both entrapped in sol–gel silica, with the aid of a diffusible electron carrier (1,4-dimethoxybenzene). Dvorak and De Armond[5] coated platinum and indium tin oxide (ITO) electrodes with films of sol–gel silica containing RuB and observed that entrapped RuB retains its photochemical and electrochemical activity upon entrapment. MacCraith et al.[6] prepared an optically coupled oxygen (O$_2$) sensor by coating optical fibers with sol–gel silica films containing RuB and [Ru(dpp)$_3$]$^{2+}$ (where dpp = 4,7-diphenyl-1,10-phenanthroline). Clearly, RuB-doped gels have stimulated research in widely varied fields, as a desirable combination of physicochemical properties may be achieved in such media.

In the preceding Chapters, it has been observed that (a) Eu(ttfa)$_3$-doped gels have significantly greater fluorescence intensities than comparable EuCl$_3$-doped gels, (b) that significant differences in the guest–host interactions are present in the three gel systems investigated, and (c) that the effects of concentration differ as a function of both dopant species and matrix. The present work involves the extension of the earlier work to include RuB, in order to characterize its luminescence behavior in the solid-state hosts and in order to gain a further understanding of dopant–matrix interactions and other parameters important for the potential development of such systems as photonic materials (e.g. phosphors and/or optical source media).

II. Experimental Methods

Tris(2,2'-bipyridyl)ruthenium(II) chloride hexahydrate, [Ru(bpy)$_3$]Cl$_2$•6H$_2$O (RuB), was obtained from Aldrich Chemical Company and used without further

purification or characterization. Silica *(matrix S)*, acrylate ormosil *(matrix A)*, and epoxide ormosil *(matrix E)* host materials were prepared according to the procedures described in the preceding Chapters.[7-9] Silica samples were prepared using tetramethoxysilane (TMOS, Fluka Chemie AG) and 0.040 molar aqueous hydrochloric acid precursors (mole ratio 1.0 TMOS : 4.0 H_2O : 2.9 × 10^{-3} HCl).[7] Acrylate ormosil samples were prepared using TMOS, 3-(trimethoxysilyl)propyl methacrylate (TMSPM, Aldrich), methyl methacrylate (MMA, Aldrich), and 0.040 *M* aqueous HCl precursors (mole ratio 1.0 TMOS : 1.0 TMSPM : 1.0 MMA : 7.0 H_2O : 5.0 × 10^{-3} HCl).[8] Epoxide ormosil samples were prepared using TMOS, 3-glycidoxypropyltrimethoxysilane (GPTMS, Aldrich), ethylene glycol (EG, Fisher Scientific Company), and 0.040 *M* aqueous HCl precursors (mole ratio 1.0 TMOS : 1.0 GPTMS : 1.0 EG : 4.5 H_2O : 3.2 × 10^{-3} HCl).[9] The hydrolysis reactions of all three precursor mixtures were initiated by the "sonogel" procedure.[7] Acrylate ormosil, epoxide ormosil, and silica xerogel specimens in this study were found to retain approximately 50%, 60%, and 30%, respectively, of their initial precursor solution volumes.

Continuous-wave luminescence (emission and excitation) spectra, software-corrected for instrumental response, were measured using a Spex Industries Model F112 spectrofluorimeter. Fluorescence decay times (τ) of RuB-doped gels were measured by exciting the samples with 464-nm laser radiation from a pulsed dye laser source (temporal pulse width of 6 ns at a repetition rate of 3 Hz). These excitation pulses were generated using a Lambda Physik LPD 3000 dye laser and coumarin 460 dye (Exciton), pumped by a Lambda Physik LEXtra xenon chloride excimer laser (308 nm). Luminescent signal was collected using a double-grating, 0.22-m monochromator (SPEX model 1680) and focused onto a thermoelectrically cooled R928 PMT. Time-resolved events were characterized using a Tektronix 2440 digital storage oscilloscope (500 MHz bandwidth) interfaced to an IBM-compatible computer. As described in the preceding

Chapters, quantum efficiencies (Q) were calculated by the reference technique of Demas and Crosby[10] using rhodamine 6G chloride in ethanol, reported to have a Q of 95%.[11]

III. Discussion of Results

The initial and final dopant concentrations of RuB in each matrix are shown in Table 7-1. RuB has been found to have relatively poor compatibility with matrix A, which may be due to the relatively low polarity of matrix A with respect to matrices E and S. RuB-doped acrylate ormosil specimens having final number densities (N) greater than 4×10^{18} cm^{-3} were observed to phase-separate.

Figures 7-1 and 7-2 show representative emission and excitation spectra for RuB in each of the three host matrices, with intensities normalized to that of the RuB:E material. The spectral intensities have been increased by factors of 4 for the RuB:A and RuB:S specimens; emission and excitation spectra were recorded at the peak excitation and emission wavelengths, respectively. The epoxide-modified silicate host was found, in general, to yield the most highly luminescent specimens. The RuB excitation feature which produces the maximum emission is due to a charge transfer process which has been designated as a metal-to-ligand charge transfer (MLCT) event.[1] These MLCT phenomena appear to be subject to significant perturbation by the local chemical environment, as demonstrated by the changes observed in the wavelength position of the RuB excitation and emission maxima ($\lambda_{ex\text{-}max}$ and $\lambda_{em\text{-}max}$, respectively) as functions of matrix and concentration (Table 7-2).

The emitting level of RuB has not been clearly elucidated, but has been generally identified as the lowest triplet MLCT state.[1] Thus, the luminescent decay from RuB species requires intersystem crossing from the initially populated singlet state. It is expected that matrix and/or concentration effects which stabilize triplet formation will simultaneously enhance the efficiency of radiative relaxation.

TABLE 7-1

Initial and Final Concentrations or Dopant Levels for RuB

Initial Sol Concentration (Molar)[a]	Initial Number Density N_0 (cm^{-3}), Sol	Final Number Density N (cm^{-3}), Xerogel A[b]	Final Number Density N (cm^{-3}), Xerogel E	Final Number Density N (cm^{-3}), Xerogel S[a]
7.0×10^{-4}	4.2×10^{17}	—	—	1.4×10^{18}
1.0×10^{-3}	6.0×10^{17}	1.2×10^{18}	1.1×10^{18}	2.1×10^{18}
3.0×10^{-3}	1.8×10^{18}	3.6×10^{18}	3.3×10^{18}	6.3×10^{18}
1.0×10^{-2}	6.0×10^{18}	1.2×10^{19}	1.1×10^{19}	2.1×10^{19}
3.0×10^{-2}	1.8×10^{19}	3.6×10^{19}	3.3×10^{19}	6.3×10^{19}
1.0×10^{-1}	6.0×10^{19}	1.2×10^{20}	1.1×10^{20}	2.1×10^{20}

[a] $N_0 = 7.0 \times 10^{-4}$ M (4.2×10^{17} cm^{-3})was reported in Ref. 1, which did not report N; the value $N = 1.4 \times 10^{18}$ cm^{-3} for RuB:S (in italics) is our estimate.

[b] RuB:A samples of $N \geq 1.2 \times 10^{19}$ cm^{-3} (in italics) phase-separated upon gellation.

TABLE 7-2

Wavelength Positions of the Excitation and Emission Maxima
($\lambda_{ex\text{-}max}$ and $\lambda_{em\text{-}max}$, nm) for RuB by Matrix and Concentration

Initial Number Density (cm^{-3})	$\lambda_{ex\text{-}max}$ Matrix A	$\lambda_{ex\text{-}max}$ Matrix E	$\lambda_{ex\text{-}max}$ Matrix S	$\lambda_{em\text{-}max}$ Matrix A	$\lambda_{em\text{-}max}$ Matrix E	$\lambda_{em\text{-}max}$ Matrix S
6.0×10^{17}	568.0	564.5	545.5	613.0	617.5	609.5
1.8×10^{18}	583.0	576.5	563.5	618.5	623.5	614.0
6.0×10^{18}	—	580.0	578.5	—	626.5	611.0
1.8×10^{19}	—	602.0	588.0	—	638.0	616.5
6.0×10^{19}	—	607.5	597.0	—	637.0	637.5
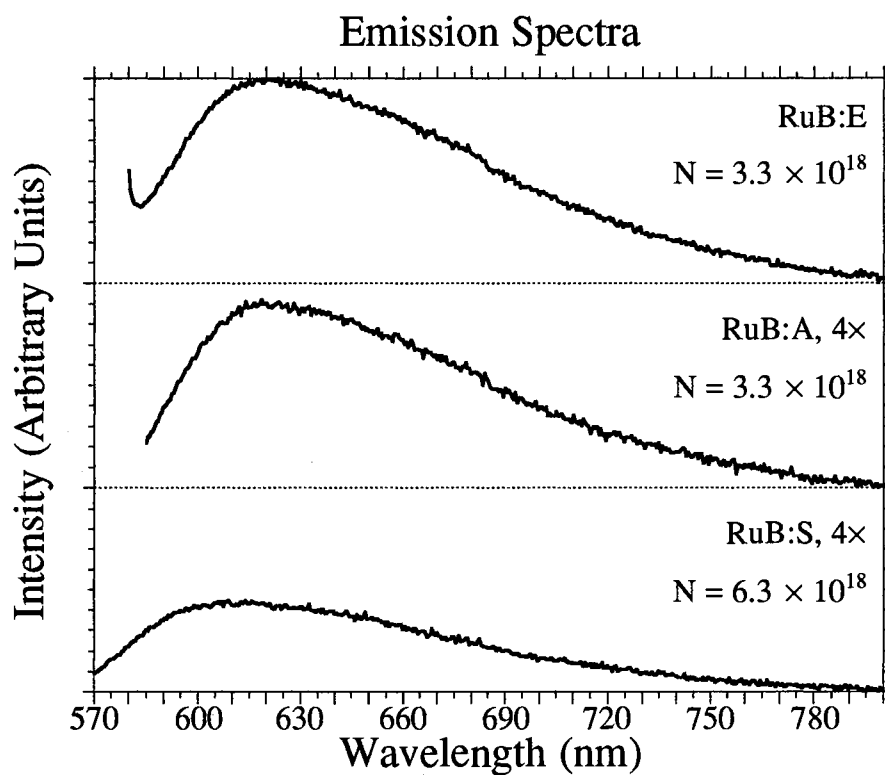
Emission Spectra

FIGURE 7-1: Representative fluorescence emission spectra: RuB:E, $N = 3.3 \times 10^{18}$ cm^{-3} (5.5 mM); RuB:A, $N = 3.6 \times 10^{18}$ cm^{-3} (6.0 mM), 4×; RuB:S, $N = 6.3 \times 10^{18}$ cm^{-3}(10 mM), 4×. Samples were excited at the maximum value of the MLCT band near 580 nm (see Figure 7-2). All emission spectra are normalized to the intensity of RuB:E. The spectra of the RuB:A and RuB:S samples are multiplied for clarity.

Excitation Spectra

Intensity (Arbitrary Units) vs **Wavelength (nm)**

RuB:E

$N = 3.3 \times 10^{18}$

RuB:A, 4×

$N = 3.3 \times 10^{18}$

RuB:S, 4×

$N = 6.3 \times 10^{18}$
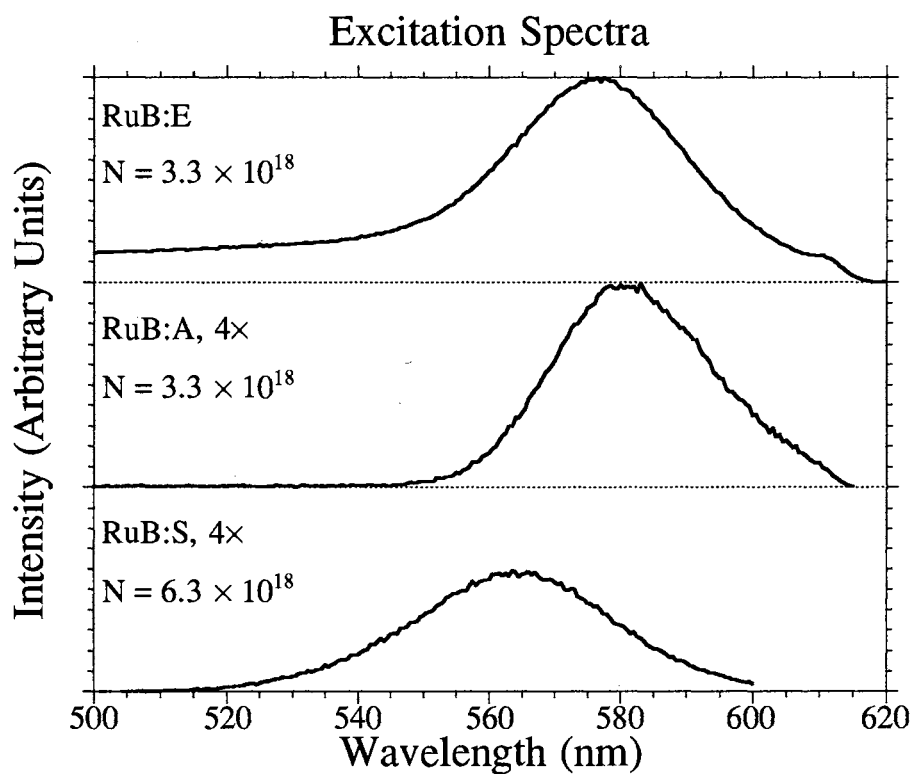
FIGURE 7-2: Representative fluorescence excitation spectra: RuB:E; RuB:A, 4×; RuB:S, 4×. Sample concentrations are the same as in Figure 7-1. Emission was viewed at the maximum value of the charge-transfer emission to the $^1A_1$ ground state near 620 nm (see Figure 7-1). All excitation spectra are normalized to the intensity of RuB:E. The spectra of the RuB:A and RuB:S samples are multiplied for clarity.

Figure 7-3 shows the quantum efficiencies (Q) of RuB in the three host matrices. Ideally, the quantum efficiency for this radiative transition would be independent of concentration at room temperature. It is observed, however, to decrease with increasing concentration in most systems. Concentration quenching is usually caused by cross-relaxation events which exist between closely-spaced dopant molecules. Q values for RuB-doped silica gels having high number densities are comparable to those previously reported in aqueous solutions (1%–5%); lower number densities in silica specimens have Q values which approach the 10% value reported by Reisfeld et al.[1] for RuB-doped silica gels containing 7×10^{-4} M ($N = 4.2 \times 10^{17}$ cm^{-3}) dopant concentrations.

RuB-doped ormosils, in general, have been found to possess substantially higher quantum efficiencies than either the liquid-phase aqueous or solid-state silica gel systems (see Figure 7-3). This is presumably due to the limited migration rate of triplet quenchers, such as oxygen (O_2), through the denser ormosil matrix. The anomalously large Q value for RuB:E at $N = 10^{19}$ cm^{-3} was reproduced in three different samples, and is consistent with visual observations of these specimens. Such behavior is not well understood, but may indicate a particularly favorable dopant–matrix interaction over restricted concentration regimes. Such maxima usually occur either by a convolution of two competing factors or as an optimum configuration (like the minimum of a quantum energy well). In this case, it is probably optimum pore packing so that the forces exerted on the dopant by the matrix are most favorable. Overall, these Q values are quite promising, and indicate that these systems merit further study for potential optical source applications.

Figure 7-4 shows the fluorescence lifetimes of the MLCT emission of RuB in all three host matrices. The lifetimes in matrix A are closest to that reported by Reisfeld et al.[1] for RuB:S, 1.34 μs. Matrix E values are comparable to the acrylate system with the pure silica gel having substantially shorter lifetimes. Lifetime reduction with increasing

dopant concentration was found to be nearly logarithmic. When considered with the observed trends in quantum efficiency, it is a strong indicator of concentration quenching.

RuB Quantum Efficiencies
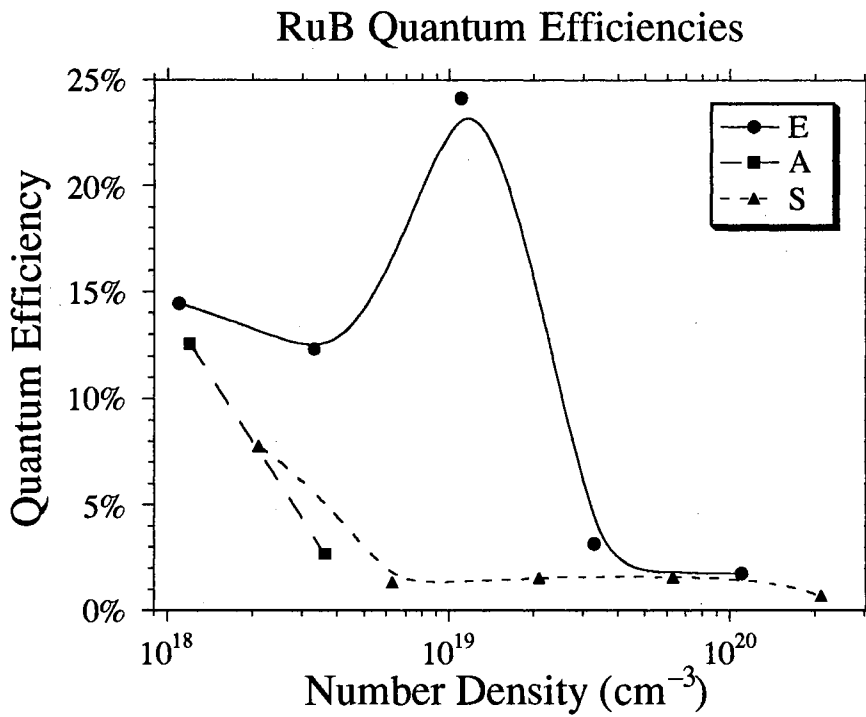
FIGURE 7-3: Quantum efficiency as a function of concentration for RuB in matrices E, A, and S. The fit is the best smooth curve.
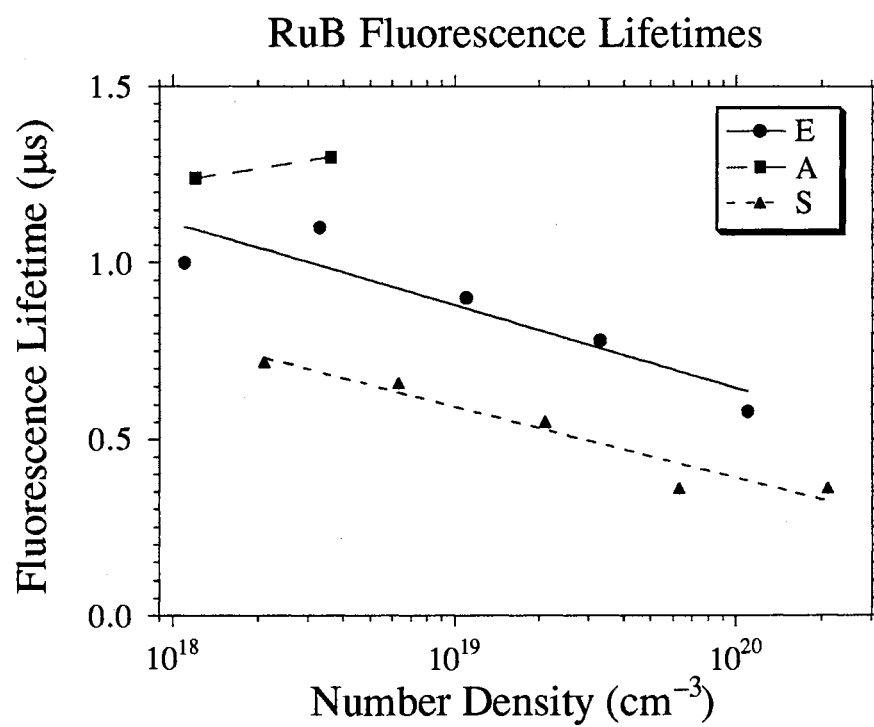
FIGURE 4: Fluorescence lifetimes (µs) of the MLCT emission for RuB. The fit is a logarithmic least-mean-square line.

IV. Conclusions

Changes in the local chemical environment experienced by the RuB dopant, as evidenced by its fluorescence spectra and other parameters, are substantially greater than those described in the earlier Chapters for organo-europium complexes, which have relatively shielded *f*-orbital electrons. Environmentally induced perturbations produce shifts in intensity and position for both excitation and emission processes. The large quantum efficiency values and broad emission and excitation characteristics exhibited by RuB in moderate to low dopant concentrations make them promising candidates for use as optical sources, or as the photoactive agent in conducting photochemical reactions.

Both RuB-doped ormosil matrices demonstrate improved quantum efficiencies and lifetime characteristics with respect to comparable RuB-doped silica gel specimens. Thus, the organically modified silicate hosts appear to be more interesting host matrices for the RuB dopant, as they were found to be in the case of $Eu(ttfa)_3$. This increased optical performance may be due in part to the denser nature of the ormosils relative to the silica xerogel, which would tend to decrease nonradiative deactivation of the RuB dopant by external triplet quenching agents such as oxygen.

V. References

1.   R. Reisfeld, D. Brusilovsky, M. Eyal, and C. K. Jørgensen, *Chimia* **43** (1989) 385, and references therein.

2.   R. Reisfeld, V. Chernyak, M. Eyal, and C. K. Jørgensen, in W. Strek, *Second International School of the Excited States of the Transition Elements* (Singapore: World Science, 1992), p. 247.

3.   K. Matsui, K. Sasaki, and N. Takahashi, *Langmuir* **7** (1991) 2866.

4. A. Slama-Schwok, D. Avnir, and M. Ottolenghi, *J. Am. Chem. Soc.* **113** (1991) 3984.

5. O. Dvorak and M. K. De Armond, *J. Phys. Chem.* **97** (1993) 2646.

6. B. D. MacCraith, C. M. McDonagh, G. O'Keeffe, E. T. Keyes, J. G. Vos, B. O'Kelly, and J. F. McGilp, *Analyst* **118** (1993) 385, and references therein.

7. (a) N. de la Rosa-Fox, L. Esquivias, and J. Zarzycki, *Diffusion and Defect Data* **53–54** (1987) 363. (b) L. Esquivias and J. Zarzycki, in J. D. Mackenzie and D. R. Ulrich, *Ultrastructure Processing of Advanced Ceramics* (New York: John Wiley & Sons, Inc., 1988), p. 255.

8. (a) C. A. Capozzi and L. D. Pye, in Proceedings of SPIE, v. 970 (Bellingham, WA: The Society of Photo-Optical Instrumentation Engineers, 1988), p. 135. (b) E. T. Knobbe, B. Dunn, P. D. Fuqua, and F. Nishida, *Appl. Opt.* **29** (1990) 2729.

9. (a) H. Schmidt and B. Seiferling, in C. J. Brinker, D. E. Clark, and D. R. Ulrich, *Better Ceramics Through Chemistry II,* Materials Research Society Proceedings, v. 73 (Pittsburgh, PA: Materials Research Society, 1986), p. 739. (b) B. Lintner, N. Arfsten, H. Dislich, H. Schmidt, G. Philipp, and B. Seiferling, *J. Non-Cryst. Solids* **100** (1988) 378.

10. J. N. Demas and G. A. Crosby, *J. Phys. Chem.* **75** (1971) 991.

11. K. H. Drexhage, (a) in F. D. Schäfer, *Dye Lasers*, second edition (New York; Berlin; Heidelberg: Springer-Verlag, 1977); (b) "Design of Laser Dyes," VII International Quantum Electronics Conference (Montreal, 1972); (c) *Laser Focus* **9** (1973) 35.

CHAPTER 8

SPECTROFLUORIMETRIC CHARACTERIZATION OF AN IONIC CONDUCTOR:
SODIUM SULFATE HIGH-TEMPERATURE PHASES DOPED WITH
EUROPIUM(III)*

I. Introduction

The highest-temperature hexagonal polymorph of sodium sulfate, Na_2SO_4 (I), which is known to be stable from 237°C to the melting point at 883°C,[1] has a number of properties of interest to specialists in solid-state ionics and crystal chemistry. Pure (I) is an ionic conductor, with a conductivity (σ) value of 1.1×10^{-5} S/cm or $(\Omega\ cm)^{-1}$ at 250°C.[2] Although this conductivity value is relatively modest, it can be increased by at least two orders of magnitude by substituting aliovalent cations into the (I) crystal structure; for example, (I) doped with 4 mol % $La_2(SO_4)_3$ has $\sigma = 1.08 \times 10^{-3}$ S/cm at 290°C (conductivity equal to that of pure phase (I) at 500°C).[3] Typical ionic crystals have σ values of only 10^{-9}–10^{-8} S/cm, while *superionic* conducting crystals have values around 0.5 S/cm.[4][†]

The example of doping (I) with La^{3+} introduces another interesting property of (I): it has significant orientational disorder in its hexagonal structure, comprised mostly of monoclinic distortions, which allows it to readily accept substitution by aliovalent cations.[5] Examples of doping (I) with aliovalent species include studies of crystals containing Y^{3+}, Sr^{2+}, Ni^{2+}, and Zn^{2+} by Höfer, Eysel and von Alpen;[6] La^{3+}, Dy^{3+}, Sm^{3+}, and

---

* Portions of the work presented in this Chapter have been accepted for presentation in the Solid-State Ionics Symposium at the Materials Research Society Fall Meeting, Boston, MA, November 28–December 2, 1994.

† In Ref. 4, lanthanum-doped Na_2SO_4 (I) is superionic ($\sigma > 10^{-3}$ S/cm). In comparison, metals have electronic conductivities of 10^4–10^6 S/cm.

In^{3+} by Prakash and Shahi;[3] and Y^{3+}, La^{3+}, Dy^{3+}, Ce^{4+}, and Ca^{2+} by Dharmasena and Frech.[1]

Aliovalent cation substitution in Na$_2$SO$_4$ (I) has at least two important effects. As mentioned above, it has the effect of increasing the ionic conductivity of (I) through the introduction of vacancies. In fact, Höfer *et al.* showed that σ depended only on the number of vacancies created and not on the valence or size of the aliovalent cation.[6] Substitution also has the effect of extending the stability region of (I) to significantly lower temperatures. Pure (I) cannot be quenched‡ to room temperature (RT) without undergoing a phase change to Na$_2$SO$_4$ (III), an orthorhombic phase which is stable from 200°–235°C and is metastable down to RT.[5, 7] (The other phases of Na$_2$SO$_4$ which have been reported are Na$_2$SO$_4$•8H$_2$O, the most stable form at ambient conditions; (V), the anhydrous orthorhombic form stable at RT and up to about 200°C; (IV), a modification of (V) which has been reported to exist from 180°–200°C; and (II), a modification of (III) which has been reported to exist from 228–235°C.[7] Both (II) and (IV) are somewhat weakly defined and hard to observe; direct (V)–(III)–(I) transitions are commonly observed.[8]) Aliovalent solid solutions of (I), however, *can* be quenched to RT because the disorder introduced into the crystal structure by aliovalent cation substitution alters the phase transition energy structure. This phase stabilization is observed to occur over a 200°C range, and it can be effected by as little as 1.2 mol % Y$_2$(SO$_4$)$_3$. At lower dopant levels, *i.e.*, less than 1 mol %, phase (III) can also form aliovalent solid solutions which are stabilized to RT.[1] As described above, a number of successful substitutions of trivalent cations into Na$_2$SO$_4$ have been reported.[1, 3, 6] In the present Chapter, the incorporation of europium(III), which has been chosen for its spectroscopic utility, into Na$_2$SO$_4$ (I) and (III) is first reported.

---

‡ The term "quenched" in this context is used to describe the process in which crystals
   are grown from a melt by controlled cooling, as opposed to its spectroscopic use, *i.e.*
   "quenched fluorescence."

The europium(III) ion is an extremely sensitive and useful probe of its immediate local environment. The presence, location, and intensity of its fluorescence transitions (particularly the $^5D_0 \rightarrow {}^7F_{0-2}$ or E_{0-2} emissions**) can provide detailed information about the symmetry, nature, and multiplicity of the individual Eu^{3+} sites which cannot be gained from techniques such as X-ray or neutron diffraction. Examples of the use of the europium(III) ion as a luminescence probe include studies of inner-sphere coordination in binary water/organic solvent systems by Lis and Choppin[9] and by Lochhead, Wamsley, and Bray;[10] and of solid-state coordination in sol–gel-derived silica glasses by McDonagh et al.;[11] tin(IV) oxide gels by Ribeiro et al.;[12] and oxide crystals by Nieuwpoort, Blasse, and Bril.[13] Finally, in a highly detailed study of a europium(III) crown ether system, Bünzli and Pradervand were able to identify three chemically differ-ent Eu^{3+} sites in two cationic and one anionic species by europium(III) fluorescence spectroscopy.[14]

In the research presented in this Chapter, europium(III) fluorescence spectroscopy is used as a probe to provide additional structural characterization for two europium-doped sodium sulfate phases, (I) and (III), both stabilized to at least room temperature. Spectra of europium(III) chloride and sulfate are included as references.

II. Experimental Methods

$EuCl_3 \cdot 6H_2O$ and $Eu_2(SO_4)_3 \cdot 8H_2O$ were obtained from Pfaltz & Bauer for use as reference compounds without further purification or characterization. The europium-doped sodium sulfate samples, Na_2SO_4 (I):Eu^{3+} (3.0 mol %) and Na_2SO_4 (III):Eu^{3+} (0.8 mol %) were obtained from Dr. Roger Frech of the University of Oklahoma, Norman, OK, and his graduate researchers Gamini Dharmasena and Renée Cole. Their synthetic

---

** As in Chapter 1, the symbol E_J ($J = 0$–4) is used as an abbreviation for the $^5D_0 \rightarrow {}^7F_J$ emission transition of europium(III).

procedure followed that previously reported by Dharmasena and Frech,[1] namely, by melting the appropriate amounts of $Eu_2(SO_4)_3 \cdot 8H_2O$ and Na_2SO_4 (both at $\geq 99\%$ purity) at 950°C for 6 h, cooling to 700°C for 3 h, and finally cooling to RT over 6 h.

Continuous-wave luminescence (emission and excitation) spectra, software-corrected for instrumental response, were measured using a Spex Industries Model F112 spectrofluorimeter by the author at Oklahoma State University, as described in the preceding Chapters. All the spectra were collected with the test subjects carefully positioned within a fused-quartz dewar in order to facilitate direct comparisons between otherwise identical spectra recorded at room temperature ($\approx$290 K) and at liquid-nitrogen temperature (77 K). The samples' full 565–715 nm emission, 605–630 nm detailed emission, and full 300–600 nm excitation spectra were recorded first at RT, then recorded at 77 K, and finally recorded a second time at RT as a safeguard against the possibility that lowering the samples' temperature to 77 K might induce a phase change. No significant differences were observed between the "before" and "after" spectra, indicating that exposing the samples to liquid nitrogen did not induce a phase change (probably due to kinetics restrictions).

Laser Raman spectra and ionic conductivity measurements were conducted by the Frech research group at the University of Oklahoma, using the techniques reported by Dharmasena and Frech.[1]

III. Discussion of Results

A. Laser-Raman Spectroscopy (Figures 8-1 and 8-2)

Figures 8-1 and 8-2 show the laser-Raman spectra used to demonstrate that doping sodium sulfate (V) with aliovalent cations causes a change to (III) at relatively low dopant levels (< 1.0 mol %), progressing to (I) at higher dopant levels ($\geq$ 1.2 mol %).

Figure 8-1: Pure Na$_2$SO$_4$ v$_4$ Raman Spectra
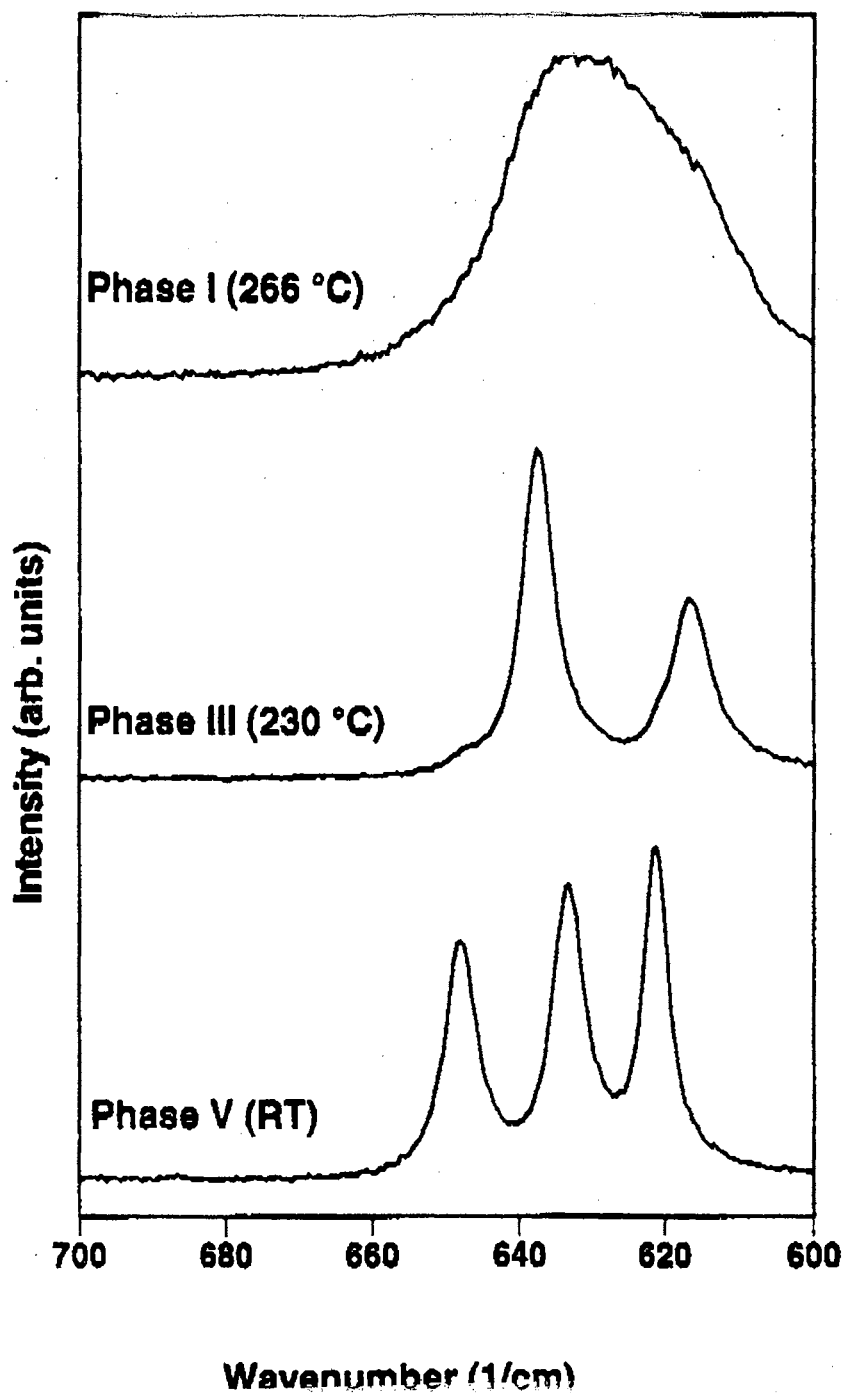
FIGURE 8-1: Temperature-dependent laser-Raman spectra of pure Na$_2$SO$_4$ powders, viewed in the v$_4$ region. This Figure was provided by Gamini Dharmasena of the University of Oklahoma and is used with permission.

Figure 8-2: Eu-Doped Na_2SO_4 v_4 Raman Spectra
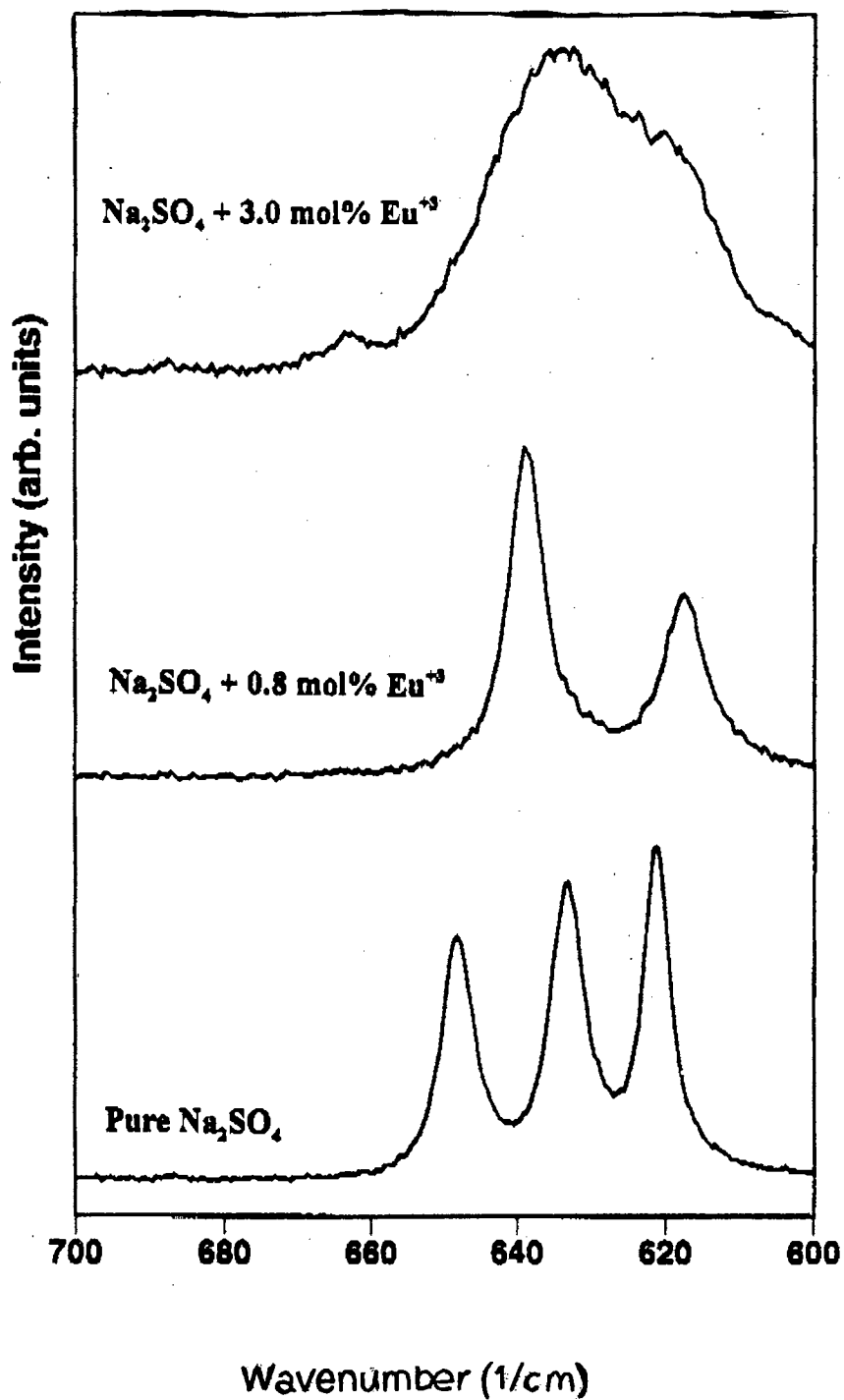
FIGURE 8-2: Room-temperature laser-Raman spectra of pure and europium-doped Na_2SO_4 powders, viewed in the v_4 region. This Figure was provided by G. Dharmasena and is used with permission.

In Figure 8-1, the triplet in pure (V); two peaks of which collapse into one, leaving a doublet, in pure (III) at 230°C; and the broad singlet in pure (I) at 266°C are characteristic of those phases both in the powder and in single crystals. These spectral features unique to (III) and (I) are faithfully reproduced in the room-temperature spectra of $Na_2SO_4:Eu^{3+}$ (0.8%), and $Na_2SO_4:Eu^{3+}$ (3.0%), respectively. These spectra demonstrate conclusively, with no other reasonable interpretations, that these doped phases are indeed isostructural with pure phases (III) and (I).[††]

B.   Ionic Conductivity (Figure 8-3 and Table 8-1)

An examination of the ionic conductivity of the europium-doped sodium sulfates, presented in Figure 8-3, also demonstrates a change in phase behavior. As a temperature-activated diffusion phenomenon, ionic conductivity has a temperature dependence which may be expressed by the following:

$$(1) \qquad \sigma = \frac{\sigma_0}{T} \exp\left(-\frac{Q_c}{kT}\right)$$

where, using the notation of Mundy,[15] σ_0 is the pre-exponential constant (S cm^{-1} K) and Q_c is the activation energy for ionic motion (J or eV); k and T have their usual physical-chemistry definitions as Boltzmann's constant (J/K or eV/K) and the absolute temperature (K), respectively. Alternatively, Equation (1) may be expressed in macroscopic units by substituting the gas constant R for k, and the equation can be made more manageable by expressing it in logarithmic form:

$$(2) \qquad \ln \sigma T = \ln \sigma_0 - \frac{Q_c}{RT} = -\left(\frac{Q_c}{R}\right)\left(\frac{1}{T}\right) + \ln \sigma_0$$

In the latter form, a plot of $\ln \sigma T$ versus $1/T$ as in Figure 8-3 allows the evaluation of Q_c from linear regression and of σ_0 by extrapolation to $T = \infty$. Besides its usefulness in determining these two quantities, this type of plot can also reveal phase changes, which are marked by discontinuities in the slopes of the lines.[8, 15] In Figure 8-3, such

---

[††]   The $Na_2SO_4:Eu^{3+}$ (0.8%) and $Na_2SO_4:Eu^{3+}$ (3.0%) solid solutions will be labeled *0.8% Eu* and *3.0% Eu* for the remainder of this Chapter.

138

discontinuities exist in pure Na_2SO_4 between 476 and 535 K (average 506 K = 233°C) and for 0.8% Eu between 485 and 526 K (average 506 K = 233°C). By converting the phase transition temperatures given in the introduction into absolute terms,[7] the (V)–(III) and (III)–(I) phase transitions are expected to occur at 473 K and 508 K, respectively, corresponding to 2.11×10^{-3} and 1.97×10^{-3} on the $1/T$ scale. For pure Na_2SO_4, this means that the discontinuity probably covers both phase transitions. Since 0.8% Eu is already in phase (III), the discontinuity is most probably the (III)–(I) transition. Additional evidence for identification of these phases is found in Table 8-1, where the Q_c and σ_0 values obtained from the data in Figure 8-3 are listed. As can also be seen from Figure 8-3, the Q_c values for all three samples at $T > 500$ K (particularly for $T > 580$ K) are very close to one another. This result is consistent with all three samples existing in phase (I) in this temperature region. It should also be noted that the Q_c values for those samples predicted to be in phase (V) (pure Na_2SO_4 at $T < 500$ K) and in phase (III) (0.8% Eu at $T < 500$ K) show significant differences from those expected for phase (I).

From the data in Figure 8-3, the ionic conductivity values at the lowest available comparable temperatures are 1.56×10^{-9} S/cm for pure Na_2SO_4 (V) at 102°C, 5.02×10^{-9} S/cm for 0.8% Eu (III) at 103°C, and 2.78×10^{-7} S/cm for 3.0% Eu (I) at 102°C. Although the value for 3.0% Eu is nearly 200 times greater than that of pure (V), at this temperature it is four decades short of the superionic threshold. Near 290°C, however, the temperature at which Prakash and Shahi reported the σ value of 1.08×10^{-3} S/cm for their *best* composition, (I)+ 4% $La_2(SO_4)_3$,[3] the value for 3.0% Eu at 308°C is 3.80×10^{-4} S/cm, fully 35% of the value of the lanthanum-doped (I) and a factor of only 2.6 below the superionic threshold.

Figure 8-3: Ionic Conductivities
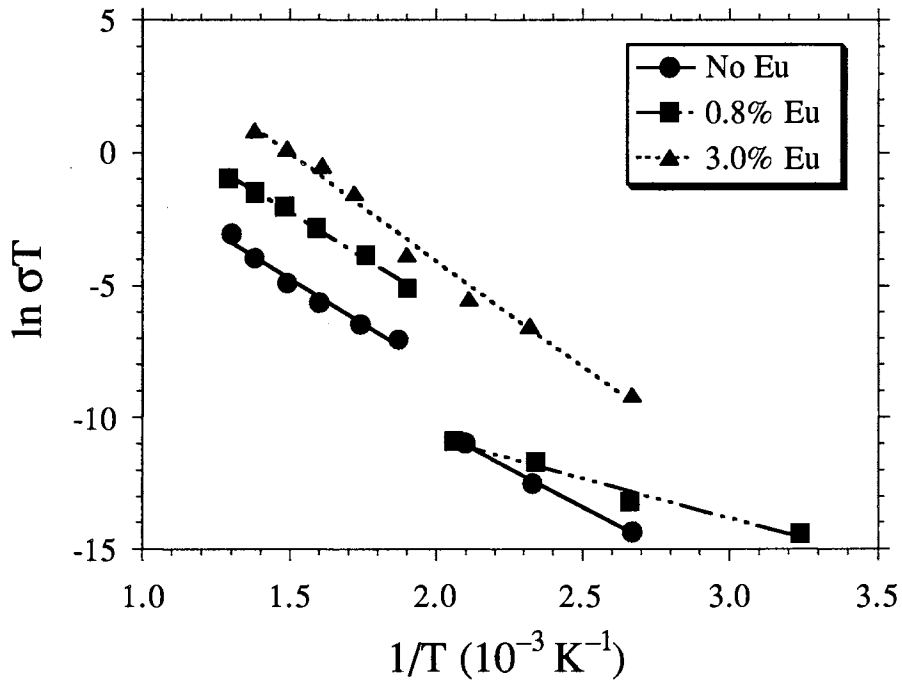
FIGURE 8-3: Ionic conductivities of pure and europium-doped sodium sulfates, fitted by linear regression. The data for this Figure was provided by G. Dharmasena and are used with permission.

TABLE 8-1

Eu Dopant Level	Q_c (J/mol)	σ_0 (S cm^{-1} K)	Corr
None, $T > 500$ K	57.5	2.84×10^2	-0.989
None, $T < 500$ K	49.0	3.82×10^0	-0.998
0.8% Eu, $T > 500$ K	55.4	2.27×10^3	-0.997
0.8% Eu, $T < 500$ K	25.3	9.09×10^{-3}	-0.986
3.0% Eu	67.1	1.76×10^5	-0.994
3.0% Eu, $T > 580$ K	56.2	2.74×10^4	-0.992

TABLE 8-1: Values of Q_c (the ion migration activation energy), σ_0 (the conductivity pre-exponential constant), and the linear regression correlation factor for pure and europium-doped sodium sulfate as functions of dopant level and temperature. These values were obtained by linear regression operations on the data in Figure 8-3.

C.   Europium(III) Spectrofluorimetry (Figures 8-4 through 8-10, Table 8-2)

The Figures and Table presented in this section display the room-temperature ($\approx$290 K) and liquid-nitrogen-temperature (77 K) europium(III) fluorescence spectra and the data generated from spectra for the purpose of conducting spectrofluorimetric characterization of the europium-doped sodium sulfates, 0.8% Eu and 3.0% Eu, and the stoichiometric references, $EuCl_3 \cdot 6H_2O$ (at both temperatures) and $Eu_2(SO_4)_3 \cdot 8H_2O$ (at RT only).

Virtually all of the features visible in the emission spectra (Figs. 8-4–8-7 and 8-10) arise from radiative emissions from the $^5D_0$ excited level of Eu^{3+}, which lies roughly 17,300 cm^{-1} above the ground state, to the first five J levels of the ^7F ground-state manifold. (The $^5D_0 \rightarrow {}^7F_{5-6}$ emissions and those emissions arising from the $^5D_1$ and $^5D_2$ levels are extremely weak.) The visible features in the excitation spectra (Figs. 8-8–8-9) arise from those absorptive transitions from the $^7F_0$ ground state to various excited states which result in population of the $^5D_0$ emitting level either directly or by internal conversion. These excited states include the $^5D_0$, $^5D_1$, $^5D_2$, $^5L_6$, $^5G_{4-6}$, $^5D_4$, and $^5H_6$, and their excitation bands are centered near 580, 530, 465, 395, 380, 360, and 320 nm, respectively; the strongest transition is the $^7F_0 \rightarrow {}^5L_6$.[16]

Because the ^5D and ^7F terms both arise from the $4f^6$ electronic configuration of Eu^{3+}, transitions between them are forbidden by the Laporte rule for electric-dipole (ED) interactions and can therefore appear only when partially allowed by the selection rules for magnetic-dipole (MD) interactions or by external perturbations which serve to mix odd-parity terms into the ion's ligand/crystal field expansion, particularly by the introduction of static and/or dynamic (vibrationally induced) asymmetry into the ligand field.[17–18] (Transitions involving a change in parity, *e.g.* $4f^6 \leftrightarrow 4f^5 5d^1$, are Laporte-allowed and therefore have very high intensities, but in Eu^{3+} these occur only at energies greater than 40,000 cm^{-1}, outside the range of conventional spectroscopic methods.[16–17]) Because the E_{0-4} transitions arise from different interaction mechanisms, their responses

to perturbations differ significantly; these differences in behavior, particularly those of the E_{0-2} transitions, can then be used to examine the Eu^{3+} ion's local ligand field.

Of the five E_J transitions, only E_1 is purely MD in character; therefore, its intensity is not sensitive to the ligand field and it may be used as a reference peak.[12, 19] In fact, in environments sufficiently symmetrical as to possess an inversion center (*e.g.* aqueous solution or $[Eu(NO_3)_6]^{3-}$), the MD E_1 transition dominates the spectrum and the other four ED features are insignificant.[14, 20]

The E_2 transition operates by a forced ED mechanism and is one of a number of rare-earth transitions so dependent upon variations in the ligand field that Judd called them "hypersensitive." Hypersensitivity is observed in those transitions which nominally obey the selection rules for electric quadrupole radiation (chiefly, $\Delta J = 2$) but which can have intensities several orders of magnitude greater than that possible under the quadrupole mechanism; hypersensitive transitions are most intense when an asymmetric electronic distribution within the rare-earth ion is produced by the external electric fields present in environments of low symmetry (classes C_s, C_n, and C_{nv}).[21] An absolute increase of the integrated intensity (S) of E_2 and a relative increase of $S(E_2)$ to $S(E_1)$ (the η_{21} ratio) is a strong indicator of the lowering of symmetry, particularly the removal of inversion symmetry,[10] and the increasing of chemical bond strength between Eu^{3+} and its surroundings.[20]

The "superforbidden" E_0 transition gains a weak MD oscillator strength in fields of low symmetry (classes C_s, C_n, and C_{nv}). Because it is a transition between $J = 0$ states, it is completely nondegenerate and has no internal structure or Stark splitting. The other four transitions have $2J + 1$ Stark components, some of which may be degenerate depending upon field symmetry. Therefore, any band structure or significant broadening of the E_0 line arises from Eu^{3+} ions in energetically different sites.[22]

Figure 8-4: Emission Spectra at Room Temperature
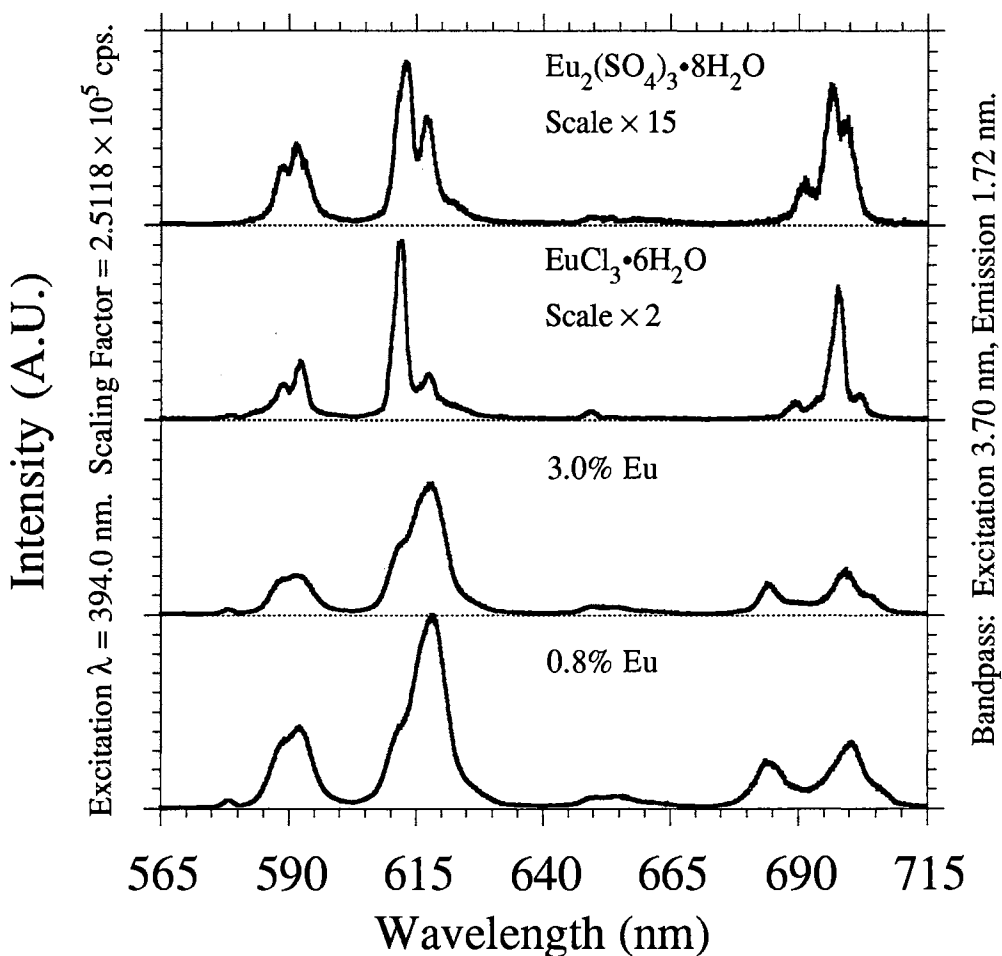
FIGURE 8-4: Full room-temperature emission spectra of 0.8% Eu, 3.0% Eu, and reference compounds $EuCl_3 \cdot 6H_2O$ and $Eu_2(SO_4)_3 \cdot 8H_2O$. The given scaling factor is that of 0.8% Eu in photon counts per second (cps), an instrument-dependent parameter removed by normalization. The europium chloride and sulfate spectra have been multiplied by 2 and 15, respectively, for clarity.

Figure 8-5: Emission Spectra at 77 K
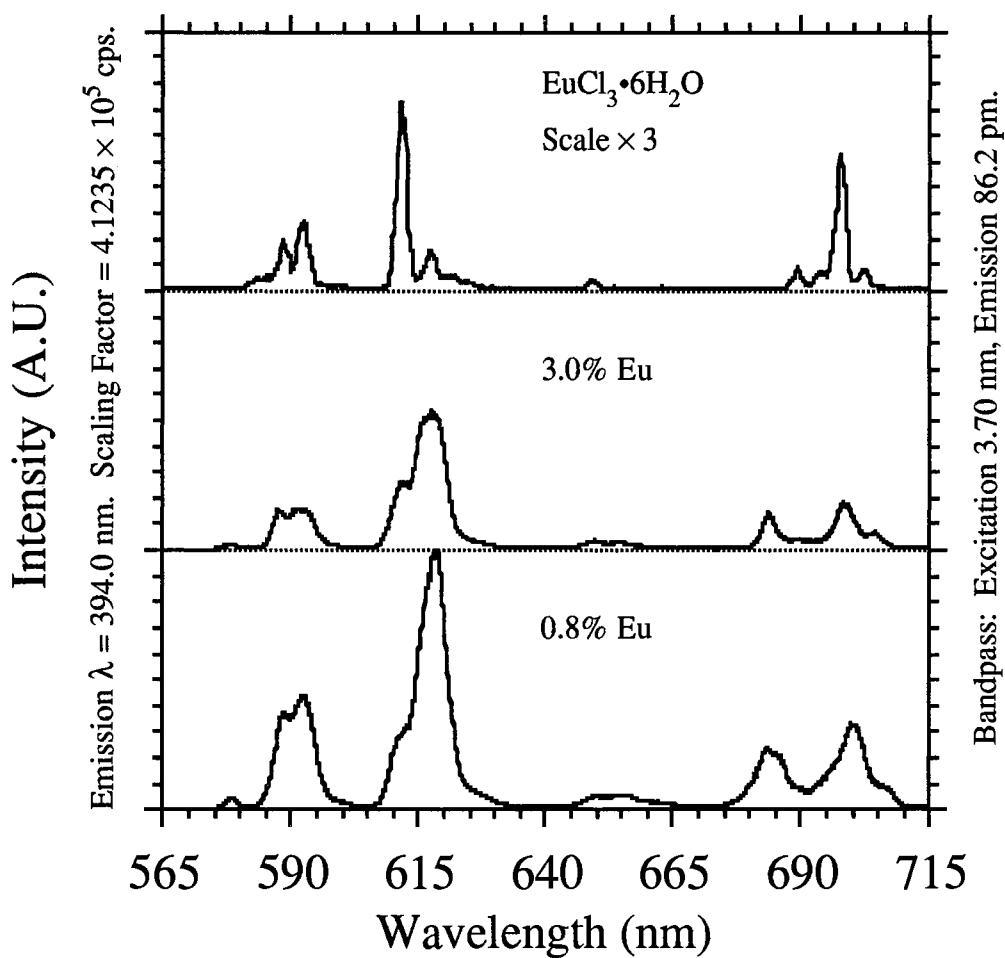
FIGURE 8-5: Full 77 K emission spectra of 0.8% Eu, 3.0% Eu, and reference compound EuCl₃•6H₂O. The given scaling factor is that of 0.8% Eu.

Figure 8-6: Emission Spectra at RT, E_2 Region
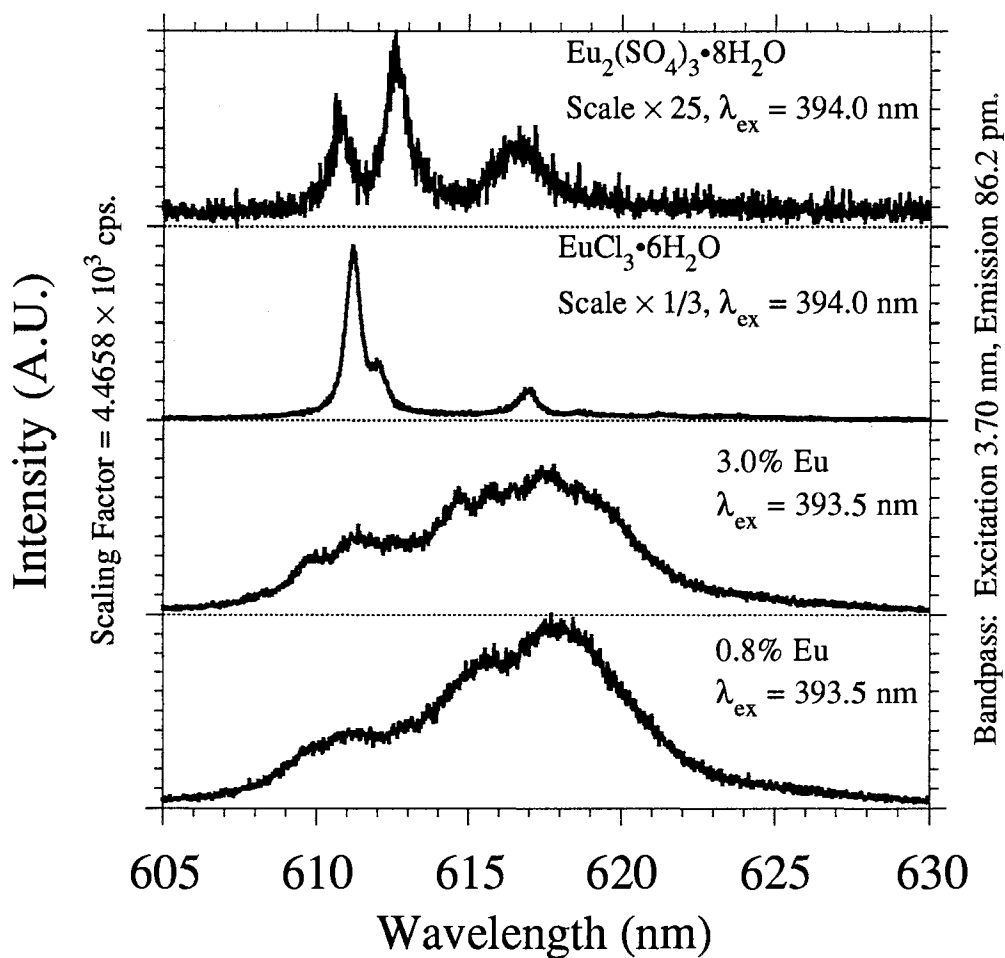
FIGURE 8-6: Detailed room-temperature emission spectra of 0.8% Eu, 3.0% Eu, and reference compounds $EuCl_3 \cdot 6H_2O$ and $Eu_2(SO_4)_3 \cdot 8H_2O$, focusing on the E_2 emission region. The given scaling factor is that of 0.8% Eu. The europium chloride and sulfate spectra have been multiplied by 1/3 and 25, respectively, for clarity.

Figure 8-7: Emission Spectra at 77 K, E_2 Region
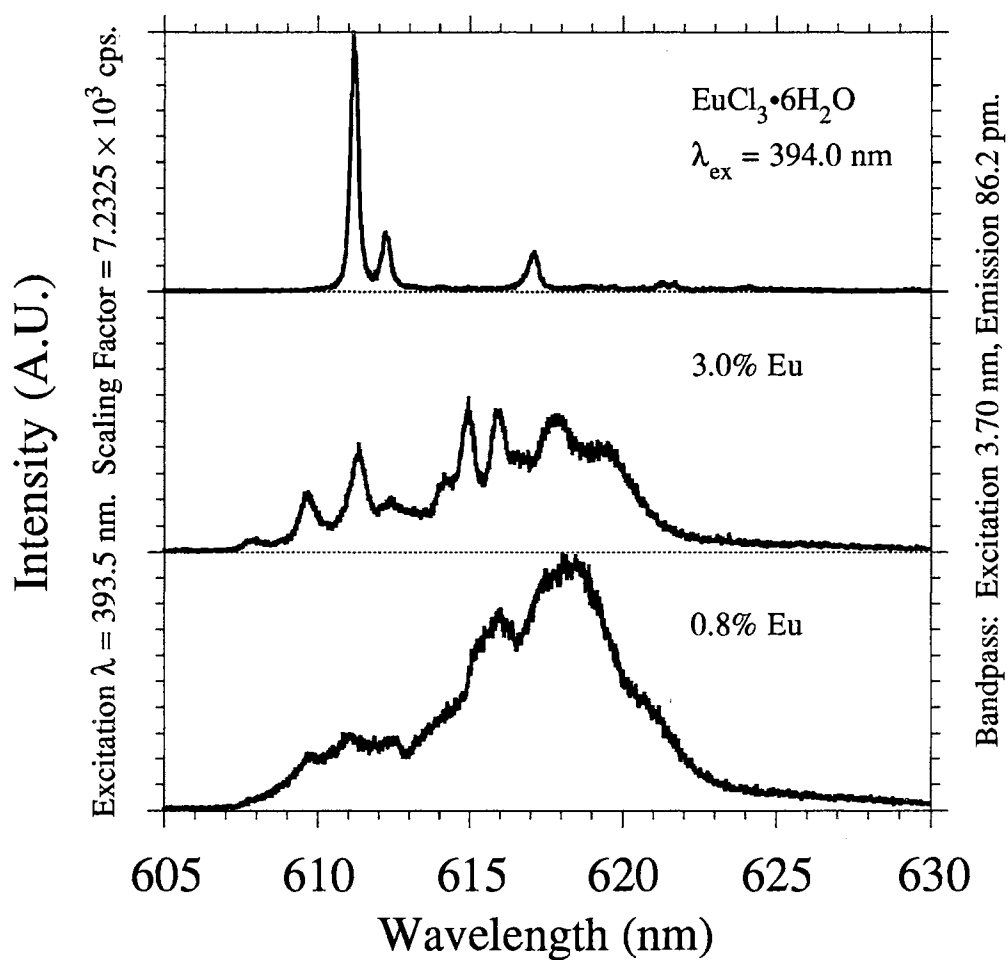
FIGURE 8-7: Detailed 77 K emission spectra of 0.8% Eu, 3.0% Eu, and reference compound $EuCl_3\cdot6H_2O$ focusing on the E_2 emission region. The given scaling factor is that of $EuCl_3\cdot6H_2O$.

Figure 8-8: Excitation Spectra at RT
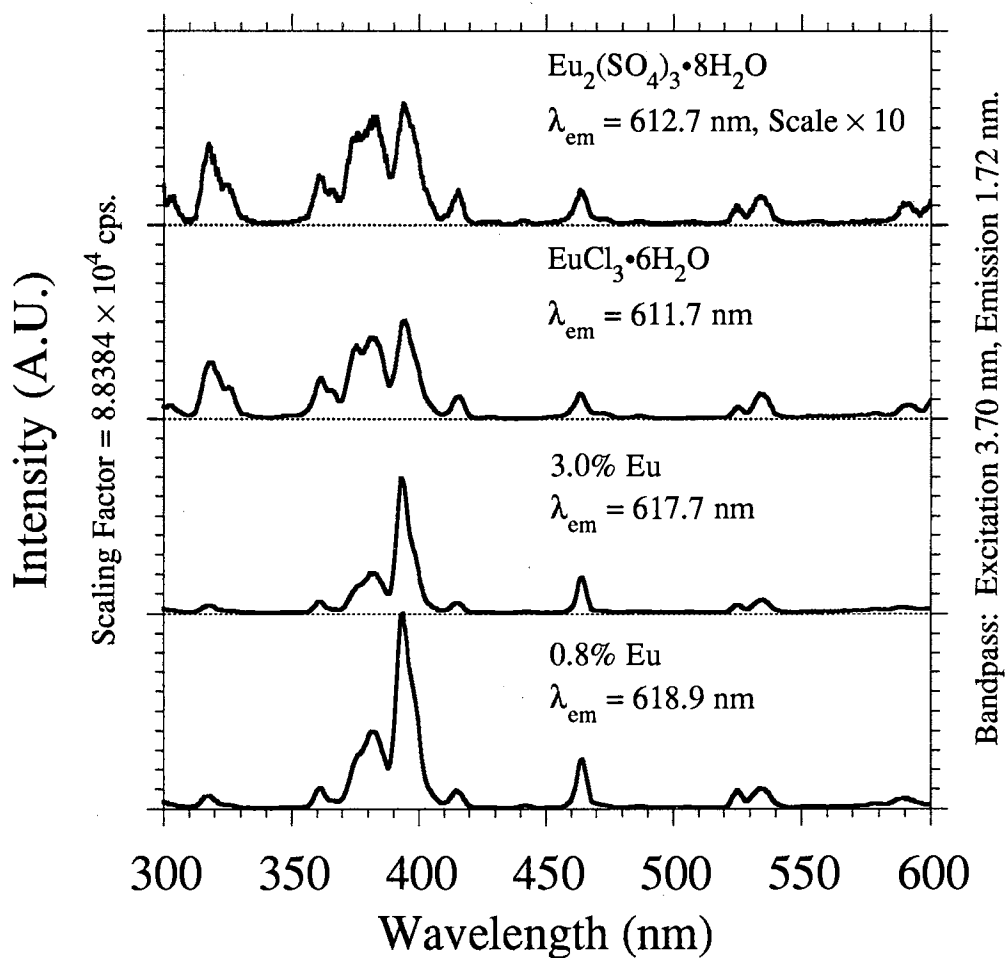
FIGURE 8-8: Full room-temperature excitation spectra of 0.8% Eu, 3.0% Eu, and reference compounds $EuCl_3 \cdot 6H_2O$ and $Eu_2(SO_4)_3 \cdot 8H_2O$, viewed at the E_2 emission. The given scaling factor is that of 0.8% Eu. The europium sulfate spectrum has been multiplied by 10 for clarity.

Figure 8-9: Excitation Spectra at 77 K
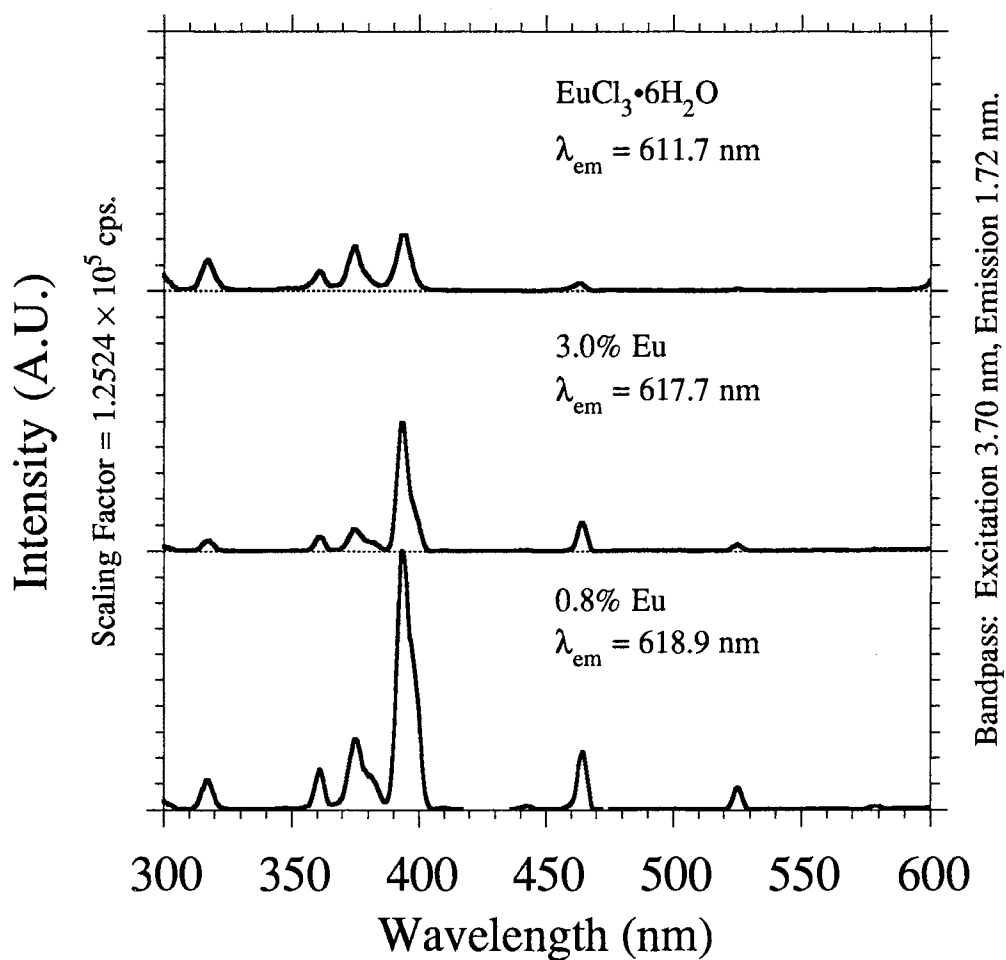
FIGURE 8-9: Full 77 K excitation spectra of 0.8% Eu, 3.0% Eu, and reference compound $EuCl_3 \cdot 6H_2O$, viewed at the E_2 emission. The given scaling factor is that of 0.8% Eu.

Figure 8-10: Emission Spectra at RT, E_0–E_1 Region

Eu$_2$(SO$_4$)$_3$•8H$_2$O
Scale × 25, λ_{ex} = 394.0 nm

EuCl$_3$•6H$_2$O
λ_{ex} = 394.0 nm

3.0% Eu
λ_{ex} = 393.5 nm

0.8% Eu
λ_{ex} = 393.5 nm

Intensity (A.U.)

Scaling Factor = 2.2526 × 10^3 cps.

Bandpass: Excitation 3.70 nm, Emission 86.2 pm.

Wavelength (nm)
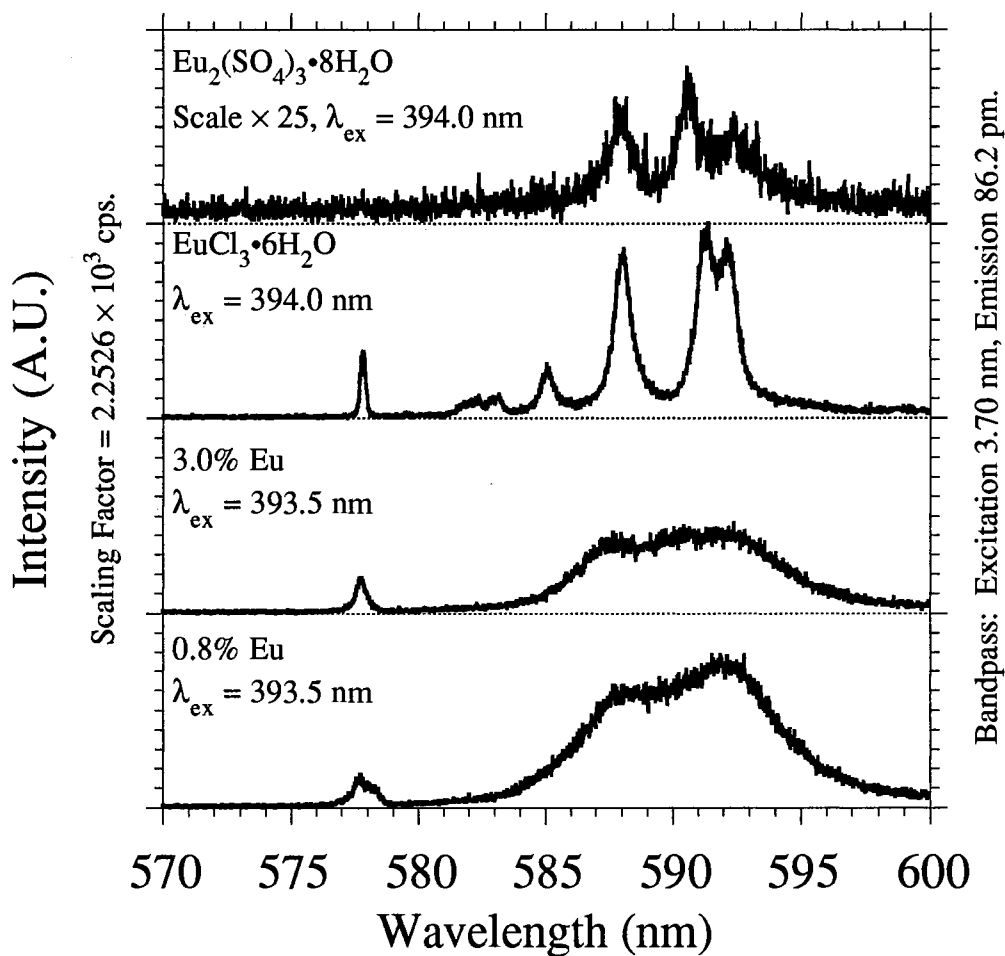
FIGURE 8-10: Detailed room-temperature emission spectra of 0.8% Eu, 3.0% Eu, and reference compounds EuCl$_3$•6H$_2$O and Eu$_2$(SO$_4$)$_3$•8H$_2$O, focusing on the E_0–E_1 emission region. The given scaling factor is that of EuCl$_3$•6H$_2$O. The europium sulfate spectrum has been multiplied by 25 for clarity.

TABLE 8-2

Part 1: RT ($\approx$290 K)

	0.8% Eu	3.0% Eu	Chloride	Sulfate
$S(E_0)$	0.135	0.085	0.048	—
$S(E_1)$	4.015	2.047	1.000	0.207
$S(E_2)$	10.421	7.295	2.346	0.441
η_{21}	**2.596**	**3.564**	**2.346**	**2.134**
$\lambda_{em\text{-}max}(E_0)$	578.3	577.9	578.4	—
$\lambda_{em\text{-}max}(E_1)$	592.2	591.7	592.2	592.2
$\lambda_{em\text{-}max}(E_2)$	618.4	617.6	612.2	612.2
FWHM E_0	2.9	2.9	3.2	—

Part 2: 77 K

	0.8% Eu	3.0% Eu	Chloride
$S(E_0)$	0.066	0.083	0.008
$S(E_1)$	0.743	2.730	0.842
$S(E_2)$	1.698	8.157	1.493
η_{21}	**2.285**	**3.442**	**1.773**
$\lambda_{em\text{-}max}(E_0)$	578.6	578.3	579.1
$\lambda_{em\text{-}max}(E_1)$	592.7	591.6	592.8
$\lambda_{em\text{-}max}(E_2)$	618.9	617.7	611.7
FWHM E_0	2.6	2.5	2.7

TABLE 8-2: Room-temperature (Part 1) and low-temperature (Part 2) parameters for the $^5D_0 \rightarrow \, ^7F_{0\text{-}2}$ ($E_{0\text{-}2}$) fluorescence emissions of europium(III) in 0.8% Eu, 3.0% Eu, and reference compounds $EuCl_3 \cdot 6H_2O$ ("Chloride") and $Eu_2(SO_4)_3 \cdot 8H_2O$ ("Sulfate"), measured with a data interval and bandpass of 0.1 and 1.72 nm, respectively. The parameters displayed are the integrated emission intensity S for each transition, normalized to the RT E_1 emission of $EuCl_3 \cdot 6H_2O$; the E_2:E_1 intensity ratio, $\eta_{21} = S(E_2)/S(E_1)$; the wavelength of maximum intensity $\lambda_{em\text{-}max}$ for each transition (nm); and the bandwidth of the E_0 peak measured as the Full Width at Half Maximum intensity (nm). The E_0 transition in $Eu_2(SO_4)_3 \cdot 8H_2O$ effectively does not exist.

1.   Full-Range Emission Spectra (Figures 8-4 and 8-5). It is readily apparent from both Figures that the emission spectra of 0.8% Eu and 3.0% Eu resemble each other much more strongly than they resemble either $EuCl_3 \cdot 6H_2O$ or $Eu_2(SO_4)_3 \cdot 8H_2O$, primarily due to differences in crystal structure as discussed below. In particular, both have higher maximum emission intensities (I) and all four E_J transitions have significantly wider bandwidths. While their intensities are relatively high, however, their E_1 and E_2 bands' Stark components are poorly resolved, effectively resulting in broad singlet peaks with a high-energy shoulder. If these two effects were to arise from chemically identical Eu^{3+} ions, there would be a contradiction—Stark degeneracy arises from high symmetry, which is associated with low emission intensity, particularly of E_2. Because the E_2 intensity is high and E_0 is present, the broadening of the E_J bands must be inhomogeneous, caused by two or more chemically distinct Eu^{3+} sites.[11, 14, 22] This interpretation is further supported by the fact that these bands are not significantly narrowed upon cooling to 77 K, although a slight resolution of the E_1 and E_2 band structures is visible.

$EuCl_3 \cdot 6H_2O$ was chosen as a reference compound because it was readily available and provides an Eu^{3+} environment of relatively low symmetry in which all five E_J transitions are visible at RT. Although its monoclinic crystal structure belongs to the centrosymmetric space group $P2/n$, it is composed of $[Eu(H_2O)_6Cl_2]^+$ ions arranged in a strongly distorted cube of C_{2h} symmetry and isolated Cl^- ions.[23] At RT, vibrational deviations from inversion symmetry allow a weak E_0 transition, which almost disappears at 77 K. After the strong differences between the $EuCl_3 \cdot 6H_2O$ spectrum and those of the 0.8% Eu and 3.0% Eu were observed, it was determined that a brief study of the stoichiometric $Eu_2(SO_4)_3 \cdot 8H_2O$ would be desirable to more directly compare the behavior of Eu^{3+} in the presence of the same anion as the doped samples. From X-ray crystallography, $Eu_2(SO_4)_3 \cdot 8H_2O$ is also monoclinic, space group $C2/c$, with C_{2h} local symmetry.[24] In spite of its belonging to the same crystal class, however, $Eu_2(SO_4)_3 \cdot 8H_2O$ clearly appears to be more symmetrical than $EuCl_3 \cdot 6H_2O$, with deviations from inversion

symmetry clearly less likely. Evidence for this assertion includes the facts that the E_0 peak is missing in $Eu_2(SO_4)_3 \cdot 8H_2O$ at RT but is present in $EuCl_3 \cdot 6H_2O$, and that the η_{21} ratio of $Eu_2(SO_4)_3 \cdot 8H_2O$ is lower than that of $EuCl_3 \cdot 6H_2O$, a measure of increasing symmetry (see Fig. 8-4 and Table 8-2). Nevertheless, the similarity in the shapes of their spectra, particularly in the number of Stark components of their E_1, E_2, and E_4 transitions, points to a similar basic symmetry different from that of 0.8% Eu and 3.0% Eu. This result is not surprising when the differences required between the monoclinic crystal structures of the stoichiometric europium compounds and the orthorhombic or roughly hexagonal structures of the europium-doped sodium sulfates are considered.

2.   *Detailed Emission Spectra, 605–630 nm (Figures 8-6 and 8-7)*. These Figures provide a more detailed picture of the $^5D_0 \rightarrow {}^7F_2$ (E_2) emission region by reducing the spectral data interval or step size from 100 to 20 pm and the emission monochromator bandpass from 1.72 nm to 86 pm. Under these experimental conditions designed to narrow peak bandwidths, $I(E_2, EuCl_3 \cdot 6H_2O)$ exceeds $I(E_2, 0.8\%$ Eu), but $S(E_2, EuCl_3 \cdot 6H_2O)$ is still less than $S(E_2, 0.8\%$ Eu). The $EuCl_3 \cdot 6H_2O$ spectrum at 77 K (Fig. 8-7) is very sharply resolved and all five Stark components allowed for a $\Delta J = 2$ transition in C_{2h} symmetry[25] are visible near 611, 612, 617, 621, and 624 nm, although the latter two are quite weak and not visible in the RT spectra of either $EuCl_3 \cdot 6H_2O$ or $Eu_2(SO_4)_3 \cdot 8H_2O$. The poor resolution in 0.8% Eu and 3.0% Eu is a strong indicator of multiple nonequivalent Eu^{3+} sites.

3.   *Full-Range Excitation Spectra (Figures 8-8 and 8-9)*. As noted earlier, the excitation spectral features arise from absorption transitions from the $^7F_0$ ground state excited states with energies greater than or equal to that of the $^5D_0$ emitting level. From low energy to high, these levels are the $^5D_0$, $^5D_1$, $^5D_2$, $^5L_6$, $^5G_{4-6}$, $^5D_4$, and $^5H_6$, and their excitation bands are centered near 580, 530, 465, 395, 380, 360, and 320 nm, respectively.[16] Besides an increase in intensity, the most notable effect of cooling the samples to 77 K is that certain features which are doublets at RT, notably the $^5D_1$, $^5G_{4-6}$, $^5D_4$, and

$^5H_6$, collapse into singlets at 77 K. The main difference between the spectra of the europium-doped sodium sulfates and those of the stoichiometric europium compounds is in the relative enhancement of the $^7F_0 \rightarrow {}^5L_6$ and diminution of the $^7F_0 \rightarrow {}^5H_6$ absorption transitions in the sodium sulfates.

4. *Detailed Emission Spectra, 570–600 nm (Figure 8-10).* These Figure provides a detailed picture of the $^5D_0 \rightarrow {}^7F_{0-1}$ (E_{0-1}) emission region by using the same step size and bandpass as in Figures 8-6–8-7. The three Stark components of $Eu_2(SO_4)_3 \cdot 8H_2O$ E_1 are noisy but clearly visible at 588.0, 590.5, and 592.5 nm. They are also visible in $EuCl_3 \cdot 6H_2O$, slightly shifted, along with a very sharp E_0 peak and two small peaks which probably arise from the weak $^5D_1 \rightarrow {}^7F_3$ emission known to lie in this region.[26] The poor resolution in E_1 of 0.8% Eu and 3.0% Eu is a strong indicator of multiple nonequivalent Eu^{3+} sites, as is the large bandwidth of E_0. In fact, the doublet structure of E_0 in 0.8% Eu points to two significantly different Eu^{3+} sites, a reasonable interpretation when the fact that the Na_I and Na_{II} sites in Na_2SO_4 (III) have different symmetries, C_{2v} and C_{2h}, is considered.[7] The Na_I and Na_{II} sites in (I) are also quite different: Na_I has four close, two intermediate, and four distant O neighbors at 252, 280, and 300 pm, respectively; Na_{II} is surrounded by six close and rather equidistant O atoms, 231–240 pm. However, the E_0 band of 3.0% Eu, while fairly wide, does not have the doublet structure of 0.8% Eu. It therefore seems probable that in (I) the Eu^{3+} ion substitutes preferentially into the Na_I site, which is both larger and has a higher coordination number, but that the strong orientational disorder in the SO_4 tetrahedra of (I) makes individual Na_I sites sufficiently nonequivalent as to cause inhomogeneous line broadening.[5]

5. *The η_{21} Ratio (Table 8-2).* The Table displays several numerical parameters evaluated from the emission spectral data, of which the most important for determination of the Eu^{3+} local environment is the ratio of the intensities of the most prominent and sensitive ED transition, E_2, to the relatively insensitive MD transition, E_1, defined by the expression $\eta_{21} \equiv S(E_2)/S(E_1)$; they are the boldface values in Table 8-2. The rule is

simply stated: higher values of η_{21} are associated with lowered symmetry and increased bond strength between Eu^{3+} and its neighbors.[10, 20] At RT (Part 1), the η_{21} values increase in the order $Eu_2(SO_4)_3 \cdot 8H_2O < EuCl_3 \cdot 6H_2O < 0.8\%$ Eu $< 3.0\%$ Eu, and this order is maintained for $EuCl_3 \cdot 6H_2O$, 0.8% Eu, and 3.0% Eu at 77 K, confirming the trends discussed in the preceding sections. Although they share the same monoclinic crystal structure at RT, $Eu_2(SO_4)_3 \cdot 8H_2O$ appears to have higher symmetry than $EuCl_3 \cdot 6H_2O$. Both of those stoichiometric europium compounds have higher local symmetries than do the europium-doped sodium sulfates, even though the sodium sulfates have crystal structures of nominally higher symmetry. Most significantly, the η_{21} values increase from 0.8% Eu to 3.0% Eu in accordance with the expected increase of disorder and hence asymmetry in going from (III) to (I). The relatively small decrease in η_{21} for these two compounds upon cooling to 77 K may arise from an increase in symmetry due to the absence of vibrational contributions expected to be present at RT. The much larger decrease in η_{21} for $EuCl_3 \cdot 6H_2O$ at 77 K may indicate that the vibrational contribution to asymmetry is much more significant in $EuCl_3 \cdot 6H_2O$ than in 0.8% Eu or 3.0% Eu or a possible phase change to a more ordered structure.

IV. Conclusions

Two high-temperature polymorphs of sodium sulfate, (I) and (III), of which at least (I) is potentially a good ionic conductor, have been stabilized to room temperature through the incorporation of Eu^{3+} ions. These Eu^{3+} ions were chosen for two reasons: first, because they are capable of stabilizing the phases (as are many other di-, tri-, and tetravalent ions); and second, because the unique spectroscopic properties of Eu3+ make it a useful probe of its local environment.

Laser-Raman spectroscopy of the europium-doped sodium sulfates has shown conclusively that characteristic features of the pure phases at their thermodynamically

154

stable temperatures also appear in doped phases at room temperature, and that the particular phase involved changes as a function of dopant level.

Measurements of the phases' ionic conductivities have demonstrated both the increases in ionic conductivity which accompany doping with aliovalent cations and the concomitant formation of cation vacancies which promotes Na^+ ion migration, and also the existence of the predicted phases and their transitions in the predicted temperatures regions. The ionic conductivity of 3.0% Eu is sufficiently high that it almost meets the threshold requirements for superionic conductors.

Finally, a series of detailed spectroscopic measurements using europium(III) fluorescence as a probe of the local Eu^{3+} ion environment has confirmed the structural predictions of previous researchers' X-ray analyses and the laser-Raman spectroscopy in showing an increase in disorder between phases (III) and (I) and a change in preference for particular Na^+ crystal sites with the changing crystal structure.

V. References

1.   G. Dharmasena and R. Frech, *J. Chem. Phys.* **99** (1993) 8929.

2.   M. A. Careem and B. E. Mellander, *Solid State Ionics* **15** (1985) 327.

3.   G. Prakash and K. Shahi, *Solid State Ionics* **23** (1987) 151.

4.   Yu. Ya. Gurevich and A. K. Ivanov-Shits, "Semiconductor Properties of Superionic Materials," in R. K. Willardson and A. C. Beer, *Semiconductors and Semimetals, Volume 26: III–V Compound Semiconductors and Semiconductor Properties of Superionic Materials* (New York: Academic Press, Inc., 1988), p. 230.

5.   W. Eysel, H. H. Höfer, K. L. Keester, and Th. Hahn, *Acta Cryst.* **B41** (1985) 5.

6.   (a) H. H. Höfer, W. Eysel, and U. von Alpen, *J. Solid State Chem.* **36** (1981) 365.

      (b) H. H. Höfer, U. von Alpen, and W. Eysel, *Acta Cryst.* **A34** (1978) S358.

7.   B. N. Mehrotra, *Z. Kristallogr.* **155** (1981) 159.

8. G. Dharmasena, *pers. commun.*, September 19, 1994.

9. S. Lis and G. R. Choppin, in W. Strek, W. Ryba-Romanowski, J. Legendziewicz, and B. Jezowska-Trzebiatowska, *The Second International School on Excited States of Transition Elements* (Singapore; New Jersey; London; Hong Kong: World Scientific Publishing Co. Pte. Ltd., 1992), p. 361.

10. M. J. Lochhead, P. R. Wamsley, and K. L. Bray, *Inorg. Chem.*, in press.

11. C. McDonagh, G. Ennis, P. Marron, B. O'Kelly, Z. R. Tang, and J. F. McGilp, *J. Non-Cryst. Solids* **147 & 148** (1992) 97.

12. S. J. L. Ribeiro, R. S. Hiratsuka, A. M. G. Massabni, M. R. Davolos, C. V. Santilli, and S. H. Pulcinelli, *J. Non-Cryst. Solids* **147 & 148** (1992) 162.

13. W. C. Nieuwpoort, G. Blasse, and A. Bril, in H. M. Crosswhite and H. W. Moos, *Optical Properties of Ions in Crystals* (New York; London; Sydney: Interscience Publishers Division of John Wiley & Sons, Inc., 1967), p. 161.

14. J.-C. G. Bünzli and G.-O. Pradervand, *J. Chem. Phys.* **85** (1986) 2489.

15. J. N. Mundy, in P. Vashishta, J. N. Mundy, and G. K. Shenoy, *Fast Ion Transport in Solids: Electrodes and Electrolytes* (New York; Amsterdam; Oxford: Elsevier North Holland, Inc., 1979), p. 159.

16. W. T. Carnall, P. R. Fields, and K. Rajnak, *J. Chem. Phys.* **49** (1968) 4412.

17. Robert D. Peacock, *Struct. Bond. (Berlin)* **22** (1975) 83.

18. (a) B. R. Judd, *Phys. Rev.* **127** (1962) 750. (b) G. S. Ofelt, *J. Chem. Phys.* **37** (1962) 511.

19. J. Huang, J. Loriers, and P. Porcher, *C. R. Acad. Sc. Paris, Série II* **294** (1982) 545.

20. R. Reisfeld, V. Chernyak, M. Eyal, and C. K. Jørgensen, in W. Strek, W. Ryba-Romanowski, J. Legendziewicz, and B. Jezowska-Trzebiatowska, *The Second International School on Excited States of Transition Elements* (Singapore; New Jersey; London; Hong Kong: World Scientific Publishing Co. Pte. Ltd., 1992), p. 247.

21. B. R. Judd, *J. Chem. Phys.* **44** (1966) 839.

22. R. Campostrini, G. Carturan, M. Ferrari, M. Montagna, and O. Pilla, *J. Mater. Res.* **7** (1992) 745.

23. N. K. Bel'skii and Yu. T. Struchkov, *Kristallografiya (Sov. Phys., Cryst.)* **10** (1965) 21 (Russian) or 15 (English).

24. (a) V. I. Ivanov, *Kristallografiya (Sov. Phys., Cryst.)* **9** (1965) 655 (Russian) or 553 (English). (b) L. L. Zaitseva, V. S. Il'yashenko, M. I. Konarev, L. N. Konovalov, L. V. Lipis, and N. T. Chebotarev, *Zh. Neorg. Khim. (Russ. J. Inorg. Chem.)* **10** (1965) 1761 (Russian) or 961 (English).

25. J. L. Prather, *Atomic Energy Levels in Crystals,* National Bureau of Standards Monograph 19 (Washington, DC: U.S. Government Printing Office, 1961), 84 pp.

26. C. Brecher, H. Samelson, and A. Lempicki, in H. M. Crosswhite and H. W. Moos, *Optical Properties of Ions in Crystals* (New York; London; Sydney: Interscience Publishers Division of John Wiley & Sons, Inc., 1967), p. 73.

BIBLIOGRAPHY

ADACHI, Tatsuhiko; SAKKA, Sumio. "Preparation of Monolithic Silica Gel and Glass by the Sol-Gel Method Using N,N-Dimethylformamide," *Journal of Materials Science* **22** (1987) 4407–4410.

ADACHI, Tatsuhiko; SAKKA, Sumio. "The Role of N,N-Dimethylformamide, a DCCA, in the Formation of Silica Gel Monoliths by Sol-Gel Method," *Journal of Non-Crystalline Solids* **99** (1988) 118–128.

ALBIN, Michael; HORROCKS, William DeW., Jr. "Europium(III) Luminescence Excitation Spectroscopy. Quantitative Correlation Between the Total Charge on the Ligands and the $^7F_0 \rightarrow {}^5D_0$ Transition Frequency in Europium(III) Complexes," *Inorganic Chemistry* **24** (1985) 895–900.

ALLAN, J. R.; CARSON, B.; PATON, A. D.; TURVEY, K.; GERRARD, D. L.; HOEY, S. "Thermal and Electrical Studies of Some Europium Compounds with Organic Ligands," *Thermochimica Acta* **157** (1990) 61–68.

ALPHA, Béatrice; BALZANI, Vincenzo; LEHN, Jean-Marie; PERATHONER, Siglinda; SABBATINI, Nanda. "Luminescence Probes: The Eu^{3+}- and Tb^{3+}-Cryptates of Polypyridine Macrobicyclic Ligands," *Angewandte Chemie International Edition in English* **26** (1987) 1266–1267.

AVNIR, David; KAUFMAN, Vered R.; REISFELD, Renata. "Organic Fluorescent Dyes Trapped in Silica and Silica-Titania Thin Films by the Sol-Gel Method. Photophysical, Film and Cage Properties," *Journal of Non-Crystalline Solids* **74** (1985) 395–406.

AVNIR, David; LEVY, David; REISFELD, Renata. "The Nature of the Silica Cage as Reflected by Spectral Changes and Enhanced Photostability of Trapped Rhodamine 6G," *The Journal of Physical Chemistry* **88** (1984) 5956–5959.

BAUER, Herbert; BLANC, Joseph; ROSS, Daniel L. "Octacoordinate Chelates of Lanthanides. Two Series of Compounds," *Journal of the American Chemical Society* **86** (1964) 5125–5131.

BEL'SKII, N. K.; STRUCHKOV, Yu. T. "The Crystal Structure and Optical Properties of Europium Chloride Hexahydrate, $EuCl_3 \cdot 6H_2O$," *Kristallografiya (Soviet Physics, Crystallography)* **10** (1965) 21–28 (Russian original) or 15–20 (English translation).

BERRY, A. J.; KING, T. A. "Characterisation of Doped Sol-Gel Derived Silica Hosts for Use in Tunable Glass Lasers," *Journal of Physics D: Applied Physics* **22** (1989) 1419–1422.

BHAUMIK, M. L. "Relaxation in Europium Chelates," *The Journal of Chemical Physics* **41** (1964) 574–575.

BHAUMIK, M. L.; EL-SAYED, M. A. "Mechanism and Rate of the Intramolecular Energy Transfer Process in Rare-Earth Chelates," *The Journal of Chemical Physics* **42** (1965) 787–788.

BONATI, Flavio. "Organometallic Derivatives of β-Diketones," *Organometallic Chemistry Reviews* **1** (1966) 379–389.

BRECHER, C.; SAMELSON, H.; LEMPICKI, A. "Laser Phenomena in Europium Chelates. III. Spectroscopic Effects of Chemical Composition and Molecular Structure," *The Journal of Chemical Physics* **42** (1965) 1081–1096.

BRECHER, C.; SAMELSON, H.; LEMPICKI, A. "The Energy Level Structure of Eu^{3+} in YVO_4," in H. M. Crosswhite and H. W. Moos, *Optical Properties of Ions in Crystals* (New York; London; Sydney: Interscience Publishers Division of John Wiley & Sons, Inc., 1967), pp. 73–84.

BREY, Wallace S. "Silicon-29 Nuclear Magnetic Resonance," in R. Anderson, B. Arkles, and G. L. Larson, *Petrarch Systems Silanes & Silicones* (Bristol, PA: Petrarch Systems, Inc., 1987), pp. 60–68.

BRINKER, C. Jeffrey; SCHERER, George W. *Sol–Gel Science: The Physics and Chemistry of Sol–Gel Processing* (Boston: Academic Press, 1990).

BÜNZLI, Jean-Claude G.; KLEIN, Bernard. "High-Coordination Polyhedra of Trivalent Rare Earth Ions," in Gregory J. McCarthy, Herbert B. Silber, and James J. Rhyne, *The Rare Earths in Modern Science and Technology*, Volume 3 (New York; London: Plenum Press, 1982), pp. 97–98.

BÜNZLI, Jean-Claude G.; PRADERVAND, Georges-Olivier. "The Eu(III) Ion as Luminescent Probe: Laser-Spectroscopic Investigation of the Metal Ion Sites in an 18-Crown-6 Complex," *The Journal of Chemical Physics* **85** (1986) 2489–2497.

BURWELL, Robert L., Jr. "Modified Silica Gels as Adsorbents and Catalysts," *Chemtech* (1974) 370–377.

CAMPOSTRINI, R.; CARTURAN, G.; FERRARI, M.; MONTAGNA, M.; PILLA, O. "Luminescence of Eu^{3+} Ions During Thermal Densification of SiO_2 Gel," *Journal of Materials Research* **7** (1992) 745–753.

CAPOZZI, Carol A.; PYE, L. David. "Preparation and Characterization of PMMA Modified SiO_2 Host Material for Organic Dye Molecules," in Proceedings of SPIE 970 (Bellingham, WA: The Society of Photo-Optical Instrumentation Engineers, 1988), p. 135.

CAREEM, M. A.; MELLANDER, B. E. *Solid State Ionics* **15** (1985) 327.

CARNALL, W. T.; FIELDS, P. R.; RAJNAK, K. "Spectral Intensities of the Trivalent Lanthanides and Actinides in Solution. II. Pm^{3+}, Sm^{3+}, Eu^{3+}, Gd^{3+}, Tb^{3+}, Dy^{3+}, and Ho^{3+}," *The Journal of Chemical Physics* **49** (1968) 4412–4423.

CHANG, N. C. "Fluorescence and Stimulated Emission from Trivalent Europium in Yttrium Oxide," *Journal of Applied Physics* **34** (1963) 3500–3504.

CHARLES, R. G.; OHLMANN, R. C. "Europium Thenoyltrifluoroacetonate, Preparation and Fluorescence Properties," *Journal of Inorganic and Nuclear Chemistry* **27** (1965) 255–259.

159

CHARLES, R. G.; RIEDEL, E. P. "Properties of Some Europium Laser Chelates Derived from Benzoyltrifluoroacetone," *Journal of Inorganic and Nuclear Chemistry* **28** (1966) 3005–3018.

CHARLES, Robert G.; RIEDEL, Ernest P. "Fluorescent Europium Chelates Derived from Fluorinated β-Diketones," *Journal of Inorganic and Nuclear Chemistry* **29** (1967) 715–723.

CHINN, S. R. In M. J. Weber, ed., *CRC Handbook of Laser Science and Technology, Volume I, Lasers and Masers* (Boca Raton, FL: CRC Press, Inc., 1982), p. 147.

CLARSON, Stephen J.; SEMLYEN, J. Anthony. *Siloxane Polymers* (Englewood Cliffs, NJ: PTR Prentice Hall, Inc., 1993).

CROSBY, G. A.; WHAN, R. E.; ALIRE, R. M. "Intramolecular Energy Transfer in Rare-Earth Chelates. Role of the Triplet State," *The Journal of Chemical Physics* **34** (1961) 743–748.

DE LA ROSA-FOX, N.; ESQUIVIAS, L.; ZARZYCKI, J. *Diffusion and Defect Data* **53–54** (1987) 363.

DEMAS, J. N.; CROSBY, G. A. "The Measurement of Photoluminescence Quantum Yields. A Review," *The Journal of Physical Chemistry* **75** (1971) 991–1024.

DEVLIN, K.; O'KELLY, B.; TANG, Z. R.; MCDONAGH, C.; MCGILP, J. F. "A Structural Study of the Sol–Gel Process by Optical Fluorescence and Decay Time Spectroscopy," *Journal of Non-Crystalline Solids* **135** (1991) 8–14.

DHARMASENA, Gamini; FRECH, Roger. "The Stabilization of Phase III and Phase I in Sodium Sulfate by Aliovalent Cation Substittution," *The Journal of Chemical Physics* **99** (1993) 8929–8935.

DIEKE, G. H.; CROSSWHITE, H. M. "The Spectra of the Doubly and Triply Ionized Rare Earths," *Applied Optics* **2** (1963) 675–686.

DREXHAGE, K. H. "Design of Laser Dyes," VII International Quantum Electronics Conference (Montreal, 1972).

DREXHAGE, K. H. In F. D. Schäfer, *Dye Lasers*, second edition (New York, Berlin, Heidelberg: Springer-Verlag, 1977).

DREXHAGE, K. H. *Laser Focus* **9** (1973) 35.

DUNN, B.; KNOBBE, E.; MCKIERNAN, J. M.; POUXVIEL, J. C.; ZINK, J. I. "The Optical Behavior of Organic and Organometallic Molecules in Sol-Gel Matrices," in C. Jeffrey Brinker, David E. Clark, and Donald R. Ulrich, *Better Ceramics Through Chemistry III*, MRS Symposium Proceedings 121 (Pittsburgh, PA: Materials Research Society, 1989), pp. 331–342.

DUNN, Bruce. "Dye-Doped Sol-Gel Tunable Lasers," Fifth International Conference on Ultrastructure Processing of Ceramics, Glasses, Composites, Ordered Polymers, and Advanced Optical Materials (Orlando, FL, February 1991).

DVORAK, Ondrej; DE ARMOND, M. Keith. "Electrode Modification by the Sol–Gel Method," *The Journal of Physical Chemistry* **97** (1993) 2646–2648.

ELBANOWSKI, Marian; LIS, Stefan; PLAZIAK, Adam S.; MAKOWSKA, Barbara. "A Mass Spectrometric Study of the Selected Lanthanide Complexes: Acetylacetonates and Ethylenediaminetetraacetates," in W. Strek, W. Ryba-Romanowski, J. Legendziewicz, and B. Jezowska-Trzebiatowska, *The Second International School on Excited States of Transition Elements* (Singapore; New Jersey; London; Hong Kong: World Scientific Publishing Co. Pte. Ltd., 1992), pp. 49–68.

ESQUIVIAS, L.; ZARZYCKI, J. In J. D. Mackenzie and D. R. Ulrich, *Ultrastructure Processing of Advanced Ceramics* (New York: John Wiley & Sons, Inc., 1988), p. 255.

EYSEL, W.; HÖFER, H. H.; KEESTER, K. L.; HAHN, Th. "Crystal Chemistry and Structure of $Na_2SO_4(I)$ and Its Solid Solutions," *Acta Crystallographica* **B41** (1985) 5–11.

GRENTHE, Ingmar; FERNELIUS, W. Conard. "Stability Relationships Among the Rare Earth Acetylacetonates," *Journal of the American Chemical Society* **82** (1960) 6258–6260.

GROMOV, D. A.; DYUMAEV, K. M.; MANENKOV, A. A.; MASLYUKOV, A. P.; MATYUSHIN, G. A.; NECHITAILO, V. S.; PROKHOROV, A. M. "Efficient Plastic-Host Dye Lasers," *Journal of the Optical Society of America B* **2** (1985) 1028–1031.

GUREVICH, Yu. Ya.; IVANOV-SHITS, A. K. "Semiconductor Properties of Superionic Materials," in R. K. Willardson and Albert C. Beer, *Semiconductors and Semimetals, Volume 26: III–V Compound Semiconductors and Semiconductor Properties of Superionic Materials* (New York: Academic Press, Inc., 1988), pp. 230–372.

HAAS, Yehuda; STEIN, Gabriel. "Pathways of Radiative and Radiationless Transitions in Europium (III) Solutions: Role of Solvents and Anions," *The Journal of Physical Chemistry* **75** (1971) 3668–3681.

HAIR, Michael L.; HERTL, William. "Acidity of Surface Hydroxyl Groups," *The Journal of Physical Chemistry* **74** (1970) 91–94.

HAMER, Andrew M.; LIVINGSTONE, Stanley E. "Lanthanide Chelates of Fluorinated β-Diketones. Part III. Mass Spectra of Lanthanide Chelates of Five Fluorinated β-Diketones," *Transition Metals Chemistry* **9** (1984) 433–438.

HAYES, A. V.; DRICKAMER, H. G. "High Pressure Luminescence Studies of Energy Transfer in Rare Earth Chelates," *The Journal of Chemical Physics* **76** (1982) 114–125.

HAZENKAMP, M. F.; BLASSE, G. "Rare-Earth Ions Adsorbed onto Porous Glass: Luminescence as a Characterizing Tool," *Chemistry of Materials* **2** (1990) 105–110.

HEBER, J.; HELLWEGE, K. H. "Fluorescence Lifetimes and Multiphonon Relaxation in Hydrated Salts of Eu and Tb," in H. M. Crosswhite and H. W. Moos, *Optical Properties of Ions in Crystals* (New York; London; Sydney: Interscience Publishers Division of John Wiley & Sons, Inc., 1967), pp. 457–466.

HÖFER, H. H.; EYSEL, W.; VON ALPEN, U. *Journal of Solid State Chemistry* **36** (1981) 365.

HÖFER, H. H.; VON ALPEN, U.; EYSEL, W. *Acta Crystallographica* **A34** (1978) S358.

HUANG, Jinggen; LORIERS, Jean; PORCHER, Pierre. "Intensités des transitions optiques de l'ion Eu^{3+} dans quelques molybdates de terres rares," *Comptes Rendus, Academie des Sciences, Paris, Série II* **294** (1982) 545–548.

ITOH, Uichi; TAKAKUSA, Michio; MORIYA, Tetsuo; SAITO, Shogo. "Optical Gain of Coumarin Dye-Doped Thin Film Lasers," *Japanese Journal of Applied Physics* **16** (1977) 1059–1060.

IVANOV, V. I. "X-Ray and Thermogravimetric Studies of the Octahydrates of the Sulfates of the Lanthanides and Yttrium," *Kristallografiya (Soviet Physics, Crystallography)* **9** (1965) 655–659 (Russian original) or 553–556 (English translation).

IZATT, Reed M.; FERNELIUS, W. Conard; HAAS, C. G., Jr.; BLOCK, B. P. "Studies on Coördination Compounds. XI. Formation Constants of Some Tervalent Ions and the Thorium (IV) Ion with the Acetylacetonate Ion," *The Journal of Physical Chemistry* **59** (1955) 170–174.

JUDD, B. R. "Hypersensitive Transitions in Rare-Earth Ions," *The Journal of Chemical Physics* **44** (1966) 839–840.

JUDD, B. R. "Optical Absorption Intensities of Rare-Earth Ions," *Physical Review* **127** (1962) 750–761.

KAMINOW, I. P.; STULZ, L. W.; CHANDROSS, E. A.; PRYDE, C. A. "Photobleaching of Organic Laser Dyes in Solid Matrices," *Applied Optics* **11** (1972) 1563–1567.

KLEINERMAN, Marcos. "Energy Migration in Lanthanide Chelates," *The Journal of Chemical Physics* **51** (1969) 2370–2381.

KNOBBE, Edward T.; DUNN, Bruce; FUQUA, Peter D.; NISHIDA, Fumito. "Laser Behavior and Photostability Characteristics of Organic Dye Doped Silicate Gel Materials," *Applied Optics* **29** (1990) 2729–2733.

LEMPICKI, A.; SAMELSON, H. "Optical Maser Action in Europium Benzoylacetonate," *Physics Letters* **4** (1963) 133–135.

LEMPICKI, A.; SAMELSON, H.; BRECHER, C. "Laser Action in Rare Earth Chelates," *Applied Optics Supplement* **2** (1965) 205–213.

LEVY, D.; REISFELD, R.; AVNIR, D. "Fluorescence of Europium(III) Trapped in Silica Gel–Glass as a Probe for Cation Binding and for Changes in Cage Symmetry During Gel Dehydration," *Chemical Physics Letters* **109** (1984) 593–597.

LINTNER, Birgit; ARFSTEN, Nanning; DISLICH, Helmut; SCHMIDT, Helmut; PHILIPP, Gottfried; SEIFERLING, Bernhard. "A First Look at the Optical Properties of Ormosils," *Journal of Non-Crystalline Solids* **100** (1988) 378–382.

162

LIS, S. "Preparation and Thermal Properties of Lanthanide Complexes of TTA," in I. Buzas, *Proceedings of the Third Analytical Chemistry Conference,* Volume 2 (Prague, Czechoslovakia, 1970), pp. 433–441.

LIS, Stefan; CHOPPIN, Gregory R. "A Luminscence Study of Preferential Solvation of the Europium(III) Ion in Binary Aqueous Solvent Mixtures," in W. Strek, W. Ryba-Romanowski, J. Legendziewicz, and B. Jezowska-Trzebiatowska, *The Second International School on Excited States of Transition Elements* (Singapore; New Jersey; London; Hong Kong: World Scientific Publishing Co. Pte. Ltd., 1992), pp. 361–366.

LOCHHEAD, M. J.; BRAY, K. L. "Spectroscopic Characterization of Doped Sol–Gel Silica Gels and Glasses: Evidence of Inner-Sphere Complexation of Europium(III)," *Journal of Non-Crystalline Solids* **170** (1994) 143–154.

LOCHHEAD, M. J.; WAMSLEY, P. R.; BRAY, K. L. "Luminescence Spectroscopy of Europium(III) Nitrate, Chloride, and Perchlorate in Mixed Ethanol–Water Solutions," *Inorganic Chemistry,* in press.

LYLE, S. J.; WITTS, Alan D. "Critical Examination of Some Methods for the Preparation of Tris and Tetrakis Diketonates of Europium(III)," *Inorganica Chimica Acta* **5** (1971) 481–484.

MACCRAITH, Brian D.; MCDONAGH, Colette M.; O'KEEFFE, Gerard; KEYES, Emmetine T.; VOS, Johannes G.; O'KELLY, Brendan; MCGILP, John F. "Fiber Optic Oxygen Sensor Based on Fluorescence Quenching of Evanescent-Wave Excited Ruthenium Complexes in Sol–Gel Derived Porous Coatings," *The Analyst* **118** (1993) 385–388.

MACK, H.; REISFELD, R.; AVNIR, D. *Chemical Physics Letters* **99** (1983) 238.

MATSUI, Kazunori; SASAKI, Kei; TAKAHASHI, Nobuyuki. "Luminescence of Tris(2,2'-bipyridine) Ruthenium (II) in Sol-Gel Glasses," *Langmuir* **7** (1991) 2866–2868.

MATTHEWS, Lowell R.; KNOBBE, E. T. "Luminescence of Rare Earth Metalorganic Complexes in Sol–Gel Derived Host Materials," in Sridhar Komarneni, John C. Parker, and George J. Thomas, *Nanophase and Nanocomposite Materials,* Materials Research Society Symposium Proceedings, v. 286 (Pittsburgh, PA: Materials Research Society, 1993), pp. 259–264.

MATTHEWS, Lowell R.; KNOBBE, Edward T. "Luminescence Behavior of Europium Complexes in Sol–Gel Derived Host Materials," *Chemistry of Materials* **5** (1993) 1697–1700.

MATTHEWS, Lowell R.; WANG, Xiao-jun; KNOBBE, E. T. "Concentration Effects on the Luminescence Behavior of Europium(III) Chloride- and Organoeuropium-Doped Silicate Gels," *Journal of Non-Crystalline Solids,* in press.

MATTHEWS, Lowell R.; WANG, Xiao-jun; KNOBBE, E. T. "Luminescence Behavior of Inorganic and Metalorganic Europium(III) Dopants Incorporated into Silica and Epoxide Ormosil Sol–Gel Hosts," *Journal of Sol–Gel Science and Technology* **2** (1994) 627 [in press].

MATTHEWS, Lowell R.; WANG, Xiao-jun; KNOBBE, E. T. "Luminescence Behavior of Organo-Ruthenium Complexes Entrapped Within Sol–Gel Hosts," in B. H. T. Chai, S. A. Payne, T. Y. Fan, A. Cassano, and T. H. Allik, *New Materials for Advanced Solid-State Lasers,* Materials Research Society Symposium Proceedings, v. 329 (Pittsburgh, PA: Materials Research Society, 1994), pp. 285–290.

MAY, P. Stanley; RICHARDSON, F. S. "Non-Radiative Deactivation of the Europium $^5D_0$ Excited State by Water Molecules Outside the Primary Coordination Sphere of Eu^{3+} in $Na_3[Eu(C_4H_4O_5)_3]\cdot2NaClO_4\cdot6H_2O$," *Chemical Physics Letters* **179** (1991) 277–281.

MCDONAGH, C.; ENNIS, G.; MARRON, P.; O'KELLY, B.; TANG, Z. R.; MCGILP, J. F. "Characterization of Sol–Gel Glasses Using Optical Probes," *Journal of Non-Crystalline Solids* **147 & 148** (1992) 97–101.

MEHROTRA, B. N. "The Crystal Structure of Na_2SO_4III," *Zeitschrift für Kristallographie* **155** (1981) 159–161.

MUNDY, John N. "Diffusion and Ionic Conductivity in Solid Electrolytes," in P. Vashishta, J. N. Mundy, and G. K. Shenoy, *Fast Ion Transport in Solids: Electrodes and Electrolytes* (New York; Amsterdam; Oxford: Elsevier North Holland, Inc., 1979), pp. 159–170.

NIEUWPOORT, W. C.; BLASSE, G.; BRIL, A. "Some Aspects of the Eu^{3+} Fluorescence in Metaloxide Host Lattices," in H. M. Crosswhite and H. W. Moos, *Optical Properties of Ions in Crystals* (New York; London; Sydney: Interscience Publishers Division of John Wiley & Sons, Inc., 1967), pp. 161–168.

O'CONNELL, Robert M.; SAITO, Theodore T. "Plastics for High-Power Laser Applications: A Review," *Optical Engineering* **22** (1983) 393–399.

OFELT, G. S. "Intensities of Crystal Spectra of Rare-Earth Ions," *The Journal of Chemical Physics* **37** (1962) 511–520.

PEACOCK, Robert D. "The Intensities of Lanthanide $f \leftrightarrow f$ Transitions," *Structure and Bonding (Berlin)* **22** (1975) 83–122.

PHILIPP, G.; SCHMIDT, H. "New Materials for Contact Lenses Prepared from Si- and Ti-Alkoxides by the Sol–Gel Process," *Journal of Non-Crystalline Solids* **63** (1984) 283–292.

PRAKASH, G.; SHAHI, K. *Solid State Ionics* **23** (1987) 151.

PRATHER, John L. *Atomic Energy Levels in Crystals,* National Bureau of Standards Monograph 19 (Washington, DC: U.S. Government Printing Office, 1961), 84 pp.

REISFELD, R.; BRUSILOVSKY, D.; EYAL, M. "Perylene Dye in a Composite Sol–Gel Glass—A New Solid-State Tunable Laser in the Visible Range," in *French-Israeli Workshop on Solid State Lasers,* Proceedings of SPIE 1182 (Bellingham, WA: The Society of Photo-Optical Instrumentation Engineers, 1988), pp. 230–239.
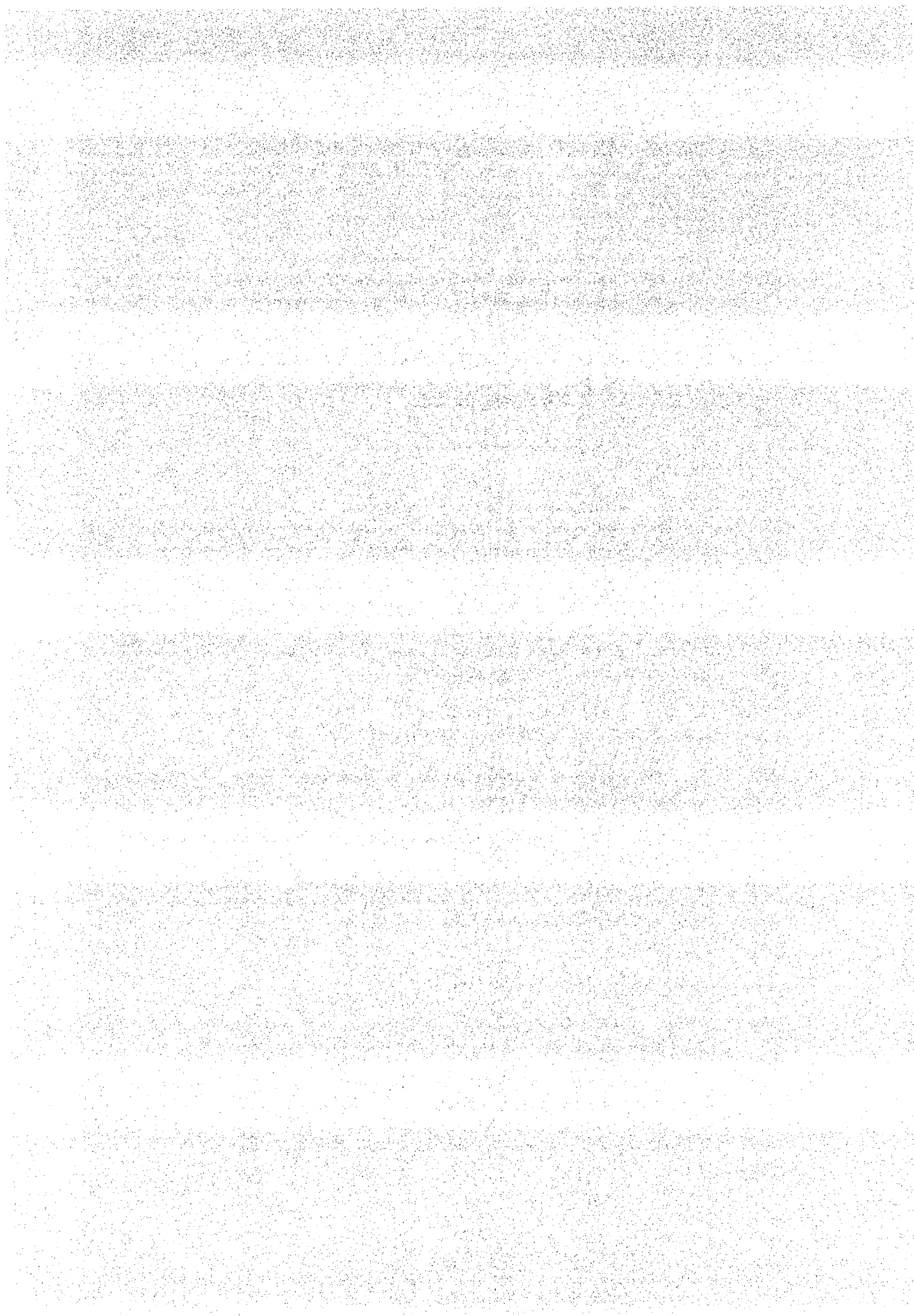
REISFELD, Renata; BRUSILOVSKY, David; EYAL, Marek; JØRGENSEN, Christian K. "Luminescence of Tris(2,2'-bipyridine)ruthenium(II) Incorporated at Moderate Temperature in Sol-Gel Glasses and Various Low-Melting Glasses," *Chimia* **43** (1989) 385–387.

REISFELD, Renata; CHERNYAK, Valery; EYAL, Marek; JØRGENSEN, Christian Klixbull. "Spectroscopy of *d*-Group Elements and Rare Earths in Glasses Prepared by the Sol–Gel Method," in W. Strek, W. Ryba-Romanowski, J. Legendziewicz, and B. Jezowska-Trzebiatowska, *The Second International School on Excited States of Transition Elements* (Singapore; New Jersey; London; Hong Kong: World Scientific Publishing Co. Pte. Ltd., 1992), pp. 247–256.

REISFELD, Renata; CHERNYAK, Valery; EYAL, Marek; JØRGENSEN, Christian Klixbull. "Spectroscopy of *d*-Group Elements and Rare Earths in Glasses Prepared by the Sol–Gel Method," in W. Strek, W. Ryba-Romanowski, J. Legendziewicz, and B. Jezowska-Trzebiatowska, *The Second International School on Excited States of Transition Elements* (Singapore; New Jersey; London; Hong Kong: World Scientific Publishing Co. Pte. Ltd., 1992), pp. 247–256.

RIBEIRO, S. J. L.; HIRATSUKA, R. S.; MASSABNI, A. M. G.; DAVOLOS, M. R.; SANTILLI, C. V.; PULCINELLI, S. H. "Study of SnO_2 Gels by Eu^{3+} Fluorescence Spectroscopy," *Journal of Non-Crystalline Solids* **147 & 148** (1992) 162–166.

ROBINSON, L. M.; LU, H.; HUPP, J. T.; SHRIVER, D. F. "Nature of the Interaction and Photophysical Properties of $[Mo_6Cl^i_8(SO_3CF_3)^a_6]^{2-}$ and $[Mo_6Cl^i_8Cl^a_6]^{2-}$ on Silica Gel," *Chem. Mater.* **1995,** *7,* 43–49.

SANCHEZ, Clément. "Optical Properties of Transition Metal Oxide Gels," in J. D. Mackenzie and D. R. Ulrich, *Sol-Gel Optics,* Proceedings of SPIE 1328 (Bellingham, WA: The Society of Photo-Optical Instrumentation Engineers, 1990), pp. 40–51.

SCHMIDT, H.; SEIFERLING, B. "Chemistry and Applications of Inorganic–Organic Polymers (Organically Modified Silicates)," in C. Jeffrey Brinker, David E. Clark, and Donald R. Ulrich, *Better Ceramics Through Chemistry II,* Materials Research Society Symposium Proceedings, v. 73 (Pittsburgh, PA: Materials Research Society, 1986), pp. 739–750.

SI, Zhi-Kun; ZHU, Gui-Yun; LI, Jie. "Study of the Fluorescence of the Europium–Thenoyltrifluoroacetone–Cetyltrimethylammonium Bromide–Triton X-100 System," *The Analyst* **116** (1991) 309–311.

SILVERSTEIN, Robert M.; SASSLER, G. Clayton; MORRILL, Terence C. *Spectrometric Identification of Organic Compounds,* Fourth Edition (New York; Toronto: John Wiley & Sons, Inc., 1981).

SINHA, S. P. *Europium* (New York: Springer-Verlag New York, Inc., 1967).

SLAMA-SCHWOK, Anny; AVNIR, David; OTTOLENGHI, Michael. "Photoinduced Electron Transfer Mediated by a Shuttling Charge Carrier between Ruthenium and Iridium Trisbipyridyl Complexes Trapped in Sol–Gel Glasses," *The Journal of the American Chemical Society* **113** (1991) 3984–3985.

165
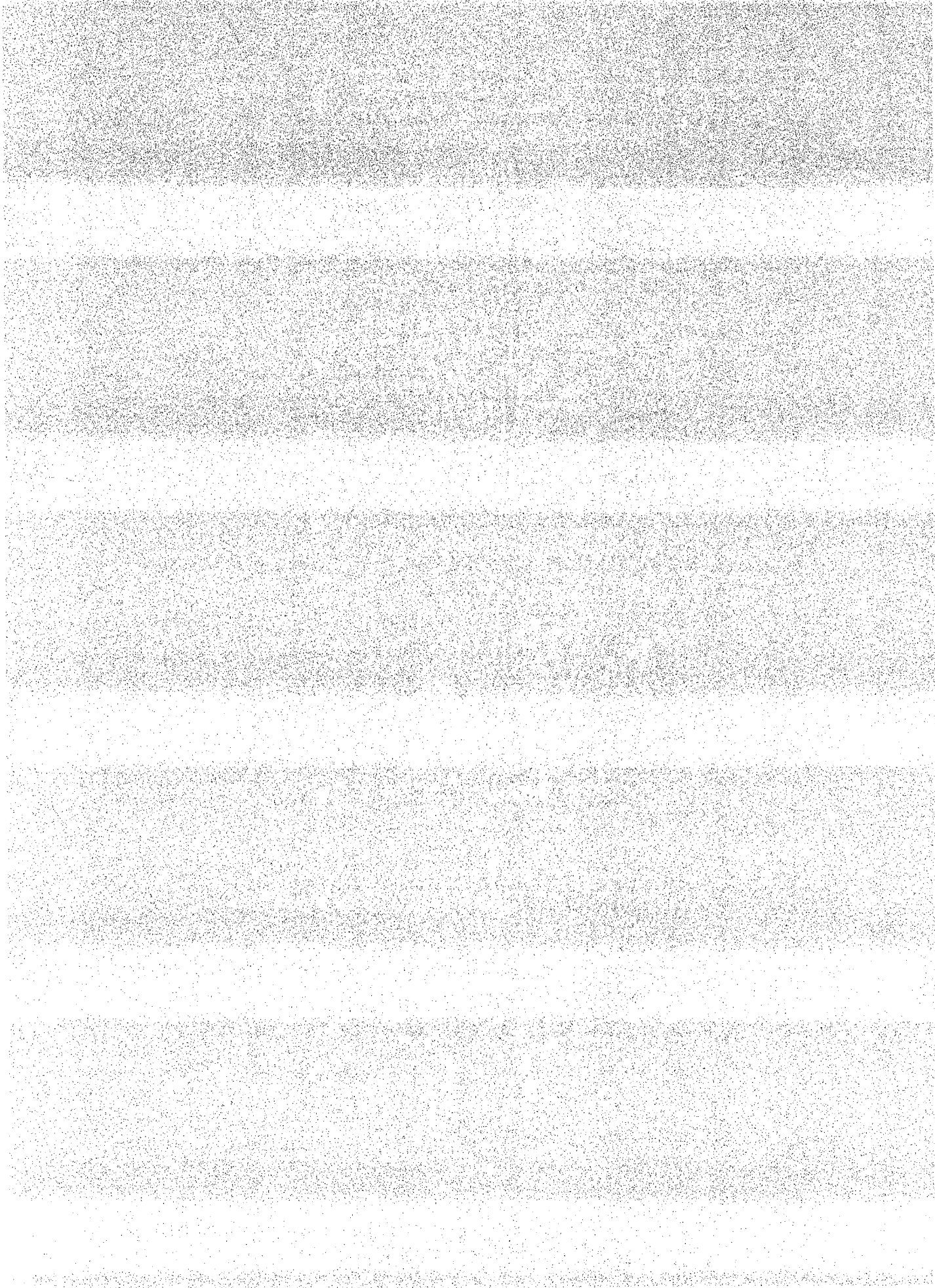
STREITWIESER, A., Jr.; HEATHCOCK, C. H. *Introduction to Organic Chemistry* (New York: Macmillan Publishing Co., Inc., 1976).

SVELTO, O. *Principles of Lasers,* second edition (New York: Plenum Press, 1982).

WANG, Xiao-jun; MATTHEWS, Lowell R.; KNOBBE, E. T. "Energy Transfer and Emission Processes in Sol–Gel Materials Doped with Europium(III) Complexes," in Anthony F. Garito, Alex K.-Y. Jen, Charles Y.-C. Lee, and Larry R. Dalton, *Electrical, Optical, and Magnetic Properties of Organic Solid-State Materials,* Materials Research Society Symposium Proceedings, v. 328 (Pittsburgh, PA: Materials Research Society, 1994), pp. 745–750.

WATSON, W. M.; ZERGER, Richard P.; YARDLEY, James T.; STUCKY, Galen D. "Examination of Photophysics in Rare Earth Chelates by Laser-Excited Luminescence," *Inorganic Chemistry* 14 (1975) 2675–2680.

WHAN, R. E.; CROSBY, G. A. "Luminescence Studies of Rare Earth Complexes: Benzoylacetonate and Dibenzoylmethide Chelates," *Journal of Molecular Spectroscopy* 8 (1962) 315–327.

WHITE, J. G. "The Crystal Structure of Europium Tris[4,4,4-trifluoro-1-(2-thienyl)-1,3-butanedione] Dihydrate," *Inorganica Chimica Acta* 16 (1976) 159–162.

WOLFF, N. E.; PRESSLEY, R. J. "Optical Maser Action in an Eu^{+3}-Containing Organic Matrix," *Applied Physics Letters* 2 (1963) 152–154.

YU, Jeong-A; LESSARD, Ronald B.; BOWMAN, Lawrence E.; NOCERA, Daniel G. "Direct Observation of Intramolecular Energy Transfer from a β-Diketonate to Terbium (III) Ion Encapsulated in a Cryptand," *Chemical Physics Letters* 187 (1991) 263–268.

ZAITSEVA, L. L.; IL'YASHENKO, V. S.; KONAREV, M. I.; KONOVALOV, L. N.; LIPIS, L. V.; CHEBOTAREV, N. T. "Physicochemical Properties of Crystalline Hydrates of Sulfates of Terbium Sub-Group Rare-Earth Elements," *Zhurnal Neorganicheskoi Khimii (Russian Journal of Inorganic Chemistry)* 10:8 (1965) 1761–1770 (Russian original) or 961–966 (English translation).

ZHANG, Xiao; LIU, Xingren. "Luminescence Properties and Energy Transfer of Eu^{2+} Doped $Ca_8Mg(SiO_4)_4Cl_2$ Phosphors," *Journal of the Electrochemical Society* 139 (1992) 622–625.

ZHU, Guiyun; SI, Zhikun; LIU, Ping; JIANG, Wei. "Study of the Fluorescence Enhancement System Europium–Gadolinium–Thenoyltrifluoroacetone–Cetyltrimetylammonium Bromide–Triton X-100 and Its Application," *Analytica Chimica Acta* 247 (1991) 37–43.

APPENDIX A

PROPERTIES OF RARE-EARTH METAL β-DIKETONATES

I. Synthetic Methods

A.   Tetrakis Chelates

As stated in the thesis, the procedures used to synthesize europium(III) β-diketo-nates were based on those described by Brecher, Samelson, and Lempicki,[1] who prepared a number of (PipH)[Eu(dik)$_4$] chelates (excluding (PipH)[Eu(acac)$_4$]) by dissolving the β-diketone (Hdik) in 95% ethanol, adding piperidine (Pip) to make the enolate ion, then adding EuCl$_3$•6H$_2$O (also in 95% ethanol). The (PipH)[Eu(dik)$_4$] precipitate was filtered, washed, and dried. With acetylacetone (Hacac), this method did not produce the desired tetrakis compound, but (PipH)[Eu(acac)$_4$] was successfully prepared by adding (PipH)(acac) to Eu(acac)$_3$ in ethanol. Differences in solubility properties (particularly of the ligands) affect yields and ease of recovery. The chelate of dibenzoylmethane (Hdbm), obtained in 70% yield, precipitates immediately from solution; in contrast, precipitation of the chelates of benzoylacetone (Hba), benzoyltrifluoroacetone (Hbtfa), and thenoyltrifluo-roacetone (Httfa) requires solvent volume reduction and are obtained in yields of 40%, 60%, and 50%, respectively.[1-2] The success of Brecher's alternate procedure in produc-ing (PipH)[Eu(acac)$_4$] was verified by measuring the variation of emission intensity with composition. "The intensity reaches a distinct maximum at the stoichiometric ratio. The fact that the other four-ligand chelates can also be produced in solution in the same manner provides additional confirmation."[1]

The base used to produce the diketonate ion from the diketone (e.g. piperidine, sodium hydroxide) must have sufficient basic strength to ionize the diketone. For example, Hdbm does not react with isoquinoline (K_b = 2.5 × 10^{-9}) to form a tetrakis europium

chelate, but does so with piperidine ($K_b = 1.6 \times 10^{-3}$); in contrast, Httfa is a stronger acid and reacts with both bases to form europium chelates.[2-3]

B.   Hydrated Tris Chelates

Brecher et al.[1] prepared all of their hydrated tris europium β-diketonates by combining $EuCl_3 \cdot 6H_2O$ with the sodium enolate (prepared from NaOH and the Hdik) in water or 50% ethanol. The $Eu(dik)_3 \cdot 2H_2O$ precipitate was subsequently washed, air dried, and vacuum dried. It has been observed that if water is not deliberately excluded from the reaction mixture, tris europium β-diketonates are always hydrated.[2]

II. Structure and Bonding

A.   Component Ions

1.   Lanthanide Ion. One of the more striking features of all the lanthanide ions is that their five $5d$, one $6s$, and three $6p$ orbitals are all completely vacant and available for bonding. Since these are the lowest-energy vacant orbitals and the ion is sufficiently large, the lanthanides exhibit both six- and eightfold coordination.[1] More specifically, in reactions with β-diketones, Eu^{3+}, Gd^{3+}, and Tb^{3+} all exhibit eightfold coordination.[3]

2.   Diketonate Ion. The acac⁻ ion (the simplest β-diketonate ion) is a special case because it is capable of bonding through (1) the oxygens to give a chelate ring; (2) C^3 (the center carbon), in which case the C=O groups may chelate a second metal ion; (3) C^1 (in R), or both C^1 and C^5 (R and R′); or (4) the enolic C=C double bond. In other diketonate ions, case (3) is not possible for R, R′ $\neq CH_3$. The absence of free C=C, C=O, and O–H stretching vibrations in the IR spectrum of diketonate compounds, together with the presence of two or three strong bands in the 1500–1600 cm⁻¹ region (assigned to mainly $v_{C=C}$ and $v_{C=O}$ vibrations), plus another strong band at 1380 cm⁻¹ (assigned to $v_{C=O}$ and v_{C-H}), are evidence for chelation. The same considerations held for the acac⁻ ion can be extended, in principle, to other diketonate ions.[4]

B. Tris Chelates

In alcohol, alcohol–DMF (N,N-dimethylformamide), and powder media, all hydrated tris chelates exhibit a multiplicity of emission spectral lines, generally more than twice the number allowed for a single chemical species. "Since the two water molecules can be oriented with respect to the three β-diketone ligands in a number of different ways, evidence for at least three different species is not unexpected. Furthermore, the highest symmetry arrangement for the dihydrate is C_{2v}, so that virtually all of the components of the $^5D_0$–$^7F_1$ and $^5D_0$–$^7F_2$ transitions should be allowed; multiple lines are indeed observed in these regions."[1] These bands are centered near 590 and 610 nm, respectively (see, for example, Figure 1-3).

C. Tetrakis Chelates

1. Possible Geometries for Coordination Number 8. Because this particular coordination occupies only eight of the lanthanide ion's nine available orbitals, "three electronic configurations of the central ion can give rise to eightfold coordination: d^5sp^2, in which the coordinating oxygens are arrayed in the symmetry of a face-centered isosceles prism; d^5p^3, which produces an Archimedean antiprism; and d^4sp^3, which can yield either the antiprism or a tetragonal dodecahedron."[1] Distinguishing between these three possible geometries is generally accomplished by comparing the observed spectral details with those allowed by group-theoretical analysis (see, for example, Chapters 1 and 8).

2. Alcohol Solution. For (PipH)[Eu(ba)$_4$], the "dodecahedral structure, having a D_{2d} symmetry, is the only one which allows two lines of different character" in the $^5D_0 \rightarrow {}^7F_2$ emission spectral region near 610 nm. In (PipH)[Eu(dbm)$_4$], the symmetry is lowered to S_4, and the eight nearest-neighbor oxygens "assume a dodecahedral arrangement about the central europium ion, subject only to slight distortion from steric or solvent interactions."[1,3]

3.   *Alcohol–DMF Solution*. DMF is such a strong electron-pair donor that it can coordinate directly to tetrakis europium β-diketonates, forming a ninefold coordination structure of symmetry C_{4v}.[1]

4.   *Powder*. The emission spectrum of (PipH)[Eu(btfa)$_4$] has two lines in the $^5D_0 \rightarrow {}^7F_0$ region near 580 nm, because btfa$^-$ "has two groups of vastly different electronegativity (CF_3 and C_6H_5) at the opposite ends of the chain. This makes it possible to have at least two distinct molecular entities: one with a permanent dipole, as, for example, with all four CF_3 groups toward one end, and the other without such a dipole." Nevertheless, it has only one crystal morphology, and the existence of isolable (PipH)[Eu(dik)$_4$]•DMF adducts shows that Pip is not directly bonded to Eu.[1]

For all the tetrakis chelates, "the piperidinium ion appears to serve the same purpose in the crystal that the dimethylformamide molecule served in [alcohol–DMF] solution: it favors the antiprism over the dodecahedron and, by its proximity, produces a C_{4v} symmetry for the immediate surroundings of the central ion."[1] "While such differences are expected between the *tris* chelate and the *tetrakis* form, significant changes in emission spectra are also observed among the solid *tetrakis* compounds which contain, nominally, the same fluorescing species," namely, Eu(btfa)$_4^-$. Differences in Stark splitting are apparent in high-resolution spectra of the $^5D_0 \rightarrow {}^7F_1$ and $^5D_0 \rightarrow {}^7F_2$ emissions; in particular, complexes containing the n-butylammonium, 2-hydroxyethylammonium, piperidinium, and tetramethylammonium cations have only one of three possible $^5D_0 \rightarrow {}^7F_1$ Stark components clearly resolved, while those containing the diethylammonium and triethylammonium cations have two and that containing the tetraethylammonium cation has all three, indicating successively greater asymmetry induced in the Eu(btfa)$_4^-$ anion. "The spectra, and hence the local symmetry of the eight bonded oxygens, about the europium are clearly dependent upon the nature of the cation. Apparently the most stable configuration about the metal is determined by the crystal packing requirements of the cation."[5]

A. *Formation Constants*

The solution equilibrium formation constants for the reaction of Eu^{3+} with $acac^-$ ($pK_a = 8.88\pm0.02$) at 30°C, two different Eu^{3+} concentrations,[6] and two different NaCl ionic strengths[6-7] are presented in Table A-1. Significantly, the *lowest* value (K_{f3}) is greater than 10^3, indicating that the product is highly favored; therefore, $Eu(acac)_3$ has significant stability in solution. Similar behavior is observed for many other rare-earth complexes.[7]

Another property relating to the fundamental stability of metalorganic complexes in aqueous solution is the tendency of the central metal ion to undergo hydrolysis. In $Ln(acac)_3$ complexes, hydrolysis "is strongly suppressed by the strong complexing with acetylacetone" as illustrated by the concentration ratio of $Ln(OH)^{2+}$ to $Ln(acac)^{2+}$. For "the most strongly hydrolyzed of the rare earths," Lu^{3+}, the ratio is only 0.02.[7]

B. *Tris–Tetrakis Equilibrium*

1. *Driving Forces.* Two driving forces determine the tris–tetrakis equilibrium reaction in lanthanide β-diketonates. Tris $(Ln(dik)_3)$ chelates are electrically neutral, but have three vacant Ln^{3+} ion bonding orbitals. On the other hand, tetrakis $(Ln(dik)_4^-)$ chelates have two more filled bonding orbitals but have excess negative charge. These two

TABLE A-1

	$\log K_{f1}$	$\log K_{f2}$	$\log K_{f3}$
$[Eu^{3+}] = 7 \times 10^{-4}\,M$, $\mu_{NaCl} = 0.0\,M$ (Ref. 6)	6.0	4.5	3.5
$[Eu^{3+}] = 7 \times 10^{-3}\,M$, $\mu_{NaCl} = 0.0\,M$ (Ref. 6)	6.1	4.6	3.4
$[Eu^{3+}] = 7 \times 10^{-4}\,M$, $\mu_{NaCl} = 0.1\,M$ (Ref. 7)	$5.87\pm.03$	$4.48\pm.03$	$3.29\pm.02$

TABLE A-1: Formation constants (after Refs. 6–7) for the reaction of Eu^{3+} with $acac^-$ in water at 30°C as functions of europium(III) concentration and ionic strength.

tendencies, to fill vacant orbitals and to achieve charge neutrality, compete, leading to the equilibrium reaction $Ln(dik)_3 + dik^- \rightleftarrows Ln(dik)_4^-$.[1]

2. *Dissociation Behavior.* The dissociation behavior of $Ln(dik)_4^-$ species vary according to the natures of the ligand and the solvent. For example, according to Brecher *et al.*,[1] $(PipH)[Eu(btfa)_4]$ almost completely dissociated in alcohol, but not in alcohol–DMF solution. The other chelates remained primarily in tetrakis form but with measurable dissociation (24–43%). The presence of two distinct $^5D_0 \rightarrow {}^7F_0$ emissions near 580 nm "demonstrates unequivocally that at least two species are present in alcohol solutions of the four-ligand chelates and that one of the species is the same as is found in solutions of the tris chelate." Because this transition is completely nondegenerate, any line multiplicity or broadening must be caused by the presence of different Eu^{3+} species.

C.   Solvent Coordination

1. *Tris Chelates.* In alcohol and alcohol–DMF, both anhydrous and hydrated tris chelates produce essentially the same species, with two or three solvent molecules coordinated to the complex in a preference order which is in theory determined by coordination strength (alcohol < water < DMF).[1,8]

2. *Tetrakis Chelates.* In alcohol–DMF (but not in alcohol), tetrakis chelates also solvate, "accepting a pair of electrons from the DMF oxygen to form a nine-coordinated compound." This phenomenon is likely attributable to the extreme donor strength of DMF.[1,8]

IV.   UV/VIS Absorption Spectra

The β-diketonate ligands have at least two ultraviolet absorption bands in the 300–400 nm region. The more intense band at longer wavelengths increases in both peak wavelength and intensity for different ligands (Table A-2). "This order probably represents increasing participation of resonance structures involving phenyl or thienyl groups with the chelate rings. A similar progression toward longer wavelength and more intense

absorption with increasing number of phenyl groups occurs with the longer wavelength band of the p-polyphenyl series of compounds."[9]

The solution UV absorption spectra of $Q[Eu(btfa)_4]$ (where Q^+ is a protonated nitrogenous base) chelates are essentially identical when Q^+ does not absorb in the same region; therefore, all these compounds dissociate into the same absorbing species, $Eu(btfa)_4^-$. Both absorption peaks of $Eu(btfa)_4^-$ are blue-shifted with respect to those of $Eu(btfa)_3$, corresponding to an increase in the ligand's S_1 energy level, but in other regards the absorption spectra of tris and tetrakis chelates are nearly identical.[5]

V. Thermal Analysis (TG and DTA)

The several thermal-analysis studies discussed below, as well as the solution equilibria described in section III.A, are included in this appendix to illustrate the room-temperature stability of europium(III) β-diketonates. Thermogravimetry (TG) measures mass loss as a function of heating, while differential thermal analysis (DTA) can determine whether a physical or chemical reaction process is endothermic or exothermic and therefore is useful in identifying the type of reaction involved.

For TG of $Eu(ttfa)_3 \cdot 2H_2O$, weight loss to 110°C corresponds to loss of water, but further heating does *not* produce anhydrous $Eu(ttfa)_3$; rather, it leads to decomposition.[9]

TABLE A-2

	λ_{max} (nm)	ε (10^4 $(M$ cm$)^{-1}$)
Eu(acac)$_3$	290	3.5
Eu(ba)$_3$	325	4.3
Eu(dbm)$_3$	342	5.5
Eu(ttfa)$_3$	352	6.0

TABLE A-2: Absorption wavelength maxima (λ_{max}) and intensities or molar extinction coefficients (ε) for four europium β-diketonates (after Ref. 9).

The difference in hydration between tris and tetrakis complexes is illustrated by the fact that $Eu(btfa)_3 \cdot 2H_2O$ has an appropriate weight loss corresponding to dehydration near 120°C, but $Eu(btfa)_4^-$ chelates show no dehydration losses.[5]

For the family of tetrakis chelates including piperidinium, $(PipH)[Eu(dik)_4]$, observable differences in thermal stability as a function of ligand species are small. Apparently, the initial thermal "attack" occurs at the piperidinium ion site common to the entire family of compounds. The differences between compounds in the $Q[Eu(btfa)_4]$ family are more significant.[10]

The study by Lis shows how TG and DTA of tris europium chelates are complementary. "All the TG curves show a distinct loss of mass at relatively low temperatures, 100–120°C, and at the same [temperature] a distinct endothermic peak appears on the DTA curve. The correlation between the TG and the DTA curves shows that in this range of temperatures the process of dehydration takes place." "Besides the dehydration section, the TG curves have a slight plateau up to 180–190°C for all the investigated complexes. Between 220 and 310°C the decomposition of the organic part of the molecule takes place and the large loss of mass results. Therefore in this range of temperature a small exothermic maximum is visible. Above 350°C the change in mass for all the investigated complexes is small and at about 550°C the TG curve reaches a plateau and the weight of the residue is, within the accuracy of a few per cent, equal to the mass of the corresponding lanthanide oxide." TG indicates that "when the dehydration process is finished, the investigated compounds show a reasonable thermal stability in the range of several tens of a degree, and then a fast decomposition process follows, resulting finally in the formation of the corresponding lanthanide oxide."[11]

As for $Eu(ttfa)_3 \cdot 2H_2O$, TG of $Eu(ba)_3 \cdot 2H_2O$ shows that the anhydrous compound is not produced upon heating. In this case, however, the hydrated compound begins losing water at 50°C and the dehydration process is complicated by hydrolysis: $Eu(ba)_3 \cdot 2H_2O \rightarrow Eu(ba)_2(OH) + H(ba) + H_2O$. This reaction appears in the DTA curve as an endothermic

peak which is followed at higher temperatures by an exothermic peak attributed to decomposition to Eu_2O_3.[12]

VI. Mass Spectrometry

A. Electron Impact Mass Spectrometry (EIMS) [13]

This technique utilizes electron bombardment to ionization the test molecule, which then fragments sequentially following a process which may be described as $M^0 - e^- \rightarrow M^{+\cdot}$ $\rightarrow A^+ + m\cdot$ or $A^{+\cdot} + m^0$, where M^0 is the test molecule (gas phase), $M^{+\cdot}$ is its molecular ion (a radical cation), A^+ is a fragment ion (which may also be a radical), and m is a neutral fragment (which may be a radical).

Lanthanide complexes of $acac^-$, $ttfa^-$, and $btfa^-$ have all been successfully investigated, three types of mass fragmentation have been observed: (1) oxidation state III is preserved (Ce, Gd); (2) III is reduced to II (Sm, Eu, Yb); and (3) both occur simultaneously (all other lanthanides).

In a study of $Eu(acac)_3$, a number of fragmentation pathways are available after the loss of the first acetylacetonate radical. Fragments and their relative intensities include $[Eu^{III}(acac)_3]^{+\cdot}$, 30; $[Eu^{II}(acac)_2]^{+\cdot}$, 100; and $[Eu^{II}(acac)]^+$, 64. "The loss of the acetylacetonate radical occurs via direct cleavage of the metal–ligand bond..."

B. Liquid Secondary Ion and Fast Atom Bombardment Mass Spectrometry (LSIMS and FAB)

These techniques differ from EIMS in that the sample is bombarded with a beam of ions (in SIMS or LSIMS) or neutral atoms (in FAB) which have energies in the keV range or higher. "As a result of the primary beam interaction, secondary ions are desorbed or sputtered from the sample (usually dissolved in the matrix) and accelerated. The ions are dispersed according to their energy and mass-to-charge ratio, and detected. ... The FAB, as well as measurements carried out using accelerated ions as the primary beam, are included in SIMS technique." "In the positive FAB/LSIMS, ions at the highest m/z

Composition	n	Relative Intensity
[Eu(acac)$_2$(acac–H)]$^-$[Eu(TEA–3H)]$_n$	0	39
	1	13
	2	22
	3	48
[Eu(acac–H)$_2$]$^-$[Eu(TEA–3H)]$_n$	0	30
	1	9
	2	13
[O=Eu(acac–H)]$^-$		30
acac$^-$[Eu(TEA–3H)]$_n$	1	100
	2	35
	3	30
	4	13
acac$^-$Eu(acac)$_3$[Eu(TEA–3H)]$_n$	0	26
	1	6
	2	—

TABLE A-3: Negative LSIMS of Eu(acac)$_3$ in triethanolamine (TEA) (after Ref. 13).

observed for organic compounds are generally [M+H]$^+$ unless [M+H+matrix]$^+$ adduct-ions are present in the spectra with distinguishably lower intensities. In the negative ion spectra, [M–H]$^-$ ions can be found. The [M+H]$^+$ ions are formed by proton addition during bombardment or by direct protonation, while [M–H]$^-$ ions are formed by proton abstraction with participation of the matrix in the proton transfer reaction."[13]

A study of europium β-diketonates which have fluorine-containing ligands shows a different fragmentation behavior from Eu(acac)$_3$.[14] "In all cases the molecular ion M$^+$· was that of the anhydrous *tris*-chelated metal complex, although the hydrated compounds were placed in the mass spectrometer. The coordinated aqua groups were removed by the very low pressure and elevated temperature operating in the mass spectrometer." The characteristics of the mass spectrum is determined by the ligand, not the lanthanide ion. In many cases, the molecular ion M first loses a ·CF$_3$ radical to produce the more stable even-electron species (M–CF$_3$). "The loss of ·CF$_3$ is facilitated by the three electron-withdrawing fluorine atoms which weaken the C–CF$_3$ bond."

In others, M loses a ligand radical to form the M–L ion. "The ion M–L can fragment in three ways: (*a*) By loss of the neutral fragment :CF_2 to yield the ion M–L–CF_2 with concomitant fluorine migration to the metal atom... No metastable peaks for this reaction have been observed either in this or any previous work. The reaction occurs presumably because of the attraction of the positive charge on the metal for the electronegative fluorine atom. (*b*) By loss of the thermodynamically stable CO molecule to yield the ion M–L–CO... (*c*) By loss of the fragment RCOF... The M–L–CF_2 loses the fragment RC(O)CH=CO to give the ion M–2L+F... The ion M–2L+F fragments by two different pathways: by loss of either CO or :CF_2... The ion M–2L+F–CF_2 can lose CO_2... The ion M–2L+F–CF_2 can lose RC(O)CH=CO to give the ion $MetF_2^+$... Alternatively, the ion M–2L+F–CF_2–CO can lose RC≡CH to give the ion $MetF_2^+$..."

"The lanthanides (Ln = Sm, Eu, Tm, and Yb) can display bivalency in addition to the more stable tervalency. The ion $MetF^+$ was found in the spectra of the complexes of these elements. The intensity of the peak varied: Eu >> Sm > Yb > Tm, reflecting the decreasing tendency among these lanthanides to display bivalency. The reaction probably takes place *via* a valency change followed by the loss of a fluorine radical ·F, as follows: $Met^{III}F_2^+ \rightarrow MetF_2^{+·} \rightarrow Met^{II}F^+ + ·F$." The mass spectrum of Eu(ttfa)$_3$ is presented in Table A-4.

"The R group generally has little effect on the mass spectra. The spectra of lanthanide complexes of (*1*) with R = C_4H_3S, Ph, *m*-MeC_6H_4, *p*-MeC_6H_4, *p*-$MeOC_6H_4$, and *p*-BrC_6H_4 are essentially similar."

TABLE A-4

Ion (R = C_4H_3S)	Relative Intensity
M	65
M–CF_3	32
M–L	39
M–L–CO	9
M–L–CF_2	39
M–L–RCO–F	32
M–2L+F	48
M–2L+F–CO	23
M–2L+F–CF_2	23
M–3L+F (MetF)	100

TABLE A-4: LSIMS relative intensity values for Eu(ttfa)$_3$ (after Ref. 14).

VII. References

1. C. Brecher, H. Samelson, and A. Lempicki, *J. Chem. Phys.* **42** (1965) 1081.

2. S. J. Lyle and Alan D. Witts, *Inorg. Chim. Acta* **5** (1971) 481.

3. H. Bauer, J. Blanc, and D. L. Ross, *J. Am. Chem. Soc.* **86** (1964) 5125.

4. F. Bonati, *Organometal. Chem. Rev.* **1** (1966) 379.

5. R. G. Charles and E. P. Riedel, *J. Inorg. Nucl. Chem.* **28** (1966) 3005.

6. R. M. Izatt, W. C. Fernelius, C. G. Haas, Jr., and B. P. Block, *J. Phys. Chem.* **59** (1955) 170.

7. I. Grenthe and W. C. Fernelius, *J. Am. Chem. Soc.* **82** (1960) 6258.

8. A. Lempicki, H. Samelson, and C. Brecher, *Appl. Opt. Suppl.* **2** (1965) 205.

9. R. G. Charles and R. C. Ohlmann, *J. Inorg. Nucl. Chem.* **27** (1965) 255.

10. R. G. Charles and E. P. Riedel, *J. Inorg. Nucl. Chem.* **29** (1967) 715.

11. S. Lis, in I. Buzas, *Proceedings of the Third Analytical Chemistry Conference*, Volume 2 (Prague, Czechoslovakia, 1970), p. 433.

12. J. R. Allan, B. Carson, A. D. Paton, K. Turvey, D. L. Gerrard, and S. Hoey, *Thermochim. Acta* **157** (1990) 61.

13. M. Elbanowski, S. Lis, A. S. Plaziak, and B. Makowska, <u>in</u> W. Strek, W. Ryba-Romanowski, J. Legendziewicz, and B. Jezowska-Trzebiatowska, *The Second International School on Excited States of Transition Elements* (Singapore: World Scientific Publishing Co. Pte. Ltd., 1992), p. 49.

14. A. M. Hamer and S. E. Livingstone, *Trans. Met. Chem.* **9** (1984) 433.

APPENDIX B

PROPERTIES OF SILICA AND DOPED SILICATES

I. Silica Surface Chemistry

A.   Surface Silanol Groups

The surface of silica in all forms, but particularly the gel, is covered with $\equiv$Si–O–H groups (variously called hydroxy groups, hydroxyls, or silanols) whose chemical reactivity allows considerable modification of the particle surface. Silica (particularly silica gel) is effectively "an amorphous condensation polymer of silicic acid" which retains large numbers of uncondensed silanols. Silica gel has a surface density of about five OH groups per square nanometer, which is equivalent to a very high concentration of surface OH groups, in the range of 2–5 molal (mol OH/kg SiO_2). Silanols are weak acids which form strong hydrogen bonds to water, alcohols, ethers, and related compounds; and weak bonds to olefins and aromatics. These bonding properties make silica gel useful in separations chromatography, where it is one of the most frequently used stationary phases.[1]

B.   Modification of the Silica Surface

The surface OH groups of silica are subject to a number of chemical reactions which can be exploited for surface modification. For example, the surface OH groups of silica gel may be replaced with (1) OCH_3 groups, by exposure to methanol vapor at 180°C; (2) Cl, by exposure to CCl_4 at 400°C (this $\equiv$Si–Cl surface is very reactive, as are chloro-silanes in general); (3) H (hydride), by reaction with lithium hydride in ether; (4) C_6H_5 groups, by reaction with phenyllithium in ether; or (5) various silicon-containing groups, by treatment with a large number silylating agents, e.g. $(CH_3)_3SiOCH_3$.[1]

C.   Surface pH and Polarity

As stated earlier, the silanol groups of silica gel are weak acids, with pK_a values near 7.1. As a consequence, the silica gel surface may readily undergo cation exchange,

particularly in basic aqueous solution, which promotes the formation of $\equiv$Si–O$^-$ species. A number of transition-metal complexes, including $[Cr(NH_3)_6]^{3+}$, $[Co(en)_2Cl_2]^+$ (en = ethylenediamine), $[Co(en)_2Cl(H_2O)]^{2+}$, and $[Ru(bpy)_3]^{2+}$ (bpy = 2,2'-bipyridine), can also ion-exchange onto partially deprotonated silica gel. "Silanol groups also serve as strong hydrogen bond donors, rendering silica gel a polar, microporous medium." Specifically but qualitatively, "silica gel is more polar than methanol and slightly less polar than 2,2,2-trifluoroethanol or water."[2]

Research on the acidity of Mg–OH, B–OH, P–OH, and Si–OH surfaces has determined that surface OH groups have lower pK_a values than do the "molecular" acids (*i.e.* magnesium hydroxide and boric, phosphoric, and silicic acids), but that there is no direct relationship between the two pK_a values (see Table B-1).[3]

D.   *Example of pH-Dependent Silica Surface Chemistry*

    1.   Interaction of Silica and Molybdenum Cluster Complexes. Robinson *et al.* (1995)[2] investigated the interaction of acid- and base-treated silica gels in three solvent systems of differing polarity (acetonitrile, methanol, and dichloromethane) with two molybdenum cluster anions of the form $[Mo_6Cl^i_8X^a_6]^{2-}$, where the superscripts i and a refer to face-bridging and axial ligands, respectively, and X = $SO_3CF_3^-$ (Tf$^-$) (**1**) or Cl$^-$

TABLE B-1

Oxide	Frequency (in cm^{-1}) of freely vibrating OH group	pK_a	Literature pK_a value for the acids in solution (first dissociation step)
SiO$_2$	3750	7.1±0.5	9.7
SiO$_2$–Al$_2$O$_3$	3750	7.1	—
P$_2$O$_5$	3670, 3700	–0.4	2.0
B$_2$O$_3$	3706	8.8±0.6	9.1
MgO	3752	15.5±0.4	—

TABLE B-1: Vibrational frequencies and observed pK_a values of surface hydroxyl groups (after Ref. 3). The nonsilicates are included for comparison purposes.

(2). The triflate ligand was chosen for its substitutional lability with respect to polar solvent molecules and the silica surface; the axial chloride ligands are much less labile.

"For a given solvent system, the uptake of **1** by the gel does not vary with the pre-treatment of the silica gel... Acetonitrile disfavors adsorption by silica gel as compared with CH_2Cl_2 and CH_3OH." In noncoordinating CH_2Cl_2, the axial Tf^- ligands remain bound to the cluster, but in solvents of higher Lewis basicity (CH_3OH or CH_3CN) they are at least partially displaced, forming the solvated clusters $[Mo_6Cl^i{}_8Tf^a{}_x(solvent)^a{}_{6-x}]^{(4-x)+}$ (**1'**). In CH_2Cl_2, acidic silica has a very high affinity for **1**, with a partition coefficient K' = 800 mL/g, but the large K' "is not due to coordinative attachment through Si–O–Mo bonds"; rather, it arises from electrostatic interactions. "In more polar, basic solvents such as CH_3CN and CH_3OH, the interaction between acidic silica gel and [**1**] is due to a combination of Si–O–Mo coordination and electrostatic interactions." This chemisorption is aided by the limited deprotonation of silanol groups in the coordinating solvents, followed by cation exchange of **1'** onto the Si–O⁻ sites, where a covalent bond can form by elimination of an axial solvent or triflate ligand. The interaction between **1'** and silica gel is even stronger under basic conditions.

Cluster **2** "can be supported on basic or acidic silica gel, when CH_2Cl_2 is the suspending solvent... No uptake of **2** by the gel is observed in more polar solvents such as CH_3CN or CH_3OH." "In CH_2Cl_2, the interaction of **2** with acidic silica gel is due to electrostatic interactions and can be expressed in terms of the partition coefficient, K'... The observed value is large (100 mL/g), indicating that association of the cluster with the polar silica gel medium is favored over interaction with the solvent phase. In more polar media, such as CH_3CN and CH_3OH, the affinity of the support for solvent molecules is greater than its affinity for the cluster, and **2** is not adsorbed by the silica gel ($K' \approx 0$ mL/g)." Neither does **2** absorb onto silica gel under basic conditions in either CH_3CN or CH_3OH, and its adsorption onto basic silica in CH_2Cl_2 reverses totally upon the addition of

tetrabutylammonium chloride to the system. Therefore, **2** does not form covalent bonds with either acidic or basic silica gel.

2. Comparisons to the Europium–β-Diketonate–Silica Gel Systems. While there is little similarity between the complex chemistries of europium and molybdenum, the study described in the preceding section illustrates principles which may be applied to the analysis of europium–silica systems. Of the two complexes studied by Robinson *et al.*,[2] only the one containing the very labile triflate ligand (**1**) participated in covalent bonding to the silica gel surface, and then predominantly at high pH when activation of the silica surface by deprotonation is more likely. As described in Appendix A (section III.A) the formation constants of europium β-diketonates are high ($K_{\beta 3} > 10^3$), meaning these complexes remain largely intact in solution; unlike Tf⁻, dik⁻ ligands are not particularly labile. Furthermore, the silicate systems described in this thesis are all in the low-pH regime. Under these conditions, therefore, the probability of direct covalent attachment of an europium β-diketonate to silica seems to be very low. As mentioned below, however, *uncomplexed* europium(III) ions have strong interactions with silica gel at all pH regimes.

II. Europium(III)-Doped Silicates

A. Europium(III) as Fluorescence Probe in Sol–Gel Silica

1. Sol, Hydrogel, and Xerogel States. The emission spectrum of Eu³⁺ in sol–gel silica at room temperature is similar to that of Eu³⁺ in aqueous solutions. In these states sol–gel silica is a solvent-rich environment, and even the xerogel still contains trapped solvent molecules ("room-temperature drying removes only the solvent molecules which are physisorbed on the walls of the open pores"[4]) which are as disordered as in the liquid state and present in sufficient numbers to form a solution-like symmetric solvation shell around the Eu³⁺ ion.[4–5] A representative sol fluorescence lifetime of 0.134 ms is comparable to the value of 0.1 ms in nitrate solution, and it decreases to 0.123 ms at the gel stage.

Comparisons with deuterated sols show that the number of water molecules in the Eu^{3+} coordination sphere is ≈ 6 in the sol, increasing to ≈ 7 at the gel point.[5]

2.   *Densified Gels and Glasses.* On heating silica xerogel above 100°C, the intensity ratio (η_{21}) and the total intensity increase to values analogous to those of Eu^{3+} in conventional silica melt glasses, in which the local environment of Eu^{3+} has much lower symmetry than a solvation shell.[4] This process was still not complete in gels partially densified at 200°C, in which the spectral degeneracy of the $^5D_0 \rightarrow {}^7F_1$ and $^5D_0 \rightarrow {}^7F_2$ emissions of Eu^{3+} was only partially lifted and the lifetime increased to only 0.380 ms. These Eu^{3+} spectra concur with ^{29}Si NMR, which "demonstrates that the 200°C glass contains silicon which is coordinated to two, three, and four other silicon atoms, via the oxygens"[5] (see also Appendix C).

At 100°C and higher temperatures, "the europium cation participates actively in the continuous polymerization–condensation reactions, and forms $(Si-O)_n Eu$ bonds, releasing HCl, which, similarly, to the release of methanol and water, results in new Si–O–Si bonds."[4] By 800°C, the spectral degeneracy of the $^5D_0 \rightarrow {}^7F_1$ transition is fully lifted, but the shape of the $^5D_0 \rightarrow {}^7F_2$ transition and the lifetime ($\tau = 1.25$ ms) still do not completely match those of conventional silicate glasses ($\tau = 2.3$ ms), they "are still not subject to a fully asymmetric silica glass environment." The ^{29}Si NMR spectrum, however, shows only four-coordinated silicon.[5]

3.   *Fluorescence as a Function of pH.* A study of the fluorescence ratio (η_{21}) of Eu^{3+} in silica at pH 1.0, 5.5, and 8.0 shows that the low-pH environment is more symmetric than the other pH regimes. The fluorescence lifetime (τ) is also shorter at low pH, which shows the presence of more O–H oscillators in the Eu^{3+} environment. Both factors "are consistent with the predicted behavior of hydrolysis and condensation as a function of pH": the hydrolysis rate is relatively faster than the condensation rate at low pH, leading to a loose network structure. At higher pH values, hydrolysis is slower and condensation is competitive, leading to a more colloidal structure.[6]

4. Fluorescence as a Function of the Water-to-Alkoxide Ratio (R). In europium-doped acid-catalyzed silica gels (pH 1.0), the Eu^{3+} ion in $R = 4$ silica has a longer τ, a larger η_{21}, and a higher fluorescence efficiency (Q) than those of Eu^{3+} ions in silicas made from sols with higher R values. "This behavior is consistent with the model for low pH materials of a loose polymer-like structure produced by fast hydrolysis..." In silicas with $R > 4$, unreacted water remains in the sol during hydrolysis, leading to lower values of τ and η_{21} for Eu^{3+} fluorescence. For sols with $R = 4$, "most of the water is used up in the hydrolysis step so the immediate environment of the Eu^{3+} contains fewer hydroxyl groups." Upon changing the pH to 5.3, the hydrolysis rate slows and becomes subject to competition for water from other reactions, which means that more water is required to complete hydrolysis. "The structure of the gel is colloidal and the europium should not be exposed to the excess water present at higher $[R]$ values, compared with the situation for acid catalysis."[6]

B. Inner-Sphere Coordination of Europium(III) in Silica

Lochhead and Bray (1994)[7] studied the effects of inner-sphere coordination of the Eu^{3+} ion in ethanol–water solution and sol–gel silica, where "the counter-ion of the europium salt affects the optical properties of Eu^{3+} in the sol and wet gel" stages of the drying process, causing significant spectral changes which "can be explained by counter-ion complexation of Eu^{3+}."

In ethanol–water solutions of three different europium salts (nitrate, chloride, and perchlorate), spectral differences "can be interpreted in terms of the relative affinity of each counter-ion for the inner coordination sphere of the Eu^{3+} ion." Nitrate ions can displace water molecules in the Eu^{3+} inner coordination sphere. This substitution distorts the Eu^{3+} local environment, thereby increasing the relative intensities of the $^5D_0 \rightarrow {}^7F_0$ and $^5D_0 \rightarrow {}^7F_2$ transitions, and also increases the fluorescence lifetime by reducing the number of quenching O–H oscillators. (Both NO_3^- and H_2O enter the Eu^{3+} inner coordination sphere more easily than ethanol.) "The Cl^- ion is less effective at entering the inner coordination

185

sphere... Inner-sphere complexation by a single Cl^- ion is achieved, however, when a significant amount of ethanol is present." In contrast, the probability of a ClO_4^- ion entering the inner coordination sphere of Eu^{3+} is very low; it remains almost exclusively in the outer coordination sphere.

The spectra of Eu^{3+} in silica sols and hydrogels are very close to those in ethanol–water solution. This "indicates that the Eu^{3+} ion experiences a liquid-like, mixed ethanol–water environment in the sols and wet gels. While the presence of silanol and ethoxy groups in the wet gel may complicate the Eu^{3+} bonding environment, the similarity between the two sets of spectra indicates that there is minimal interaction between the Eu^{3+} ion and the silica matrix at these early stages of the process. ...inner-sphere counter-ions and solvent molecules dominate the Eu^{3+} coordination shell in the early stages of the sol–gel reactions."

When doped silica gels are heat-treated, spectral differences due to counter-ion complexation disappear. "In addition to driving off excess water and solvent, heat treatment appears to also destroy the inner-sphere complexation of NO_3^- [and Cl^-] ions."

III. References

1. R. L. Burwell, Jr., *Chemtech* (1974) 370, and references therein.

2. L. M. Robinson, H. Lu, J. T. Hupp, and D. F. Shriver, *Chem. Mater.* **7** (1995) 43, and references therein.

3. M. L. Hair and W. Hertl, *J. Phys. Chem.* **74** (1970) 91.

4. D. Levy, R. Reisfeld, and D. Avnir, *Chem. Phys. Lett.* **109** (1984) 593, and references therein.

5. K. Devlin, B. O'Kelly, Z. R. Tang, C. McDonagh, and J. F. McGilp, *J. Non-Cryst. Solids* **135** (1991) 8, and references therein.

6. C. McDonagh, G. Ennis, P. Marron, B. O'Kelly, Z. R. Tang, and J. F. McGilp, *J. Non-Cryst. Solids* **147 & 148** (1992) 97.

7. M. J. Lochhead and K. L. Bray, *J. Non-Cryst. Solids* **170** (1994) 143, and references therein.

APPENDIX C

SOLID-STATE MAGIC-ANGLE-SPINNING (MAS)
NUCLEAR MAGNETIC RESONANCE (NMR) SPECTRA

I. Silica Gel

Figure C-1 presents the ^{29}Si MAS NMR spectrum obtained by the one-pulse-with-proton-decoupling (OPD) procedure, which is designed to identify all ^{29}Si environments present in the material, in this case a silica xerogel dried for months at room temperature. Two peaks are evident near –18 and –28 ppm, consistent with Q^1 ($\equiv$SiOSi(OR)$_3$, R = H or CH$_3$, and Si is the ^{29}Si atom in question) and Q^2 environments (($\equiv$SiO)$_2Si$(OR)$_2$).[1] There is no evidence for the presence of monomeric Q^0 (Si(OR)$_4$) species from the tetra-methoxysilane (TMOS) precursor or its hydrolysis products, nor for Q^3 (($\equiv$SiO)$_3Si$OR) or fully condensed Q^4 (($\equiv$SiO)$_4Si$) species, all of which lie at substantially more negative values. Figure C-2 shows the complementary spectrum obtained by the ^{1}H–^{29}Si cross-polarization (CP) procedure, which is designed to identify those ^{29}Si environments which are closely coupled to ^{1}H, in this case by OH groups. There is only one large peak near –18 ppm, with a small satellite peak near –10 ppm and a shoulder near –28 ppm. The peak near –18 ppm therefore probably arises from a $\equiv$SiOSi(OH)$_3$ species.

From this evidence it becomes apparent that while the precursor has been largely hydrolyzed in the xerogel, the gel structure is only partially condensed and presumably consists of long, intertwined chains similar to those observed in glassy polymers. At first, this structural concept seemed inconsistent with the observed optical and mechanical properties of the xerogel specimen, namely, transparency and glasslike brittle fracture. However, upon further contemplation of the works of Levy *et al.*,[2] who reported that room-temperature drying removes only physisorbed solvent molecules and not chemisorbed or entrapped solvent molecules; and of Devlin *et al.*,[3] who observed the

presence of significant amounts of Q^2 and Q^3 species in gels heated to 200°C and full condensation only in gels heated to 800°C, the postulation of the xerogel existing primarily as Q^1 and Q^2 species becomes the most likely explanation. Such an interpretation can be confirmed by a thoroughly detailed future investigation, which seems to be justified by the dearth of work on unheated gel systems.

The best-known Q^2 siloxane polymers are the silicones, particularly poly(dimethylsiloxane), which contains the $[(CH_3)_2SiO]_n$ repeat unit, and the argument can be made that a partially condensed polysilicic acid chain should have similar properties. The problem is that poly(dimethylsiloxane) and similar polymers containing various organic functionalities have significantly different physical properties from those observed in the silica gel. Many polysiloxanes are liquids at room temperature, and most solid polysiloxanes are elastic materials with very low glass-transition temperatures, near 150 K for poly(dimethylsiloxane). These properties are a direct consequence of the insulation of the polar siloxane backbone of the polymer by the hydrophobic alkyl groups, which prevents strong intermolecular interactions. In fact, a literature survey revealed no unambiguous examples of organopolysiloxanes exhibiting properties consistent with those observed in silica gel. However, it has been observed that when polysiloxanes are functionalized with such polar groups as carboxylic acids and amines, even at low levels of functionalization, the introduction of the potential for new types of intermolecular interactions significantly changes the polymer's physical properties, specifically through the action of intermolecular hydrogen bonding.[4]

This phenomenon of intermolecular hydrogen bonding appears to be the best approach to reconciliation of the nominally conflicting observations obtained from the NMR spectra of the silica gels and their physical properties. While it is true that linear Q^2 polysilicic acid would have the same Si–O–Si backbone structure as organopolysiloxanes, the difference in the chemical properties of its side groups is crucial. As has been described in Appendix B, silanol groups in particular are capable of forming strong hydrogen bonds.

Therefore, while alkyl groups insulate the siloxane backbone from intermolecular attractive forces, the silanol (and a few alkoxysilane) species present in silica gel will interact strongly with neighboring polysilicic acid molecules, producing a material with a sufficiently high glass-transition temperature to exhibit glasslike behavior.

II. Doped Silica Gel

Figure C-3 presents the ^{29}Si MAS OPD NMR spectrum of a silica xerogel doped with tris(4,4,4-trifluoro-1-(2'-thienyl)-1,3-butanedionato-O,O')europium(III) trihydrate at 0.100 M initial concentration and dried for months at room temperature to a final concentration near 0.5 M. As in Figure C-1, two large peaks are evident, near -16 (shifted from -18) and -28 ppm, again consistent with Q^1 and Q^2 environments.[1] A new small peak near -6 ppm and the very broad, low peak between $+50$ and -150 ppm may arise from the presence of the Eu^{3+} complex. Because Eu^{3+} is strongly paramagnetic, its complexes are widely used as NMR shift reagents and even long-distance interactions are observable, leading to much shorter relaxation times and hence broad peaks.[5] In contrast, the CP/MAS NMR spectrum in Figure C-4 is nearly identical to that in Figure C-2, so the presence of the dopant apparently does not alter cross-polarization. Once again, the structural information is consistent with the xerogel being a glassy polymer composed of Q^1 and Q^2 species.

III. Epoxy–Diol Ormosil

Figure C-5 presents the ^{29}Si MAS OPD NMR spectrum of an epoxy–diol ormosil xerogel, prepared from TMOS and 3-glycidoxypropyltrimethoxysilane (GPTMS) in a 1:1 mole ratio and dried for months at room temperature. The two peaks observed in silica (Fig. C-1) appear once more near -17 and -27 ppm, corresponding to the Q^1 and Q^2 silica environments.[1] Two new peaks near $+26$ and $+15$ ppm presumably arise from Q1 and Q2 species which contain one Si–C bond from the 3-glycidoxypropyl group. The ^{1}H–^{29}Si CP/MAS spectrum in Figure C-6 shows the same four peaks in nearly identical positions,

namely, +26, +18, –18, and –27 ppm, indicating that all four ^{29}Si species are coordinated to OH groups. The structural information is consistent with the xerogel being a polymer composed of Q^1 and Q^2 species, but this ormosil is noticeably more elastic than silica gel.

The ^{1}H–^{13}C CP/MAS spectrum in Figure C-7 shows six observable ^{13}C peaks near 73, 63, 52, 45, 24, and 9 ppm. The "ideal structure" presented in Figure C-8 illustrates the possible ^{13}C environments. Two of these peaks (9 and 24 ppm) may be unambiguously assigned to the $\equiv$SiCH$_2$– and –CH$_2$– methylene carbons (1 and 2 in Fig. C-8), respectively. The peaks and broad base in the 63–73 ppm region probably correspond to the –CH$_2$O– ether carbons (3 and 4).

IV. Methacrylate Ormosil

Figures C-9 and C-10 present the ^{29}Si OPD and ^{1}H–^{29}Si CP MAS NMR spectra, respectively, of a methacrylate ormosil xerogel, prepared from TMOS, 3-(trimethoxysilyl)-propyl methacrylate (TMSPM), and methyl methacrylate (MMA) in a 1:1:1 mole ratio and dried for months at room temperature. The spectra in these two figures are very similar to those in Figures C-5 and C-6, respectively, indicating that the same type of ^{29}Si environments exist, namely, Q^1 and Q^2 silica species and Q^1 and Q^2 species containing a Si–C bond, in this case from the 3-(trimethoxysilyl)propyl group. It should be readily apparent that the local ^{29}Si environments in the methacrylate ormosil should be similar to those in the epoxy–diol ormosil because the organic functionalities in both are isolated from the silicon atom by a propyl group. Again, the ^{29}Si structural information is consistent with the xerogel being a polymer composed of Q^1 and Q^2 species, and the methacrylate ormosil, like the epoxy–diol ormosil, is noticeably more elastic than silica gel, even more so than the epoxy–diol ormosil.

The ^{1}H–^{13}C CP/MAS spectrum of the methacrylate ormosil in Figure C-11 shows eight observable ^{13}C peaks near 167, 137, 126, 67, 51, 23, 19, and 10 ppm, while that of poly(methyl methacrylate) (PMMA) in Figure C-12 contains only five, near 184, 132, 59,

191

51, and 24 ppm. The "ideal structure" presented in Figure C-13 illustrates the possible ^{13}C environments. For this sample it was possible to unambiguously assign peaks to all eight expected ^{13}C environments: (1) the methacrylate methyl $-CH_3$ (19 ppm), (2) the methacrylate quaternary carbon (51 ppm), (3) the methacrylate-polymer methylene $-CH_2-$ (67 ppm), (4) the methacrylate carbonyl (167 ppm), (5) the methacrylate ester $-OCH_3$ (137 ppm), (6) the propyl ester methylene $-OCH_2-$ (126 ppm), (7) the propyl methylene $-CH_2-$ (23 ppm), and (8) the propyl silyl methylene $\equiv Si-CH_2-$ (10 ppm). As expected, the spectrum of PMMA is quite similar, but assignations are slightly more difficult. The unambiguous assignments are (1) the methyl $-CH_3$ (24 ppm), (2) the quaternary carbon (51 ppm), (3) the ester methoxy $-OCH_3$ (59 ppm), and (5) the carbonyl (184 ppm). The small peak at 132 ppm has not been conclusively identified, but could arise from the terminal methylene $CH_2=$ of unpolymerized methyl methacrylate. The methacrylate-polymer methylene $-CH_2-$ (4) is believed to appear as a shoulder near 63 ppm, but this assignment is not conclusive.

V. References

1. W. S. Brey, in R. Anderson, B. Arkles, and G. L. Larson, eds., *Petrarch Systems Silanes & Silicones* (Bristol, PA: Petrarch Systems, Inc., 1987), pp. 60–68.

2. D. Levy, R. Reisfeld, and D. Avnir, *Chem. Phys. Lett.* **109** (1984) 593.

3. K. Devlin, B. O'Kelly, Z. R. Tang, C. McDonagh, and J. F. McGilp, *J. Non-Cryst. Solids* **135** (1991) 8.

4. S. J. Clarson and J. A. Semlyen, *Siloxane Polymers* (Englewood Cliffs, NJ: PTR Prentice Hall, Inc., 1993).

5. R. M. Silverstein, G. C. Sassler, and T. C. Morrill, *Spectrometric Identification of Organic Compounds,* Fourth Edition (New York; Toronto: John Wiley & Sons, Inc., 1981).

Figure C-1

OkSU CMX-300
MAS=4kHz 12/22/93
One Pulse with proton decoupling
ppfn=s1pulse
cdir=d1
cfn=sio21p.001
cfp=0
sf1=59.800843 MHz
sf2=300.998455 MHz
sw=50 KHz
a=150
a1=150
ad=100 usec
al=1k cplx
aqtm=20.481 msec
dw=20 usec
extm=50.021 sec
p=0 deg
pd=50 sec
pw=5 usec
rd=150 usec
dpc=1 scns
ac=64 scns
dl=2k cplx
tlb=50 Hz
rmp=0.61072 virt
rmv=-0.0418877 ppm
fdsc=4069K
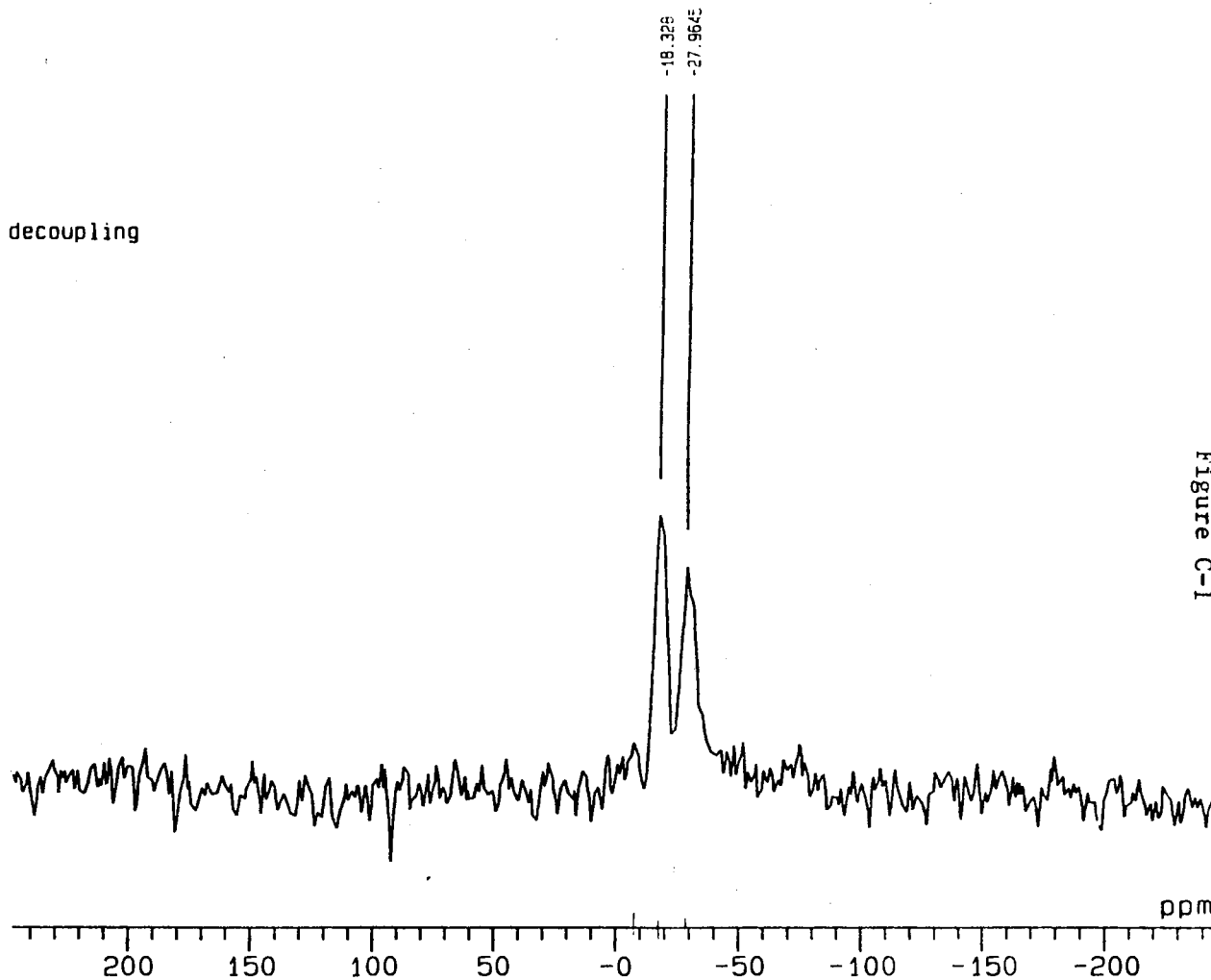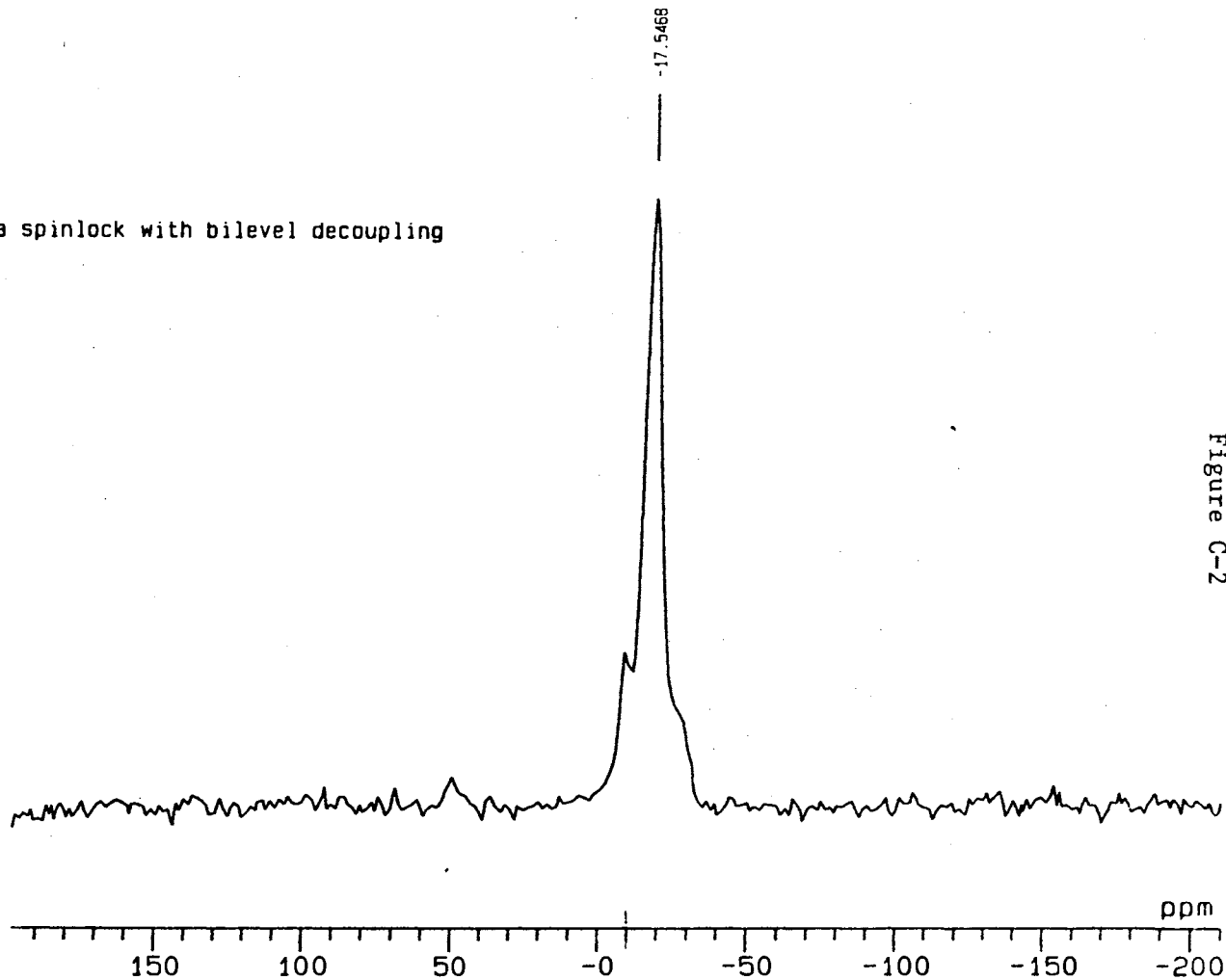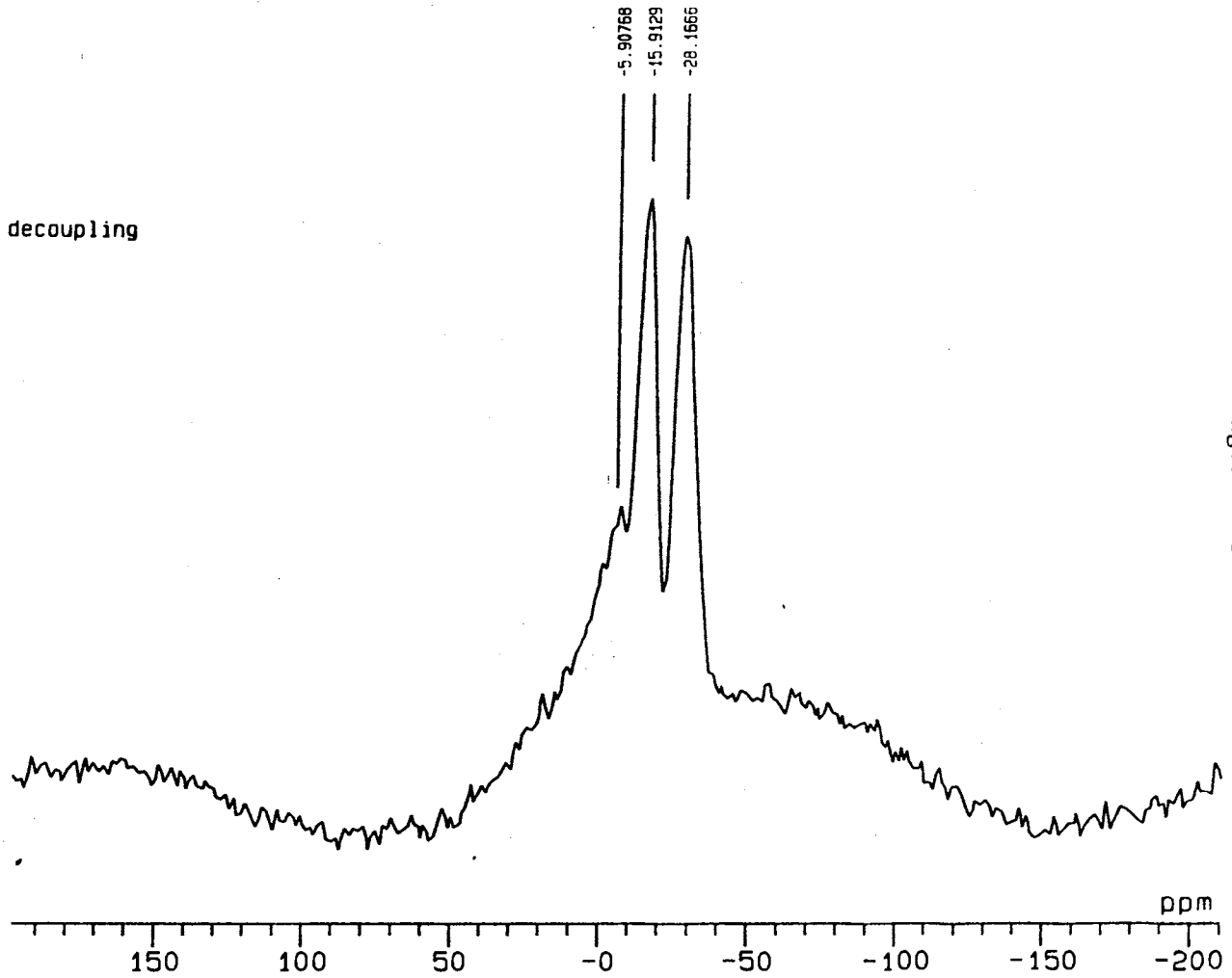tph0=108 deg
tph1=91 deg
disle=247.212 ppm

193

OkSU CMX-300
MAS=4kHz 1/5/94
cross polarization via spinlock with bilevel decoupling
ppfn=scp7
cdir=d1
cfn=silicacp.001
cfp=0
sf1=59.800843 MHz
sf2=300.998455 MHz
sw=50 KHz
a=150
a1=150
a2=150
ad=10 usec
al=1k cplx
aqtm=20.481 msec
ct=200 usec
dw=20 usec
extm=2.0207 sec
lc=5
p=0 deg
pd=2 sec
pw=5 usec
rd=10 usec
dpc=1 scns
ac=1000 scns
dl=2k cplx
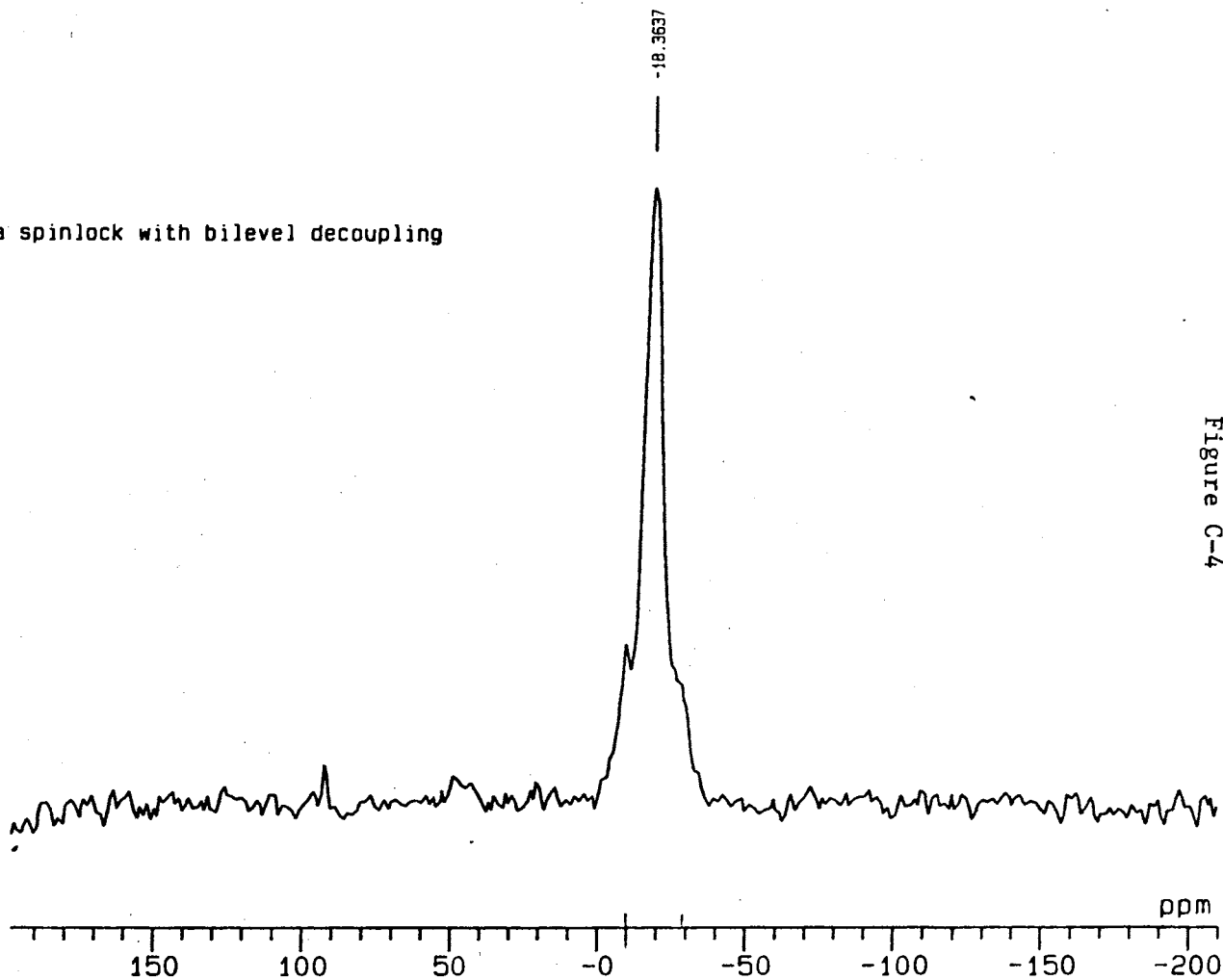tlb=50 Hz
rmp=0.61072 virt
rmv=-0.0418877 ppm
fdsc=1.512e+04K

-17.5468

Figure C-2

Chemagnetics

OkSU CMX-300
MAS=4kHz 1/4/94
One Pulse with proton decoupling
ppfn=s1pulse
cdir=d1
cfn=eut3si1p.001
cfp=0
sf1=59.800843 MHz
sf2=300.998455 MHz
sw=50 KHz
a=150
a1=150
ad=100 usec
al=1k cplx
aqtm=20.481 msec
dw=20 usec
extm=20.021 sec
p=0 deg
pd=20 sec
pw=5 usec
rd=150 usec
dpc=1 scns
ac=1000 scns
dl=2k cplx
tlb=50 Hz
rmp=0.61072 virt
rmv=-0.0418877 ppm
fdsc=1.224e+04K
tph0=33.291 deg
tph1=-1621 deg
disle=197.882 ppm

Peak labels: -5.90768, -15.9129, -28.1666

ppm axis: 150, 100, 50, -0, -50, -100, -150, -200

Figure C-3

OkSU CMX-300
MAS=4kHz 1/3/94
cross polarization via spinlock with bilevel decoupling
ppfn=scp7
cdir=d1
cfn=eut3sicp.001
cfp=0
sf1=59.800843 MHz
sf2=300.998455 MHz
sw=50 KHz
a=150
a1=150
a2=150
ad=10 usec
al=1k cplx
aqtm=20.481 msec
ct=200 usec
dw=20 usec
extm=2.0207 sec
lc=5
p=0 deg
pd=2 sec
pw=5 usec
rd=10 usec
dpc=1 scns
ac=1000 scns
dl=2k cplx
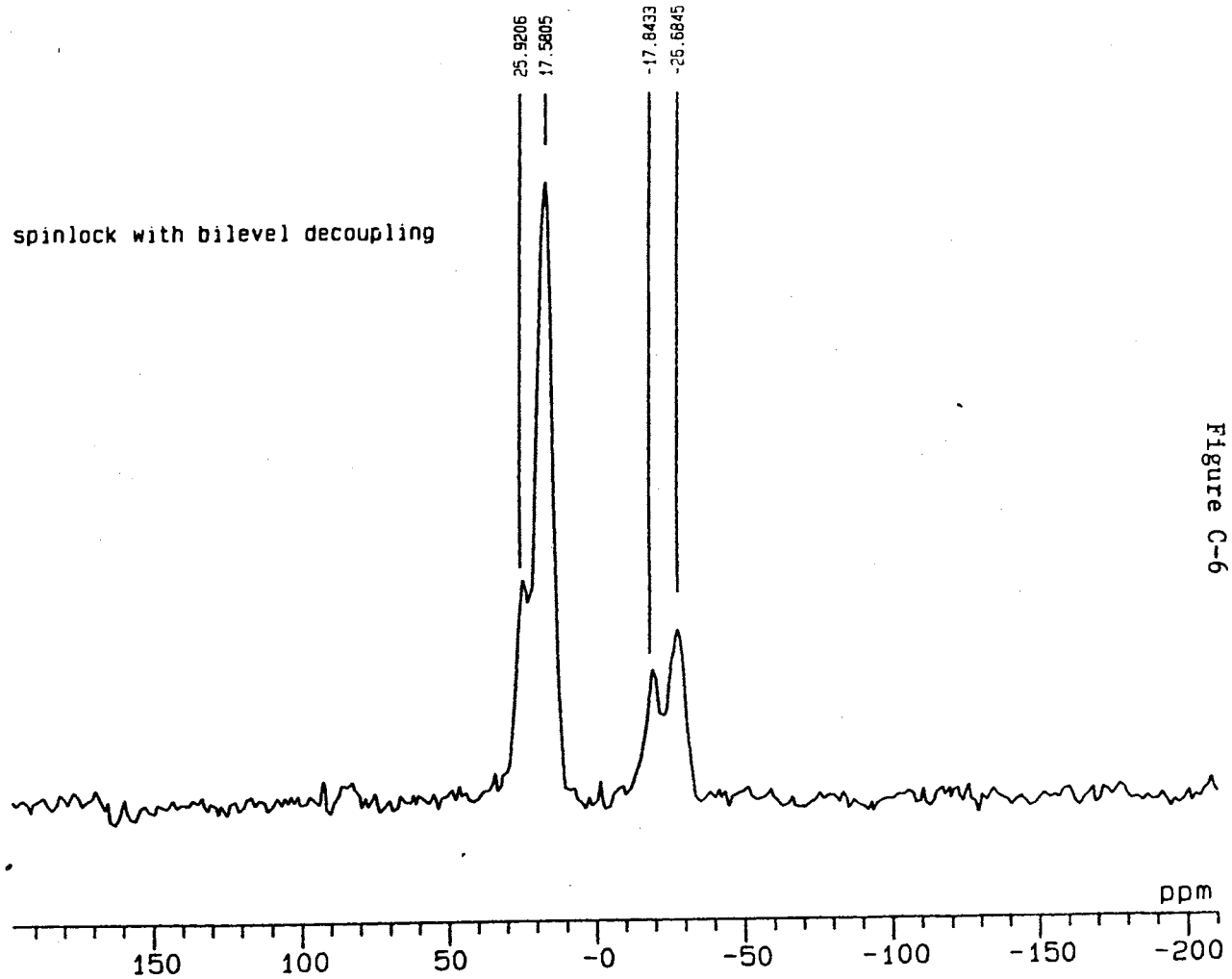tlb=50 Hz
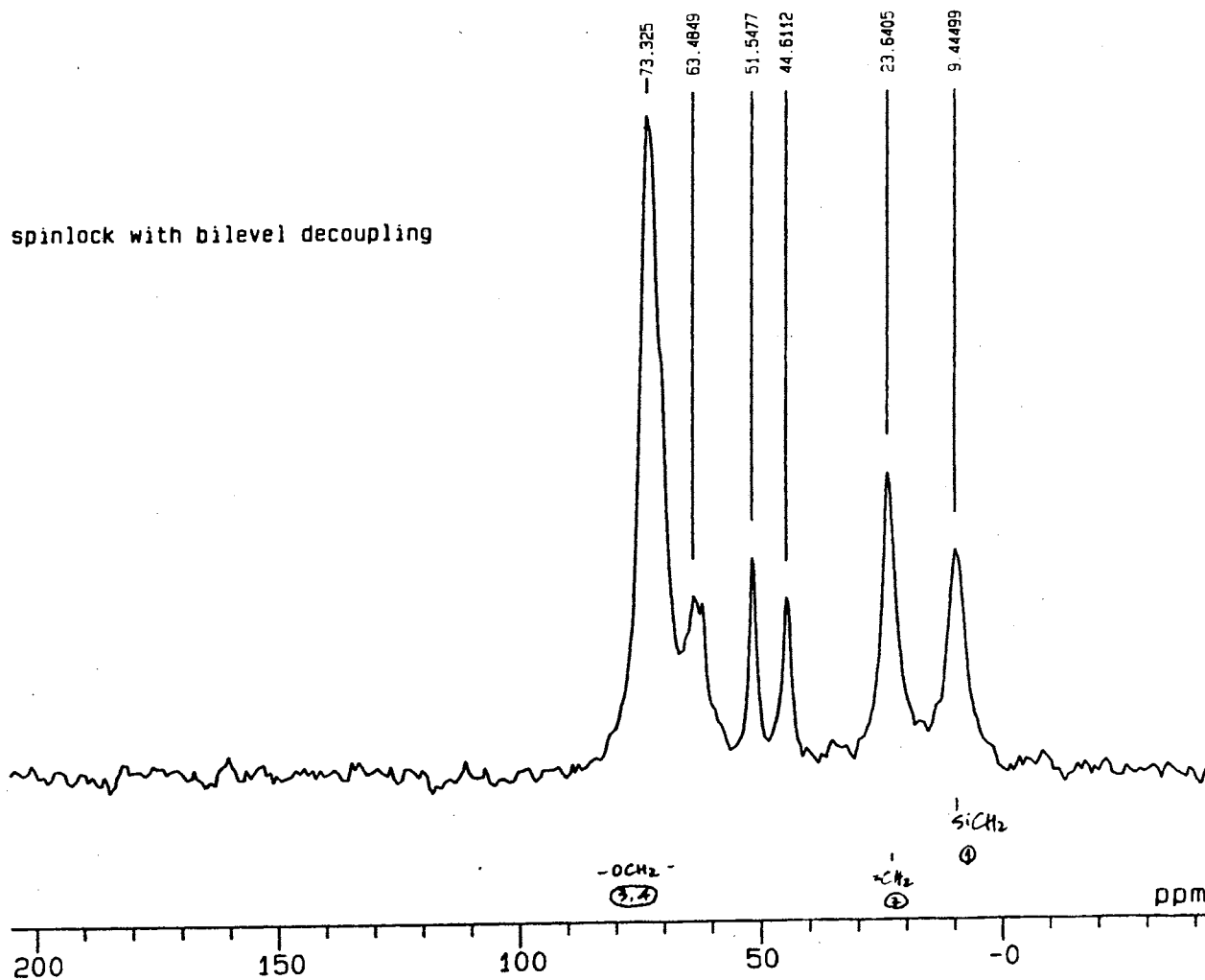rmp=0.61072 virt
rmv=-0.0418877 ppm
fdsc=1.224e+04K

-18.3637

Figure C-4

OkSU CMX-300

MAS=4kHz 1/3/94
One Pulse with proton decoupling
ppfn=s1pulse
cdir=d1
cfn=eormsi1p.001
cfp=0
sf1=59.800843 MHz
sf2=300.998455 MHz
sw=50 KHz
a=150
a1=150
ad=100 usec
al=1k cplx
aqtm=20.481 msec
dw=20 usec
extm=20.021 sec
p=0 deg
pd=20 sec
pw=5 usec
rd=150 usec
dpc=1 scns
ac=1000 scns
dl=2k cplx
tlb=50 Hz
rmp=0.61072 virt
rmv=-0.0418877 ppm
fdsc=1.092e+04K
tph0=33.291 deg
tph1=-1621 deg
disle=197.882 ppm
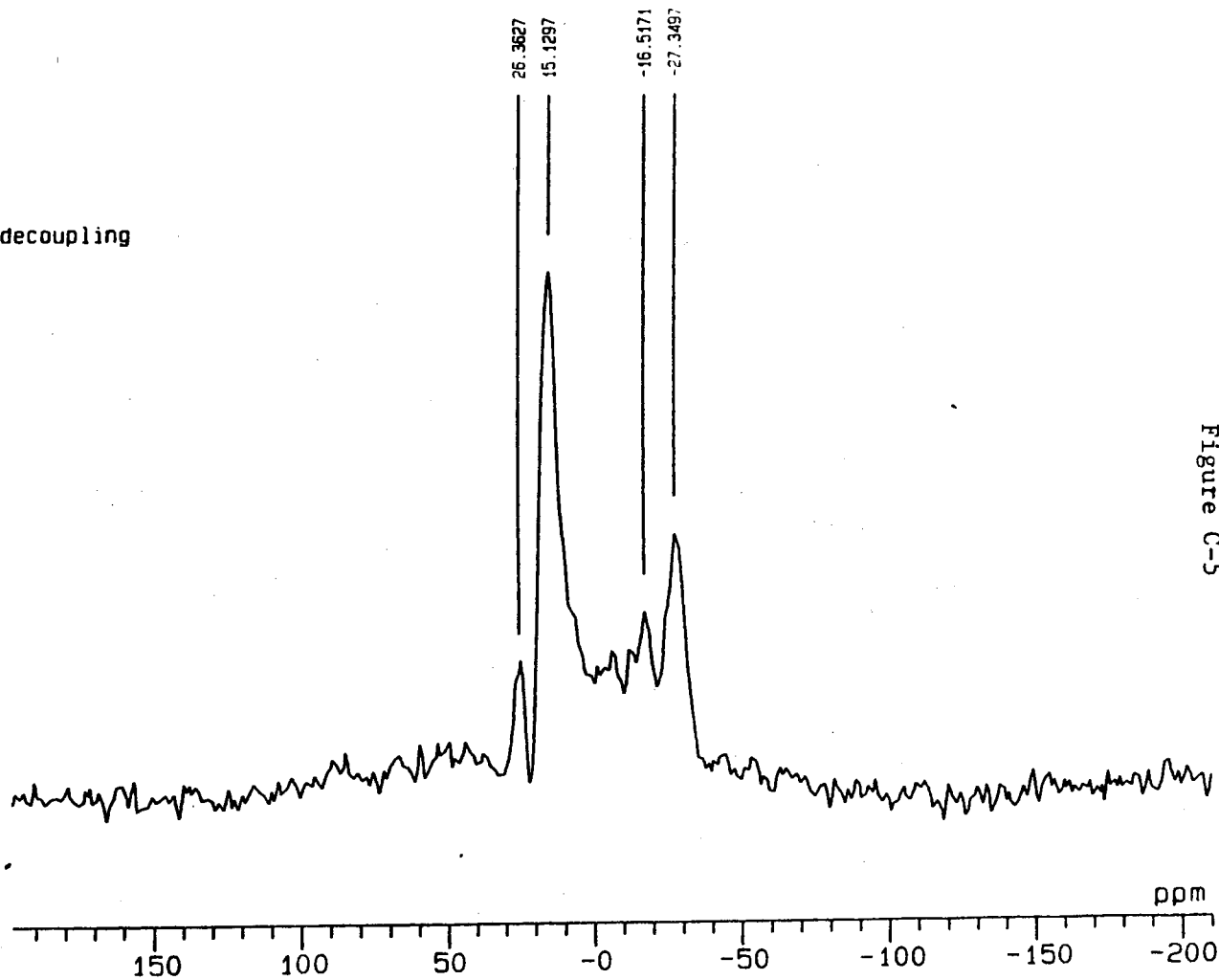
Figure C-5

26.3627 15.1297 -16.5171 -27.3497

ppm

150   100   50   -0   -50   -100   -150   -200

Figure C-6

OkSU CMX-300
MAS=4kHz 1/3/94
cross polarization via spinlock with bilevel decoupling
ppfn=scp7
cdir=d1
cfn=eormsicp.001
cfp=0
sf1=59.800843 MHz
sf2=300.998455 MHz
sw=50 KHz
a=150
a1=150
a2=150
ad=10 usec
al=1k cplx
aqtm=20.481 msec
ct=200 usec
dw=20 usec
extm=2.0207 sec
lc=5
p=0 deg
pd=2 sec
pw=5 usec
rd=10 usec
dpc=1 scns
ac=1000 scns
dl=2k cplx
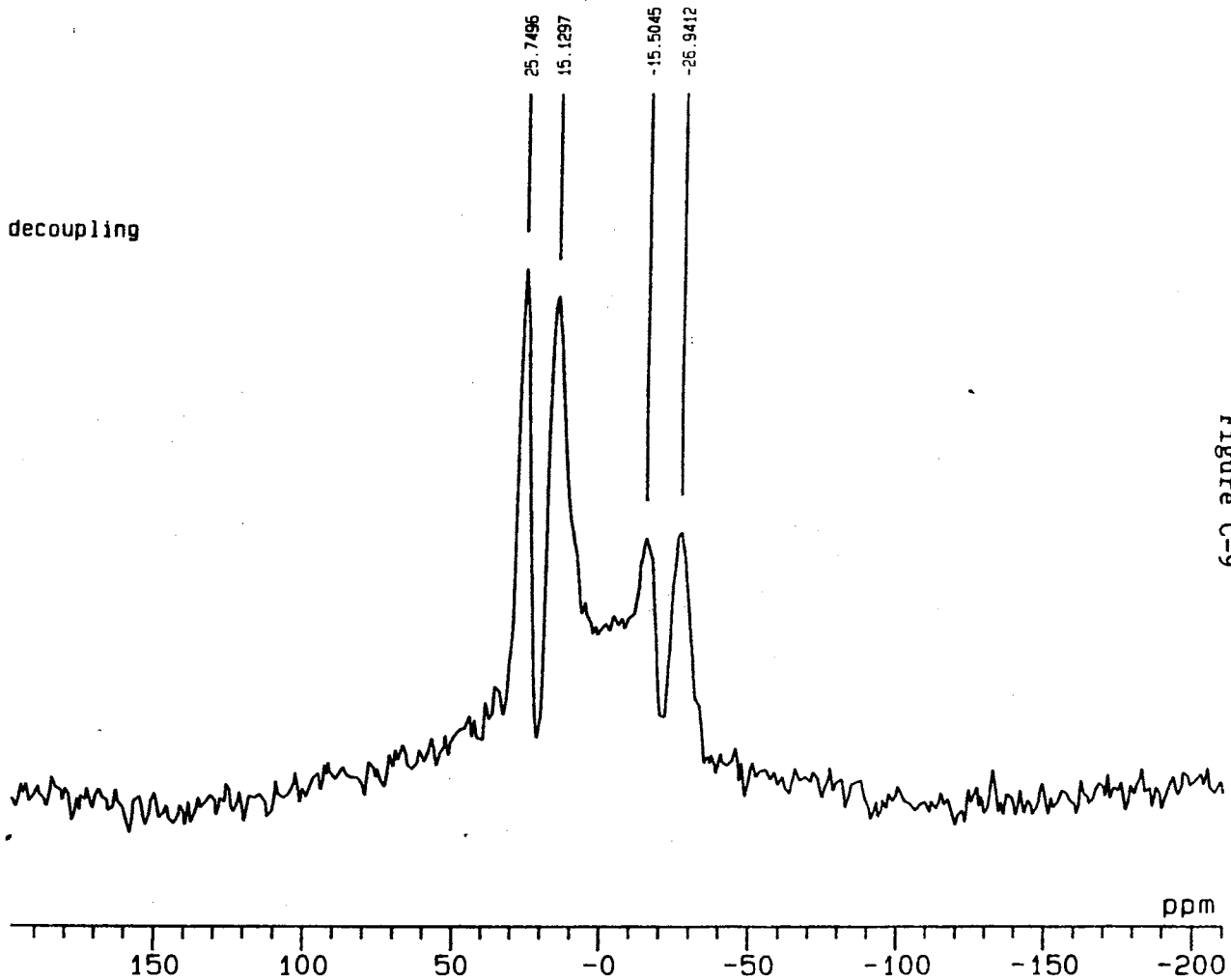tlb=50 Hz
rmp=0.61072 virt
rmv=-0.0418877 ppm
fdsc=1.594e+04K

Figure C-7

OkSU CMX-300

MAS=4khz 12/20/93
cross polarization via spinlock with bilevel decoupling
ppfn=scp7
cdir=subdata
cfn=eorm.001
cfp=0
sf1=75.691414 MHz
sf2=300.998455 MHz
sw=50 KHz
a=152
a1=152
a2=152
ad=10 usec
al=1k cplx
aqtm=20.481 msec
ct=100 usec
dw=20 usec
extm=2.0206 sec
lc=3
p=0 deg
pd=2 sec
pw=5 usec
rd=10 usec
dpc=1 scns
ac=100 scns
dl=4k cplx
tlb=50 Hz
rmp=0.59701 virt
rmv=-0.0331074 ppm
fdsc=5022K

Epoxy-Diol ORMOSIL Ideal Structure

ORMOSIL

Silica

Ethylene Glycol Linkage

Poly(Ethylene Oxide) Linkage

Figure C-8

OkSU CMX-300
MAS=4kHz 1/3/93
One Pulse with proton decoupling
ppfn=s1pulse
cdir=d1
cfn=mormsi1p.001
cfp=0
sf1=59.800843 MHz
sf2=300.998455 MHz
sw=50 KHz
a=150
a1=150
ad=100 usec
al=1k cplx
aqtm=20.481 msec
dw=20 usec
extm=20.021 sec
p=0 deg
pd=20 sec
pw=5 usec
rd=150 usec
dpc=1 scns
ac=1000 scns
dl=2k cplx
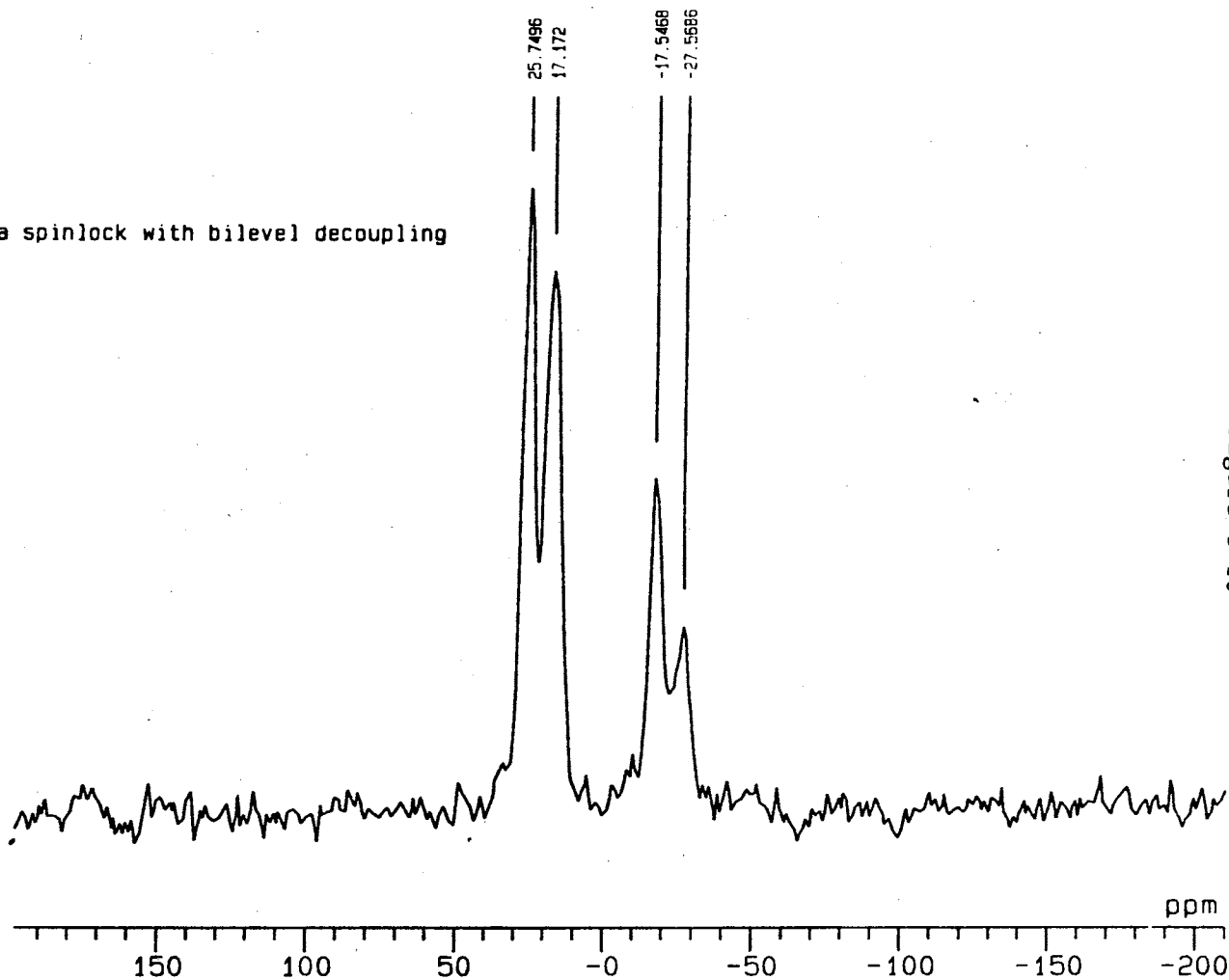tlb=50 Hz
rmp=0.61072 virt
rmv=-0.0418877 ppm
fdsc=9392K
tph0=33.291 deg
tph1=-1621 deg
disle=197.882 ppm

25.7496 15.1297 -15.5045 -26.9412

ppm

150   100   50   -0   -50   -100   -150   -200

Figure C-9

Figure C-10

OkSU CMX-300

MAS=4kHz 1/3/94

cross polarization via spinlock with bilevel decoupling

ppfn=scp7

cdir=d1

cfn=mormsicp.001

cfp=0

sf1=59.800843 MHz

sf2=300.998455 MHz

sw=50 KHz

a=150

a1=150

a2=150

ad=10 usec

al=1k cplx

aqtm=20.481 msec

ct=200 usec

dw=20 usec

extm=2.0207 sec

lc=5

p=0 deg

pd=2 sec

pw=5 usec

rd=10 usec

dpc=1 scns

ac=1000 scns

dl=2k cplx

tlb=50 Hz

rmp=0.61072 virt

rmv=-0.0418877 ppm

fdsc=9392K

CHEMAGNETICS

OkSU CMX-300
MAS=4kHz 12/20/93
cross polarization via spinlock with bilevel decoupling
ppfn=scp7
cdir=subdata
cfn=morm.001
cfp=0
sf1=75.691414 MHz
sf2=300.998455 MHz
sw=50 KHz
a=152
a1=152
a2=152
ad=10 usec
a1=1k cplx
aqtm=20.481 msec
ct=100 usec
dw=20 usec
extm=2.0206 sec
lc=3
p=0 deg
pd=2 sec
pw=5 usec
rd=10 usec
dpc=1 scns
ac=100 scns
dl=4k cplx
tlb=50 Hz
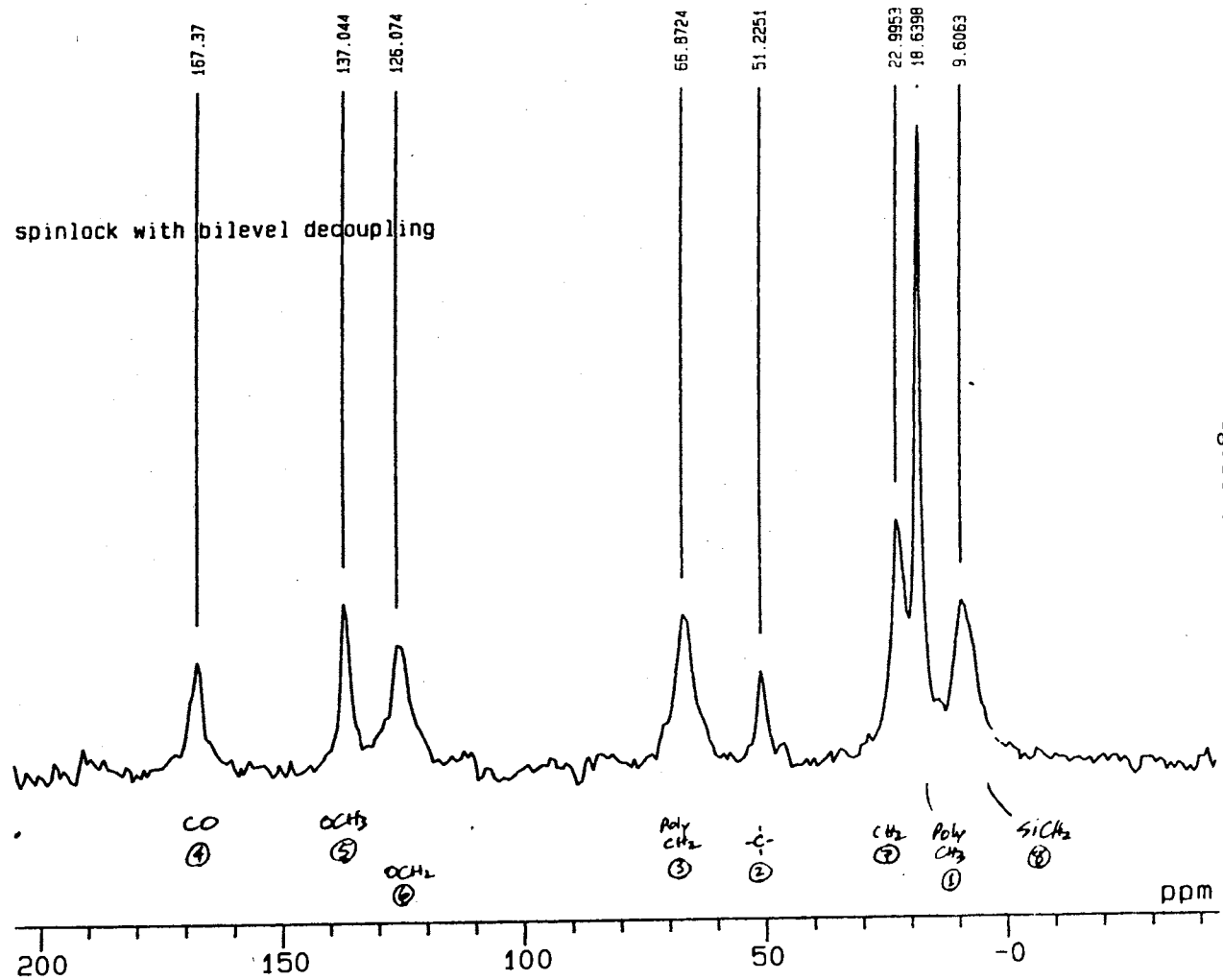rmp=0.59701 virt
rmv=-0.0331074 ppm
fdsc=5022K

167.37
137.044
126.074
66.8724
51.2251
22.9953
18.6398
9.6063

CO ④
OCH₃ ⑤
OCH₂ ⑥
Poly CH₂ ③
-C- ②
CH₂ ⑦
Poly CH₃ ①
SiCH₂ ⑧

200   150   100   50   -0   ppm

203

Figure C-11

Figure C-12

Figure C-13

Auils 160-160   E-withdrawing - uphill

Esters 160-170

for > 175.

Methacrylate ORMOSIL Ideal Structure
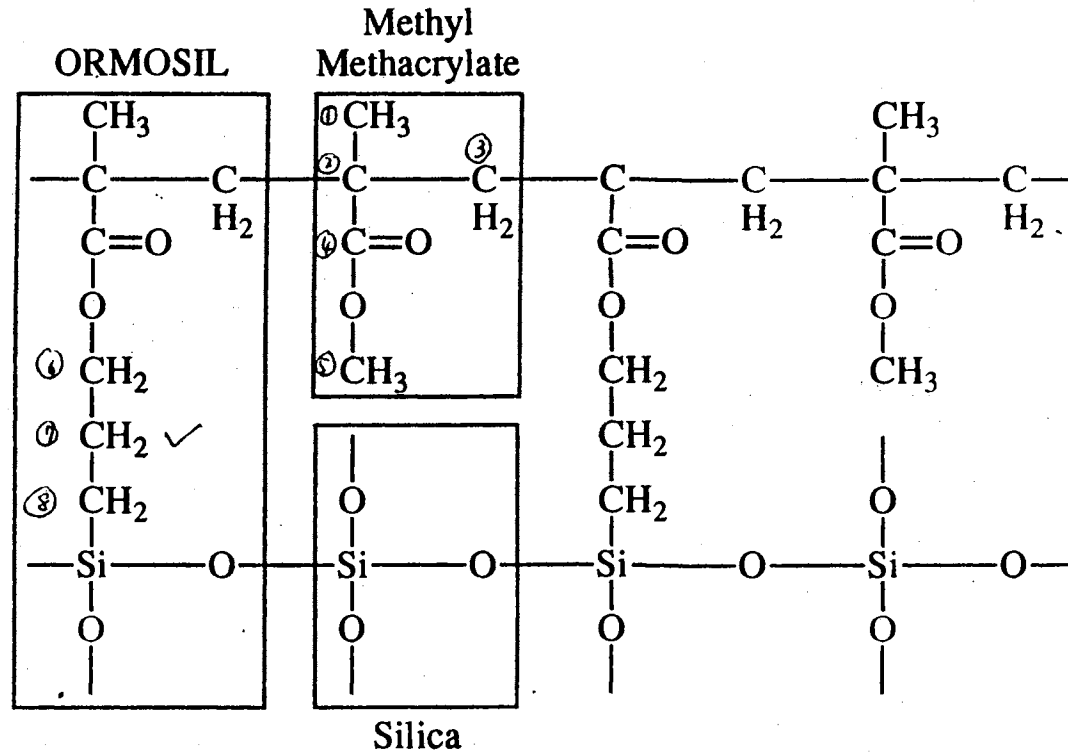
After Capozzi and Pye (1988).

2

VITA

Lowell Ralph Matthews

Candidate for the Degree of

Doctor of Philosophy

Thesis: ON THE SYNTHESIS AND CHARACTERIZATION OF THE OPTICAL PROPERTIES OF EUROPIUM- AND RUTHENIUM-DOPED SOL–GEL-DERIVED MATERIALS AND SODIUM SULFATES

Major Field: Chemistry

Biographical:

> Personal Data: Born in Tulsa, Oklahoma, on March 9, 1961, the son of Ralph A. and Hazel J. Matthews.

> Education: Graduated from Charles Page High School, Sand Springs, Oklahoma in May 1979; received Bachelor of Science degree in Chemistry from the University of Tulsa in May 1990, Magna Cum Laude. Completed the requirements for the Doctor of Philosophy degree with a major in Chemistry at Oklahoma State University in May 1995.

> Experience: Employed by Oklahoma State University, Department of Chemistry, as a graduate teaching and research assistant; Oklahoma State University, Department of Chemistry, 1990 to present.

> Professional Memberships: American Chemical Society, Materials Research Society.